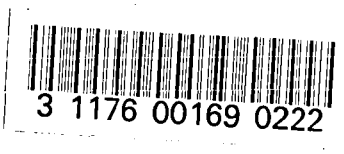

NASA Contractor Report 163105

THE DAST-I REMOTELY PILOTED RESEARCH VEHICLE DEVELOPMENT AND INITIAL FLIGHT TESTING

Alexandros Kotsabasis

Contract NSG 4017
February 1981

NASA

NASA Contractor Report 163105

THE DAST-I REMOTELY PILOTED RESEARCH VEHICLE DEVELOPMENT AND INITIAL FLIGHT TESTING

Alexandros Kotsabasis
University of Kansas Center for Research, Incorporated
Lawrence, Kansas

Prepared for
Dryden Flight Research Center
under Contract NSG 4017

National Aeronautics and
Space Administration
Scientific and Technical
Information Office

1981

Intentionally Left Blank

FOREWORD

This report was made possible by a National Aeronautics and Space Administration grant, NSG-4017, to the University of Kansas.

Intentionally Left Blank

TABLE OF CONTENTS

PAGE

LIST OF ACRONYMS

ACT	active controls technology
ADC	analog-to-digital converter
ADI	altitude director indicator
ALTH	altitude hold
AP	autopilot
ARW-I	aeroelastic research wing I
ATTH	attitude hold
CAS	command augmentation system
CAT	communication and tracking
CD	computer direct
CG	center of gravity
CRT	cathode-ray tube
DAC	digital-to-analog converter
DFRC	Dryden Flight Research Center
FAA	Federal Aviation Administration
FCB	flight control box
FPS	fixed radar special type
FSS	flutter suppression system
GRT	ground resonance test
GVT	ground vibration test
HF	high frequency
IFF	identification friend or foe
LaRC	Langley Research Center
LC	logic card
LPO	launch panel operator
LRO	long range optics

MAC	mean aerodynamic chord
MARS	mid-air recovery system
NASA	National Aeronautics and Space Administration
PCM	pulse code modulation
PHIH	bank angle hold
RAV	remotely augmented vehicle
RD	rate damper
RP	remote pilot
RPM	revolutions per minute
RPRV	remotely piloted research vehicle
RS	recovery system
SAF	spectral analysis facility
SCB	software control board
SCW	super critical wing
S&L	straight and level
TM	telemetry
TMR	tip mass release
UHF	ultrahigh frequency
USAF	United States Air Force
VHF	very high frequency
W&B	weight and balance

LIST OF FIGURES

LIST OF TABLES

LIST OF SYMBOLS

SYMBOL	DEFINITION	USUAL DIMENSION
b	wing span	
$\bar{c}$	mean aerodynamic chord	
$C_D = \frac{D}{\bar{q}S}$	drag coefficient	
$C_{D_\alpha} = \frac{\partial C_D}{\partial \alpha}$	variation of drag coefficient with angle of attack	deg^{-1}
$C_{D_{\delta_E}} = \frac{\partial C_D}{\partial \delta_E}$	variation of drag coefficient with elevator angle	deg^{-1}
$C_\ell = \frac{L}{\bar{q}Sb}$	rolling moment coefficient	
$C_L = \frac{L}{\bar{q}S}$	lift coefficient	
$C_{\ell_p} = \frac{\partial C_\ell}{\partial\left(\frac{pb}{2U_1}\right)}$	variation of rolling moment coefficient with roll rate	
$C_{L_q} = \frac{\partial C_D}{\partial\left(\frac{\bar{q}c}{2U_1}\right)}$	variation of lift coefficient with pitch rate	
$C_{\ell_r} = \frac{\partial C_\ell}{\partial\left(\frac{rb}{2U_1}\right)}$	variation of rolling moment coefficient with yaw rate	
$C_{L_u} = \frac{\partial C_L}{\partial\left(\frac{U}{U_1}\right)}$	variation of lift coefficient with speed	
C_{L_o}	effective lift curve slope intercept	

SYMBOL	DEFINITION	USUAL DIMENSION
$C_{L_\alpha} = \frac{\partial C_L}{\partial \alpha}$	variation of lift coefficient with angle of attack	deg^{-1}
$C_{L_{\dot{\alpha}}} = \frac{\partial C_L}{\partial\left(\frac{\dot{\alpha}\bar{c}}{2U_1}\right)}$	variation of lift coefficient with rate of change of angle of attack	
$C_{\ell_\beta} = \frac{\partial C_\ell}{\partial \beta}$	variation of rolling moment coefficient with sideslip angle	deg^{-1}
$C_{\ell_{\delta_A}} = \frac{\partial C_\ell}{\partial \delta_A}$	variation of rolling moment coefficient with aileron angle	deg^{-1}
$C_{L_{\delta_E}} = \frac{\partial C_L}{\partial \delta_E}$	variation of lift coefficient with elevator angle	deg^{-1}
$C_{L_{\delta_R}} = \frac{\partial C_\ell}{\partial \delta_R}$	Variation of rolling moment coefficient with rudder angle	deg^{-1}
$C_m = \frac{M}{\bar{q}S\bar{c}}$	pitching moment coefficient	
$C_{m_q} = \frac{\partial C_m}{\partial\left(\frac{q\bar{c}}{\partial U_1}\right)}$	variation of pitching moment coefficient with pitch rate	
C_{m_o}	effect pitching moment curve slope intercept	
$C_{m_\alpha} = \frac{\partial C_m}{\partial \alpha}$	variation of pitching moment coefficient with angle of attack	deg^{-1}
$C_{m_{\dot{\alpha}}} = \frac{\partial C_m}{\partial\left(\frac{\dot{\alpha}\bar{c}}{\partial U_1}\right)}$	variation of pitching moment coefficient with elevator angle	deg^{-1}

SYMBOL	DEFINITION	USUAL DIMENSION
$C_n = \frac{N}{\bar{q}Sb}$	yawing moment coefficient	
$C_{n_p} = \frac{\partial C_n}{\partial\left(\frac{pb}{\partial U_1}\right)}$	variation of yawing moment coefficient with roll rate	
$C_{n_r} = \frac{\partial C_n}{\partial\left(\frac{rb}{\partial U_1}\right)}$	variation of yawing moment coefficient with yaw rate	
$C_{n_\beta} = \frac{\partial C_n}{\partial \beta}$	variation of yawing moment coefficient with sideslip angle	deg^{-1}
$C_{n_{\delta_A}} = \frac{\partial C_n}{\partial \delta_A}$	variation of yawing moment coefficient with aileron angle	deg^{-1}
$C_{n_{\delta_R}} = \frac{\partial C_n}{\partial \delta_R}$	variation of yawing moment coefficient with rudder angle	deg^{-1}
$C_Y = \frac{Y}{\bar{q}Sb}$	side force coefficient	
$C_{Y_p} = \frac{\partial C_Y}{\partial\left(\frac{pb}{\partial U_1}\right)}$	variation of side force coefficient with roll rate	
$C_{Y_r} = \frac{\partial C_Y}{\partial\left(\frac{rb}{\partial U_1}\right)}$	variation of side force coefficient with yaw rate	
$C_{Y_\beta} = \frac{\partial C_Y}{\partial \beta}$	variation of side force coefficient with sideslip angle	deg^{-1}
$C_{Y_{\delta_A}} = \frac{\partial C_Y}{\partial \delta_A}$	variation of side force coefficient with aileron angle	deg^{-1}

SYMBOL	DEFINITION	USUAL DIMENSION
$C_{Y_{\delta_R}} = \frac{\partial C_Y}{\partial \delta_R}$	variation of side force coefficient with rudder angle	deg^{-1}
D	FSS control system parameter	
db	decibel	
g	acceleration of gravity	m/sec^2
G(S)	transfer function	
$\dot{h}$	altitude rate	m/sec^2
HP	altitude	m
Hz	frequency	cycle/sec
I_x	Moment of inertia about the X-axis	$kg\text{-}m^2$
I_y	moment of inertia about the Y-axis	$kg\text{-}m^2$
I_z	moment of inertia about the Z-axis	$kg\text{-}m^2$
I_{xz}	product of inertia referred to X- and Z-axes	$kg\text{-}m^2$
k	gain constant	
KCAS	calibrated airspeed	m/sec
m	mass	kg
M	Mach number	
P	roll rate	rad/sec
P_I	impact pressure	kgf/m^2
P_s	static pressure	kgf/m^2

SYMBOL	DEFINITION	USUAL DIMENSION
P_t	total pressure	kgf/m^2
q	pitch rate	rad/sec
$\bar{q}$	dynamic pressure	N/m^2
r	yaw rate	rad/sec
rpm	revolutions per minute	
S	Laplace variable	sec^{-1}
spc	samples per cycle	
sps	samples per second	
THR	throttle setting	% rpm
V	velocity	m/sec
V_T	true airspeed	m/sec
W	weight	kg
α	angle of attack	deg
β	sideslip angle	deg
γ	flight path angle	deg
δ_a	FSS aileron deflection	deg
$\delta_{A,a,d}$	differential tail deflection, $\delta_{A,a,d} = \delta_L - \delta_R$	deg
$\delta_{E,e}$	elevator deflection, $\delta_{E,e} = \frac{\delta_L + \delta_R}{2}$	deg
δ_{h_L}	left elevator deflection	deg
δ_{h_R}	right elevator deflection	deg

SYMBOL	DEFINITION	USUAL DIMENSION
$\delta_{R,r}$	rudder deflection	deg
ζ	damping ratio	
Θ	pitch attitude angle	deg
Φ	bank angle	deg

Subscripts:

AP	autopilot
B.P.	break point
C	command
IC	initial condition
L	left hand
R	right hand
P	pilot's command
THR	throttle

Table and figure labels:

ALP	angle of attack
AP	autopilot
BATTLO	battery voltage low
CHANA	channel A
CHANB	channel B
CLOSS	carrier loss
DA	computer differential tail command
DE	computed elevator command
DHL	left elevator deflection
DHR	right elevator deflection

SYMBOL	DEFINITION
EMER	emergency recovery
GENFL	generator failure
H	altitude
PHI	bank angle
RECVRY	normal recovery
THA	pitch attitude angle
THABIS1	pitch attitude bias 1
THABIS2	pitch attitude bias 2
THR	computed throttle command

CHAPTER 1

INTRODUCTION

Rapidly increasing fuel costs during the past decade has lead to a renewed and intensive interest in improving aircraft efficiency. A number of research programs supported by the National Aeronautics and Space Administration are aimed at enhancing aircraft efficiency by improving aerodynamics, increasing propulsion system efficiency, and reducing aircraft weight.

Aircraft weight reductions generally are accompanied by a combination of reduction in flutter speed, decrease in aircraft fatigue life, and reduction in vehicle stability.

The DAST (Drones for Aerodynamic and Structural Testing) program is directed at applying Active Controls Technology (ACT) in order to achieve wing weight reduction without incurring the penalties mentioned above.

The first application of ACT by the DAST program will be through the testing of an active Flutter Suppression System (FSS) designed to suppress explosive flutter modes of the supercritical Aeroelastic Research Wing (ARW-I) in the transonic region.

The most effective use of active controls is to incorporate the ACT concept into aircraft configurations at the preliminary design stage. For that, an accurate and reliable method is needed to predict the structural and transonic aerodynamic characteristics. The DAST program is anticipated to provide valuable information that will advance the technology required for reliable prediction of structural and unsteady aerodynamics.

The primary research objective of the flutter suppression experiment is to validate the active control system synthesis and analysis for the first Aeroelastic Research Wing, ARW-I. The experiment, known as the DAST-I, is unique in that it is designed to suppress flutter characteristics that have been analytically predicted. Past ACT applications have only demonstrated the suppression of well-defined flutter modes.

The validation of the DAST-I active control system for flutter suppression will be to demonstrate an increase of the ARW-I flutter boundary speed by 20 percent.

The DAST program is a NASA intercenter effort involving the Dryden Flight Research Center (DFRC) at Edwards AFB in California and the Langley Research Center (LaRC) in Langley, Virginia. Flight testing of the DAST-I vehicle will be conducted by the NASA Dryden Flight Research Center.

In this report, a description is given of the DAST-I remotely piloted research vehicle development, operation, and initial flight testing.

In Chapter 2, a description of the modified Firebee II test vehicle is presented. A description of the ARW-I and FSS is given in Chapter 3. The supporting ground facilities and aircraft systems are presented in Chapter 4. A description of the real time simulation facility and the design and specification of the RAV control system is included in Chapter 5. A summary of the preflight and test flight procedures common to the RPRV operation is presented in Chapter 6, followed by an evaluation of the Blue Streak test flight and the first and second ARW-I test flights in Chapter 7. A summary

of conclusions concerning the RPRV operation in general and the testing of the DAST-I in particular is presented in Chapter 8.

This report emphasizes the software aspects of the DAST program. Minimal information is given about the actual hardware systems utilized by the program. This was done in order to reflect the author's activities in this program, which were mainly related to the development of the ground-based software control system, the software specification and software validation testing via piloted simulation.

CHAPTER 2

DAST-I REMOTELY PILOTED RESEARCH VEHICLE

The DAST program utilizes a modified BQM-34E/F Firebee II supersonic aerial target drone for flight testing. The use of a remotely piloted vehicle was necessary because of the high technical risks involved in flight testing of an active flutter suppression system. Because of the explosive nature of ARW-I flutter modes, design errors or system malfunctions could lead to major structural failures, which in turn could jeopardize the safety of the pilot of a manned test vehicle.

The modified Firebee II research vehicle will be tested at the NASA Dryden Flight Research Center. Remote control of the vehicle is achieved through a facility, developed by this center, that utilizes a flight testing concept known as the Remotely Piloted Research Vehicle (RPRV) technique. The technique involves a pilot who controls the flight test vehicle from a ground cockpit and a ground-based digital computer for computation of command signals. The remote pilot cockpit and the computer are coupled to the flight test vehicle through telemetry uplink and downlink channels. The RPRV concept evolved from the interest in developing a low-cost alternative to full-scale manned testing for high risk flight test programs.

Flight test operations of remotely piloted vehicles require a significant support. The elements involved in testing the Firebee II drone are presented in figure 2.1. The flight test operation involves a B-52 aircraft as a carrier and launch vehicle, an F-104 chase aircraft as a backup control station, and a U.S. Air Force

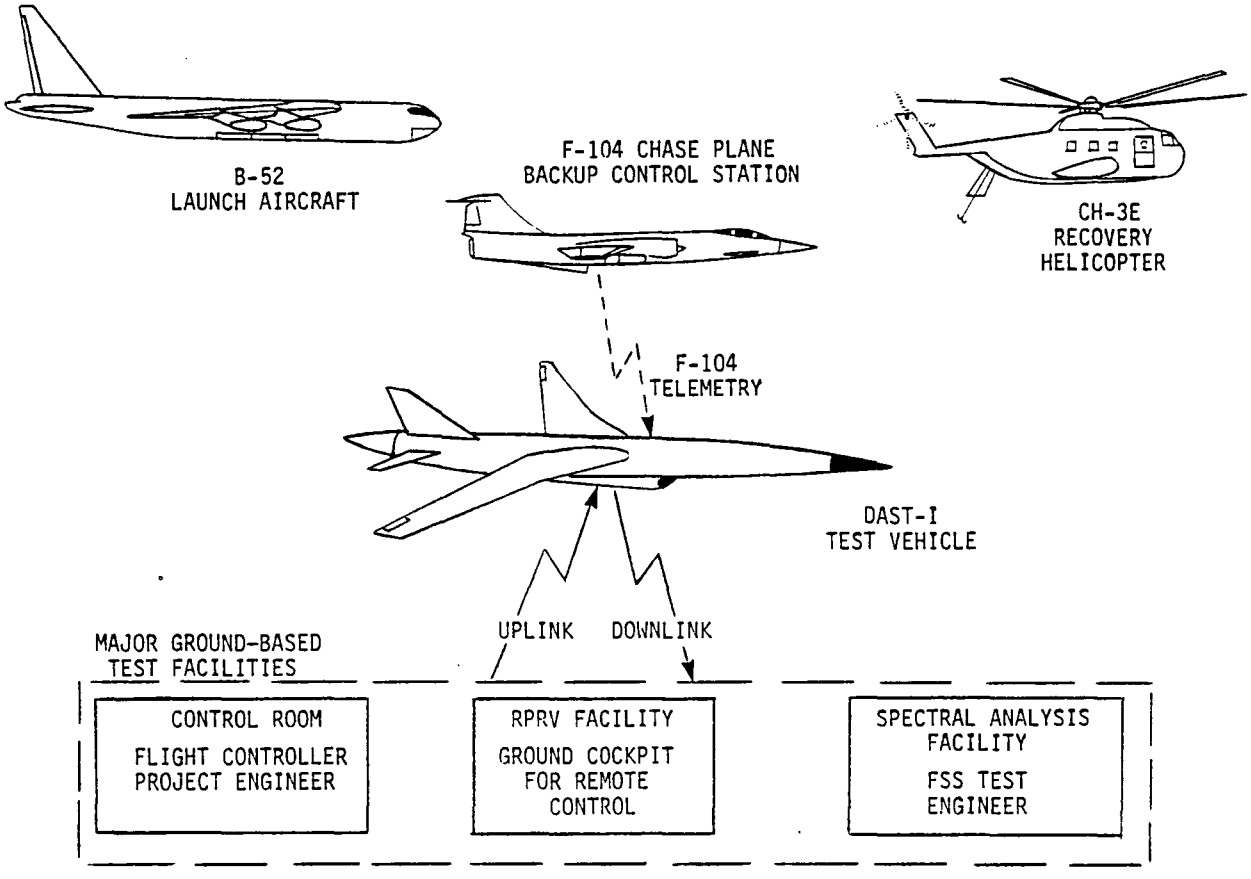

Figure 2.1. A simplified presentation of the DAST-I RPRV flight test operation.

CH-3E helicopter for the mid-air recovery of the test vehicle. Photographic coverage is provided by another F-104 aircraft. Several ground facilities are also involved during the flight test operation. Only the major supporting ground facilities are shown in the above figure.

In this chapter a general description is given of the BQM-34E/F Firebee II drone that is utilized as a test bed by the DAST program. Aerodynamic and stability and control characteristics are also presented.

2.1 DAST-I Test Vehicle

The BQM-34E/F Firebee II target drone was selected as the test bed for the DAST program because of its size, relatively clean aerodynamic shape, performance, and flight envelope. The vehicle has a flight envelope suitable for flutter testing and high altitude experiments. The equipment compartment offers the necessary volume for additional research instrumentation. Five drones were purchased from the Air Force. Only one would be modified to become the test bed for the first aeroelastic wing, ARW-I. A three-view drawing of the Firebee II drone is shown in figure 2.2. The DAST vehicle fitted with the ARW-I wing is presented in figure 2.3. Excluding the replacement of the original Firebee II wing by the aeroelastic research wing, hardly any external modifications were made to the vehicle. The new configuration is known as the DAST-I test vehicle.

In this section the test vehicle will be described. A list of modifications made to the original drone, is also presented. These modifications were made to fulfill special NASA Dryden Flight Research Center flight test requirements.

Physical Characteristics:

	WING	HORIZONTAL TAIL	VERTICAL TAIL
Gross Area (m^2)	2.97	0.85	0.8
Aspect Ratio	2.5	3.5	1.1
Taper Ratio	0.3	0.4	0.3
Incidence (degrees)	0.0	All-movable	-
Dihedral (degrees)	0.0	0.0	-
Rudder Area (m^2)	-	-	0.056

Clean Zero Fuel Weight 730 kg
Clean Full Internal Fuel Weight 853 kg

Power Plant:
Continental YJ69-T-406
Rated Thrust 871 kgf (Sea level static)

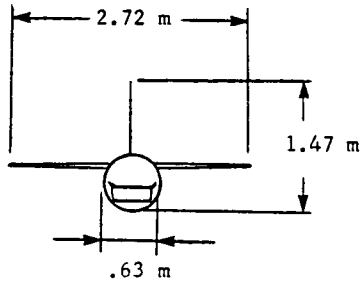

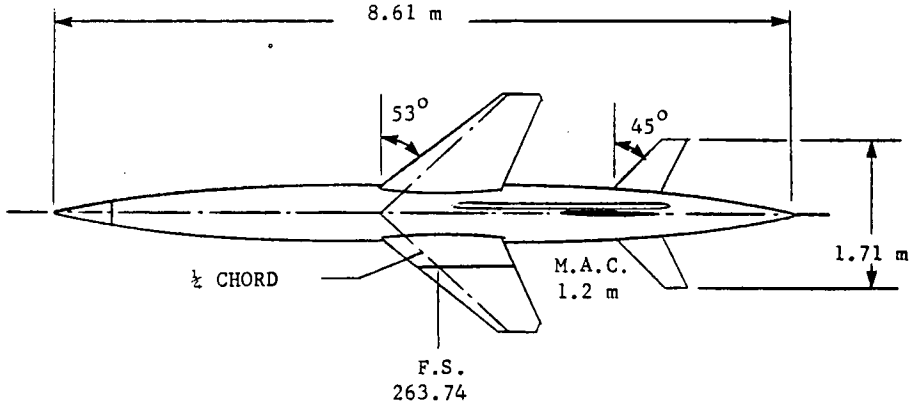

Figure 2.2. BQM-34E/F Firebee II drone general configuration.

Physical Characteristics:

	WING	HORIZONTAL TAIL	VERTICAL TAIL
Gross Area (m^2)	2.787	0.85	0.8
Aspect Ratio	6.8	3.5	1.1
Taper Ratio	0.36	0.4	0.3
Incidence (degrees)	0.0	All-movable	-
Dihedral (degrees)	0.0	0.0	-
Rudder Area (m^2)	-	-	0.056

Clean Zero Fuel Weight 870 kg
Clean Full Internal Fuel Weight 1008 kg

Power Plant:
Continental YJ69-T-406

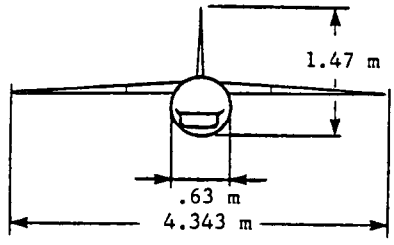

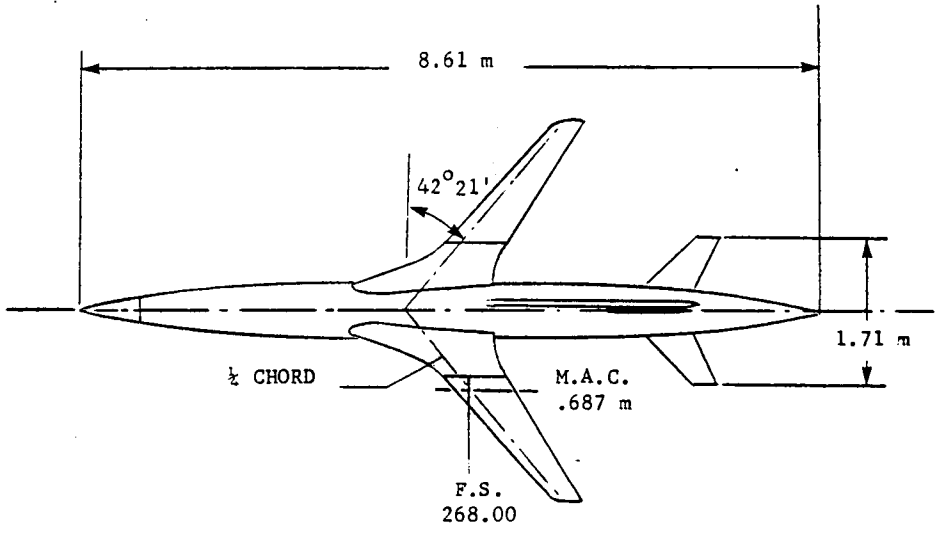

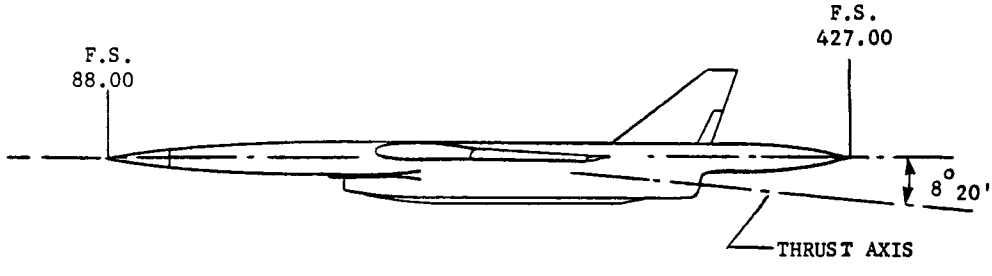

Figure 2.3. DAST-I test vehicle general configuration.

2.1.1 General Description

The dimensions of the test vehicle and other general information are presented in figure 2.3. The DAST-I flight envelope is shown in figure 2.4. The operational ceiling is limited due to the unsteady pitchup characteristics of the ARW-I supercritical wing at high angles of attack. Performance data were based on results obtained from wind tunnel test of a 1/6-scale force model. Throttle settings lower than 80 percent of the maximum rpm value can cause an engine flameout. Therefore, the minimum flight speed at most altitudes is limited by the minimum allowable throttle setting rather than by aircraft stall.

Control in the pitch and roll axes is achieved by the all-movable differential horizonatal tail. Yaw control is obtained through the rudder.

Trim conditions for the test vehicle were determined utilizing the real time simulation. The trim angle of attack and trim elevator setting as a function of altitude and Mach number are shown in figures 2.5 and 2.6 for full and empty fuel conditions, respectively. Throttle settings for the above trim conditions are given in figure 2.7. Fuel quantity hardly affects the throttle setting, therefore the data presented in this figure are valid for full and empty fuel conditions. The empty fuel conditions were calculated with 23 kg of fuel remaining in the main tank. This is the minimum fuel condition at which recovery will be initiated during flight operations. Conditions with less than 23 kg of fuel will not be flown during normal operations for safety reasons.

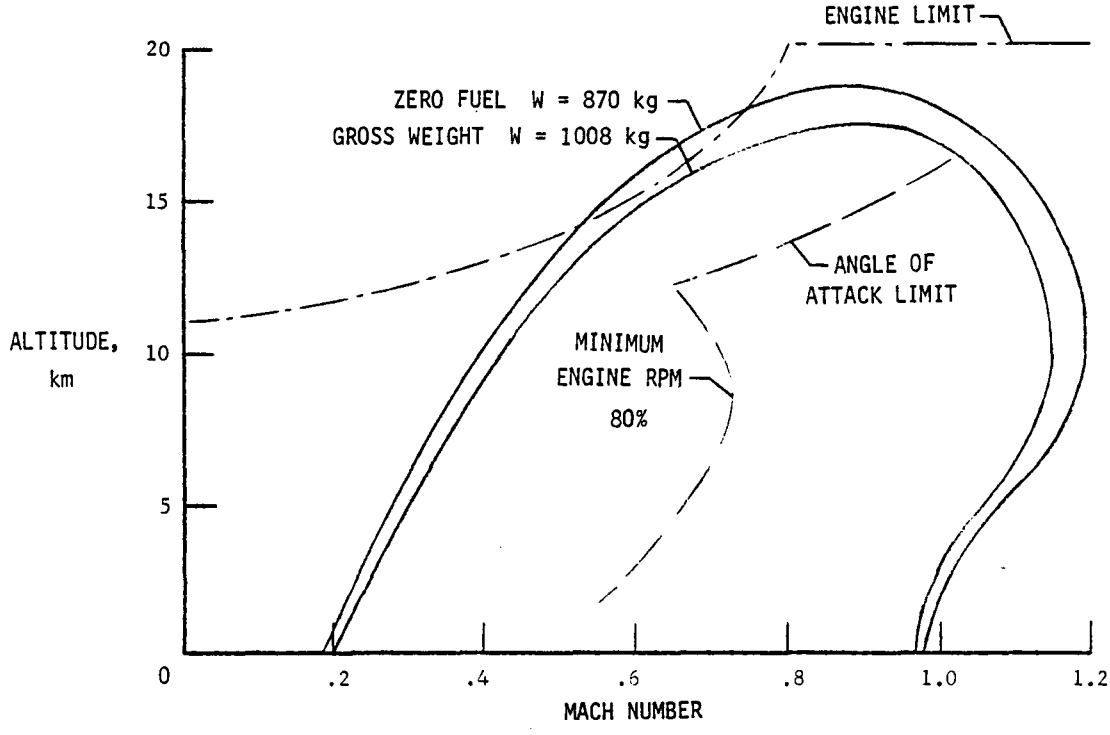

Figure 2.4. Flight envelope of the DAST-I test vehicle.

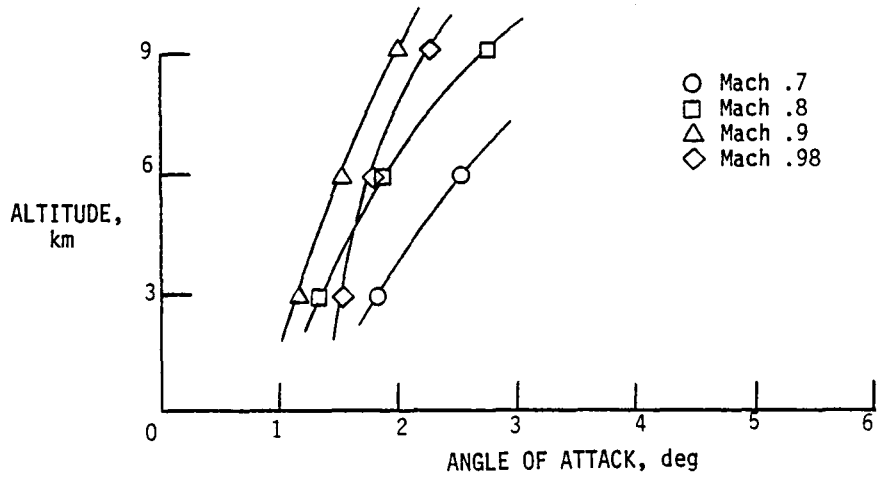

(a) Trim angle of attack.

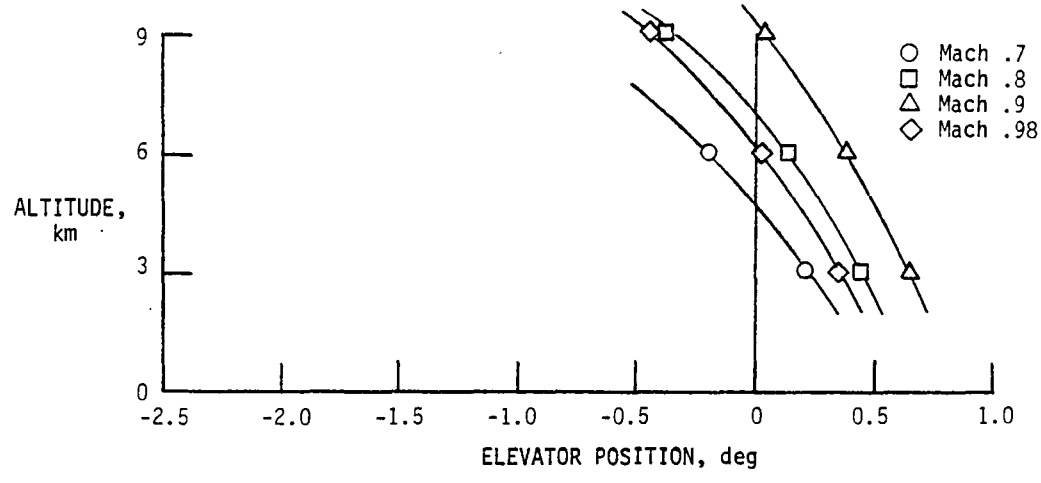

(b) Trim elevator position.

Figure 2.5. DAST-I trim conditions at full fuel weight. W = 1008 kg; c.g. = 264.4 F.S.

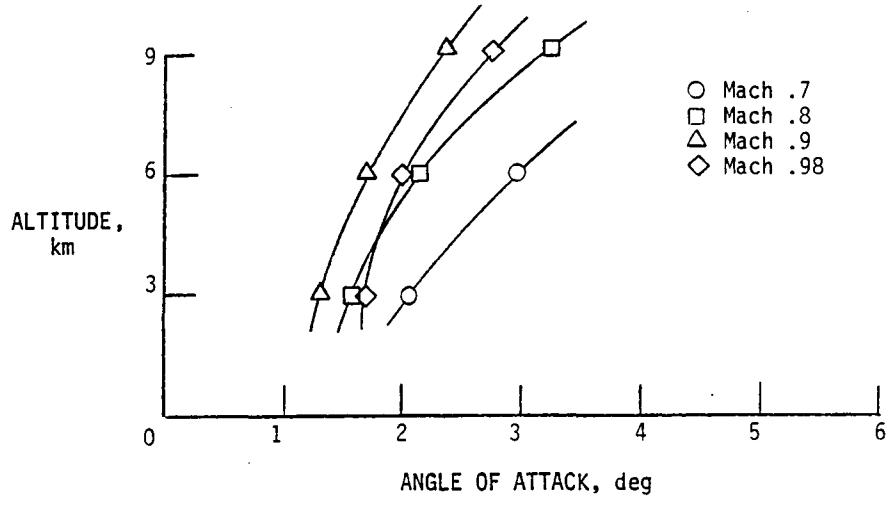

(a) Trim angle of attack.

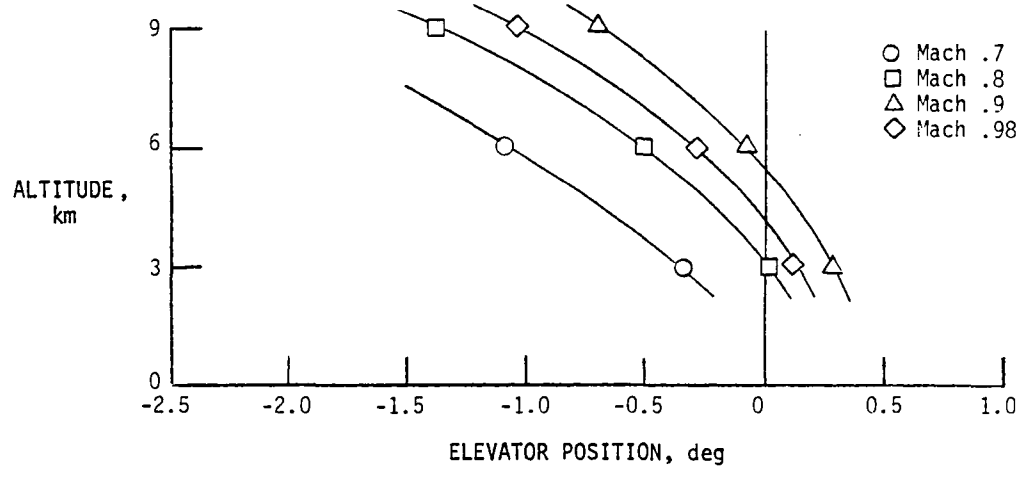

(b) Trim elevator position.

Figure 2.6. DAST-I trim conditions at 23 kg of fuel remaining. W = 893 kg; c.g. = 267.7 F.S.

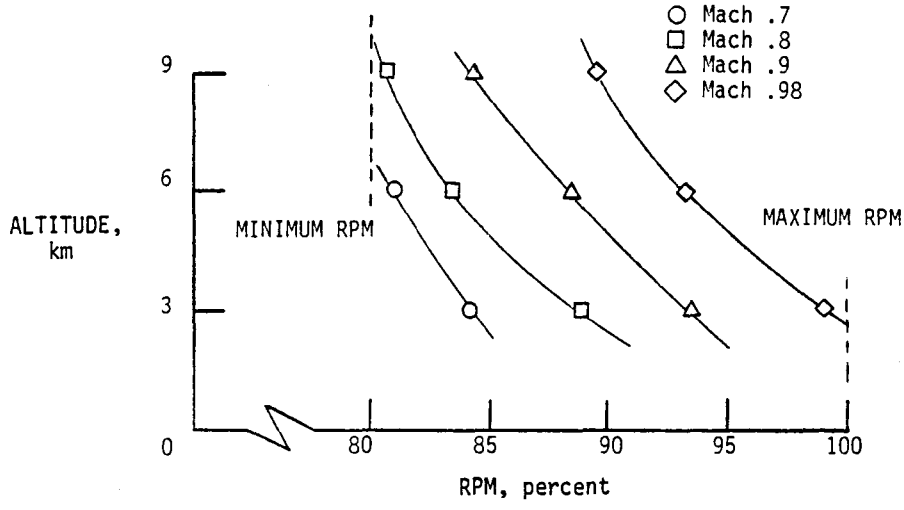

Figure 2.7. Throttle command required at trimmed conditions.

The vehicle is powered by the Continental YJ69-T-406 powerplant, with a rated thrust of 871 kgf at 100 percent rpm (22,150 rpm) and at sea level conditions. The engine's thrust axis makes an angle of 8.3 degrees with the waterline of the vehicle. The distance between the thrust axis and the center of gravity changes as fuel is consumed. This change results in a considerable pitching moment about the center of gravity, which has to be accounted for when simulating the vehicle.

The relatively large sized engine for the Firebee II drone results in gyroscopic effects that are most evident in the pitch and yaw axes. The engine rotation moment of inertia is equal to .375 $kg/m^2/rad/sec$. This is the value specified by the engine manufacturer.

The operational rpm for this engine is limited between 80 and 100 percent. Net thrust and fuel flow versus Mach for four different altitudes and three rpm settings is shown in figures 2.8 and 2.9, respectively. Thrust and fuel consumption show, in general, an increase with decreasing altitude. Engine efficiency becomes poor at lower altitudes and low rpm settings.

The gross and empty vehicle weight and the respective location of the center of gravity (c.g.) are given in table 2.1. The gross weight presented in this table was experimentally determined during weight and balance (W&B) tests. The empty weight was calculated by subtracting the auxiliary and main fuel weight from the gross weight.

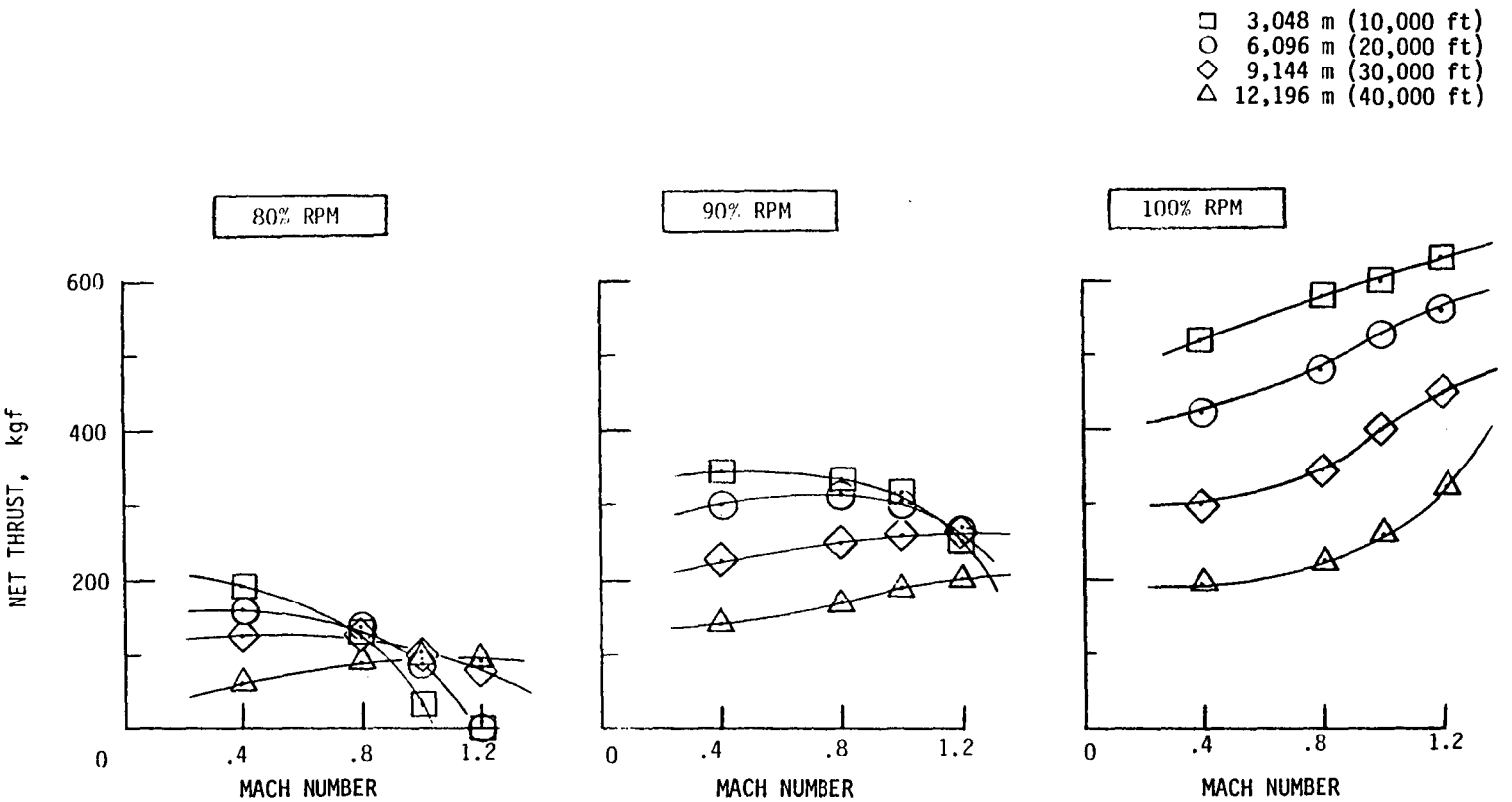

Figure 2.8. Net thrust of the YJ69-T-406 Firebee II engine versus Mach number.

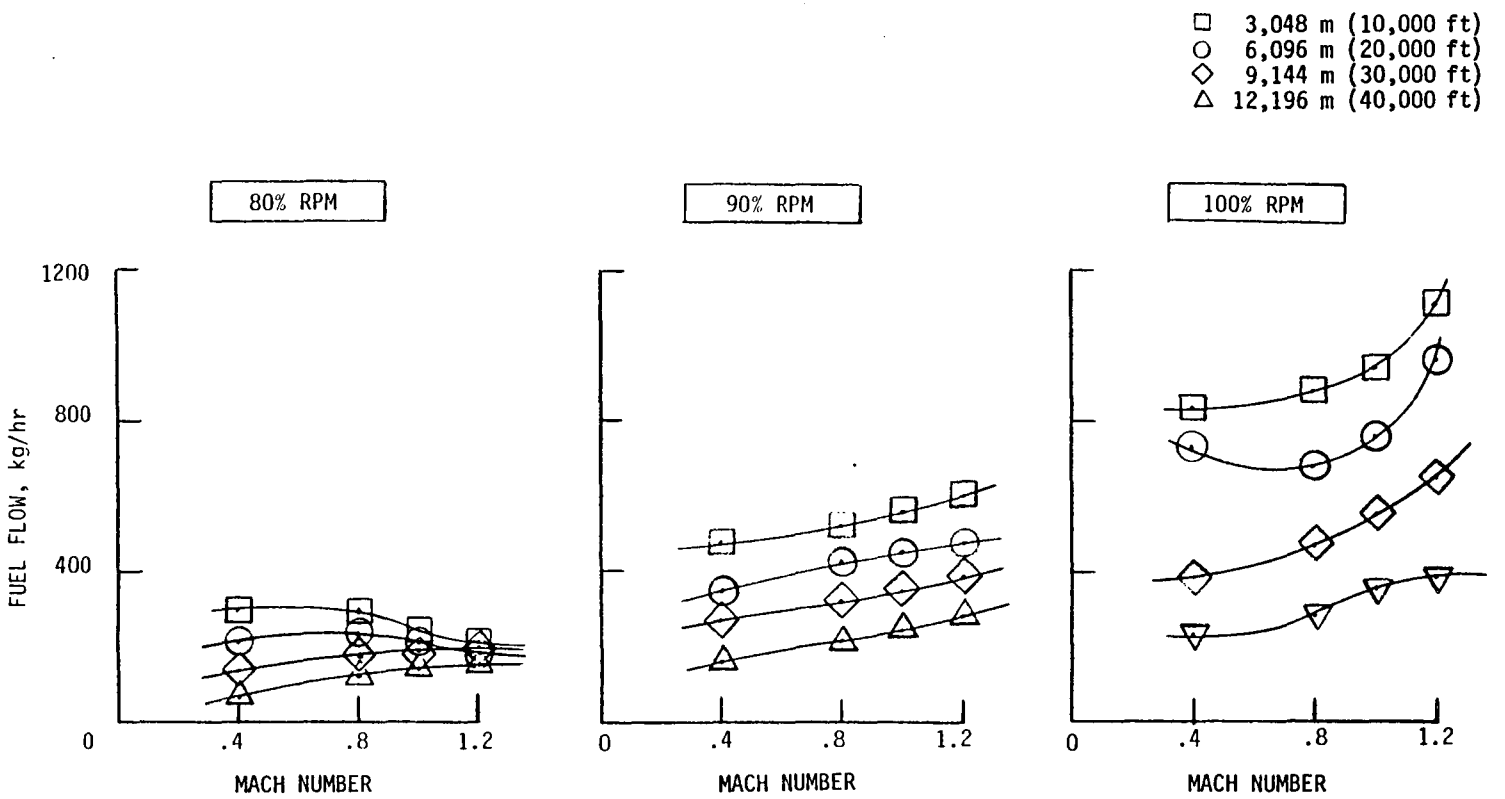

Figure 2.9. Fuel flow of the YJ69-T-406 Firebee II engine versus Mach number.

TABLE 2.1 DAST-I WEIGHT AND C.G. LOCATION

Vehicle Configuration	Vehicle weight*, kg	C.G. Location		
		Horizontal		Vertical
		% MAC**	F.S.	Waterline
Gross weight	1008	11.7	264.4	53.60
Empty auxiliary Tank	977	19.2	266.4	53.62
Zero fuel	870	25.0	268.0	54.17

* Includes smoke and engine oil
** MAC = .687 m

The c.g. location of the vehicle with full fuel is balanced to a predetermined fuselage station during W&B tests. The other c.g. locations presented in table 2.1 were analytically determined. The c.g. travel versus vehicle weight is shown in figure 2.10. The horizontal c.g. travel is largely affected by the auxiliary fuel quantity due to the forward location of the auxiliary tank. A fuel flow regulating mechanism is designed to empty the auxiliary fuel tank first. This results in a substantial aft c.g. travel within the first few minutes of a free flight.

The DAST-I moments of inertia were determined by extensive inertia tests conducted at the NASA Dryden Flight Research Center. Test results determined the empty vehicle inertia, while moments of inertia at other fuel conditions were analytically obtained.

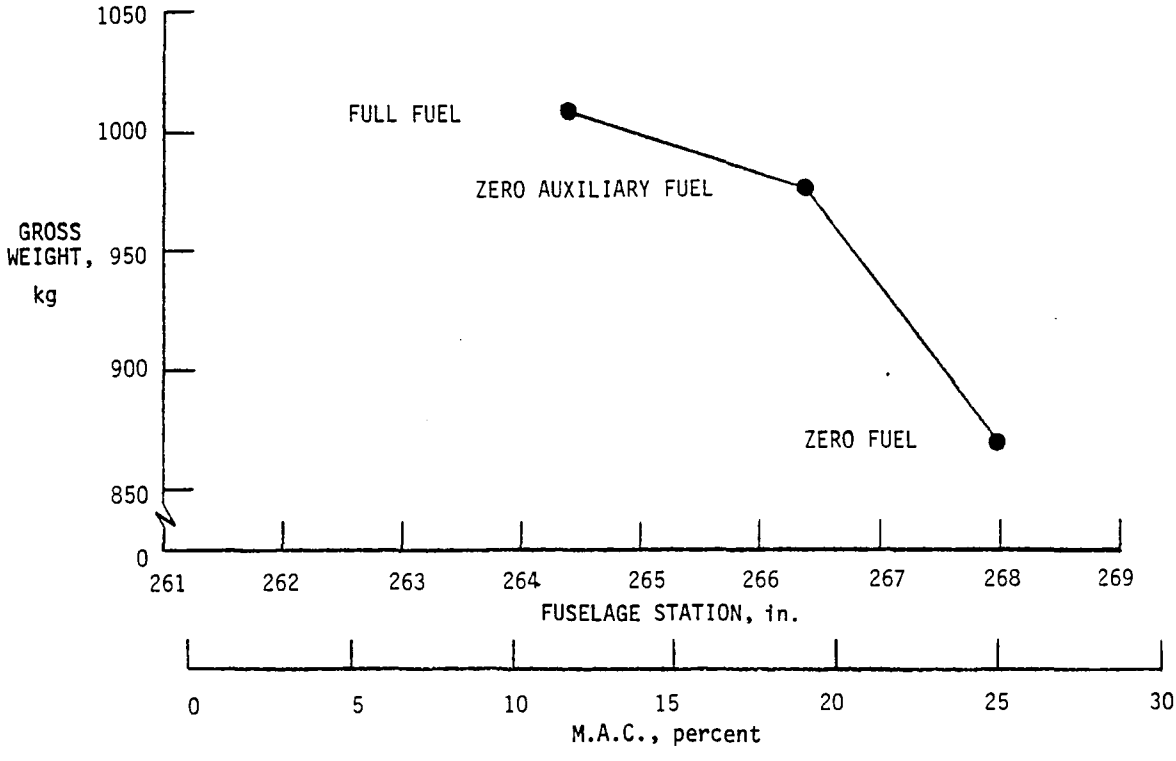

Figure 2.10. DAST-I center of gravity travel versus vehicle weight.

TABLE 2.2 DAST-I MOMENTS OF INERTIA

Vehicle configuration	Vehicle weight*, kg	C.G. fuselage station	I_x Roll, kg-m^2	I_y Pitch, kg-m^2	I_z Yaw, kg-m^2	I_{xz} Product, kg-m^2
Gross weight Empty	1008	264.4	239	3075	3200	-11.9
Auxiliary tank	977	266.4	238	2986	3118	-12.9
Zero fuel	870	268.0	237	2958	3090	-14.6

* Includes smoke and engine oil

The inertia tests were conducted in June 1979. Due to several additions and modifications to the vehicle the zero fuel weight was altered. The c.g. location at the empty fuel condition was also intentionally shifted forward by 5.08 cm. The inertia values presented in table 2.2. were corrected for the new empty vehicle weight and c.g. shift.

The duration of the DAST-I flight is limited by the vehicle's relatively low fuel capacity. Altitude and airspeed conditions during flight will determine the actual duration of flight. In general, a test flight is expected to provide approximately 25 minutes of flight data.

2.1.2 Firebee II Modifications

The equipment compartment of the Firebee II drone was highly modified for the DAST program. The modifications were made partially to fulfill NASA Dryden Flight Research Center flight test requirements. Other modifications were related to the addition of FSS equipment and the aeroelastic wing.

A summary of the equipment modifications and additions made to the original Firebee II vehicle follows:

- In order to utilize the Remotely Augmented Vehicle (RAV) system the original remote control system was replaced by a new receiver encoder, transmitter, and two Pulse Code Modulation (PCM) systems. Sensors were replaced and new instruments were added to provide the necessary data for the ground-based control system and for evaluation of the FSS performance.

- The Firebee II autopilot was replaced by an analog autopilot, designed and fabricated by NASA Dryden Flight Research Center.

- A microprocessor was added to perform the necessary onboard digital and proportional signal routing and logic switching.

- The Firebee II wing tip antennas were replaced by a wrap-around nose cone antenna, designed and fabricated by NASA Langley Research Center.

- In the aft section of the equipment compartment the FSS hydraulic pump and hydraulic fluid reservoir were installed.

- The FSS control box, containing the FSS control system and other electronics, was also included in the equipment compartment.

- Temperature-regulating heater blankets were added to most of the electronic instruments following the first ARW-I flight.

Several Firebee II systems are still utilized by the DAST-I. These systems perform the following functions:

- Power distribution

- Engine and engine control

- Fuel control

- Recovery

The only external modification to the vehicle was the addition of an air scoop and air vent for temperature control of the equipment compartment.

2.1.3 DAST-I Equipment Layout

A layout of the front section of the DAST-I vehicle including the equipment compartment is given in figure 2.11.

The nose boom provides temperature and pressure information. Attached are the angle of attack and sideslip angle vanes. The wrap-around antenna is located in the nose cone. The front section of the equipment compartment includes the RAV system instrumentation. The FSS equipment is located in the aft section of this compartment adjacent to the wing.

The center section is shown in figure 2.12. It consists of the main fuel tank and engine air inlet. The fuel dump valve is located at the lower side of the fuselage. This valve opens during recovery to allow the release of excess fuel. The main chute hangers are also shown in this figure.

FSS instruments are located in the wing center section and underneath the wing gloves attached to the front wing spar. Accelerometers, FSS aileron actuators, and the tip mass release system are located at the wing tips.

The aft section containing the Continental YJG9-T-406 engine and engine exhaust is shown in figure 2.13. Surface actuators are located aft of the tail cone. The tail cone contains the drag, main, engagement and stabilization chutes along with the associated pyrotechnics for chute deployment and tail cone separation. The pyrotechnics are controlled by the recovery system described in section 2.4.3.

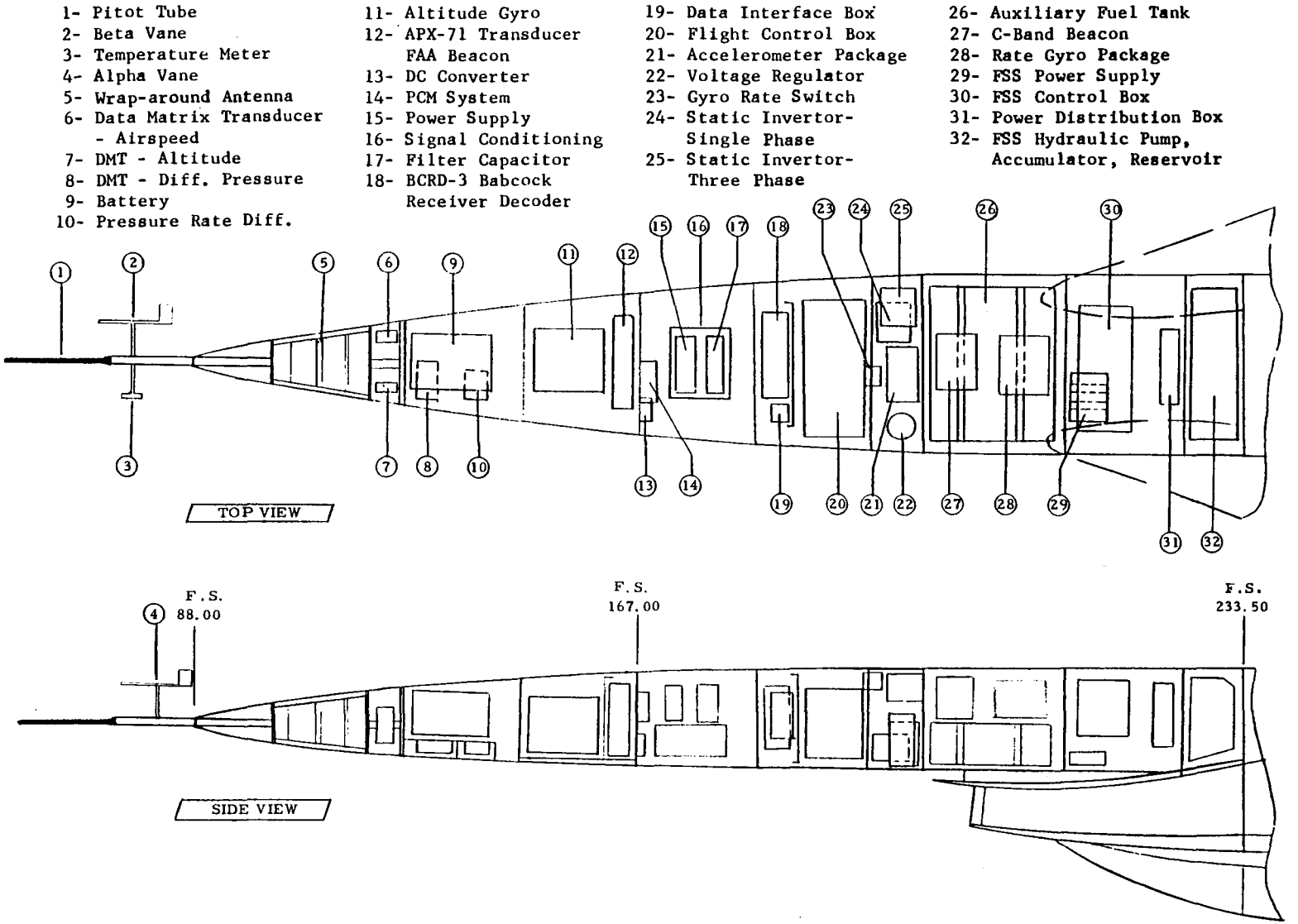

Figure 2.11. Equipment compartment layout.

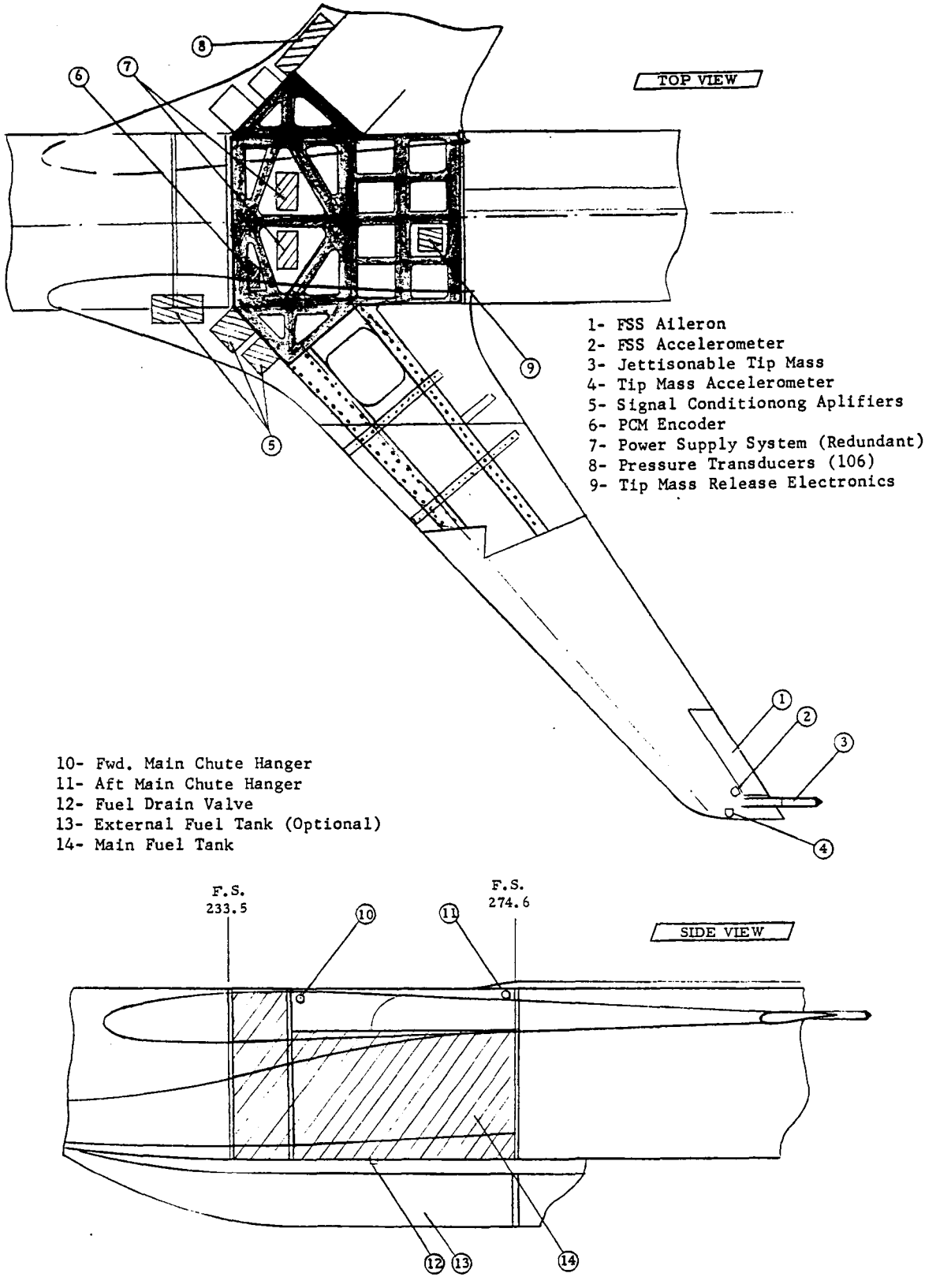

Figure 2.12. Center section layout.

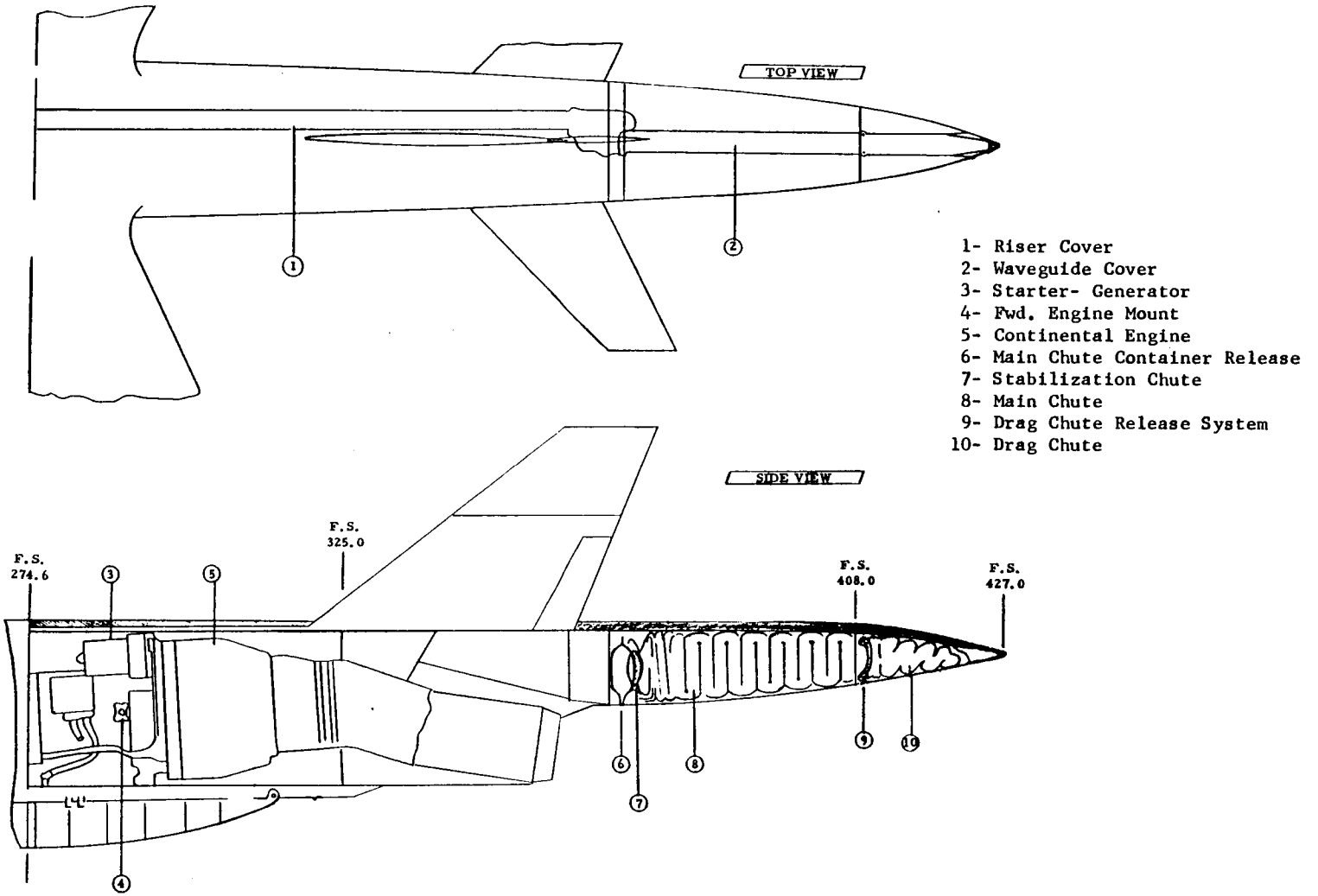

Figure 2.13. Aft section layout.

2.2 Aerodynamic Characteristics

Wind tunnel tests were conducted by the NASA Langley Research Center to determine the rigid body static longitudinal and lateral-directional aerodynamic characteristics of the DAST-I test vehicle.

A 1/6-scale force model was used to obtain data. The model was equipped with a supercritical wing, elevons, and rudder. The Langley 8-foot (2.44 m) tunnel was utilized for the tests. A summary of the test conditions is given in table 2.3. A complete description of the tests and test results is presented in reference 1.

Dynamic longitudinal and directional derivatives were estimated using the wind tunnel results. The analytical methods utilized to determine the dynamic derivatives are presented in reference 2.

TABLE 2.3 DAST-I 1/6-SCALE MODEL WIND TUNNEL TEST CONDITIONS

Variable	Range
Mach number	.4 to .98 Mach
Angle of attack	-4 to 12 degrees
Sideslip angle	-6 to 6 degrees
Symmetric elevon deflection	-9 to 3 degrees
Asymmetric elevon deflection	0 to 6 degrees
Rudder deflection	0 to -10 degrees
Reynolds number	6.6×10^6 per meter

In appendix A the DAST-I aerodynamic derivatives are presented as a function of Mach number and angle of attack. The derivatives are referenced to the 1/4-chord point of the ARW-I. Data for Mach numbers between .98 and 1.2 were determined by extrapolating flight test results obtained from the F-8 Supercritical Wing (SCW) program conducted at the NASA Dryden Flight Research Center. Evaluation of this F-8 program is given in reference 3.

Discrepacies between the data presented in reference 2 and in appendix A are the result of several modifications made to improve the quality of the aerodata model.

The aerodata model is utilized by the six-degree-of-freedom real time simulation. The model allows non-linear characteristics to be included in the simulation. This is achieved by defining the rigid body, static and dynamic aerodynamic coefficients in a matrix format in which every element is defined by angle of attack and Mach number breakpoints. In between breakpoints, the value of a coefficient is defined by interpolation.

A summary of observations concerning the aerodynamic characteristics of the DAST-I wind tunnel model follows:

- Most of the longitudinal and lateral-directional static derivatives are non-linear in angle of attack and Mach number. Dynamic derivatives show similar non-linear behavior.

- Wind tunnel results indicate that the model exhibited pitchup characteristics at approximately 7 degrees of angle of attack. This is attributed to the C_{m_α} derivative becoming positive at the above conditions.

- Elevon effectiveness appeared to be sufficient to trim the model throughout the Mach number range. The effectiveness in roll and yaw control was also positive throughout the Mach range.

- Derivatives defined by the wind tunnel tests are for a rigid body vehicle. Linear analysis results, later verified by flight test results, indicate that due to flexibility effects of the wing the estimated c_{m_α} value could increase considerably. This would in turn result in a decrease of the longitudinal stability of the vehicle. A compensation for the flexibility effect was added to the aerodata model by superimposing a correction to the pitching moment coefficient as follows:

$$C_{m_f} = C_m + 57.3 * K * \bar{q} * \alpha \qquad (2.1)$$

where

C_{m_f} flexible pitching moment coefficient

C_m rigid body coefficient

K_f flexibility constant = .00001

$\bar{q}$ dynamic pressure

α angle of attack

Additional comments concerning the static and dynamic derivatives are given in reference 2.

2.3 Stability and Control Characteristics

The DAST-I open loop longitudinal and lateral-directional stability characteristics are presented in this section. Analysis results were obtained by utilizing the CONTROL program described in reference 4.

For the analysis, the rigid body equations of motion were implemented in this program. A C_{m_α} flexibility correction was introduced by superimposing a flexibility term to the pitching moment coefficient, C_m, as shown in equation (2.1). The vehicle weight and c.g. location used for the analysis are given in table 2.1. The corresponding moments of inertia are included in table 2.2. The aerodata package presented in appendix A was utilized to model the vehicle's aerodynamic characteristics.

Longitudinal open loop analysis results at full internal fuel conditions are presented in figure 2.14. The short period and phugoid root loci are shown as a function of altitude and Mach number.

The results show that damping ratio and frequency of the short period decrease with increasing altitude at a certain Mach number. The best damping ratio is achieved at 3,048 m and .9 Mach. The phugoid is stable at low Mach numbers. At high Mach values one pole on the real axis becomes positive. The worst case is obtained at an altitude of 12,196 m and .9 Mach. In general, the phygoid damping will decrease with increasing altitude.

The effect of fuel quantity on the longitudinal characteristics is shown in figure 2.15. At an altitude of 3,048 m the decrease in fuel quantity results in an increase in short period damping up to .34 at .9 Mach. The increase in short period damping due to decreasing fuel quantity is less at higher altitudes. The phugoid is hardly affected by the fuel quantity.

Lateral-directional open loop results are shown in figure 2.16. The dutch roll root locus is presented for a series of Mach numbers at two different altitudes. The results show an increase in frequency and decrease in damping with increasing Mach. An increase in altitude hardly affects the damping ratio, while it slightly decreases the frequency. The roll mode appears to be a strong function of altitude and Mach number. The best response is achieved at 3,048 m and .95 Mach.

The spiral mode is almost neutral. For certain conditions the mode becomes unstable. For the worst case, the time constant is

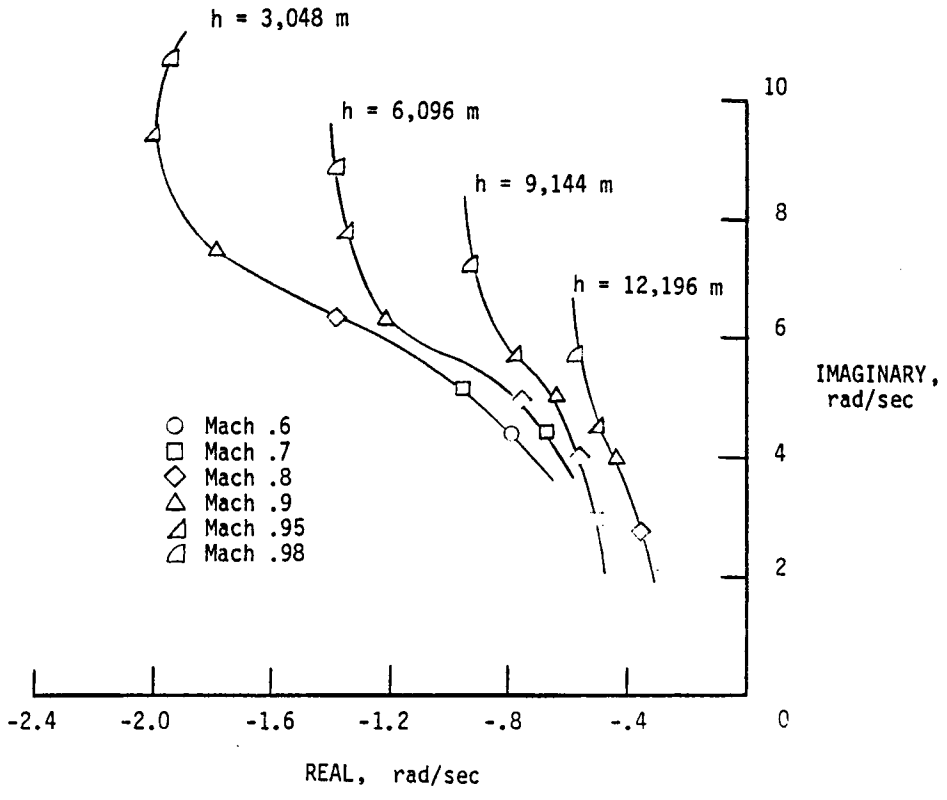

(a) Short period open loop root locus.

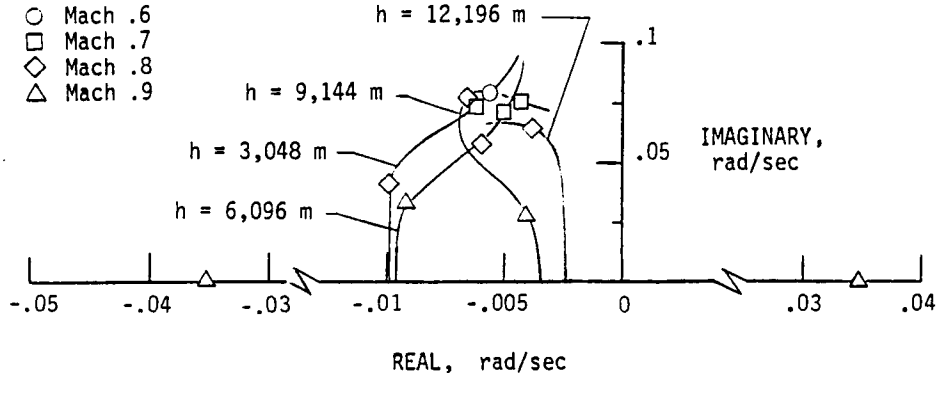

(b) Phugoid open loop root locus.

Figure 2.14. Open loop root locus in longitudinal axis at selected flight conditions with full fuel. W = 1008 kg; c.g. = 264.4 F.S.

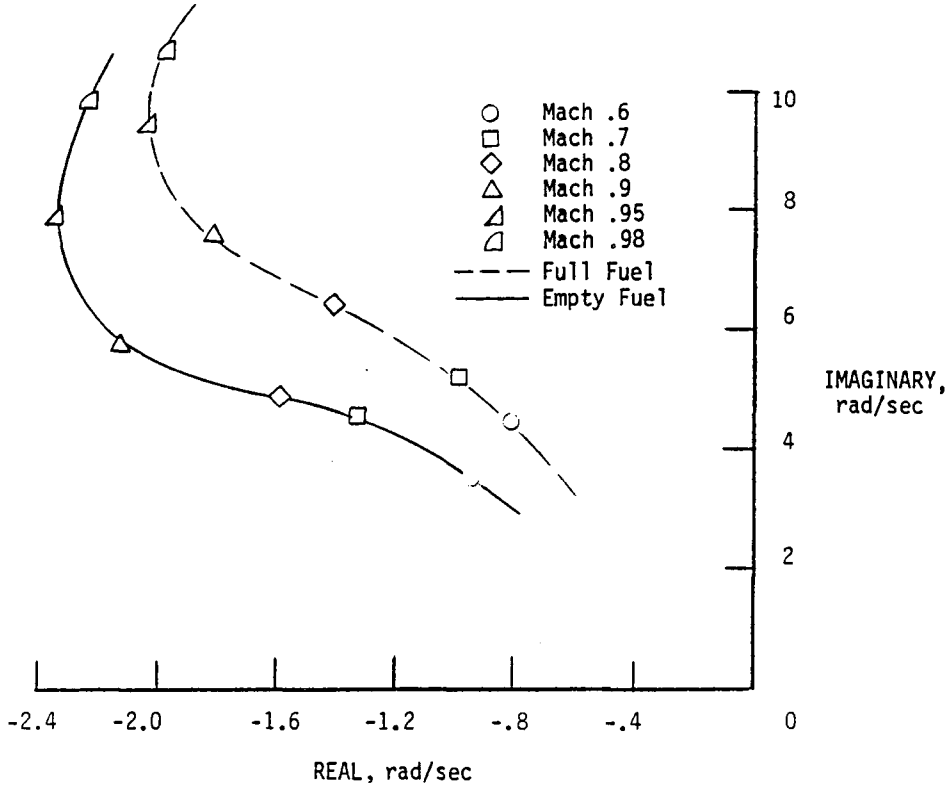

(a) Short period open loop root locus.

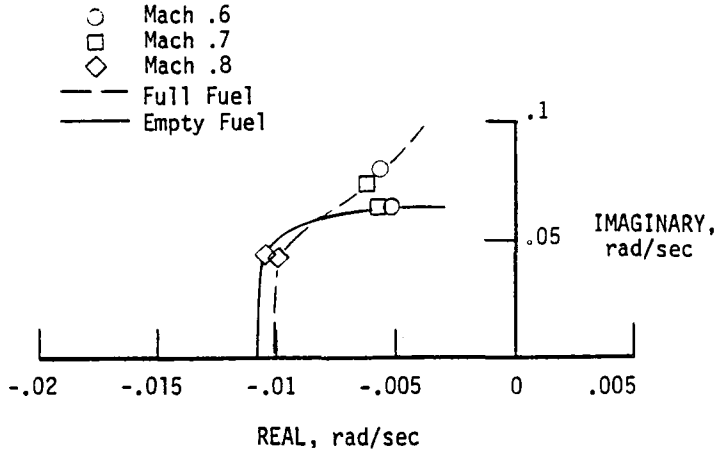

(b) Phugoid open loop root locus.

Figure 2.15. Open loop root locus in longitudinal axis at full and zero fuel conditions. At full fuel W = 1008 kg, c.g. = 264.4 F.S.; at zero fuel W = 870 kg, c.g. = 268.0 F.S.

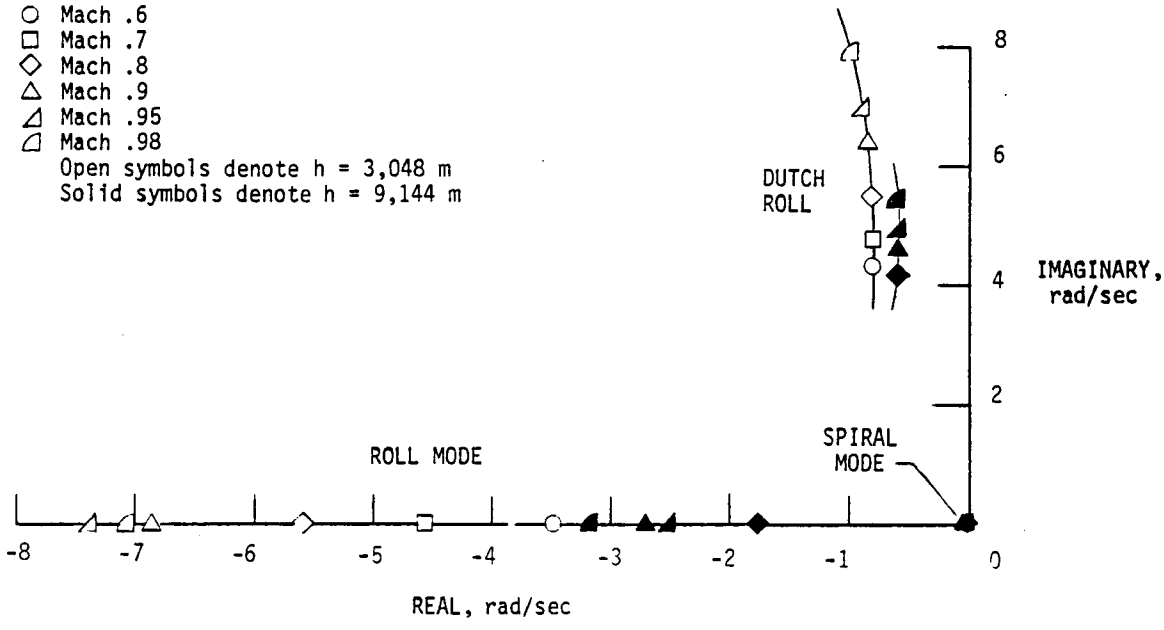

Figure 2.16. Open loop root locus in lateral-directional axis at selected flight conditions with full fuel. W = 1008 kg; c.g. = 264.4 F.S.

less than 100 seconds.

Fuel quantity has little or no effect on the lateral-directional characteristics of the vehicle.

2.4 Onboard Systems

The onboard instrumentation consists of equipment that can be divided in three groups. The first group has as primary function: the reception, decomutation and distribution of discrete and proportional uplink signals. The second consists of the actual onboard systems such as the autopilot. The data acquisition system forms the third group. This group of onboard equipment provides the necessary vehicle information to the ground facilities through downlink telemetry. The flutter suppression instrumentation constitutes the actual flight test equipment that is described in Chapter 3.

A functional block diagram of the onboard systems is given in figure 2.17. The data acquisition and FSS systems are not included. This figure shows the uplink signal routing through the Babcock receiver, the data interface box, and the data decoder. The uplink signal is received by a wrap-around nose cone antenna with an approximate radius of 96.5 km. The antenna signal strength pattern, given in figure 2.18, shows evident decrease in signal strength forward and aft of the vehicle.

The received discrete signals are directed to a microprocessor, known as the logic card, and the FSS. The digital proportional commands are converted to analog signals and directed to the appropriate servos and the onboard autopilot.

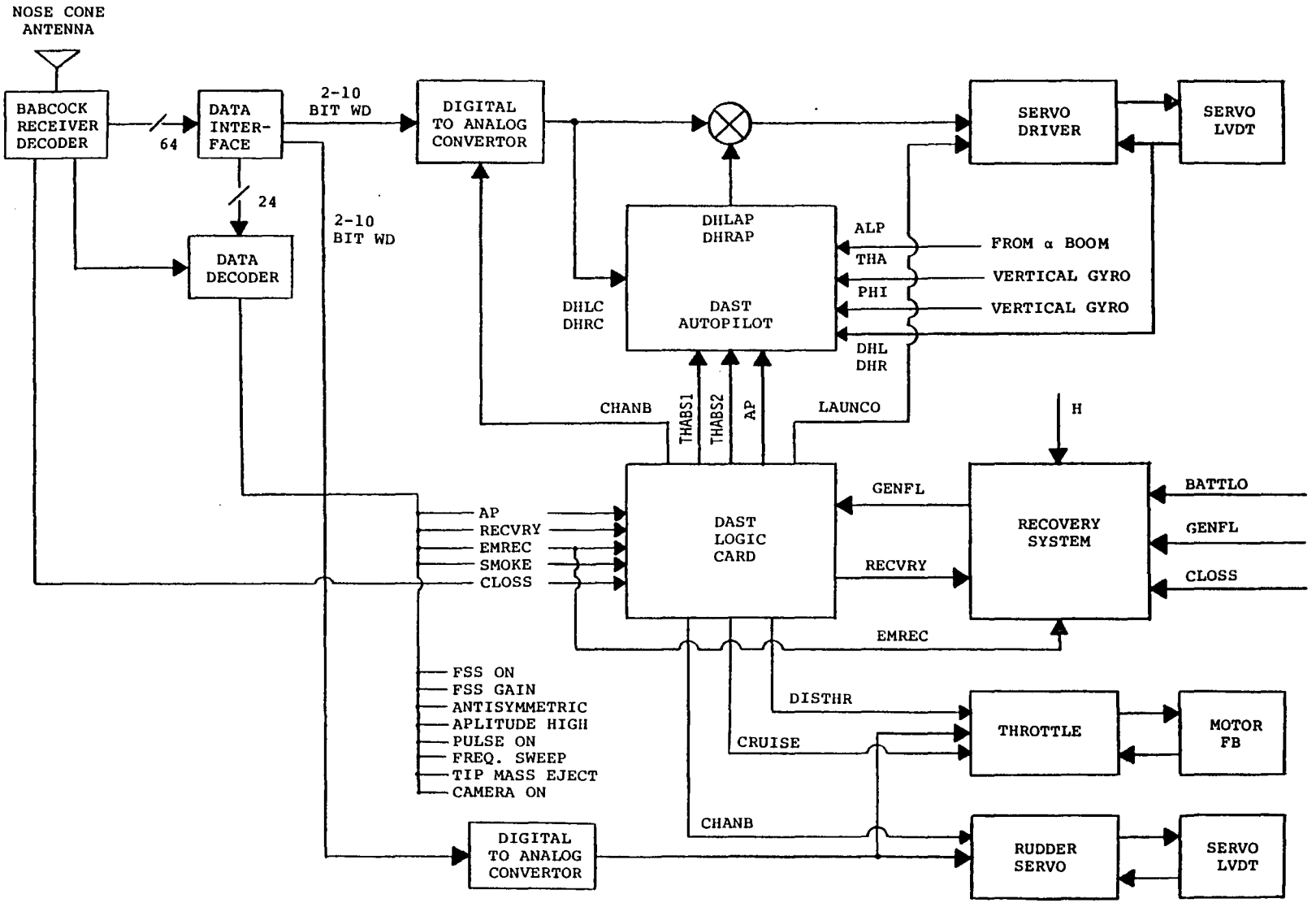

Figure 2.17. Functional block diagram of the DAST-I onboard system interface (FSS system not included).

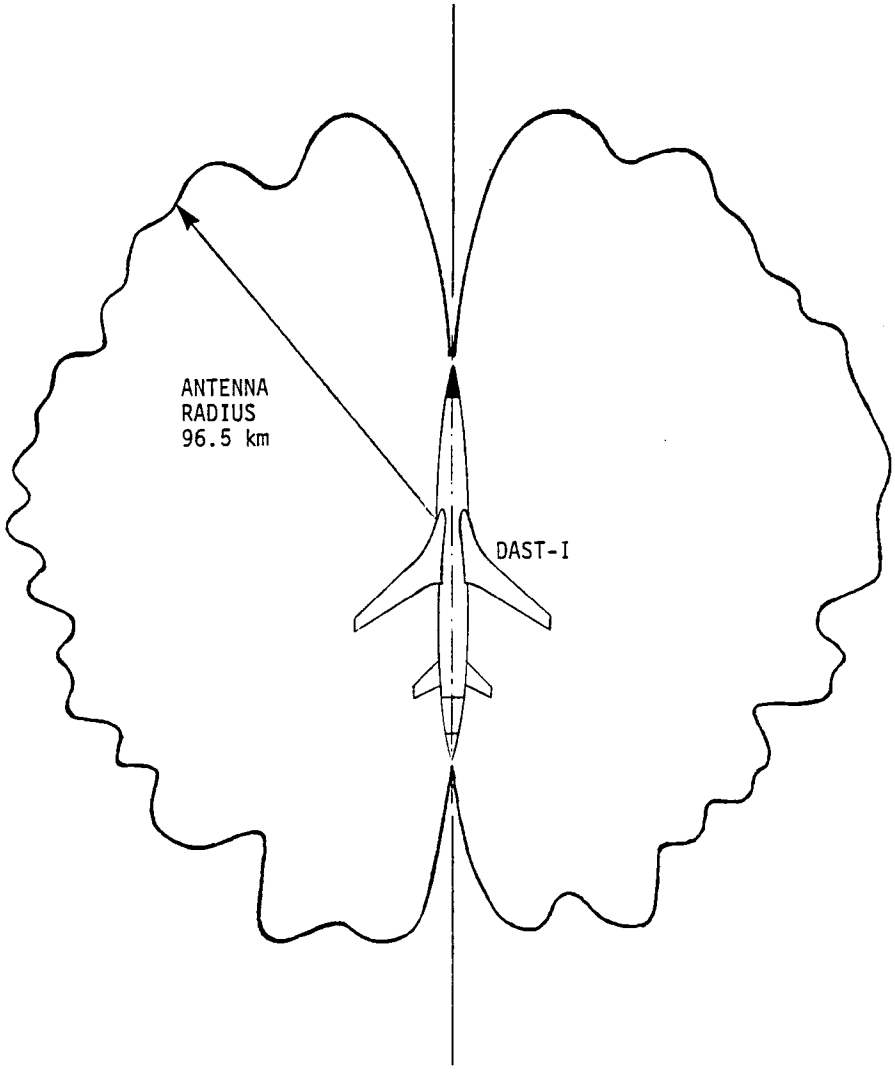

Figure 2.18. Signal strength pattern of the wrap-around antenna.

In this section we will describe in detail the function and characteristics of the following major onboard systems:

- Autopilot (AP)
- Logic card (LC)
- Recovery system (RS)

From the above onboard systems only the RS is an authentic Firebee II system. The AP and LC are physically located in the equipment compartment as one unit, known as the Flight Control Box (FCB).

2.4.1 Autopilot

The DAST-I analog onboard autopilot (AP) is a backup control system designed and fabricated by the NASA Dryden Flight Research Center.

The system is automatically engaged in case of uplink telemetry loss and whenever recovery is initiated. The AP can also be selected from the ground cockpit.

The primary function of this system is to maintain constant altitude and wings level. While the AP is engaged the F-104 backup controller has limited control authority of the test vehicle. This remote control feature is provided to allow the F-104 controller to fly the test vehicle back to the recovery area in case of uplink telemetry loss.

In case of a ground computer failure, the test pilot can select AP from the ground cockpit. In this mode of operation the pilot has limited control authority through the right-hand side panel of the ground cockpit.

The AP interface with the onboard systems is shown in figure 2.17. A block diagram of the AP control system is presented in figure 2.19. The system utilizes angle of attack and pitch attitude information for longitudinal stabilization. Bank angle feedback is used to maintain wings level.

Original design requirements for the AP excluded the use of gyros for additional augmentation. This design requirement was based on the philosophy that the AP, being a backup of the ground based control system, should not utilize the same source of information as the primary control system.

The left- and right-hand elevon uplink commands, $\delta_{h_{L_C}}$ and $\delta_{h_{R_C}}$, will bypass the AP if this system is not engaged. When remote control is in effect, the above signals will be the commands initiated either by the F-104 controller or the ground-based test pilot. The elevator position information, δ_{h_L} and δ_{h_R}, is utilized to reduce the AP engagement transient.

The pitch attitude biases, Θ_{bias1} and Θ_{bias2}, are initiated by the logic card circuitry during recovery. These inputs cause the AP to initiate a climb. The resulting decrease in dynamic pressure is expected to be sufficient for a safe drag chute deployment. The bias value is determined by the flight condition at which recovery is initiated. This AP input is ramped into the system through an RC circuit with a 10-second time constant to ensure a smooth transition.

The "AP" discrete which results in AP engagement is a command initiated by the logic card.

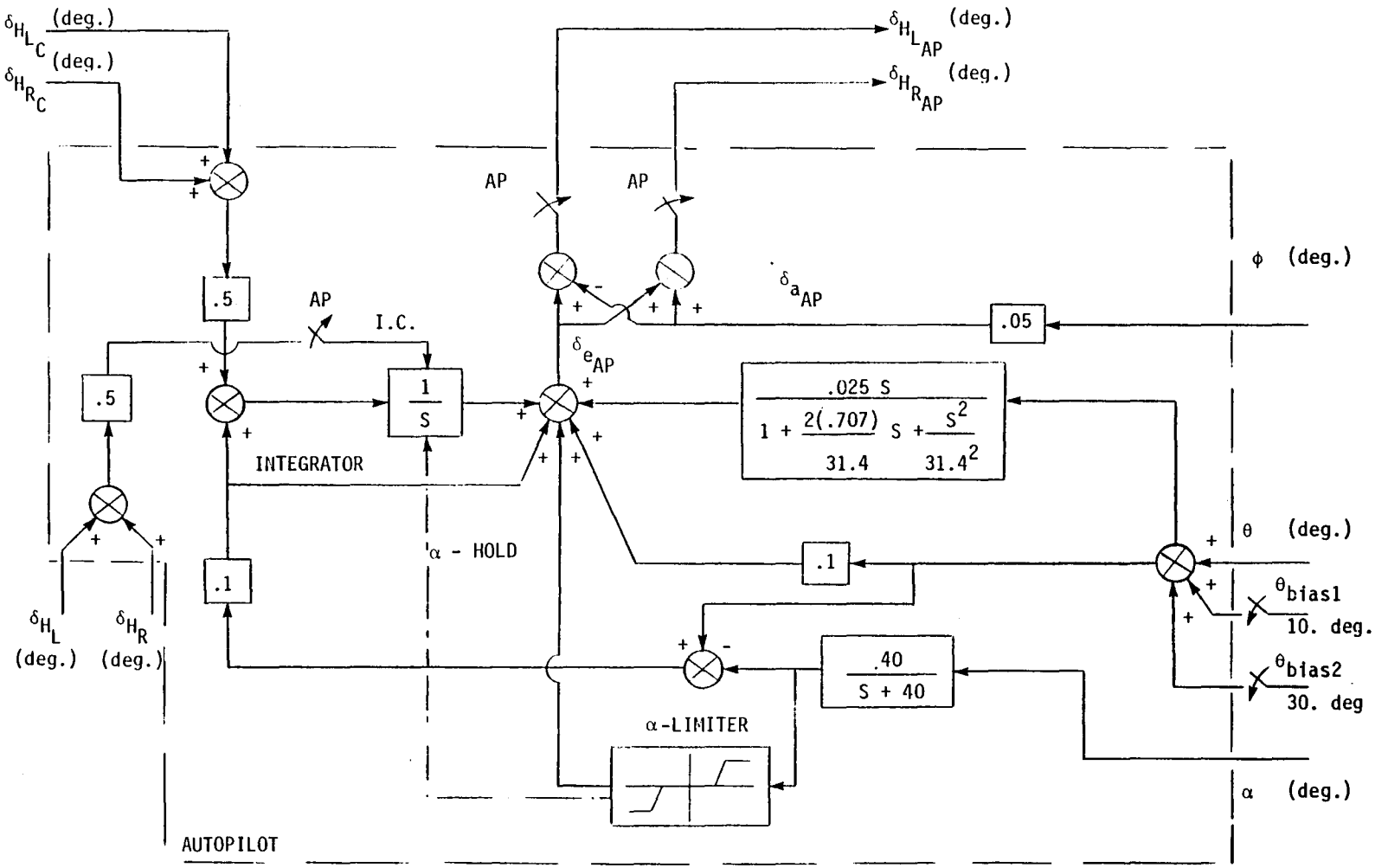

Figure 2.19. DAST-I onboard autopilot.

The AP performs the following longitudinal and lateral-directional functions:

- Pitch rate damping, achieved through differentiation of the pitch attitude signal.
- Pitch attitude hold function, provided through direct pitch attitude feedback.
- Glide slope hold function, provided by the proportional plus integral flight path angle feedback.
- Angle of attack limiter. A schedule results in a reduction of AP authority when α exceeds the limits of +6 and -4 degrees. The integrator is also set to a hold mode when α exceeds the limits. This prevents the α-limiter signal from being overpowered by the integrator output. The α-limiter authority is limited to 1.5 degrees of elevator command.
- Bank angle hold function, provides the necessary wings leveling capability through bank angle feedback.

A 40 radian/sec low pass filter is used to suppress the high frequency components of the angle of attack signal that are generated by the nose boom structural dynamics.

Longitudinal and lateral-directional linear analysis results are presented in figures 2.20 and 2.21, respectively. The AP root locations are presented for selected altitudes and Mach number conditions. The open loop poles of longitudinal and lateral-directional modes at an altitude of 3,048 m and Mach .8 are also included for comparison. Figure 2.20 shows that the damping of the short period and phugoid is increasing with descreasing altitude. The short period frequency shows an increase with increasing Mach number. The phugoid frequency is less affected by Mach number. The open loop poles indicate that there is a significant increase in phugoid damping and frequency due to the AP augmentation. The short period is hardly affected.

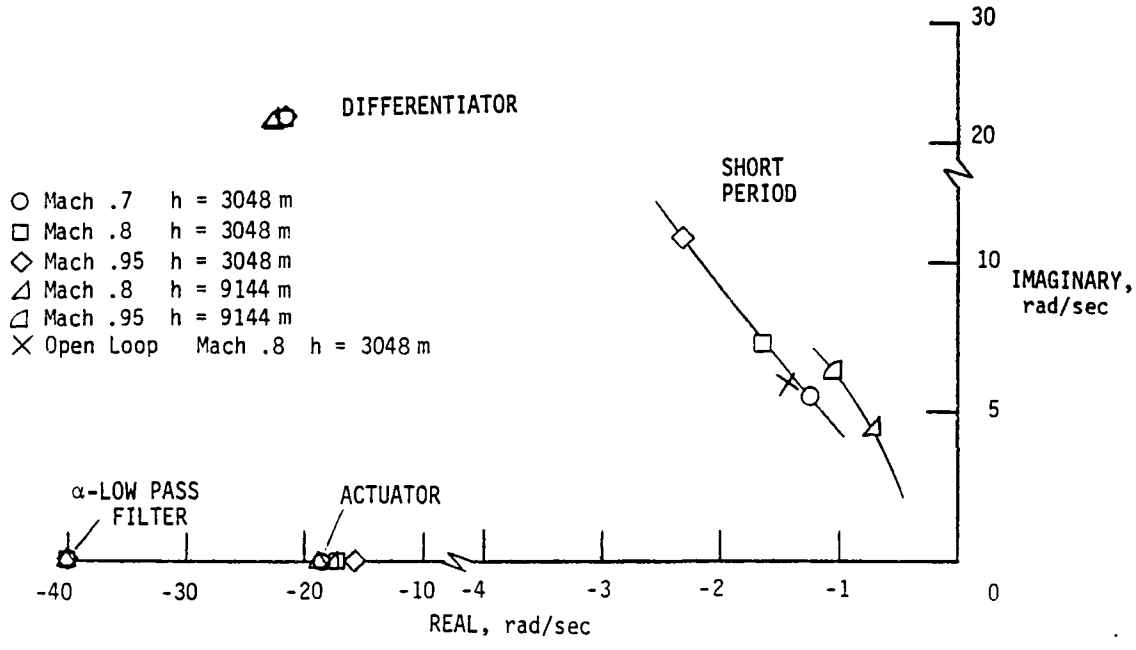

(a) Root locus.

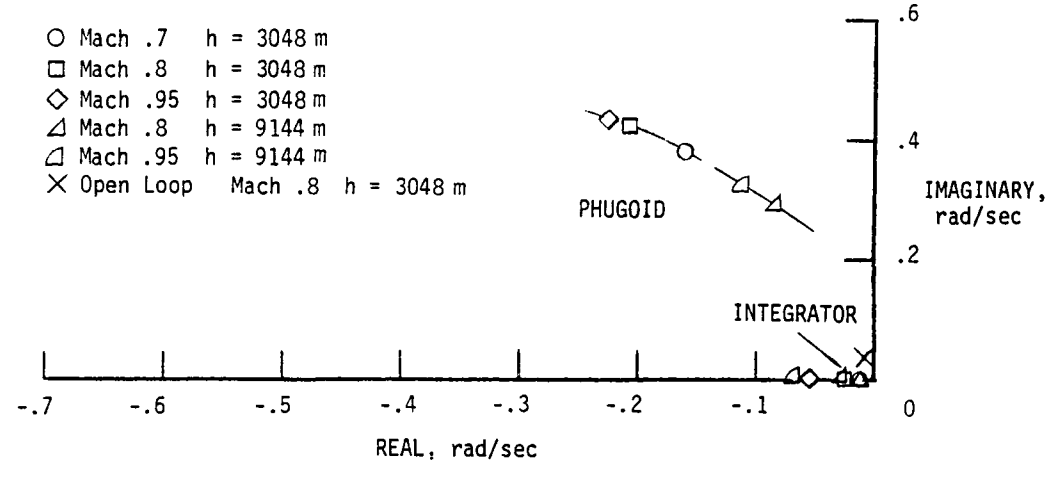

(b) Expanded view of root locus near origin.

Figure 2.20. Longitudinal autopilot s-plane root locus at selected flight conditions. W = 1008 kg; c.g. = 264.4 F.S.

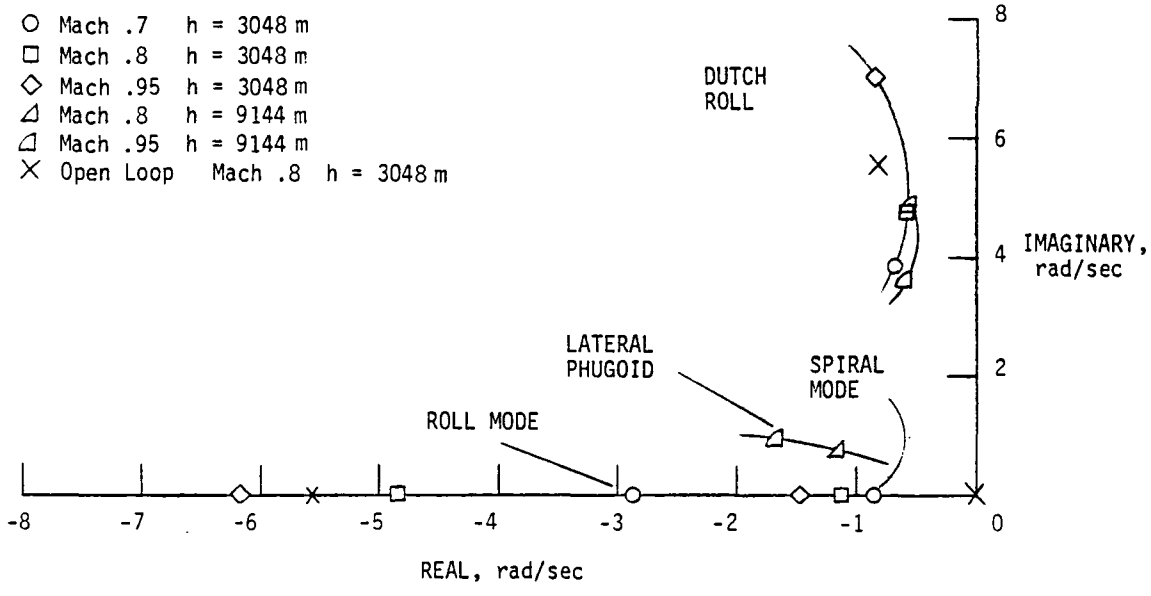

Figure 2.21. Lateral-directional autopilot s-plane root locus at selected flight conditions.

Lateral-directional open and closed loop root locations are shown in figure 2.21. The best dutch roll damping is obtained at 3,048 m and Mach .6. The roll and spiral mode time constants decrease with increasing Mach number. At higher altitudes the roll and spiral mode real poles are combined in two complex poles (lateral phugoid). The open loop poles indicate that the bank angle feedback has a slight, negative effect on the dutch roll and roll mode. A considerable increase in spiral mode damping is achieved. The lateral phugoid mode is well damped and shows a slight increase in damping and frequency with increasing Mach number.

The fuel quantity effect on the longitudinal AP characteristics is shown in figure 2.22. In general the phugoid and short period roots show an increase in damping with decreasing fuel. At higher altitudes the effect becomes less. The fuel effect on the lateral-directional modes is insignificant.

Remote control in the autopilot mode can be obtained from the ground cockpit and the F-104. The ground-based pilot has to select AP in order to control the vehicle through the AP. The F-104 telemetry will automatically engage AP.

The F-104 backup controller has limited control authority through a set of panels shown in figure 2.23. He has the ability to engage the F-104 transmitter and encoder separately and generate commands such as "smoke," "recovery," and "emergency recovery."

The proportional elevon commands are generated by the circuitry shown in figure 2.24. The rudder is set to zero while the elevator and differential stabilizer commands are defined by the integrator outputs. The integrator for the elevator is position limited to ± 1.

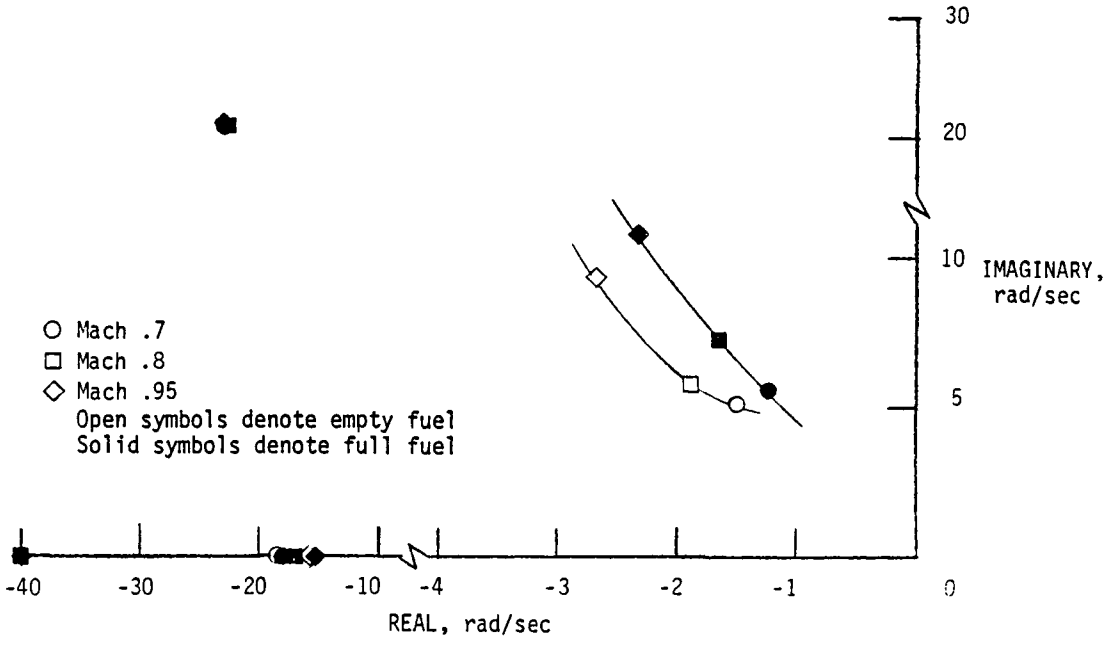

(a) Root locus.

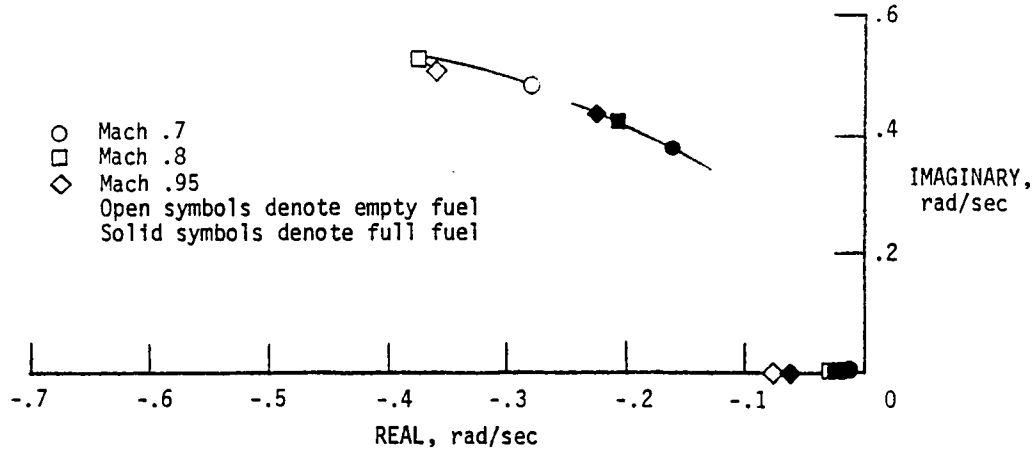

(b) Expanded view of root locus near origin.

Figure 2.22. Longitudinal autopilot s-plane root locus at full and empty fuel conditions. At full fuel W = 1008 kg, c.g. = 264.4 F.S.; at zero fuel W = 870 kg, c.g. = 268.0 F.S.; h = 3048 m.

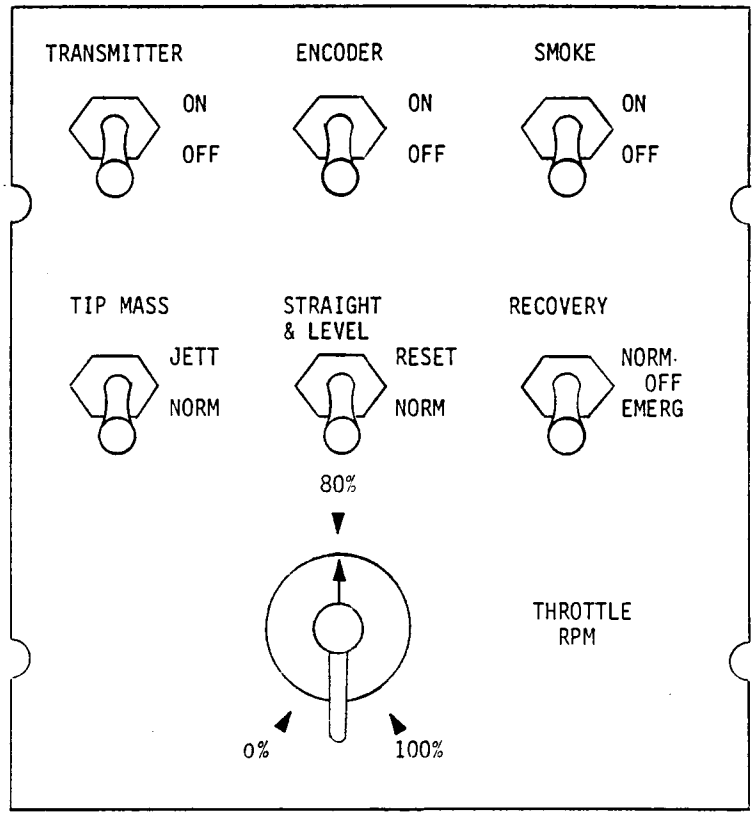

(a) Discrete commands and proportional throttle control panel.

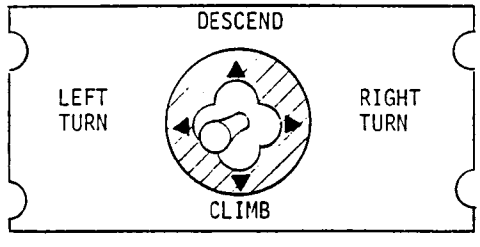

(b) Proportional elevator and aileron control panel.

Figure 2.23. F-104 remote control panels.

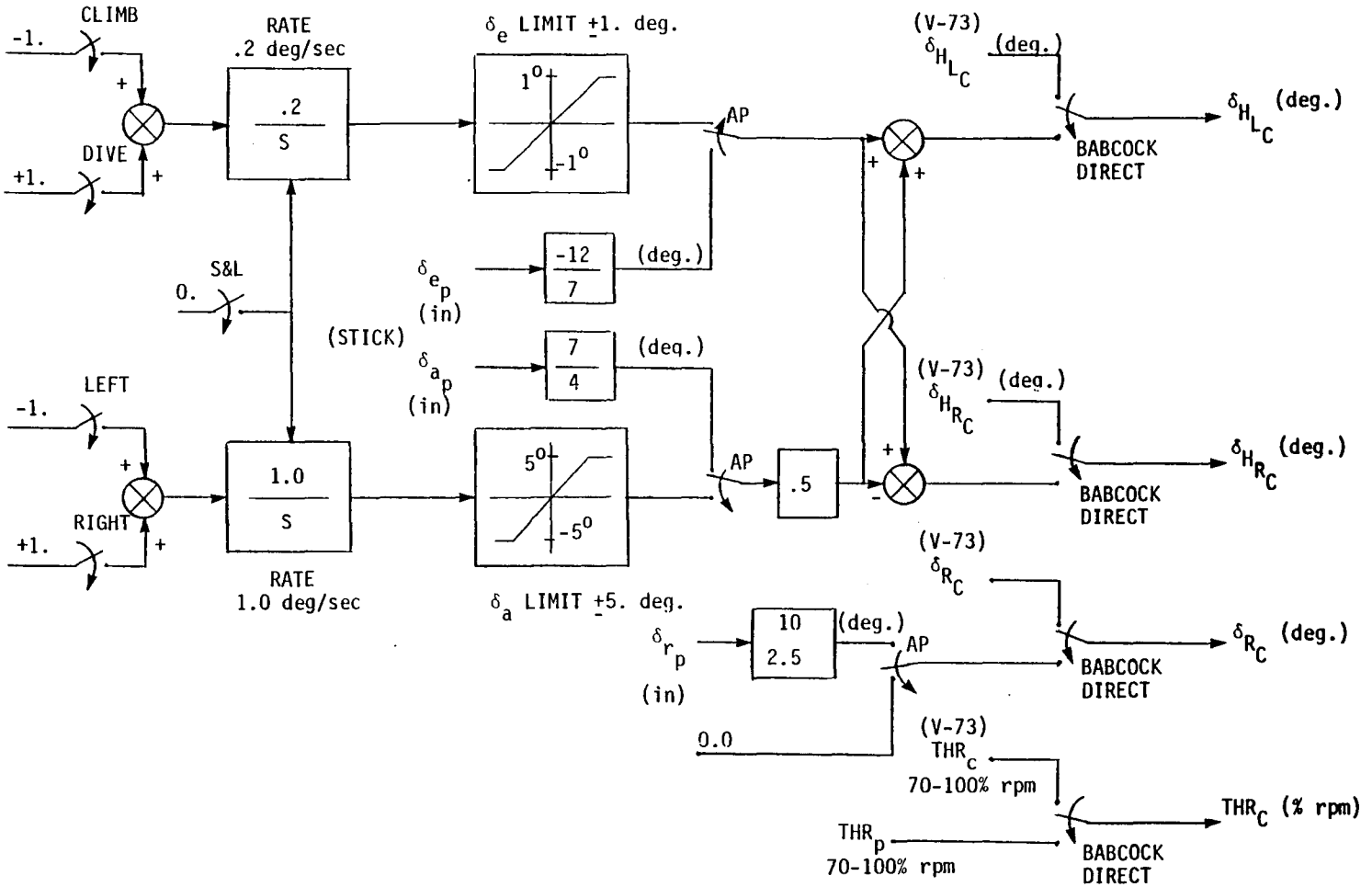

Figure 2.24. F-104 and ground cockpit circuitry for the generation of proportional autopilot commands.

degree and rate limited to $\pm$.2 deg/sec. The differential stabilizer is poisition limited to $\pm$5. degrees and rate limited to $\pm$1 deg/sec. Both integrators are controlled by a four-way switch that generates the climb, dive, left turn, and right turn commands.

The straight and level (S&L) command will drive both integrators to zero at the prescribed integration rates. Integration will take place as long as the switch is commanding S&L.

The backup controller has full throttle authority from 0 to 100 percent rpm. A detent at 80 percent prevents the controller from commanding lower rpm settings unintentionally, which could cause an engine flameout. Additional information concerning the F-104 remote control feature is given in section 4.5.2.

In the AP mode the test pilot has limited vehicle control through the right-hand side panel of the ground cockpit, assuming no uplink telemetry loss has occured. The uplink commands are defined by a circuitry similar to the F-104, shown in figure 2.24. The only difference between the two circuitries is the function of the S&L command. The ground cockpit S&L command will drive the circuitry integrators to zero following a first order exponential delay with a 2-second time constant. The delay will be operational only when the S&L switch is held forward (i.e. commanding S&L).

Throttle control is obtained through the cockpit throttle lever. The authority is limited between 70 and 100 percent rpm.

2.4.2 Logic Card

The interface of the logic card (LC) with the other onboard systems is shown in figure 2.17. This sub-system is a micropros-

sesor that utilizes uplink and onboard generated discrete commands to perform the necessary switching and routing of discrete and proportional signals.

A block diagram of the LC is presented in figure 2.25. The system has four different modes of operation as indicated in the above figure. These modes are:

- Launch
- Remote pilot or autopilot
- Carrier or telemetry loss
- Recovery

The launch mode is in effect while the vehicle is attached to the B-52 carrier and for three seconds after launch. In this mode, initial launch conditions can be set, such as elevator position and throttle setting. Following the actual release from the carrier and three seconds in flight, the LC will engage the remote pilot/autopilot (RP/AP) mode. This is the mode wherein the vehicle can be controlled from the ground and the F-104 backup controller.

Loss of the uplink signal results in the engagement of the carrier loss mode. In this mode, the microprocessor automatically engages the onboard AP and waits for the uplink signal strength to exceed the limit of -92 db. If uplink is regained, the LC will return to the RP/AP mode. Evaluation of the signal strength is accomplished every three seconds. If uplink is not regained within 20 seconds, the LC will enter the recovery mode.

The recovery mode will also be engaged in case "recovery" or "emergency recovery" is commanded by the ground-based pilot or backup controller. This mode is nonreversible, as there is no

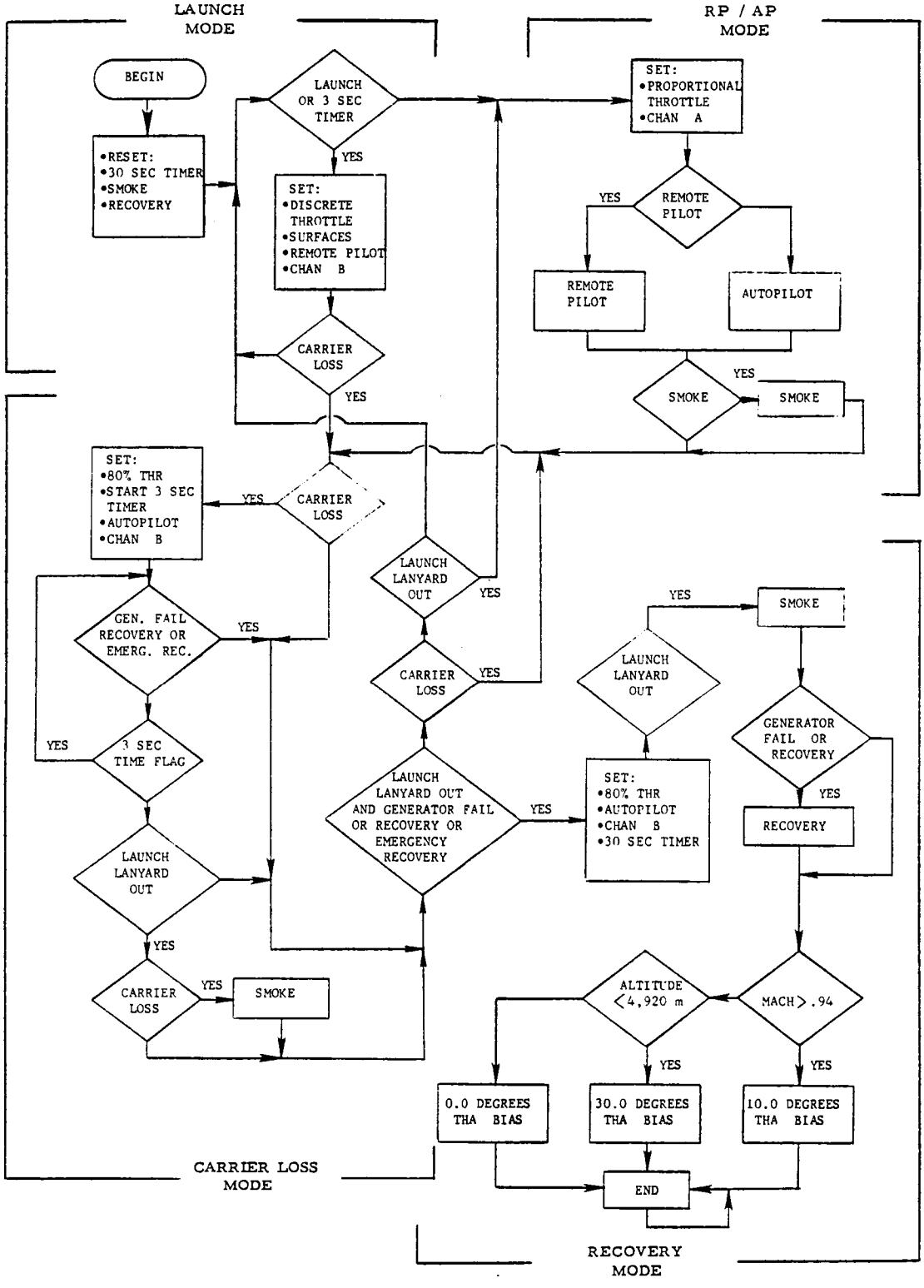

Figure 2.25. Logic card flow chart.

internal or external command that could alter this mode of operation.

A third command that could also engage the recovery mode is the "generator fail" discrete.

In the recovery mode, the LC will engage the AP, cut off the uplink signal, command an rpm setting of 80 percent, and generate a pitch attitude bias as shown in figure 2.25.

The smoke command, generated by the LC, results in a series of eight smoke pulses of 1-second duration each, separated by a 2-second, pause. This feature, when activated, provides a smoke trail that enhances the visibility of the test vehicle. This command is automatically triggered when recovery is initiated.

2.4.3 Recovery System

The recovery system (RS) is a major onboard system, designed and fabricated by Teledyne Ryan Aeronautical. The principal function of this system is to generate discrete commands that result in the deployment of the drag, main, and stabilization chutes. A high altitude normal recovery sequence is shown in figure 2.26. The drag chute is deployed first and is designed to reduce the drone's speed to a level where safe main chute deployment can take place. The main chute, much greater in size than the drag chute, is attached to the hangers located at the center section of the vehicle. While the main chute is deployed, the helicopter will attempt to "catch" the engagement chute that is directly connected to the load line. When the helicopter has control of the vehicle through the load line, the main chute is automatically disengaged and a small stabilization

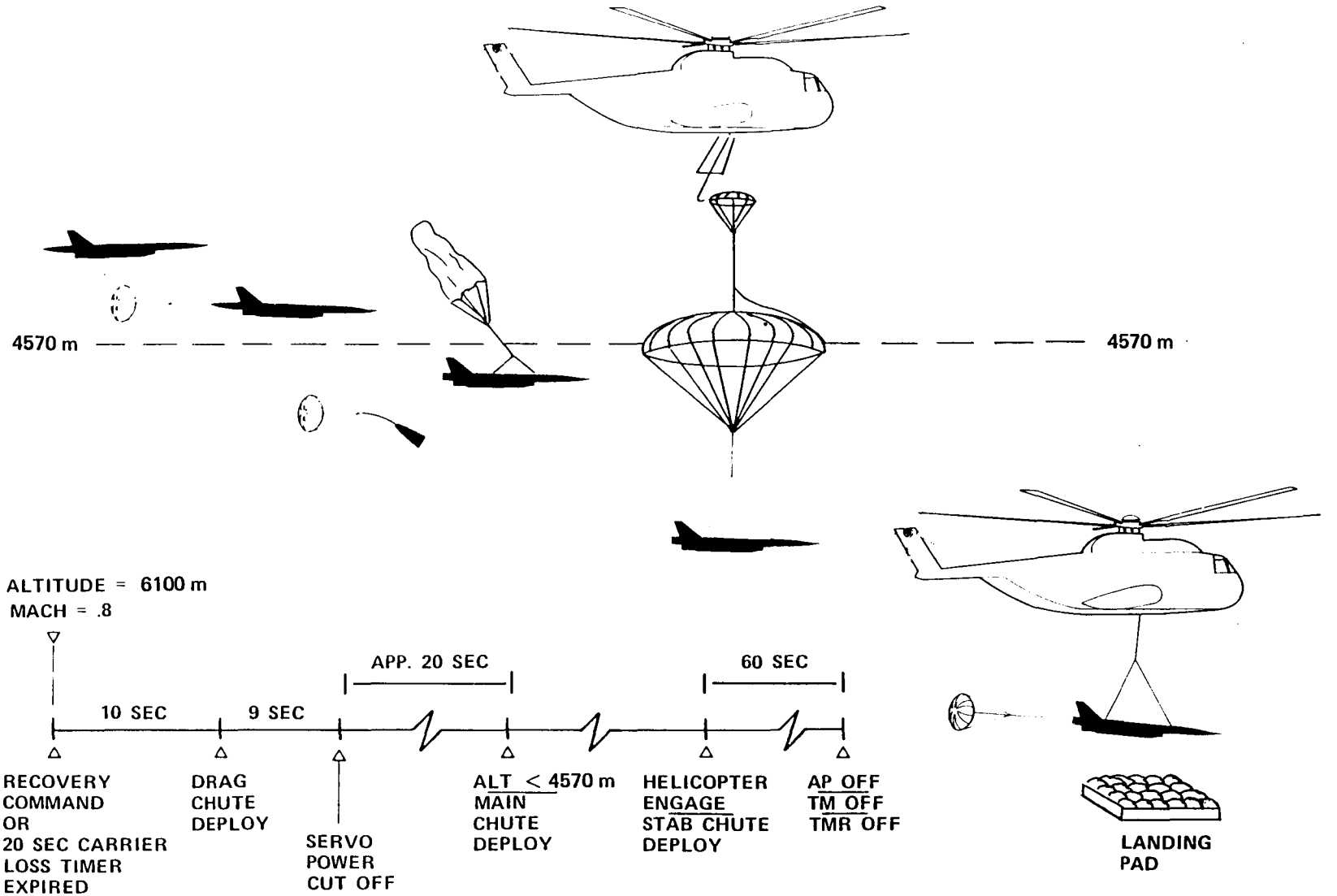

Figure 2.26. DAST-I high altitude, normal mid-air recovery sequence.

chute is deployed. This chute will stabilize the test vehicle while it is transported back to the base underneath the helicopter.

Another function of the RS is the power cut-off of onboard systems such as the servos, the AP and LC and the downlink telemetry and data acquisition systems.

The RS is physically a combination of timers and relays. The primary inputs to the system are the discrete commands "normal recovery" and "emergency recovery." Discrete commands such as "generator fail" (commanded when the generator output is < 25 volts which is equivalent to an engine rpm < 60 percent) and "carrier loss" (telemetry loss) will also activate the RS.

The system has four modes of operation, as indicated by figure 2.27. The command and the altitude will determine the mode of operation. The circuitry that is associated with every one of these four modes is presented in the form of a flow chart in figures 2.28 through 2.31. The four modes of operation presented in the above figures are not actually independent sub-systems. They all utilize common timers and relays. The actual circuitry of a mode will be defined when the mode is selected.

In order to prevent drag chute deployment at dynamic pressures higher than the prescribed limits, the RS povides a circuitry that will not allow chute deployment unless the Mach number is lower than a predetermined value.

If the battery voltage drops below 21.5 volts, the resulting "battery under voltage" discrete will override the Mach number check and deploy the chutes. This is due to the fact that the pyrotechnics utilized for the actual chute and tail cone release are activated by

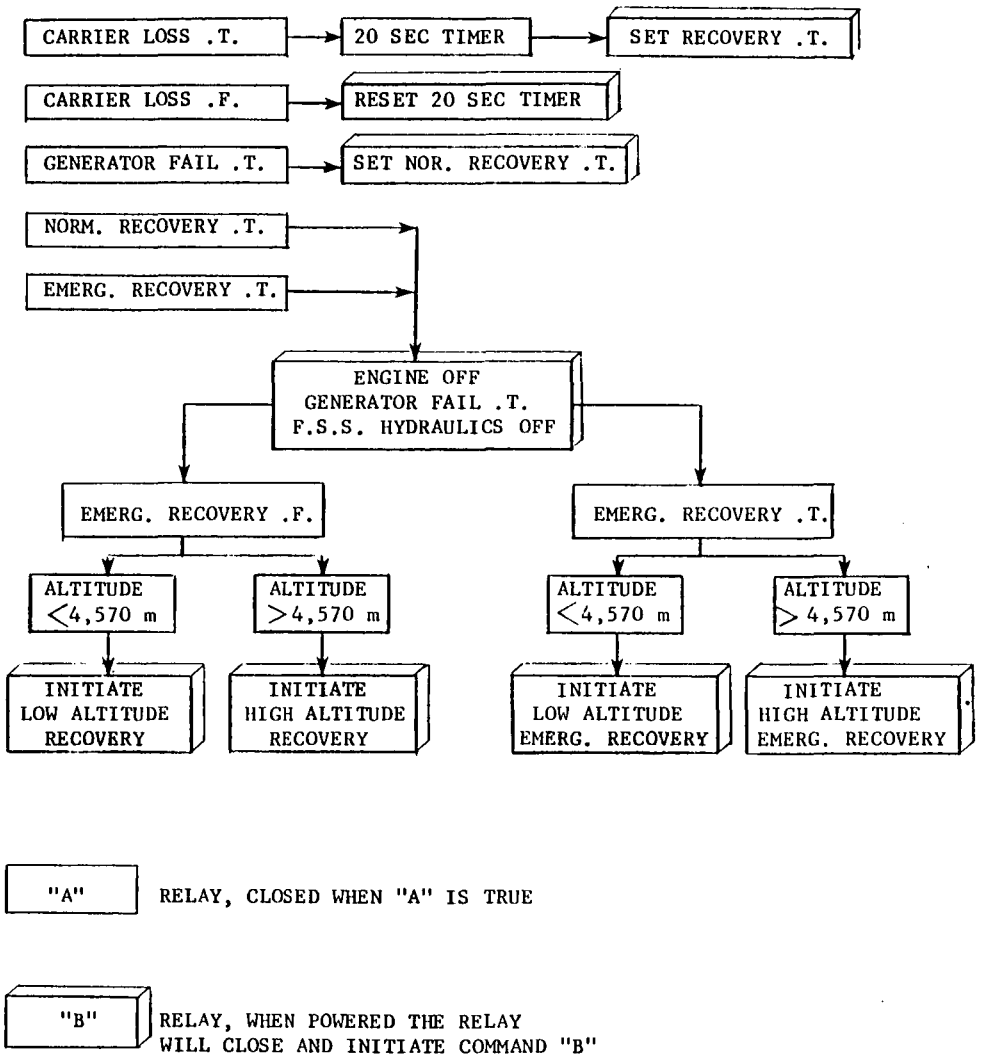

Figure 2.27. Recovery system mode selection flow chart.

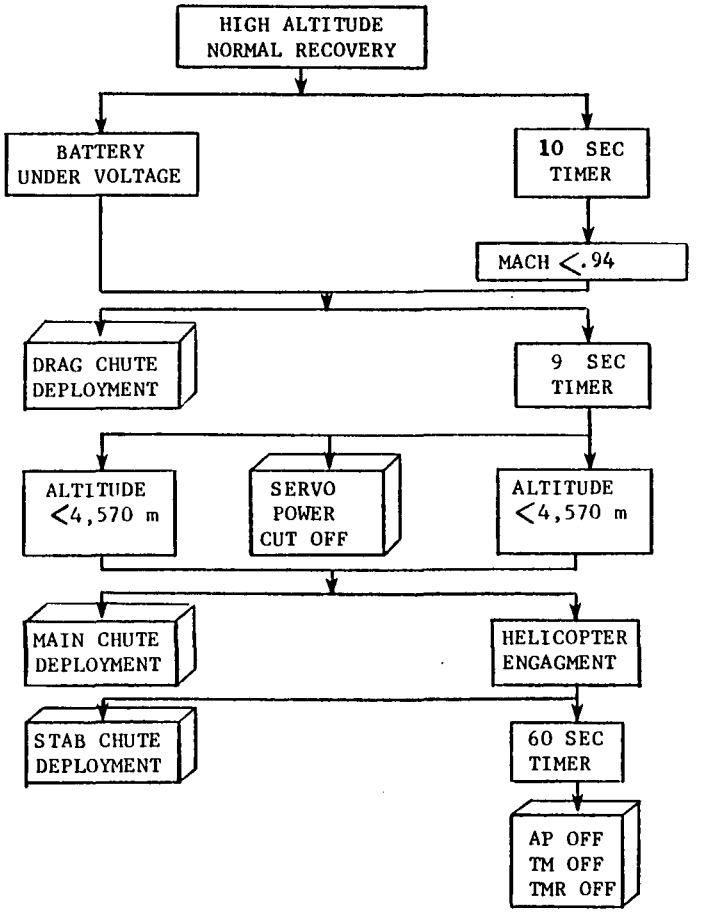

Figure 2.28. High altitude normal recovery flow chart.

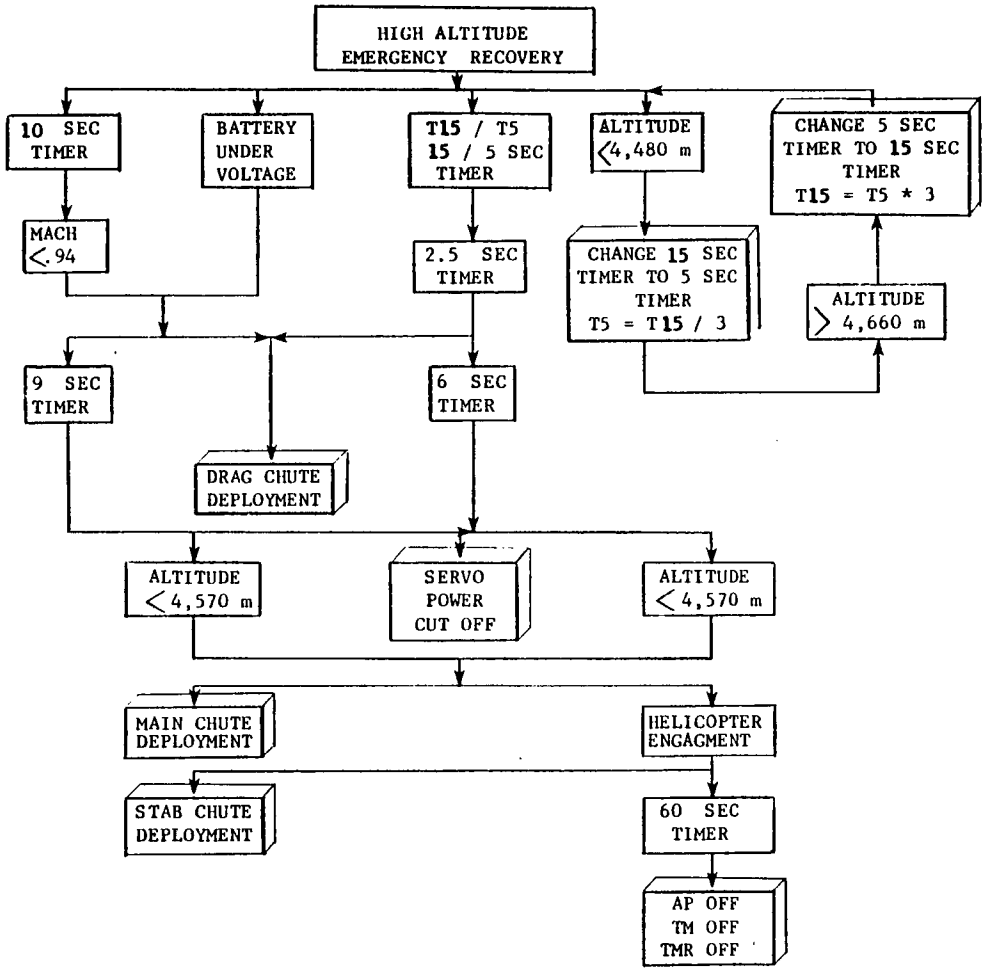

Figure 2.29. High altitude emergency recovery flow chart.

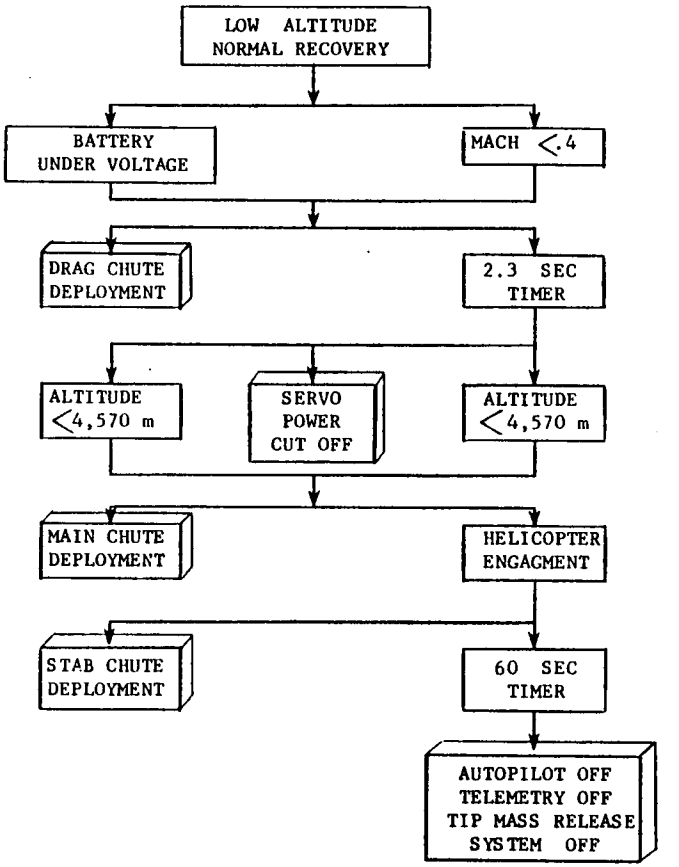

Figure 2.30. Low altitude normal recovery flow chart.

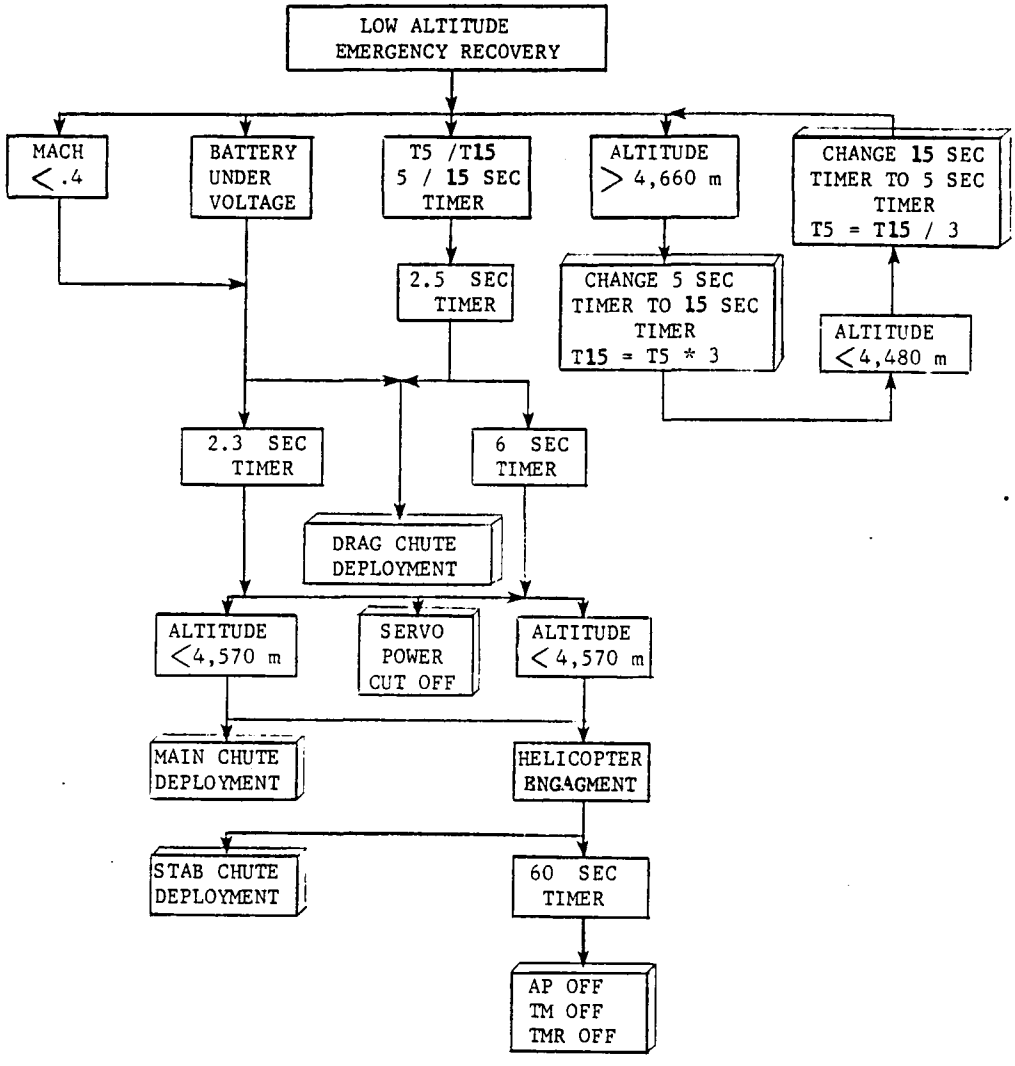

Figure 2.31. Low altitude emergency recovery flow chart.

the battery. A low battery voltage will not be sufficient to fire the pyrotechnics; therefore, such a condition has to be avoided by any means.

Emergency recovery is an optional command that causes an early chute deployment. This command can be initiated from the ground cockpit and the F-104. In case of an emergency, both normal and emergency recovery modes can be commanded simultaneously as figure 2.27 indicates. The premature chute deployment caused by the emergency recovery command increases the risk of chute deployment at dynamic pressures that exceed the chute dynamic pressure limit. The main and drag chute limits, as a function of altitude and Mach number, are presented in figure 2.32. The flight condition at which, during flight test operations, recovery is initiated is also indicated. The actual vehicle response during recovery is shown in figure 2.33. The drag chute deployment results in a slight pitching up moment and a considerable decrease in airspeed. Main chute deployment occurs at an altitude of approximately 4500 m. The main and drag chute deploy at dynamic pressures lower than their limits. The above vehicle response represents the operation of the high altitude, normal recovery mode. The flow chart of this mode is given in figure 2.28.

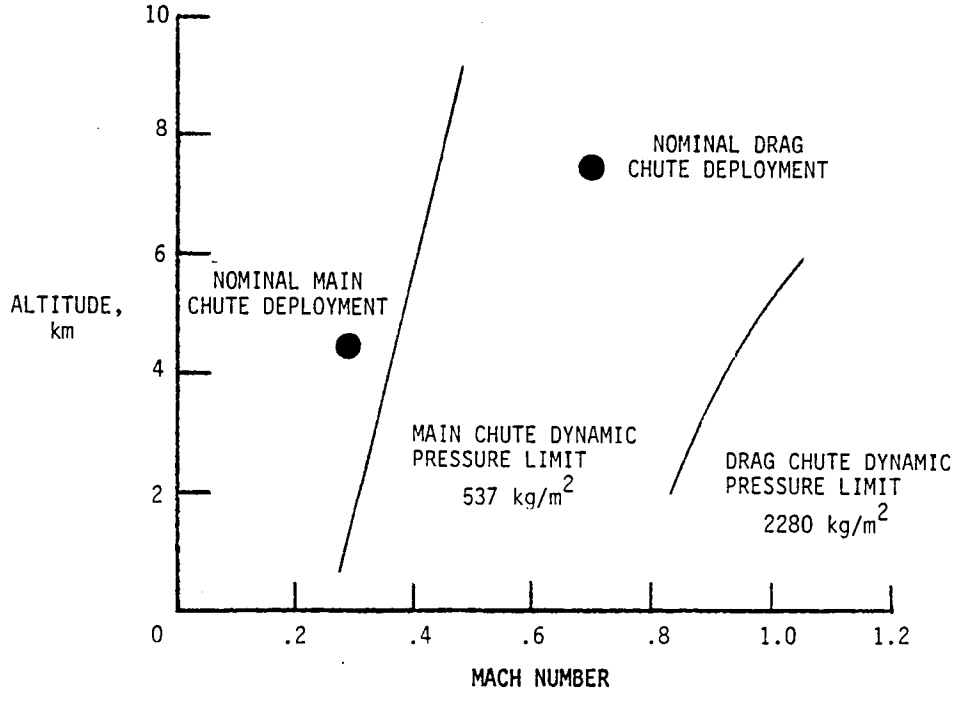

Figure 2.32. Drag chute and main chute deployment dynamic pressure limits.

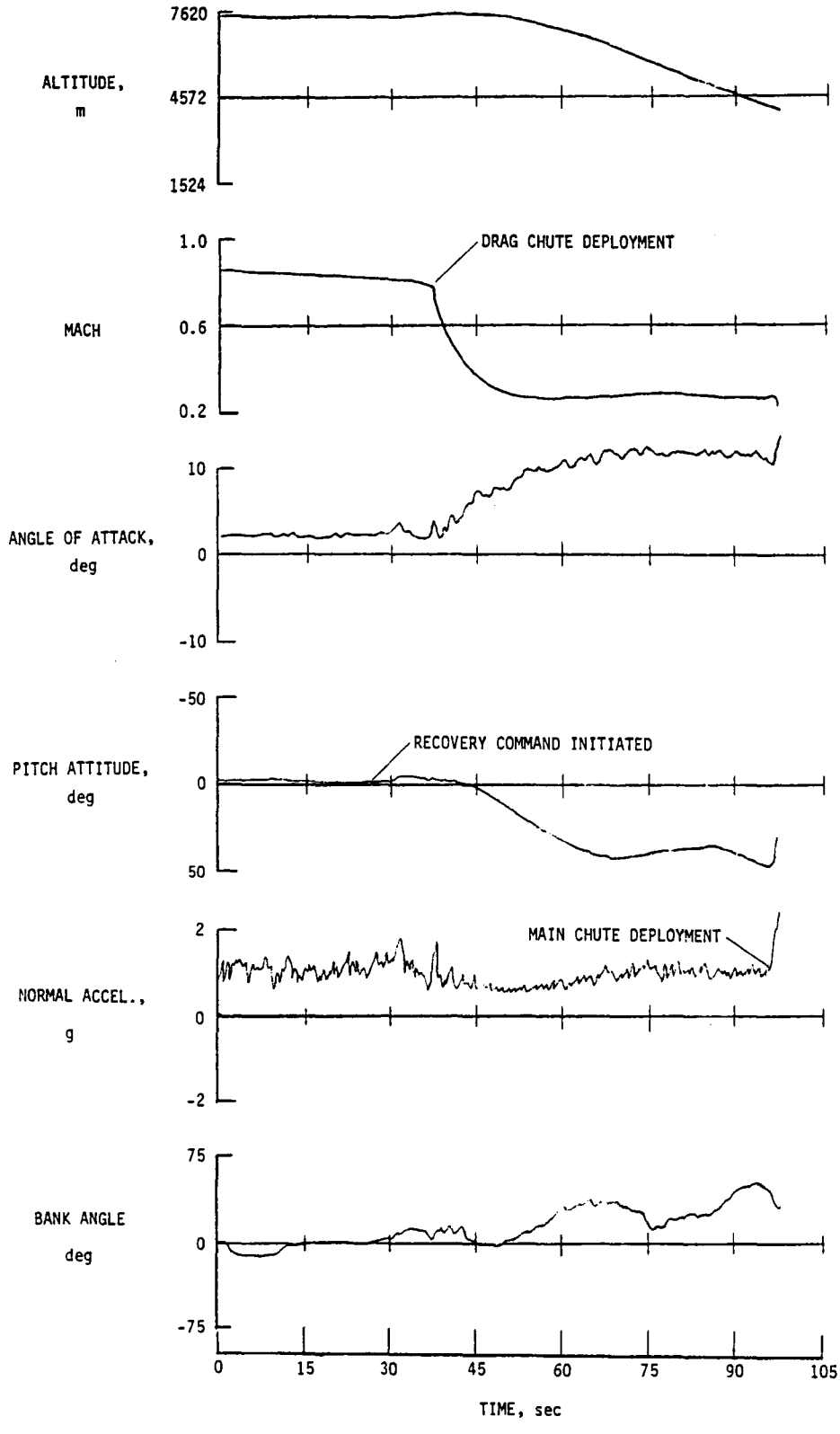

Figure 2.33. Response of the DAST-I vehicle during recovery.

CHAPTER 3

FIRST AEROELASTIC RESEARCH WING FLUTTER SUPPRESSION SYSTEM

Flutter is an aeroelastic phenomenon characterized by a dynamic instability occuring in flight when the elasticity of the structure becomes an essential component of the instability.

The ARW-I was designed to exhibit flutter within the operational envelope of the Firebee II test vehicle, and especially in the transonic region. Flutter prediction theory in this region involves a great deal of accurate determination of structural and unsteady aerodynamic characteristics of the structure.

The development of the ARW-I flutter suppression system was based on analytical models of the unsteady airloads in the transonic region. The principal objective of the first ARW-I experiment is to validate the unsteady aerodynamic prediction techniques and the active controls technology for flutter suppression.

Validation of the flutter suppression system will be accomplished by demonstrating an in-flight increase of the flutter boundary by 20 percent and by providing data that correlate with the theoretically obtained results.

In this chapter, a description is given of the first aeroelastic wing and the active control system for flutter suppression. The hardware required for the flutter suppression experiment is also presented.

3.1 Aeroelastic Research Wing ARW-I

The first research wing selected for flight testing was designed and fabricated by the NASA Langley experimental shop facilities. The wing, shown in figure 3.1 and referred to as the ARW-I, has a supercritical airfoil, originally conceived by Dr. Richard T. Whitcomb at NASA Langley. The airfoil is representative of a transport design. The ARW-I is a 3/8-scale model of the TF-8A supercritical wing (reference 3) previously tested on an F-8 aircraft by NASA Dryden. Table 3.1 presents a list of the physical characteristics of the ARW-I.

TABLE 3.1 PHYSICAL CHARACTERISTICS OF THE ARW-I WING

Airfoil type	Supercritical
Area, m^2	2.7871
Span, m	4.343
Mean aerodynamic chord, m	0.6882
Aspect ratio	6.77
Taper ratio	.366
Thickness-to-chord ratio, percent	
Root	11
Tip	7
Dihedral angle, deg	0
Quarter-chord sweep, deg	42.24
Incidence (root), deg	0
Twist, deg	-5
Aileron	
Area, m^2	0.034
Span, m	0.305
Chord, percent wing chord	26
Deflection, deg	±12
Hingeline, percent chord	23
Designed cruise condition	
Mach number	.98
Altitude, m	13,716
Design lift coefficient	.36
Design load limit (1.25 safety factor)	
Positive g	2.5
Negative g	-1.5

The wing structure was designed for a maneuver limit load of 2.5 g and was purposely designed to exhibit flutter within the

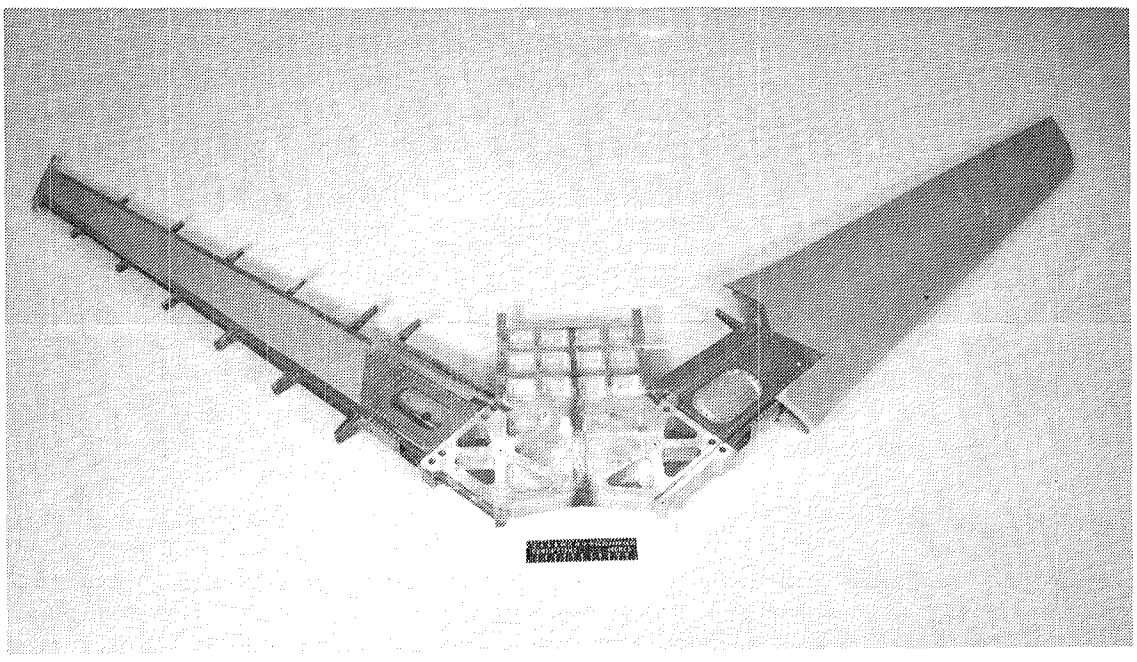

Figure 3.1. First aeroelastic research wing ARW-I.

operating envelope of the flight configuration. This was achieved by reducing torsional stiffness through the use of fiberglass wing skins. The fiber glass material used for the fabrication appeared to have an understated or conservative torsion by as much as 50 percent. The resulting torsion stiffness was much greater than anticipated, causing the wing to be flutter-free over a larger portion of the flight envelope than acceptable for the research test. Reduction of the wing torsion stiffness was achieved by adding ballast weight aft of the trailing edge. Ground vibration tests and analysis of a NASTRAN model of the wing and wing center section structure provided symmetric and antisymmetric vibration modes. Results are presented in table 3.2. The analytically predicted wing modes are in good agreement with ground vibration tests. There are considerable discrepancies in the predictions of the fuselage modes. Further testing is expected to determine the source of the discrepancy.

The flight envelope, including the predicted basic flutter boundary M_f of the test vehicle fitted with the ARW-I, is shown in figure 3.2. The flutter boundary of the wing without the ballast is also shown. The primary flutter modes of the ARW-I are a combination of bending and torsion. The predicted damping ratio versus dynamic pressure for both the symmetric and antisymmetric flutter modes is presented in figure 3.3. This figure indicates the explosive flutter onset of the ARW-I and the fact that both symmetric and antisymmetric modes become unstable at about the same flight conditions.

In figure 3.4, the predicted symmetric and antisymmetric open loop flutter boundaries are presented as a function of altitude and

TABLE 3.2 SYMMETRIC AND ANTISYMMETRIC ELASTIC MODE DESCRIPTION

Elastic mode	SYMMETRIC			ANTISYMMETRIC		
	Frequency, Hz		Mode description	Frequency, Hz		Mode description
	Analysis	GVT		Analysis	GVT	
1	10.04	9.8	Wing bending	12.16	13.5	Wing bending
2	16.34	14.9	Fuselage bending	21.56	17.1	Fuselage and fin bending
3	29.70	27.7	Wing bending and torsion	29.95	27.2	Wing chordwise bending
4	34.14	38.7	Wing torsion	34.31	30.5	Wing torsion and fin bending
5	40.58	46.6	Fuselage bending	36.19	47.2	Fin bending
6	49.03		Wing bending and torsion	48.32		Wing bending and torsion
7	65.72		Stabilizer bending	52.78		Wing and fuselage bending
8	73.34		Stabilizer bending and wing torsion	56.51		Stabilizer bending
9	80.76		Wing torsion	82.04		Wing torsion, fin and stabilizer bending
10	104.33		Fuselage and stabilizer bending	83.64		Wing torsion, fin and stabilizer bending

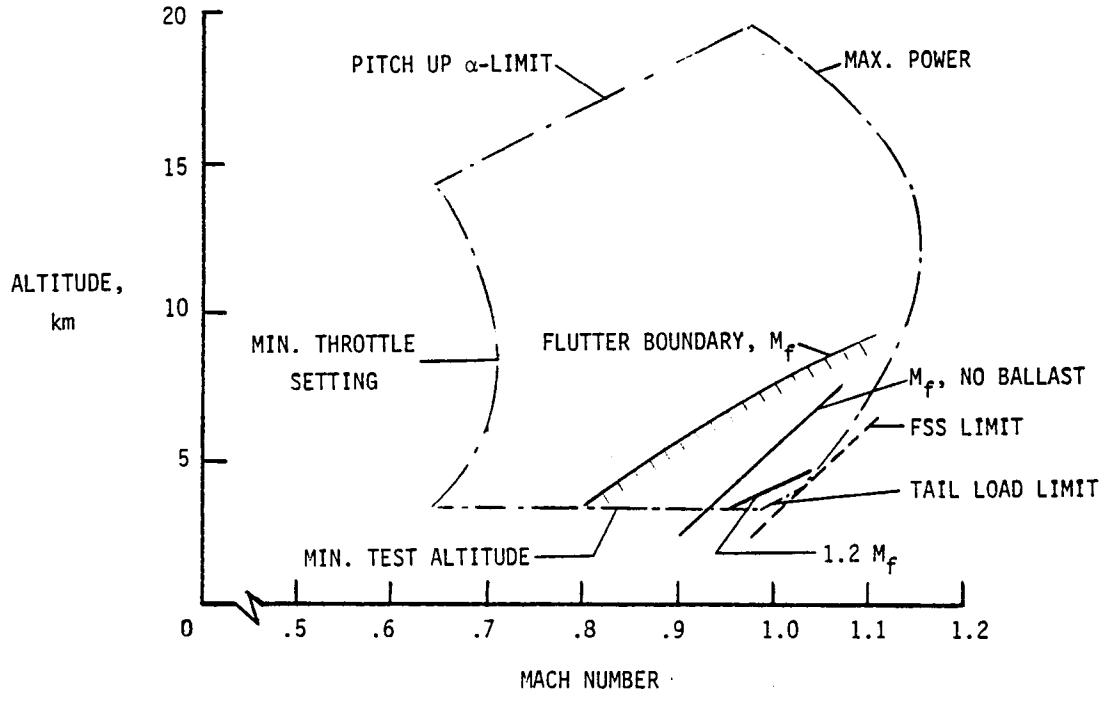

Figure 3.2. ARW-I flight envelope and predicted flutter boundaries.

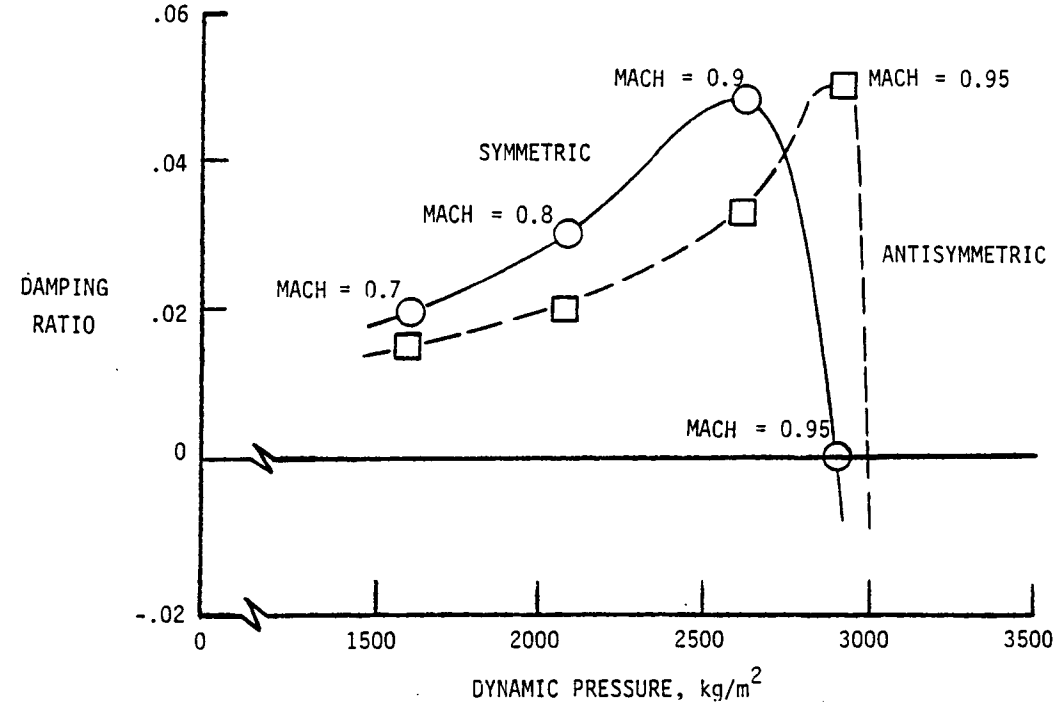

Figure 3.3. Predicted symmetric and antisymmetric open loop flutter onset of the ARW-I at an altitude of 6100 meters.

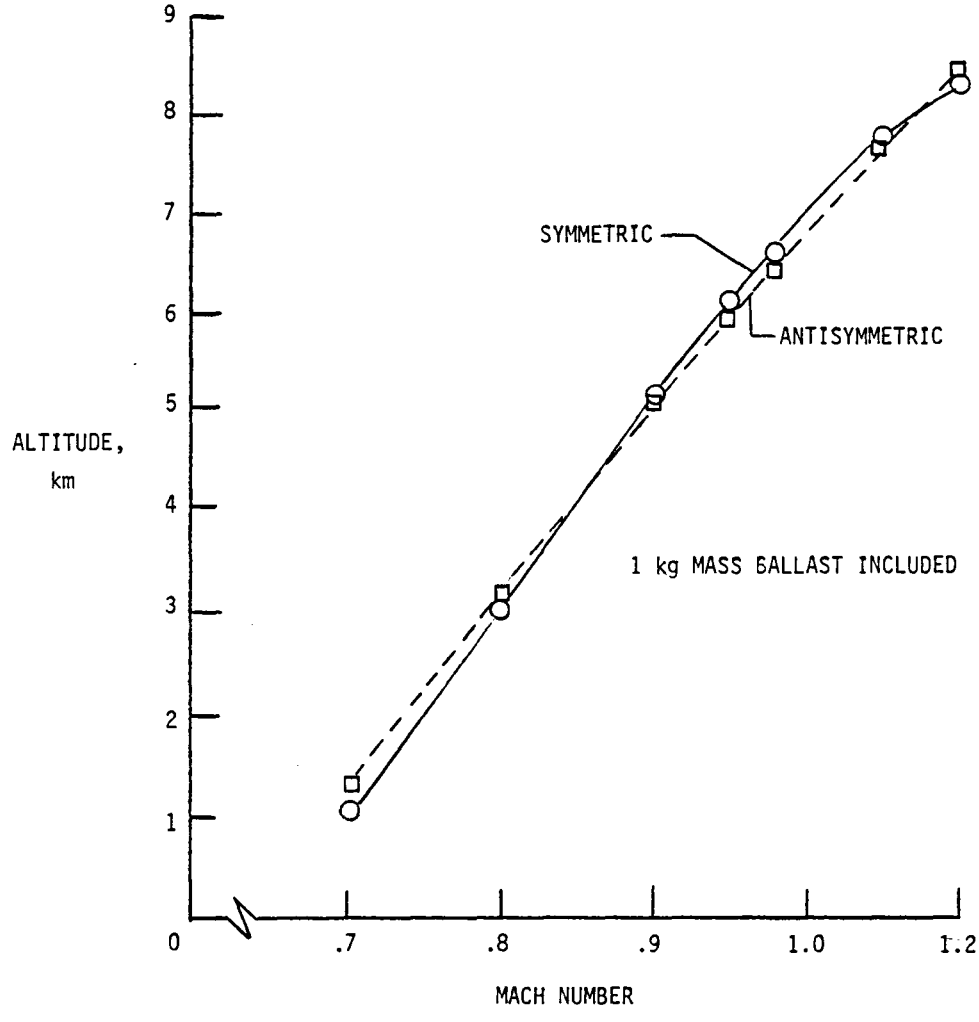

Figure 3.4. Predicted ARW-I symmetric and antisymmetric open loop flutter boundaries.

Mach number. The figure shows that symmetric flutter will occur first at altitudes above 4270 m, while the antisymmetric flutter will proceed the symmetric at lower altitudes.

The ballast weights added to each wing tip were made ejectable. In case of an FSS malfunction within the flutter boundary, jettison of both tip masses will cause the wing to become flutter-free up to a significantly higher dynamic pressure.

The tip mass release (TMR) system is shown in figure 3.5. Two tip mass cylinders, each containing 1 kg of lead shot, are located on each wing tip. The system can be activated manually from the ground and the F-104 chase plane. Under normal operating conditions, the system is controlled by an electronic circuit that integrates the accelerometer signal, sensed by the TMR accelerometers located on each wing tip. Integration will take place only when the accelerometer output exceeds the trigger level of 15. g. When the integrated signal exceeds a pre-set value, the electronic circuit will fire the pyrotechnic actuators in the mass cylinders, causing the pushrod mechanism to release the lead shot.

The integration scheme prevents spikes in the accelerometer signal from firing the pyrotechnics, and ensures that the wing will indeed be fluttering before jettisoning the lead shot.

3.2 Flutter Suppression System (FSS)

The flutter suppression system (FSS) is an analog system designed and fabricated by the Boeing Wichita Company under a NASA Langley contract. The major contract requirement was to provide an active

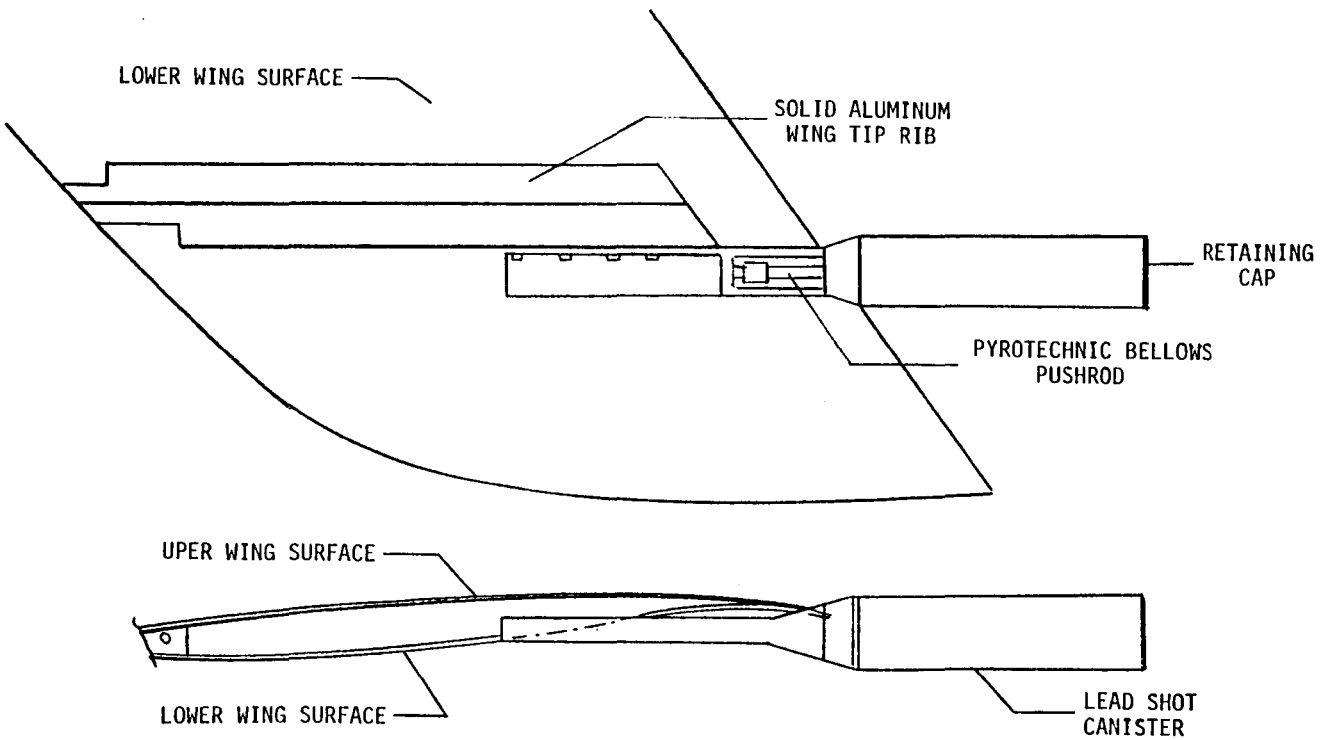

Figure 3.5. Tip mass release system ballast attachment.

control system that would extend the flutter boundary of the DAST-I vehicle by 20 percent.

The FSS primary function is to generate artifical stiffness in a system such as the ARW-I, by utilizing an augmentation control system that will produce forces which oppose motion in the system. When the system is operating properly, it will suppress the divergent motion of the wing caused by flutter.

The development of the FSS follows an analysis sequence presented in figure 3.6. Unsteady aerodynamic techniques and NASTRAN vibration solutions provide the basis for the generation of the equations of motion. The procedure in generating the equations is described in more detail in reference 2.

The FSS block diagram is shown in figure 3.7. Four accelerometer signals are utilized as inputs to the system. Two of these accelerometers are located on each wing tip and two are mounted in the fuselage. The last two accelerometers are used to subtract the rigid body vertical and roll accelerations from the wing sensors. The filter, common to the symmetric and antisymmetric paths, contains the D parameter. This parameter is a function of impact pressure, P_I, and is expected to provide adequate gain margins at all flight conditions.

Notch filters were added to the system to achieve proper gain and phase at the corresponding symmetric and antisymmetric flutter frequencies. The gain and phase characteristics of the actual hardware FSS versus frequency are presented in figures 3.8 and 3.9 for the symmetric and antisymmetric conditions, respectively.

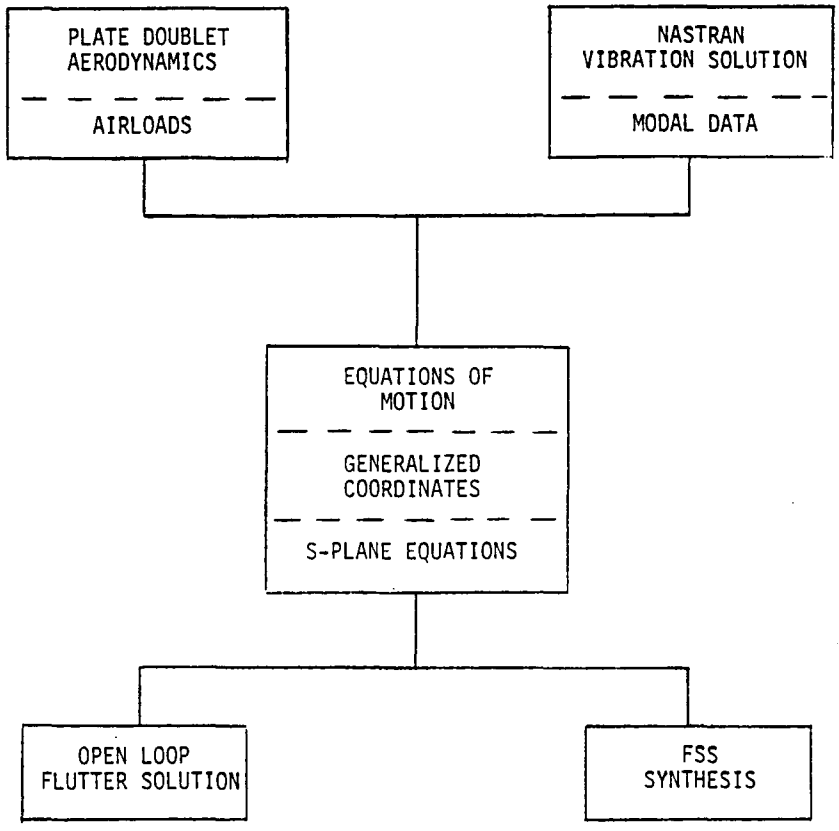

Figure 3.6. Flutter analysis sequence.

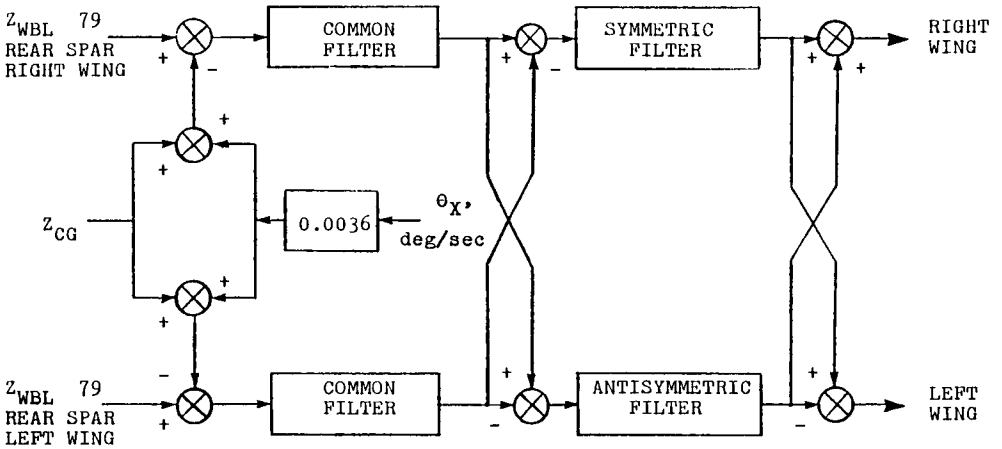

COMMON FILTER :

$$\frac{1.8\times10^{5}S(S^2+DS+200^2)\,(S^2+360S+333^2)}{(S+2)\,(S+40)\,(S^2+(D+40)S+40D)\,(S^2+1700S+848.5^2)\,(S+900)}$$

SYMMETRIC FILTER :

$$\frac{1.581\times10(S^2+80S+85^2)\,(S^2+80S+295^2)\,(S^2+62.2S+1037^2)}{(S^2+220S+156^2)\,(S^2+1100S+550^2)\,(S^2+5185+1037^2)}$$

ANTISYMMETRIC FILTER :

$$\frac{3.6755\times10(S^2+60S+80.8^2)\,(S^2+62.2S+1037^2)\,(S+125)\,(S^2+48S+480^2)\,(S^2+22.6S+133^2)\,(S^2+195S+1218.9^2)\,(S^2+80S+295^2)}{(S^2+180S+175^2)\,(S^2+518S+1037^2)\,(S+200)\,(S^2+274S+456^2)\,(S^2+106.4S+133^2)\,(S^2+609.5S+1218.9^2)\,(S^2+1300S+295^2)}$$

$$D = \frac{364081.0}{P_I-.382P_S+556.6} - 1490.0$$, D Limited to 4267 m and 7315 m , P_I Impact pressure, P_S Static pressure, (kg/m^2)

Figure 3.7. Flutter suppression system block diagram.

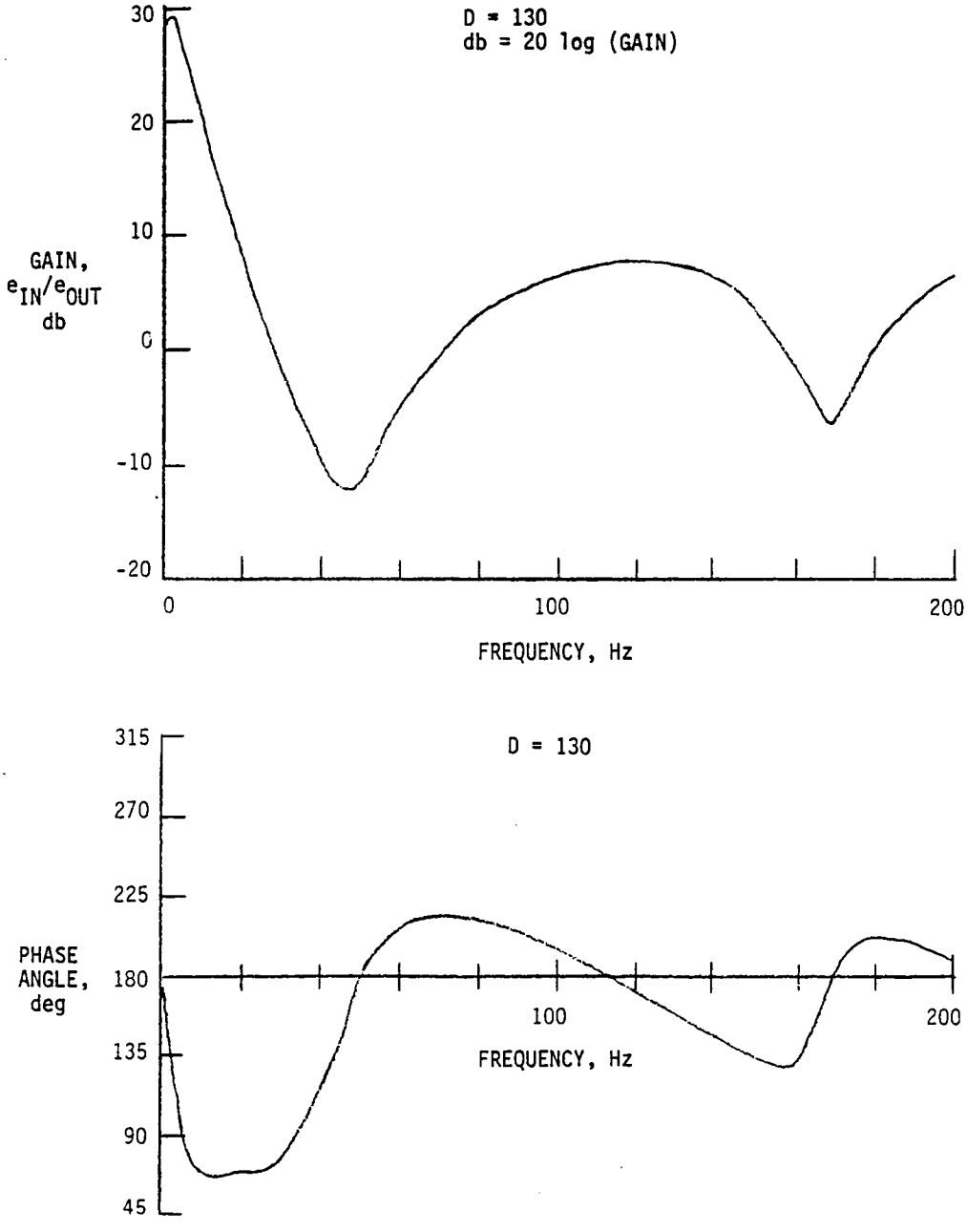

Figure 3.8. FSS symmetric mode gain and phase angle versus frequency.

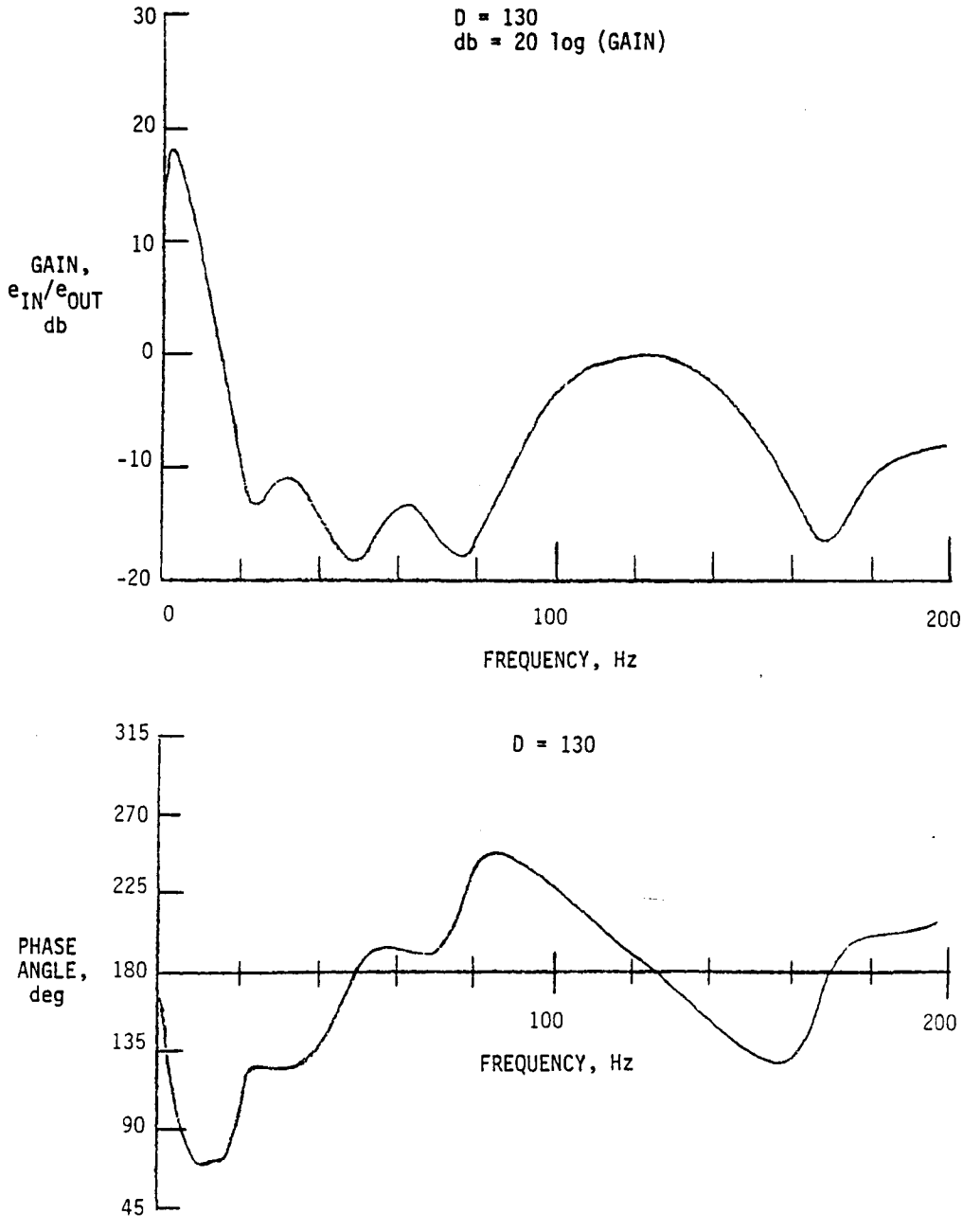

Figure 3.9. FSS antisymmetric mode gain and phase angle versus frequency.

The flutter boundary shift caused by the FSS is shown in figure 3.2 as a function of altitude and Mach number. The 1.2 M_f goal for the FSS is also shown.

The improvement in the damping ratio of symmetric and antisymmetric flutter modes is shown in figures 3.10 and 3.11, respectively. The analysis results indicate that the required 20 precent increase in flutter boundary speed can be achieved.

A model of the ARW-I wing equipped with an FSS was tested in a wind tunnel to provide data to support the FSS flight test program. The tests were conducted in the NASA Langley 16-foot (4.8 m) Transonic Dynamics Tunnel. The primary objective of the tests was to validate the methods used to synthesize the FSS and demonstrate the suitability of the test methods proposed for the flight tests with the DAST-I vehicle. The wind tunnel results verified the FSS synthesis methods. The flight test methods could not be evaluated due to the model response to wind tunnel turbulence.

The model was successfully tested at about 42 percent above the open loop flutter boundary dynamic pressure, which is equivalent to an increase in flutter speed of 19 percent. At that condition, the system saturated. This was attributed to the turbulence of the tunnel which is significantly higher than the turbulence expected in the atmosphere. Tests also verified that jettison of the 1 kg ballast will stop flutter at dynamic pressure conditions within the flutter boundary region.

Additional information concerning the design and sythesis of the FSS can be found in references 5 and 6.

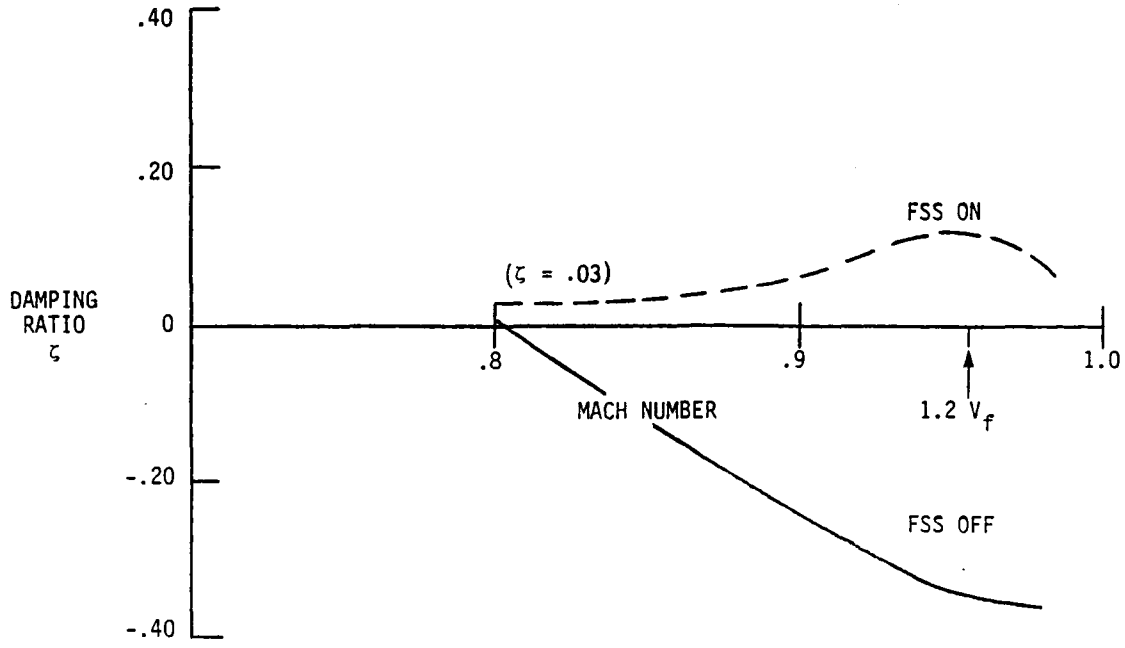

Figure 3.10. Predicted ARW-I symmetric flutter mode damping ratio. h = 3048 m.

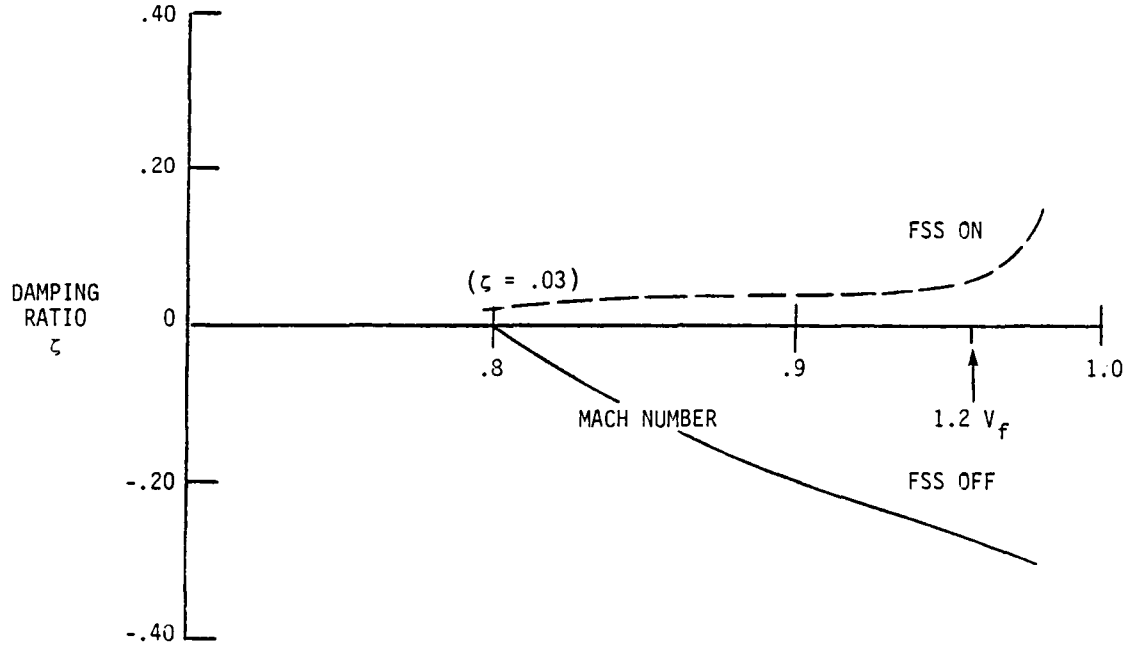

Figure 3.11. Predicted ARW-I antisymmetric flutter mode damping ratio. h = 3048 m.

3.3 FSS Instrumentation

A layout of the onboard FSS equipment is shown in figure 3.12. This section gives a description of the following FSS components:

- FSS electronic box
- Hydraulic pump
- FSS aileron servoactuators
- Motion sensors

The FSS electronic box contains major electronic components such as the electronics for the implementation of the FSS control laws and the sweep excitation generator. The FSS is an analog system controlled by digital uplink commands. These uplink commands are shown in table 3.3. General information concerning the flutter excitation generator is presented in table 3.4.

The hydraulic pump, utilized only during the first ARW-I flight, was an electrically driven Sundstrand-Pesco Model 165-100. The difficulty to operate the pump satisfactorily and the lack of spare parts resulted in the purchase of a new system. The new ABEX pump is electrically driven by an EEMCO engine. The hydraulic pump is rated at 3.785×10^{-3} cubic meters of fluid per minute at a pressure of 1.0×10^{7} N/m^2. The accumulator has a capacity of 3.18×10^{-4} m^3. A reservoir on the low pressure side of the pump, has a capacity of 3.2×10^{-4} m^3.

According to the original design requirements, the surface actuators had to be located within the ARW-I airfoil. In order to comply with this requirement, the hydraulic servovalves were placed in the fuselage and connected to the actuators through hydraulic lines. Analysis of the hydraulic line effect on the actuator characteristics indicated that this concept was acceptable.

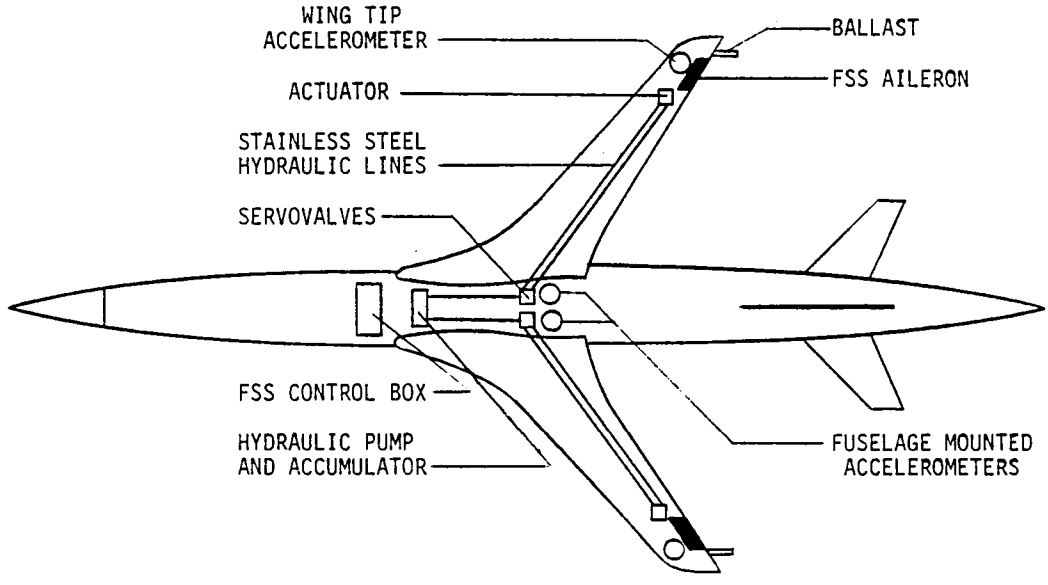

Figure 3.12. FSS equipment layout.

TABLE 3.3 FSS UPLINK COMMANDS

Command	Parameter identification	Range
FSS box engage	FSSON	on/off
Excitation pulse	PULCOM	on/off
Excitation sweep	SWECOM	on/off
Excitation symmetry	SYMCOM	sym./antisym.
Excitation amplitude	AMPCON	high/low
FSS gain	FSGAIN	high/low

TABLE 3.4 THE ONBOARD FLUTTER EXCITATION GENERATOR

Sinusoidal sweep	
Frequency range	10 to 40 Hz
Duration	10 sec
Type of sweep	$f = f_0 e^{kt}$
Amplitudes (only two in flight)	1 or 2 deg
Doublet (one cycle square wave)	
Frequency	25 Hz
Amplitudes (only two in flight)	1 or 2 deg
Flexibility on the ground	
Sweep duration	5 to 20 sec
Sweep frequency (end points individualy)	± 5 Hz
Sweep and doublet amplitudes	.5 to 5.0 deg

Automatic reset capability provided when the excitation is disengaged.

Each function starts at zero amplitude.

Soft start and stop is provided. Nominal ramp time .5 second up and down, variable symmetric or nonsymmetrical ±.2 second.

The actuator is a single-vane rotary design. The control surface is directly coupled to the shaft. This system was sized so that the stall torque equals the maximum expected hinge moment. The actuator maximum torque is 3.18 kg/m at 1.0×10^7 N/m^2 of pressure.

The FSS utilizes four miniature high frequency ICP quartz accelerometers, one on each wing and two in the fuselage. The inboard accelerometer signal is summed and subtracted to provide normal and angular fuselage accelerations, respectively. The accelerometers are fabricated by PCB-Piezotronics (Model 303A03) and have a range of ±500.0 g.

CHAPTER 4

SUPPORTING GROUND FACILITIES AND AIRCRAFT SYSTEMS

The remotely piloted vehicle operations conducted at NASA Dryden require a substantial support from ground and range facilities. This chapter describes the facilities involved in the DAST-I operation along with the airborne support. Facilities and systems not directly involved in the DAST-I flight test operation are not included in this description.

4.1 Remotely Piloted Research Vehicle (RPRV) Facility

The RPRV facility is a major element of support for all remotely piloted vehicle programs. This facility is enhanced by a remotely augmented vehicle (RAV) system which can provide remote augmentation for manned and unmanned test vehicles.

A block diagram of the RPRV concept is shown in figure 4.1. Downlink telemetry containing vehicle response variables is routed to the ground cockpit instrument panel and a ground-based computer. Telemetry data are also routed to the data acquisition system and analog strip chart recorders and mapping displays for real time monitoring. Pilot proportional control functions are processed by an analog-to-digital converter and directed to the ground computer together with digital ground cockpit commands. Ground computer proportional commands are provided to the uplink encoder and transmitted to the vehicle.

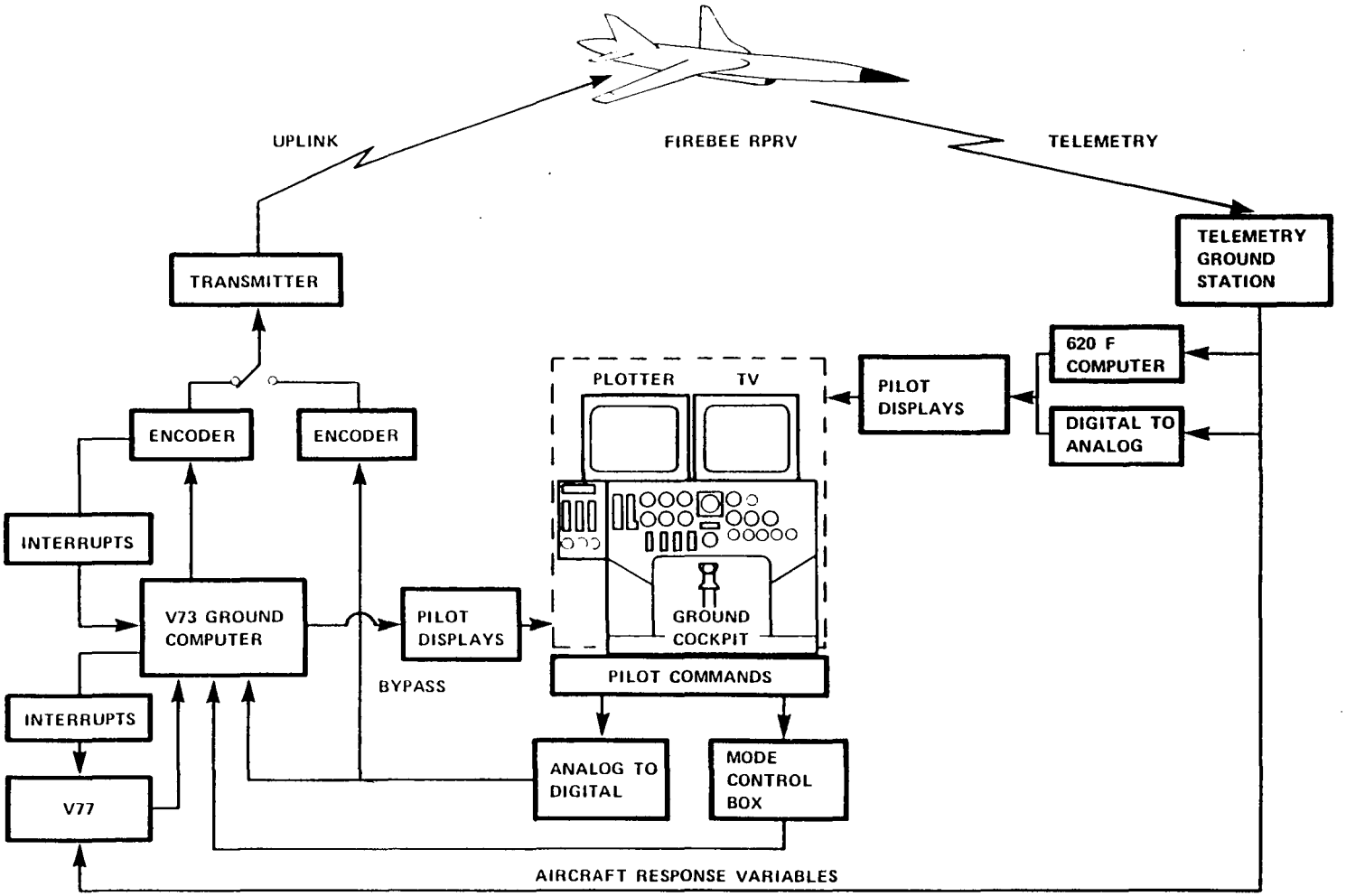

Figure 4.1. Functional block diagram of the RPRV system.

Proportional control of the remotely piloted vehicle can also be obtained without the use of the RAV system. This mode of operation, known as the Babcock Direct mode, does not utilize the Varian computers. Analog commands obtained from the stick computer are routed through an analog-to-digital converter and directed to the uplink encoder.

A layout of the RPRV facility is shown in figure 4.2. A description of the ground cockpit and the RPRV computational equipment is presented in the following sections.

4.1.1 Ground Cockpit

Through the ground-based cockpit the test pilot has direct proportional control of the test vehicle. This allows the use of experienced test pilots so that the maximum research capability can be realized from the system.

The RPRV facility has three ground cockpit crew stations. Two of these are installed in 2.7 x 3.3 m isolation cubicles. The third is installed in a 4.3 x 4.8 m area that is designated as a special displays area. The DAST program is utilizing one of the smaller cubicles.

The cockpit crew station enclosures are soundproofed to lessen extraneous noise, inside walls and ceiling are painted flat black to decrease peripheral vision distractions, and controlled lighting is used to focus the pilot's attention on the more important panels and controls. Display panels and side consoles can be interchanged to provide multi-program capability.

A picture of the DAST ground cockpit is shown in figure 4.3. A more detailed description of the instrument panel is shown in figure

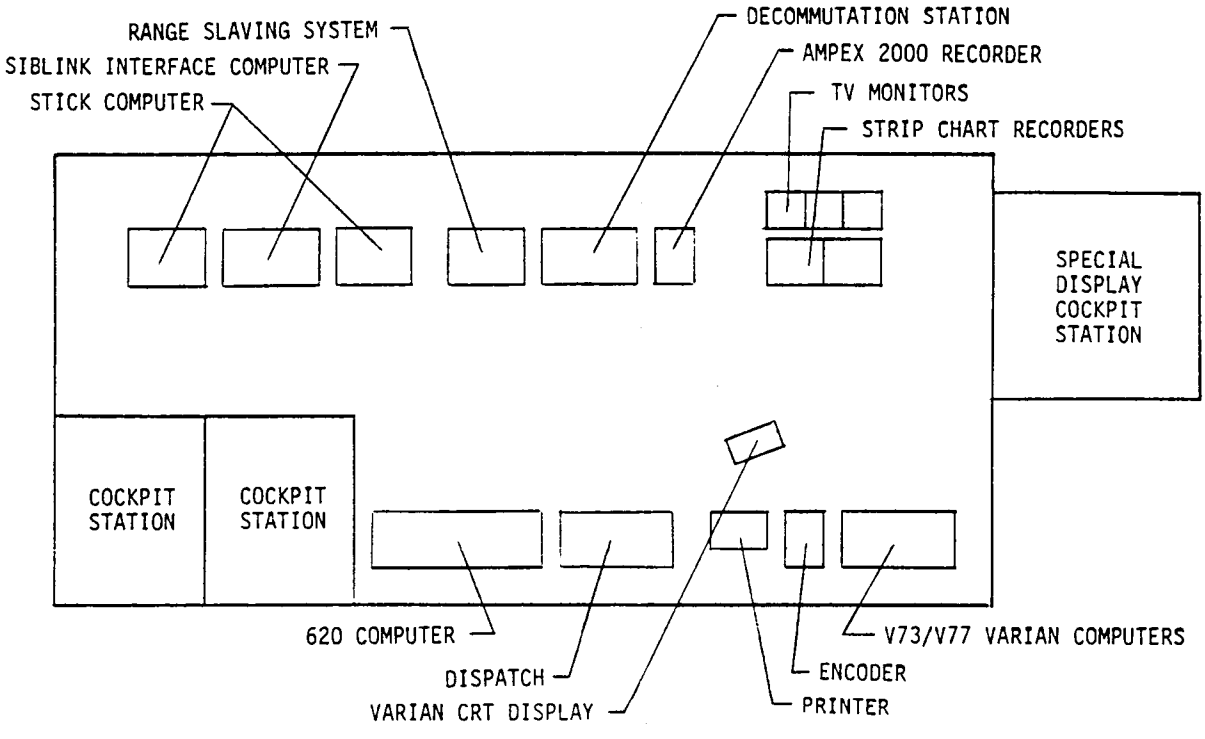

Figure 4.2. RPRV facility layout.

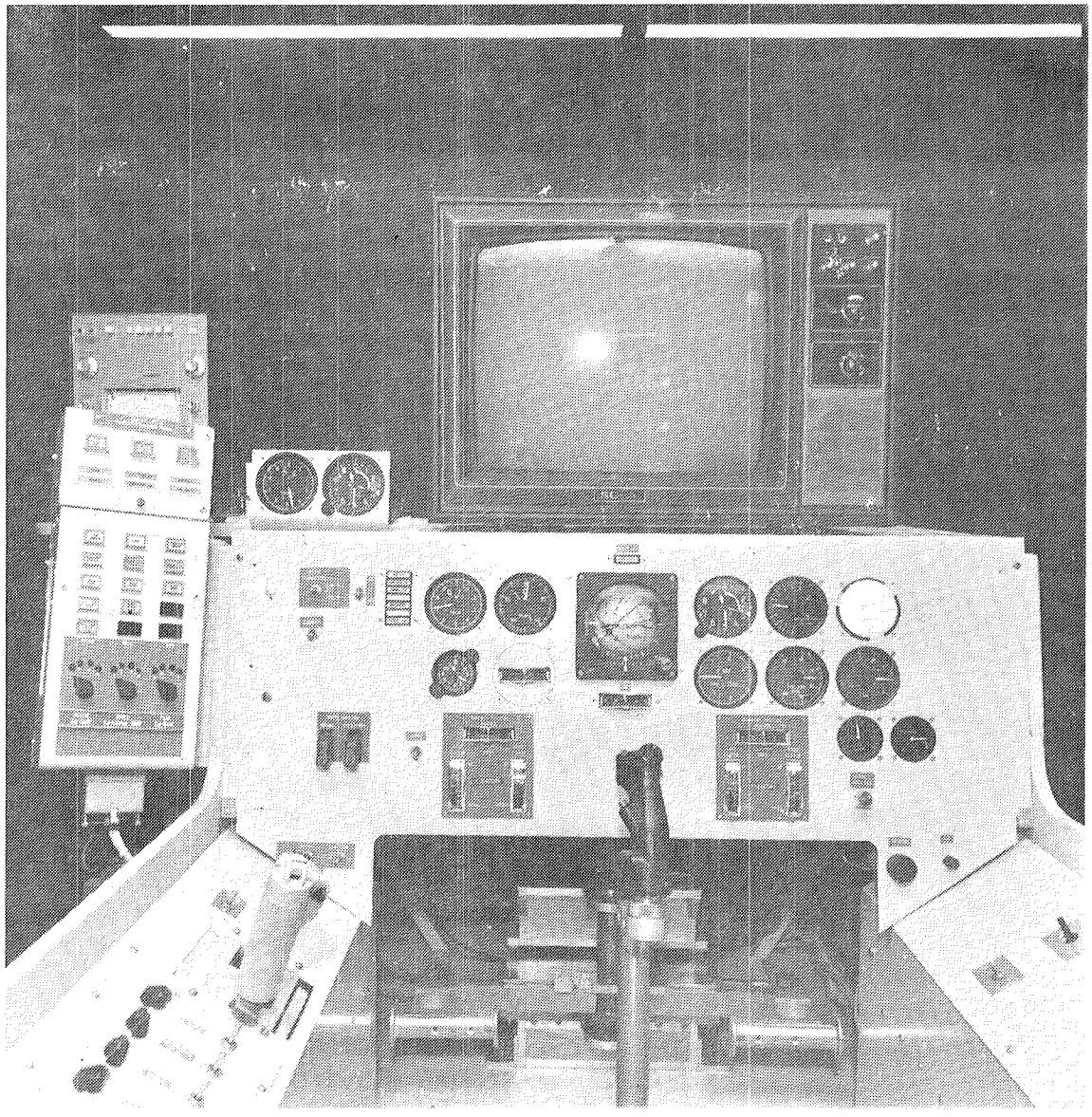

Figure 4.3. RPRV ground cockpit.

4.4. The information displayed on this panel is either a downlink parameter or a ground computer output. All instruments are scaled by the Siblinc interface computers. Altitude and airspeed information is provided by the USAF FPS-16 tracking radar and is displayed on the upper left corner of the instrument panel. The radar is a backup source of information in case of downlink telemetry failure. In table 4.1, a list is presented of the variables displayed on the main instrument panel. Their respective range and source is included. In table 4.2 the annunciator lights are described.

TABLE 4.1 GROUND COCKPIT INDICATORS

Indicator	Displayed parameter	Source
MACH	Mach number	V-73 computer
KNOTS	Calibrated airspeed	V-73 computer
ALITMETER	Altitude	V-73 computer
ADI	Altitude, heading, and bank angle indicator	V-73 computer
HDOT	Altitude rate, bank angle compensated	V-73 computer
FUEL	Amount of fuel remaining	V-73 computer
LONGITUDINAL ACCEL.	Longitudinal acceleration	V-73 computer
FPA	Flight path acceleration	V-73 computer
GAMMA (HORIZ. ILS)	Flight path angle, bank angle compensated	V-73 computer
NORMAL ACCEL.	Normal acceleration	Downlink telemetry
ALPHA	Angle of attack	Downlink telemetry
BETA	Sideslip angle	Downlink telemetry
FUEL FLOW	Fuel flow rate	Downlink telemetry
% RPM	Needle 1 shows commanded rpm	RPRV cockpit
	Needle 2 shows actual A/C rpm	Downlink telemetry
RADAR AIRSPEED	Ground speed	FPS-16 radar
RADAR ALTIMETER	Altitude	FPS-16 radar

The left- and right-hand side panels and the stick and pedals are shown in figure 4.5. The left-hand side panel contains the

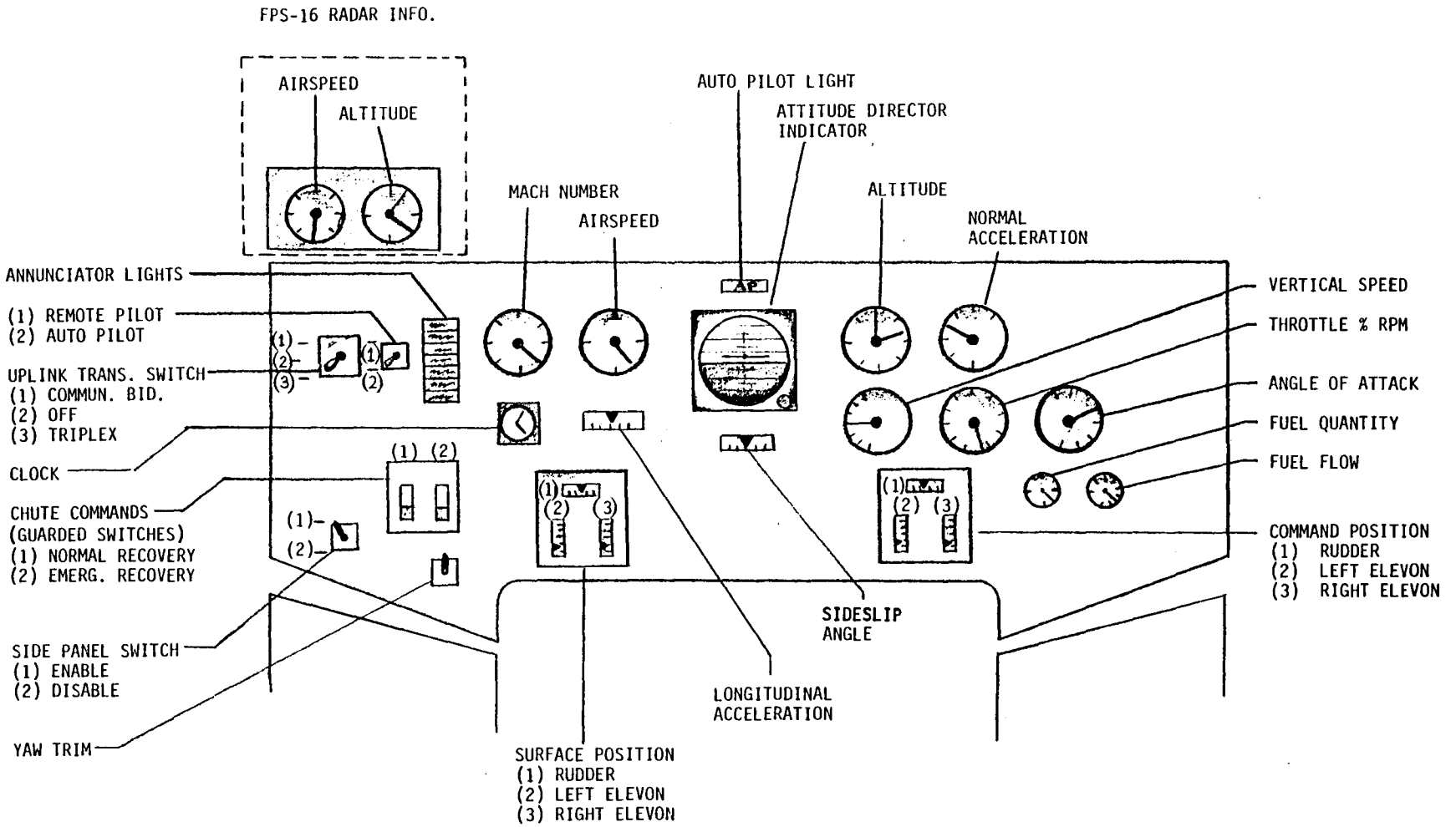

Figure 4.4. Ground cockpit instrument panel layout.

TABLE 4.2 GROUND COCKPIT ANNUNCIATOR LIGHTS

Light	Function	Source
ANT. SW.	Lit when source of uplink other than triplex antenna	RPRV ground cockpit
COMPUTER FAIL	Lit when V-73 or V-77 has failed	Computer monitoring hardware
CARRIER LOSS	Lit when uplink signal strength below limit. (-92db)	Downlink telemetry
RECOVERY	Lit only when normal recovery has been initiated	Downlink telemetry
HORN DISABLE	Lit when alpha warning horn is disabled	RPRV ground cockpit
PROGRAM CONT.	Lit when pilot is using the pulse panel step and pulse commands	V-73 computer
AUTO PILOT	Lit when onboard autopilot is engaged	Downlink telemetry

throttle lever and the pulse panel. The pulse panel is only active when the switch located on the lower left side of the instrument panel is placed in the enable position. The stick and rudder force control switch is used only during preflight checks for stick force and displacement calibration. The horizontal ADI needle is utilized to display flight path angle.

The right-hand panel is mainly used for remote AP control. An audio buzzer is also installed with a reset and disengage capability. The buzzer is activated whenever the angle of attack exceeds 6 degrees. The communication panel provides to the pilot the ability to communicate via UHF and any of the intercom channels. The stick and rudder system is an electric feel system that operates on all three control axes. It has the capability of simulating feel characteristics to most aircraft flight control systems. The characteristics that can be obtained are force gradients, aerodynamic feedback, and mechanical parameters such as mechanical stops, damping, and trim friction.

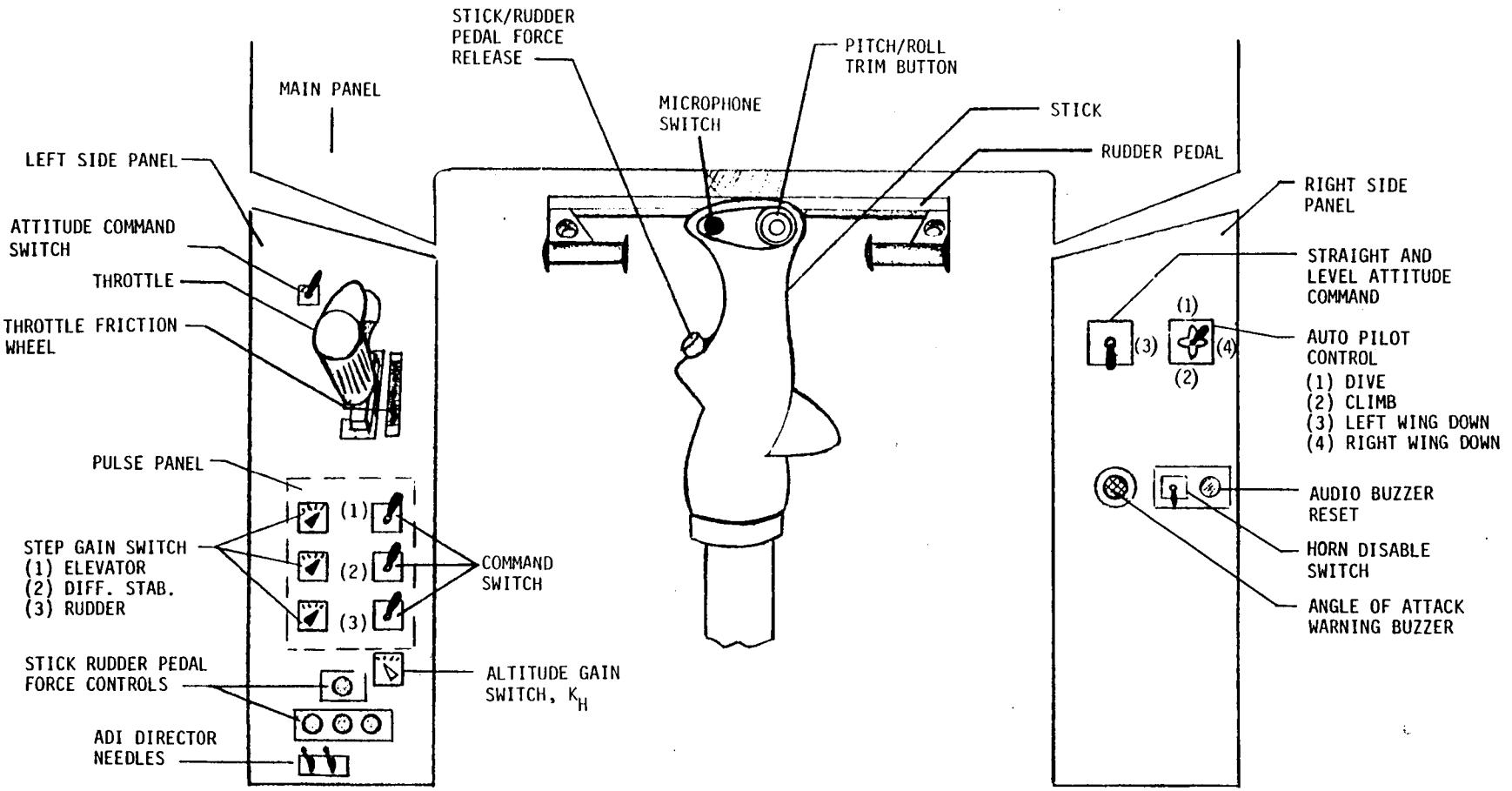

Figure 4.5. Ground cockpit side panel and stick functions.

The mode control panel is shown in figure 4.6. It provides control mode switching and selectable feedback gains in all three axes. The RAV mode is engaged through this panel.

The FSS monitor panel, located on top of the mode control panel, is shown in figure 4.7. This panel provides information to the pilot concerning the progress of the FSS testing.

During flight test operations, the ground cockpit is manned by the test pilot and the project engineer. The project engineer has control over the mode control panel, and functions as an additional communication link between the ground cockpit and the control room.

4.1.2 Varian Computers

Essential to the RAV system are the V-73 and V-77 Varian computers that perform the control system computations and downlink signal decommutation respectively.

The V-73 is a 32K, 16-bit computer, programmed in FORTRAN IV and machine language. The primary task of this computer is to perform control law computations during hangar checkout of the test vehicle and during flight test operations. A secondary task is to perform calculation for cockpit display purposes. Downlink data are obtained from the V-77 computer. Analog control inputs from the ground cockpit are converted into digital signals and directed to this computer. Discrete inputs are also obtained from the ground cockpit. The output of the computer is a 16-bit word operated under external clock control. The proportional output commands are directed to the uplink encoder and transmitter.

The V-77 receives the downlink telemetry signal from the tri-

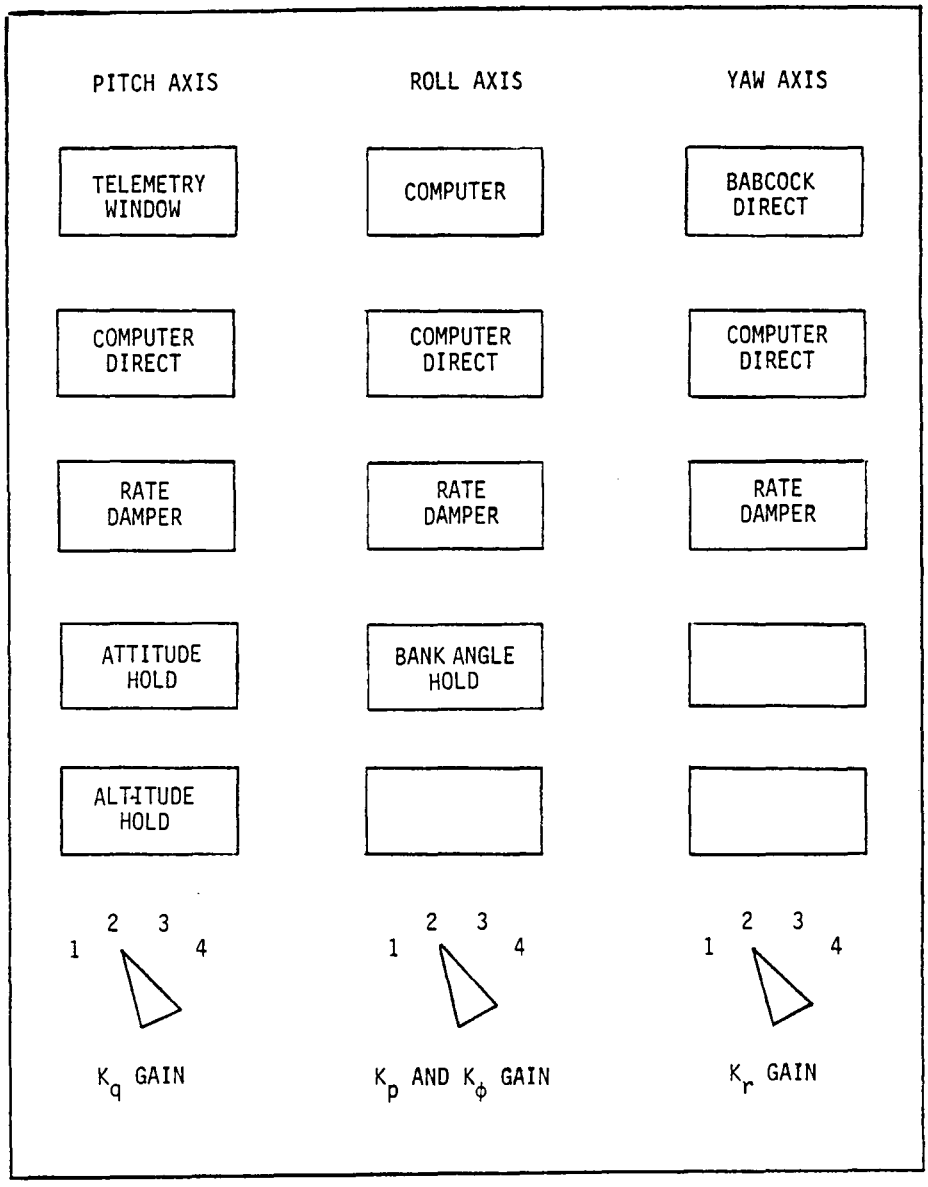

Figure 4.6. Mode control panel.

plexed antenna system. This computer operates utilizing a program that reads data from the downlink telemetry interface buffer/controller, decommutates the telemetry and transfers processed downlink variables to the V-73 on an "as needed" basis.

4.1.3 Siblinc Interface Computer

The Siblinc computer is used to interface the ground cockpit display panels with the dispatch system. This computer is mainly used for signal scaling, offsetting, and inverting.

4.1.4 Uplink System

The uplink signal routing is schematically shown in figure 4.8. In the RAV mode, the input to the uplink system is a combination of digital proportional commands generated by the V73 computer and discrete commands initiated in the ground cockpit. The proportional and discrete commands are merged by a discrete timing and control system. In the Babcock direct mode, the proportional commands are digitalized analog control signals from the ground cockpit.

The uplink system was developed by the U.S. Navy for multiple remote control of drone vehicles. The ability to control one to several drones simultaneously provides a high-update-rate system when controlling a single vehicle.

The characteristics of this system are:

- 16 bits per data frame (10-bit proportional command signal and 6 discrete signals)
- 4 data frames per cycle
- 106 cycles per second
- 2 parity checks per data frame
- Synchronization and parity checks on each cycle
- UHF band transmission
- Frequency shift keying

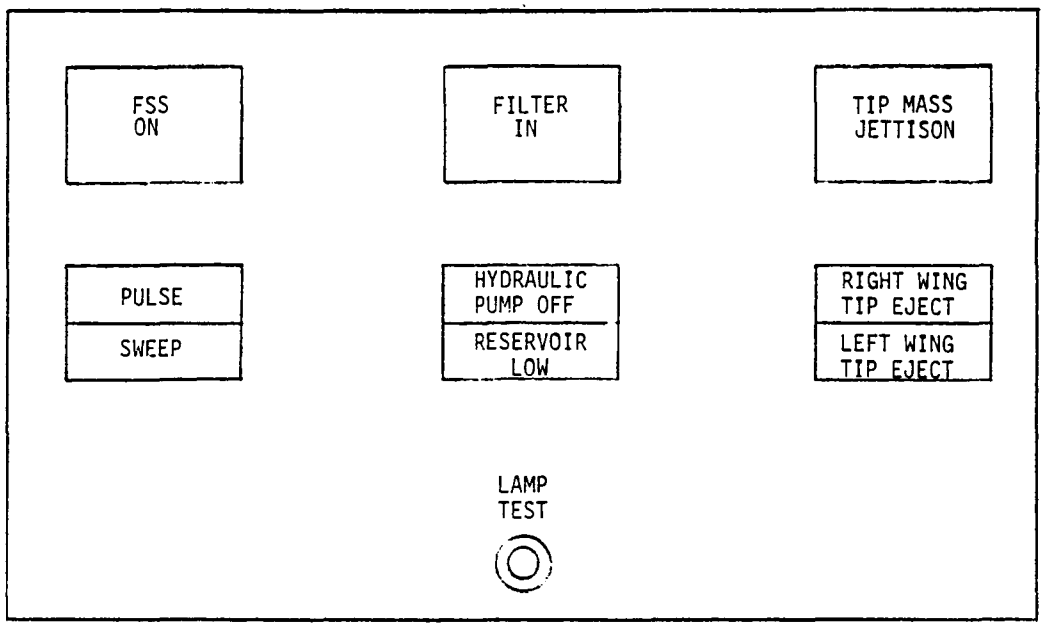

Figure 4.7. FSS monitor panel.

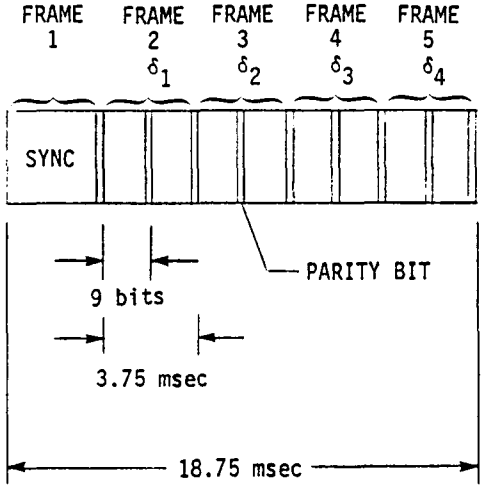

Figure 4.8. Uplink telemetry time schedule.

The telemetry uplink cycle shown in figure 4.8 consists of four 16-bit data words (frames) and one sync word transmitted at 53.33 samples per second. This implies a 18.75 milliseconds cycle time. The four proportional command signals, generated by the V-73 computer are coded in the 10 most significant bits of the uplink words, with the remaining 6 bits being available for the discrete signals. The uplink encoder interrupts the discrete timing and control system every 3.75 milliseconds to request one of the 16-bit command words. The uplink interrupt servicing routine tests five sense lines to determine the correct output variable. In case the timing system and the uplink encoder should get out of synchronization, the timing system sends the variable that the encoder requests even though it may have anticipated sending a different word. The uplink system output is transmitted to the test vehicle from the triplexed telemetry antenna located at the AN/FPS-16 site on the Buckhorn Ridge or the directional backup antenna located at the communications building.

4.1.5 Downlink System

The NASA Dryden telemetry flight data acquisition system is used for the telemetry downlink portion of the RPRV system. The system provides aircraft response variables to the ground station at high sample rates. A ground-based system is also utilized for the recording of RPRV facility parameters.

The general characteristics of the pulse code modulation (PCM) known as the Vector MMP-600 system are:

- Bit rate, variable from 1K (1,000) to 2,000 Kbits/sec
- Word length, variable from 8 to 12 bits/word

- Frame length, variable from 4 to 254 words/frame
- Frames per subframe, $2 \leqq n \leqq 32$
- Frames per second, K = bit rate/bits/frame

The first word for every frame contains a frame identification number. The last two words are used for frame synchronization.

The DAST program utilizes two onboard PCM systems, system 1 and 2, and one ground-based system, system 3. The specific characteristics are presented in table 4.3.

TABLE 4.3 DAST PCM SYSTEM CHARACTERISTICS

	System 1	System 2	System 3
Bit rate, bits/sec	110K	130K	160K
Word length, bits/word	10	9	10
Frame length, words/frame (1 ID word, 2 sync words included)	22	48	80
Frames per cycle	10	10	----
Frames per second (words)	500 (11)	300 (32)	200 (77)
Subframe rates (words)	250 (3) 100 (2) 50 (3)	30. (13)	

System 1 is the primary system containing all major FSS and control system parameters. System 2 contains loads data and some FSS variables. The third PCM system is located in the RPRV facility and contains signals from the ground cockpit and Varian computer. The table indicates that not all parameters are transmitted at the highest sample rate. The system 1 format, presented in figure 4.9, shows that 6 variables are transmitted every other two frames (250 samples per second), 10 at every other 5 (100 sps) and 30 at every other 10 (50 sps). Only 11 FSS parameters are calculated at 500 sps.

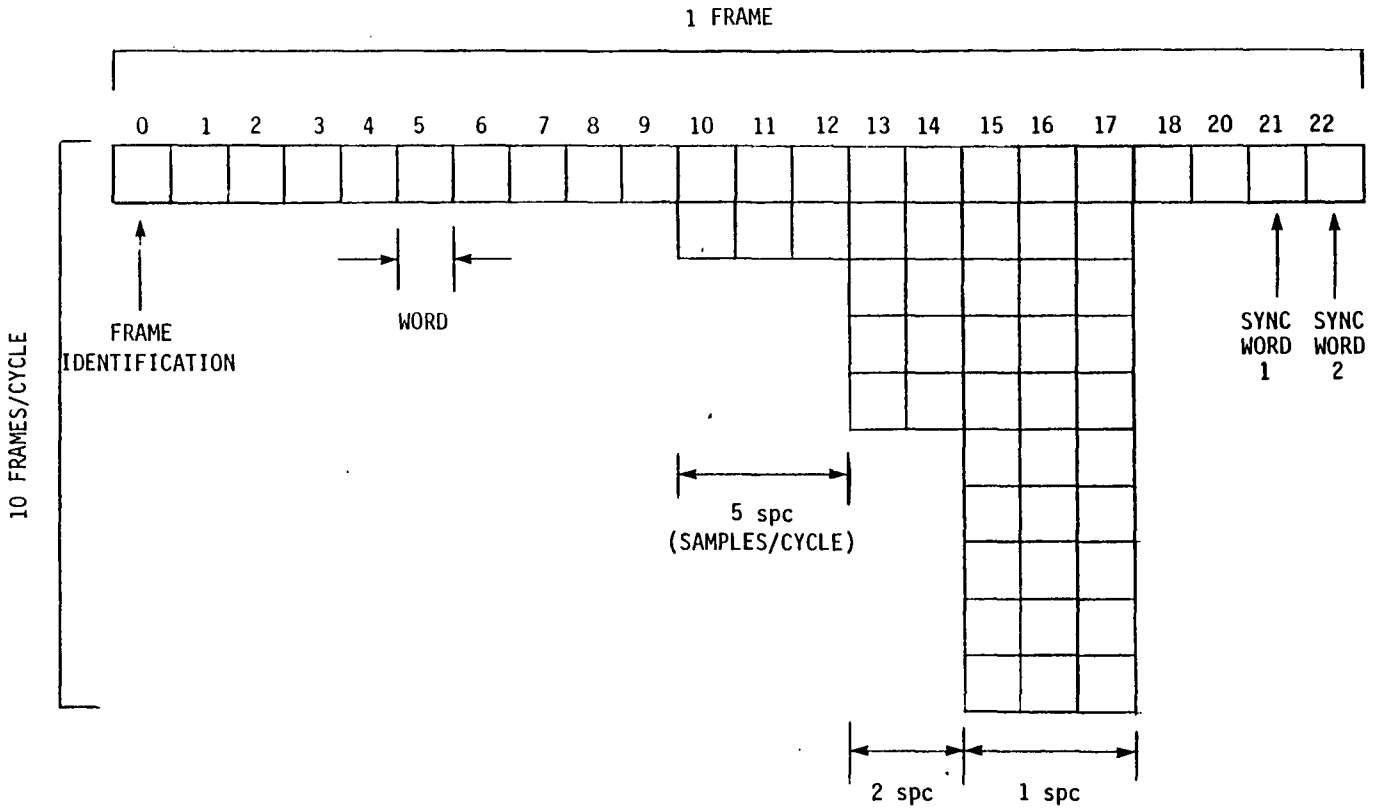

Figure 4.9. PCM system 1 cycle format.

The digital video data stream, received from systems 1 and 2 by the telemetry receiver, is decoded and directed through a digital-to-analog converter. A co-axial cable transfers the data to the RPRV, SAF, and other monitoring stations. System 3 data are processed in a similar fashion.

4.2 Spectral Analysis Facility (SAF)

A layout of the SAF is shown in figure 4.10. The facility occupies a central position in the DAST-I operation by performing the FSS testing.

Raw downlink data obtained from the triplex antenna are decommutated and processed to a HP-5451C Fourier analyser and a real time voltage analyser. Downlink parameters are also routed to strip chart recorders for real time monitoring. Special digital displays provide information concerning the FSS status. Results obtained from the Fourier analyser are displayed on the Tektronix graphics terminal. A hardcopy unit is attached to this terminal. Predicted and actual damping ratios of flutter modes are plotted during flight testing on the flutter test display panel. Digital FSS commands initiated by the FSS controller are routed to the RPRV encoder.

The SAF is provided with two-way intercom channels between the control room and the RPRV facility. The FSS controller also has two-way radio communication in UHF. This is a unique feature to the DAST program. In general, flight test operations conducted at NASA Dryden allow only the flight controller, the test pilot, and the supporting aircraft to have two-way radio commuinication in UHF.

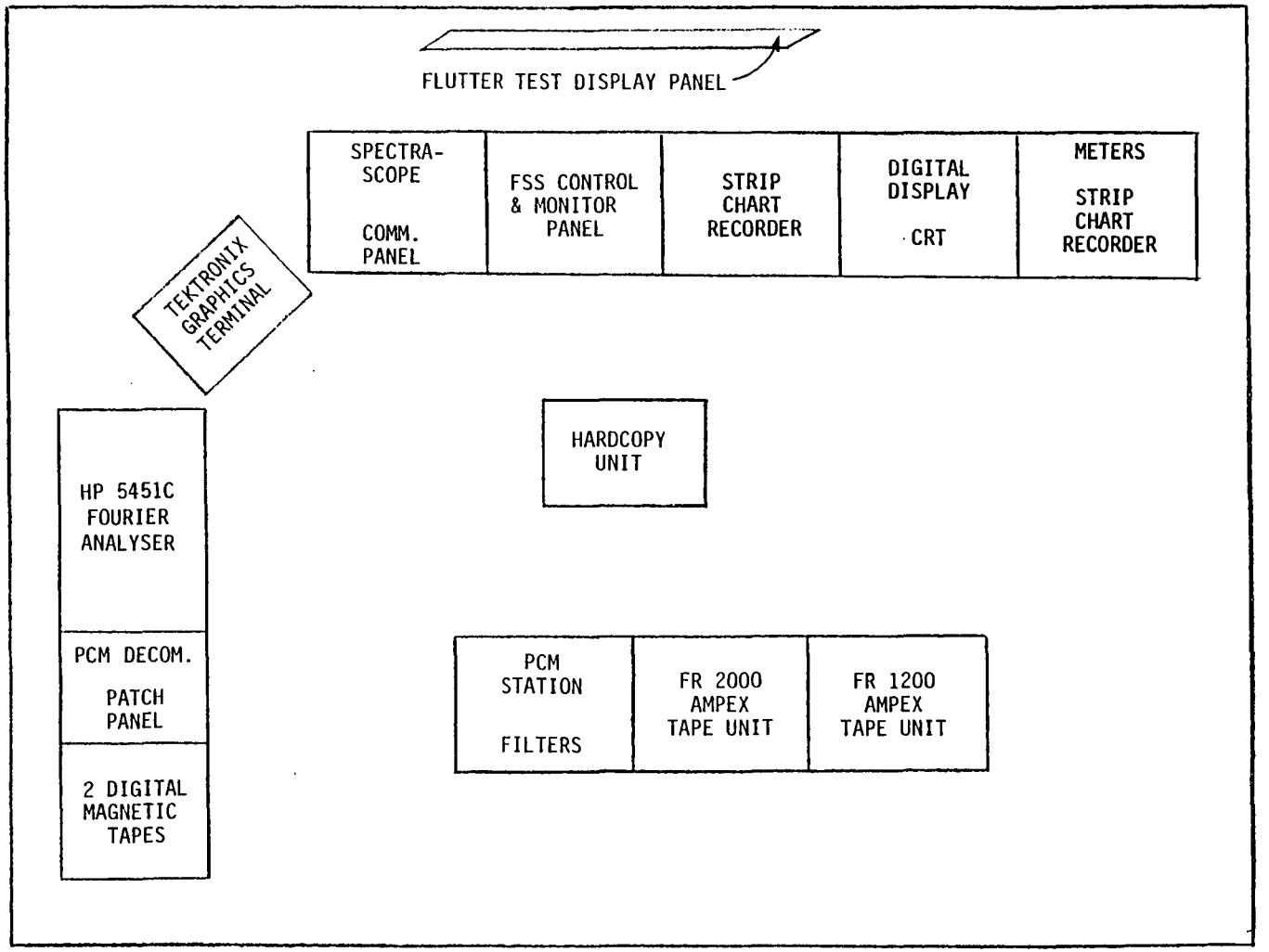

Figure 4.10. Spectral analysis facility layout.

Allowing the FSS controller to communicate in UHF was a necessity due to the importance of the FSS testing.

4.3 Control Room

The control room is located in the main building (4800) of the NASA Dryden Flight Research Center. A layout of this facility is shown in figure 4.11.

This facility has a decision-making authority. The project engineer is informed about the status of the test flight by the operations engineer, range operation engineer, flight controller, and FAA Dryden flight safety officer.

The flight controller is an experienced test pilot. His primary task is to guide the ground-based pilot around the predetermined flight track. Position information of the test vehicle is presented to the flight controller through a set of plotboards that are driven by the FPS-16 radar signal.

Vehicle status information is also provided to the project engineer by a number of research engineers monitoring onboard system status, FSS performance, and vehicle stability and control characteristics. Real time monitoring is intended to ensure that test conditions are attained, to provide information for decision-making purposes during normal operation and emergency conditions, and to verify condition and proper functioning of the vehicle and all onboard sub-systems.

The control room can be seen as an information center supplied by the following data sources:

- Vehicle and FSS downlink parameters

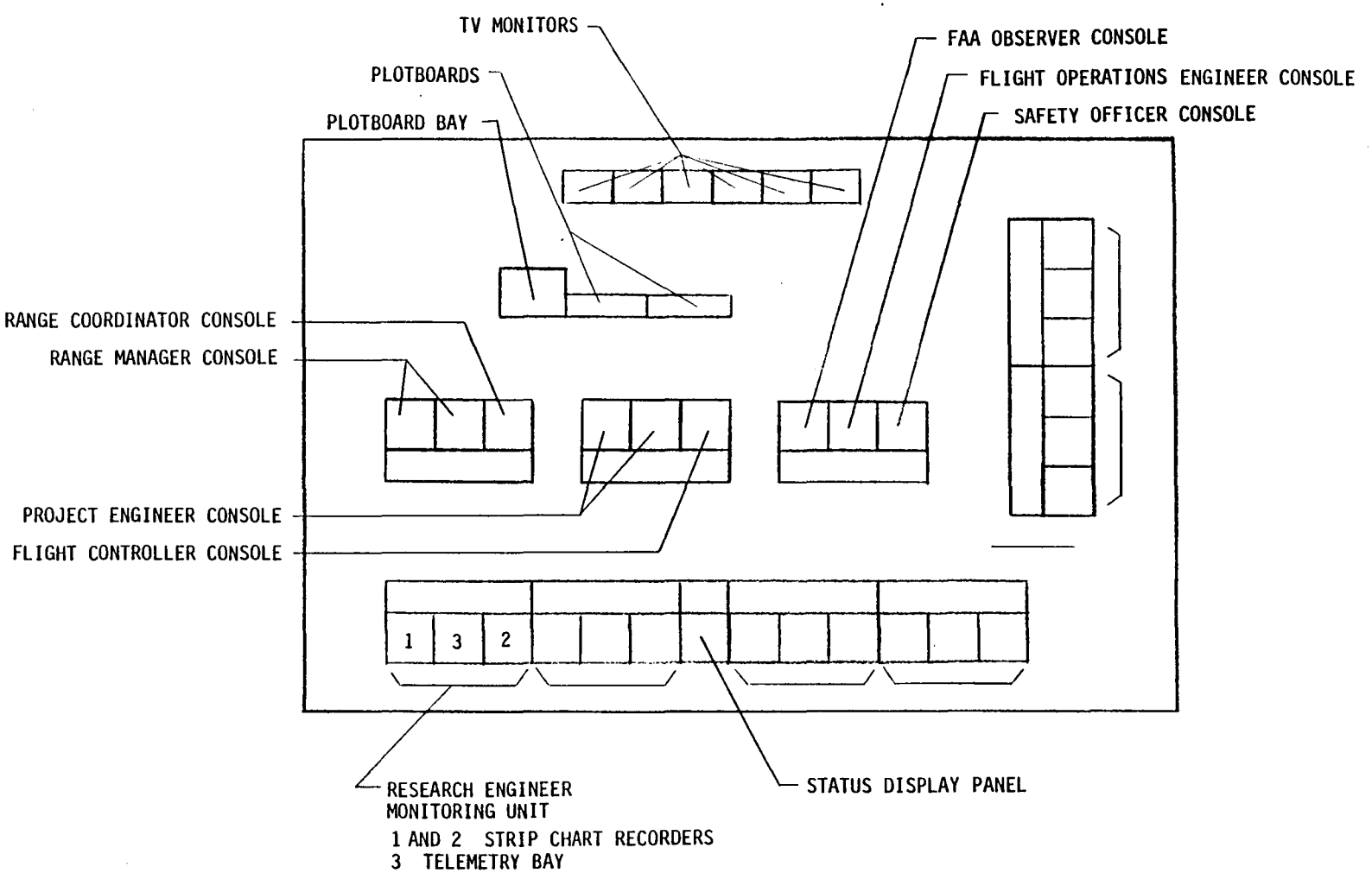

Figure 4.11. Control room layout.

- RPRV ground cockpit signals
- Computed SEL 8602 output variables
- Vehicle position presented on two plotboards
- Video pictures of the test vehicle and ground cockpit

The project engineer and flight controller have the ability to communicate in VHF, UHF, and all intercom channels. An emergency battery-powered UHF transceiver is also available in case of a major power failure.

4.4 Signal Routing and Range Facilities

Data streams obtained by the onboard data acquisition systems (section 4.1) and the RPRV facility are routed to several ground facilities.

The command and signal routing is shown in figure 4.12. There are three telemetry systems, PCM-1, PCM-2, and PCM-3. The primary system, PCM-1, generated by the onboard acquisition system, transmits all downlink data pertaining to aircraft operation, flight and atmospheric conditions, and FSS operation. In addition, it duplicates the transmission of flutter observation accelerometer signals and static pressure differential which are also transmitted by the secondary system, PCM-2. The secondary system transmits all data pertaining to the operation of the loads experiment including strain gage bridge outputs, wing surface pressures, and systems temperatures and voltages. As an alternate means of monitoring flutter, the secondary system also carries flutter observation strain gage bridge signals. The third PCM system contains signals generated in the RPRV facility. It includes computer-generated signals, analog and

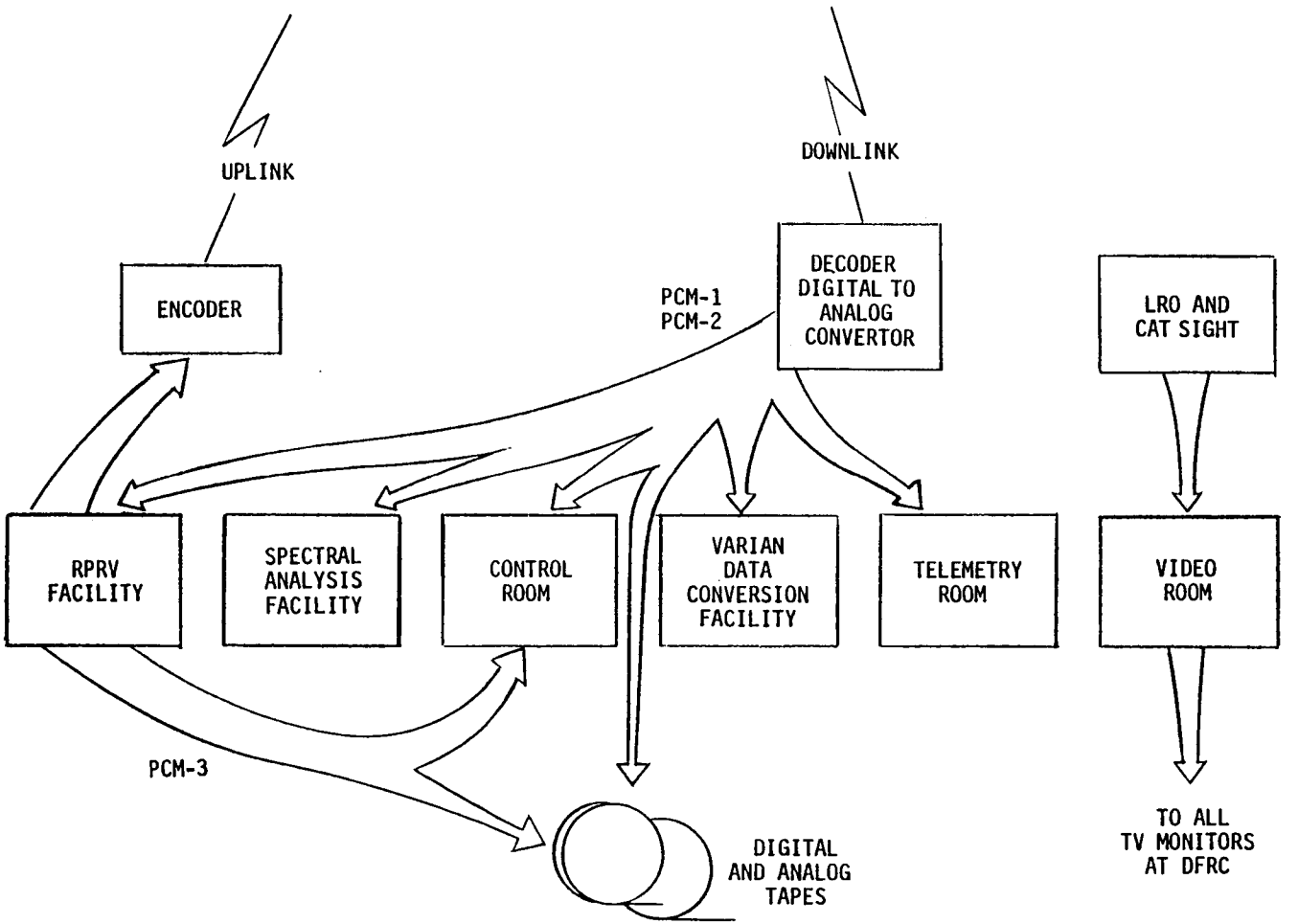

Figure 4.12. Command, telemetry, and video signal routing.

discrete cockpit outputs, and proportional and discrete uplink commands. All three data streams are routed to the major facilities as shown in figure 4.12.

In the telemetry room, all PCM systems are decommutated and recorded on tape for post flight analysis. The SEL 8602 computer is utilized to generate computed data that are required for special display purposes in other facilities.

The video room has as primary function the recording and distribution of video data obtained from the low range optics (LRO) color camera, the communications and tracking sight triplex 40-inch camera, and other ground-based and airborne cameras.

The range facilities utilized for data transmission and reception and vehicle tracking are the communication and tracking sight (CAT sight) and the Communications Building.

The CAT sight is the primary telemetry station. The triplex antenna transmits the uplink signal and receives the downlink telemetry data while slaved to the FPS-16 tracking radar. The antenna has a range of 320 kilometers for high altitude aircraft. A 40-inch camera is attached to the triplex antenna.

The Communication Building is a backup uplink telemetry station. The uplink signal is transmitted by an omni-directional antenna. This facility also receives and records UHF, VHF, and HF communications during test flights.

A triplex backup reception antenna is located on the main building of the NASA Dryden center. Also located on the main building is the low range optics color camera. The LRO camera can be slaved to the FPS-16 radar signal or manually controlled from the video room.

4.5 Airborne Support

A substantial airborne support is required during the flight test operations of the DAST-I test vehicle. It includes the B-52 launch vehicle, the F-104 backup command station, and the CH-3E helicopter for mid-air recovery of the drone. In this section, a description is given of the above vehicles. The T-38 photo chase aircraft is not included in this description.

4.5.1 B-52 Launch Aircraft

The B-52 aircraft has been utilized by NASA Dryden for a number of missions throughout the last 15 years. The vehicle is equipped to perform preflight tests on the ground and in the air, up to the moment the test vehicle is launched.

The DAST-I drone is attached to the B-52 right wing through an adapter. In figure 4.13, the test vehicle is shown attached to the B-52 carrier. The upper part of the adapter was originally utilized by the X-24 program. The lower part was specially fabricated for the DAST program and is known as the minipylon. The figure also presents information concerning the position of the test vehicle in relation to the B-52.

The launch vehicle provides the ability to control and monitor the DAST-I onboard systems through the launch panel operator's (LPO) console. The operator has the ability to supply DC power to the vehicle while the engine of the test vehicle is off. With the engine on, the LPO can select internal or external power. The power panel along with the Firebee II engine monitor and control panel are shown in figure 4.14.

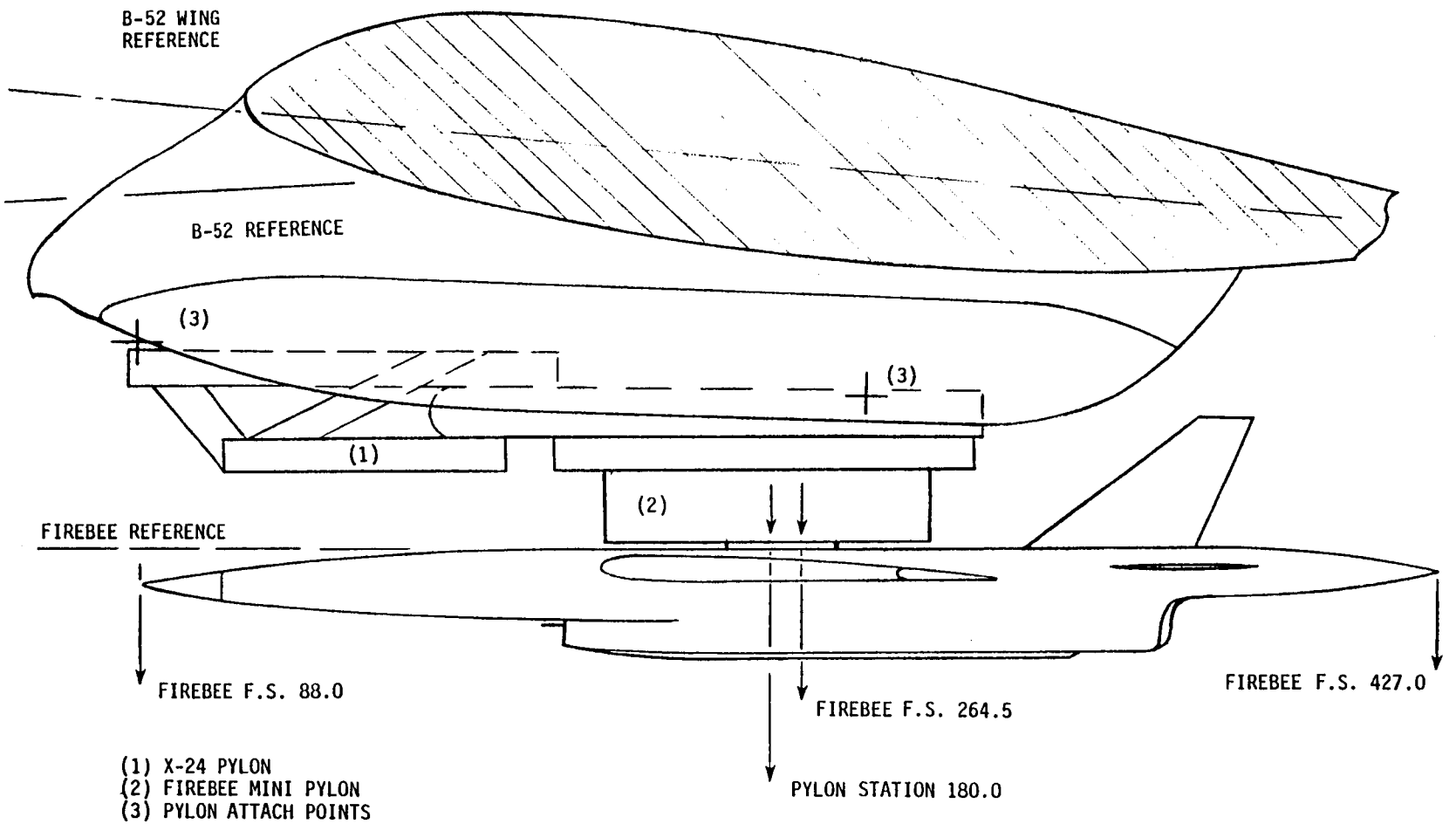

(a) DAST-I drone attached to the B-52 wing.

Figure 4.13. The DAST-I test vehicle attached to the B-52 launch aircraft.

LAUNCH CONDITIONS

ALTITUDE	5180 m
MACH	.415
B-52 GROSS WEIGHT	107,050 kg
FIREBEE LAUNCH WEIGHT	1008 kg

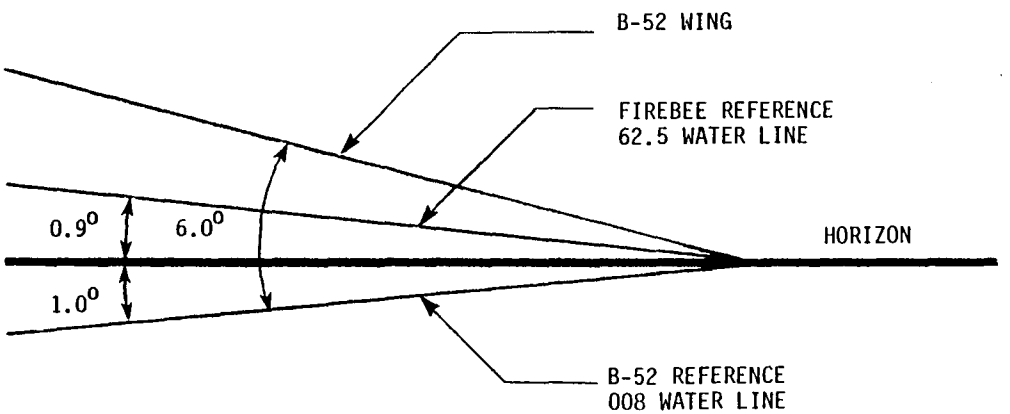

(b) B-52 and DAST-I angle of attack at launch conditions.

Figure 4.13. Concluded.

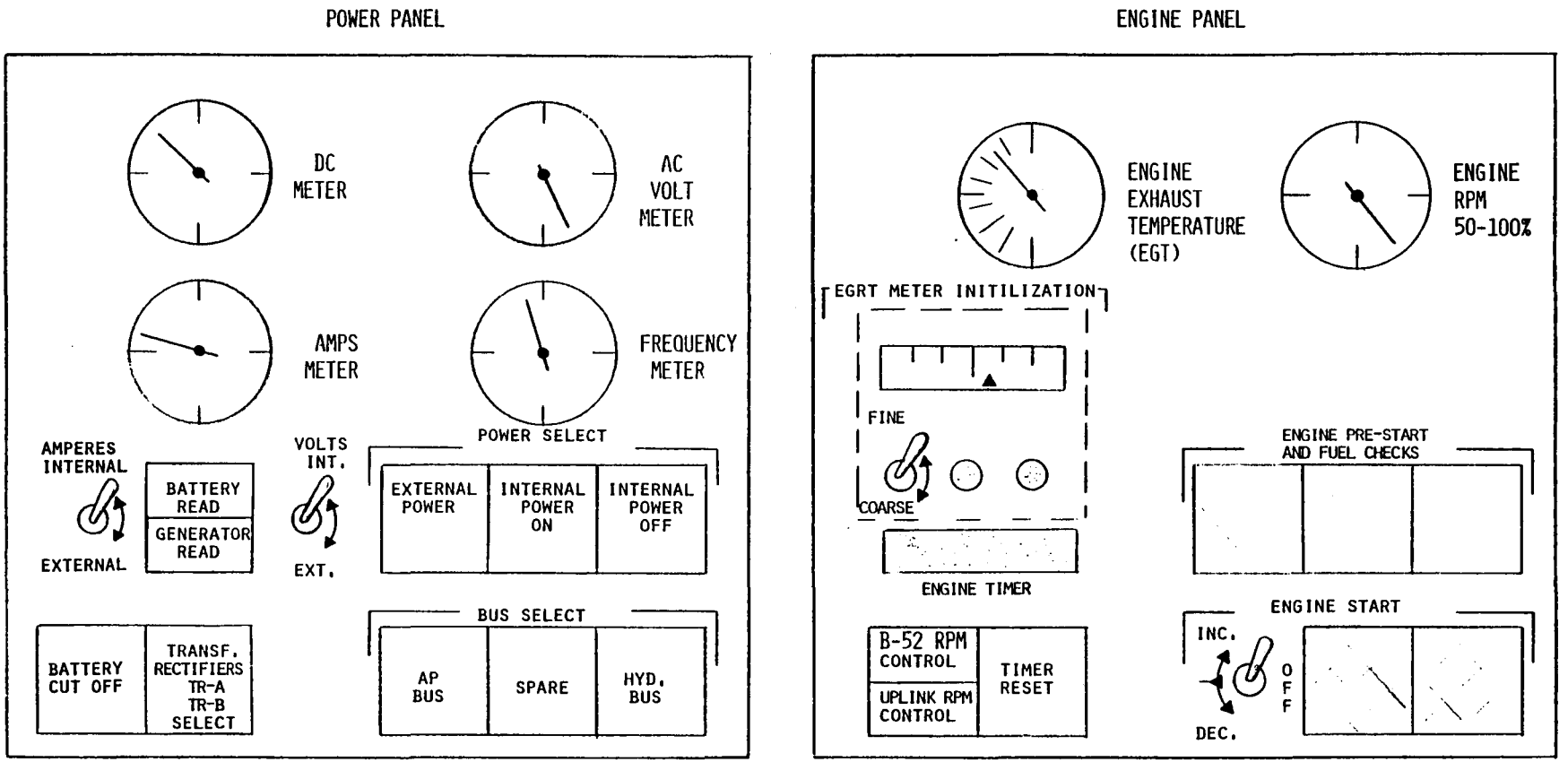

(a) Internal and external power control and monitor panel.

(b) Firebee II engine control and monitor panel.

Figure 4.14. Power and Firebee II engine panels.

In figure 4.15, the fuel top-off and MARS panels are shown. The first panel monitors the 303.0 l adaptor fuel tank. The fuel top-off system is also controlled through this panel. The fuel top-off feature is essential to this limited fuel endurance test vehicle because it provides the ability to launch the vehicle with full fuel tanks.

The MARS panel is utilized for recovery system check out. The guarded switch, when activated, results in the complete jettison of the recovery chutes. This is a safety feature in case chute deployment occurs while the vehicle is still attached to the B-52.

The flight control system panel is utilized to initiate discrete commands for onboard system checkout. The panel is shown in figure 4.16. The normal and emergency launch panels are also included in this figure.

Release of the drone is achieved by firing two explosive pins that connect the test vehicle and the minipylon.

4.5.2 F-104 Backup Command Station

According to Edwards AFB requirements, all powered RPRV drones need to have a backup command station that has the ability to control the drone in the event of uplink telemetry loss.

The DAST program utilizes a two seat F-104 aircraft as a backup station. From the rear seat of the aircraft, the backup controller utilizes two panels to generate the necessary commands. Both panels are shown in figure 2.23. The panel that initiates discrete commands and provides proportional throttle control is located on the left-hand side of the controller. The panel for proportional elevator

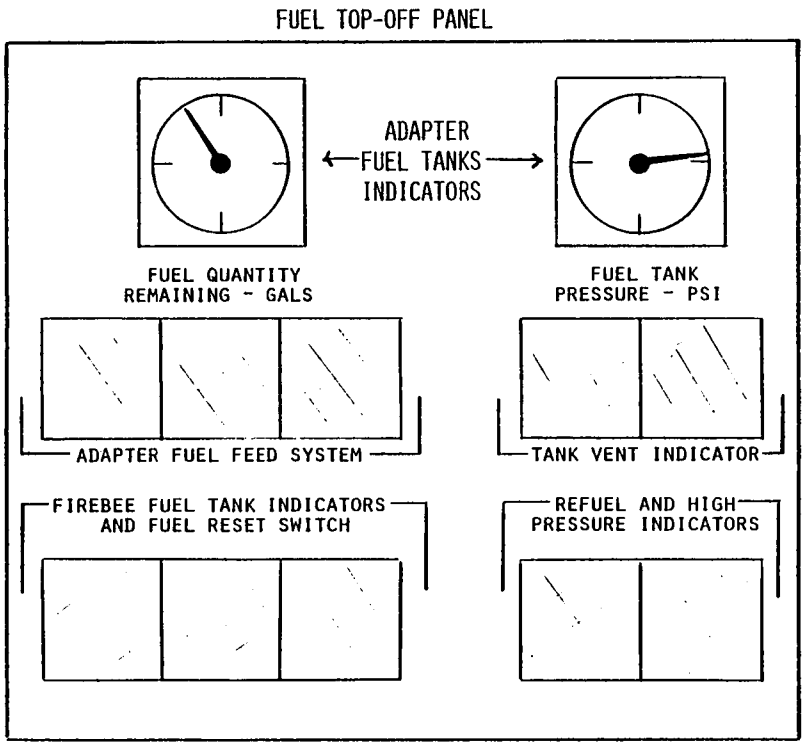

(a) Adapter fuel monitor and fuel top-off control panel.

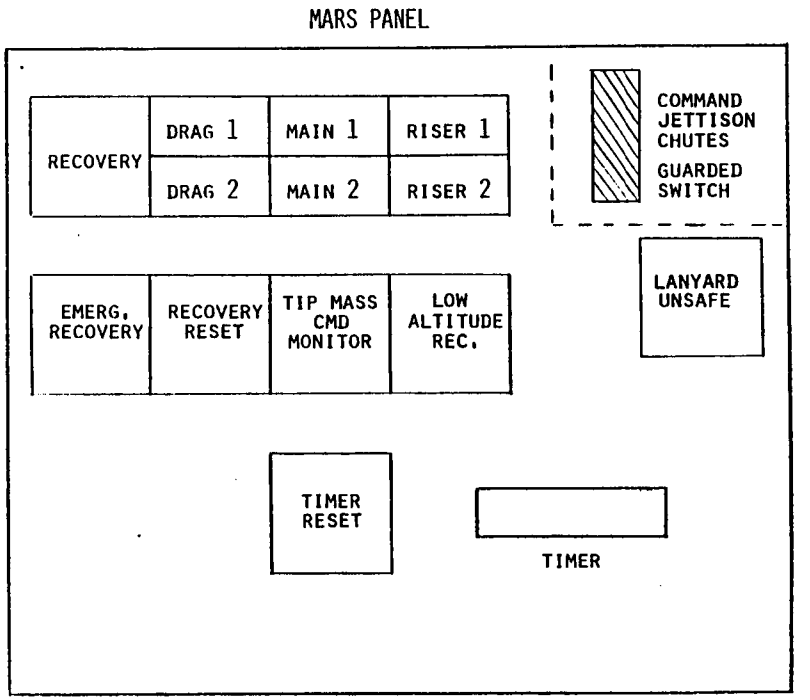

(b) Recovery system check out panel.

Figure 4.15. B-52 adapter fuel and MARS monitor panels.

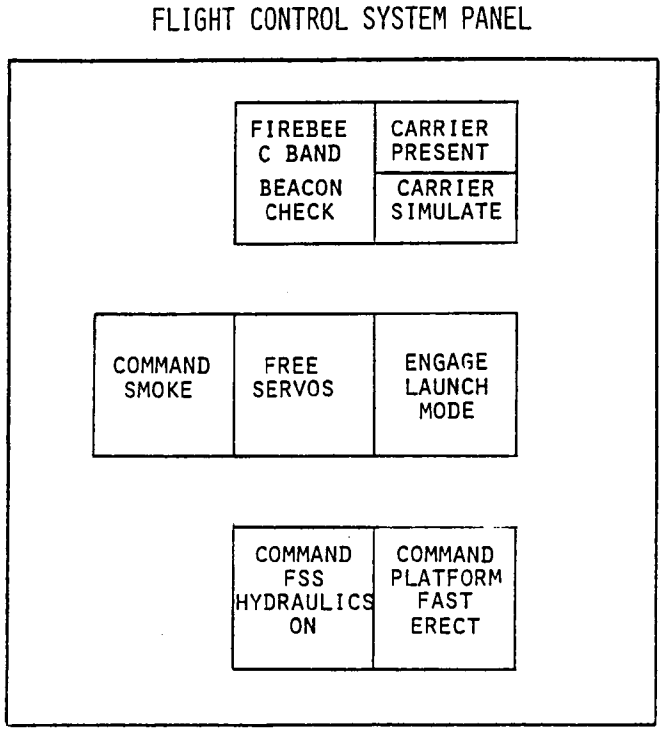

(a) Check-out panel for the Firebee II onboard control systems.

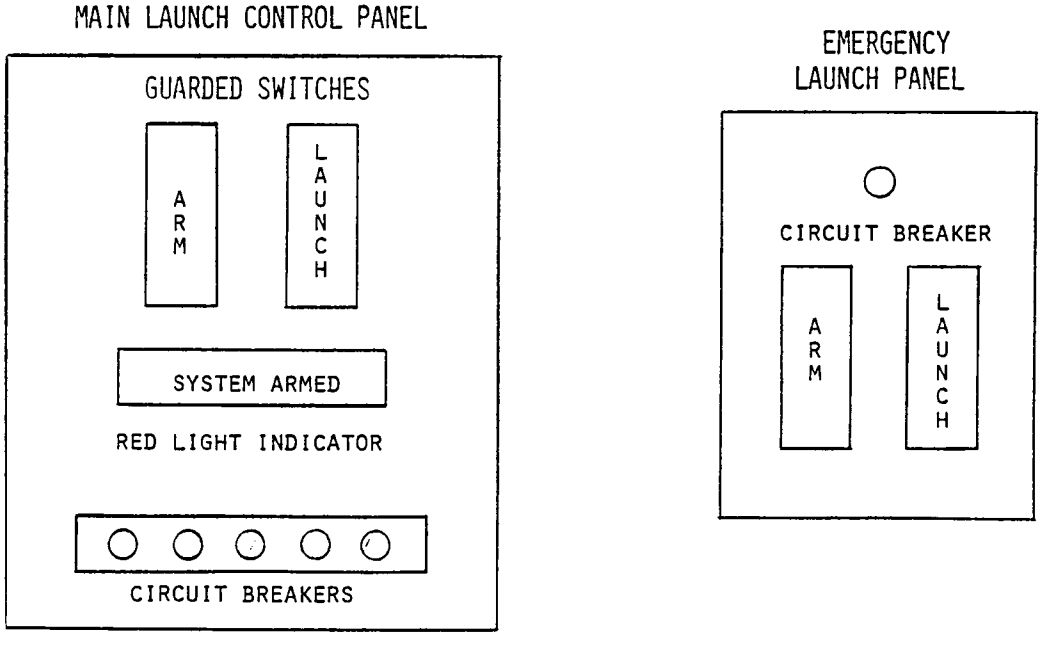

(b) Main and emergency launch panels.

Figure 4.16. Control system and launch panels.

and differential stabilizor commands is located on the right-hand side.

The discrete commands are:

- Transmitter, on/off
- Encoder, on/off
- Smoke, on/off
- Tip mass release, jettison/normal
- Recovery, normal/off/emergency
- Straight and level, reset/normal

Through the proportional elevator and aileron control panel, the controller has a limited authority of ±10 degrees in flight path angle and ±50 degrees in bank angle.

4.5.3 MARS Recovery Helicopter

A USAF CH-3E helicopter configured for mid-air recoveries is utilized by the DAST program. The helicopter is manned by a specially trained crew in such operations.

A normal recovery sequence is shown in figure 2.26. The helicopter crew performs a hook-up of the engagement chute that is directly connected to the vehicle through the load line. Load line hook-up will result in the release of the main chute and deployment of the stabilization chute. This chute will provide the needed stability while the helicopter is returning to the base from the recovery area. Finally, the vehicle is placed on an inflated landing pad that is meant to protect the fragile wings.

Following the main chute deployment, at an altitude of approximately 4,550 m, the vehicle assumes a descent rate of approximately

410 m/min. At this rate, the helicopter has approximately 8 minutes to perform a mid-air recovery. A maximum of three trials is feasible under normal conditions. The success rate of mid-air recoveries, as advertised by the USAF, is about 80 percent.

4.6 Communications

Communication between the ground facilities and aircraft involved in the DAST-I flight test operation is achieved through UHF two-way radio and intercom. In figure 4.17, a diagram is presented that shows the major communication channels. Communications between the flight controller, the ground-based test pilot and the supporting aircraft is obtained through UHF two-way radio. The FSS test engineer is also communicating in UHF frequency.

Two-way intercom channels are utilized for communication between the ground-based facilities such as the RPRV facility, the control room, and the SAF. Within a facility, direct voice control between research engineers is also an approved way of communication. A battery-powered UHF transceiver is used as a backup communication unit for the flight controller in case of a power failure.

UHF frequencies are assigned to the program upon request, made prior to each test flight. General telemetry and radar frequencies are given in table 4.4.

TABLE 4.4 TELEMETRY AND RADAR FREQUENCIES

Downlink Telemetry	
PCM-1	1441.5 MHz
PCM-2	1480.5 MHz
Uplink Telemetry	1804.5 MHz
FPS-16 Radar (C-band)	5660.0 MHz
IFF FAA Tracking	
Reception	1030 MHz
Transmission	1090 MHz

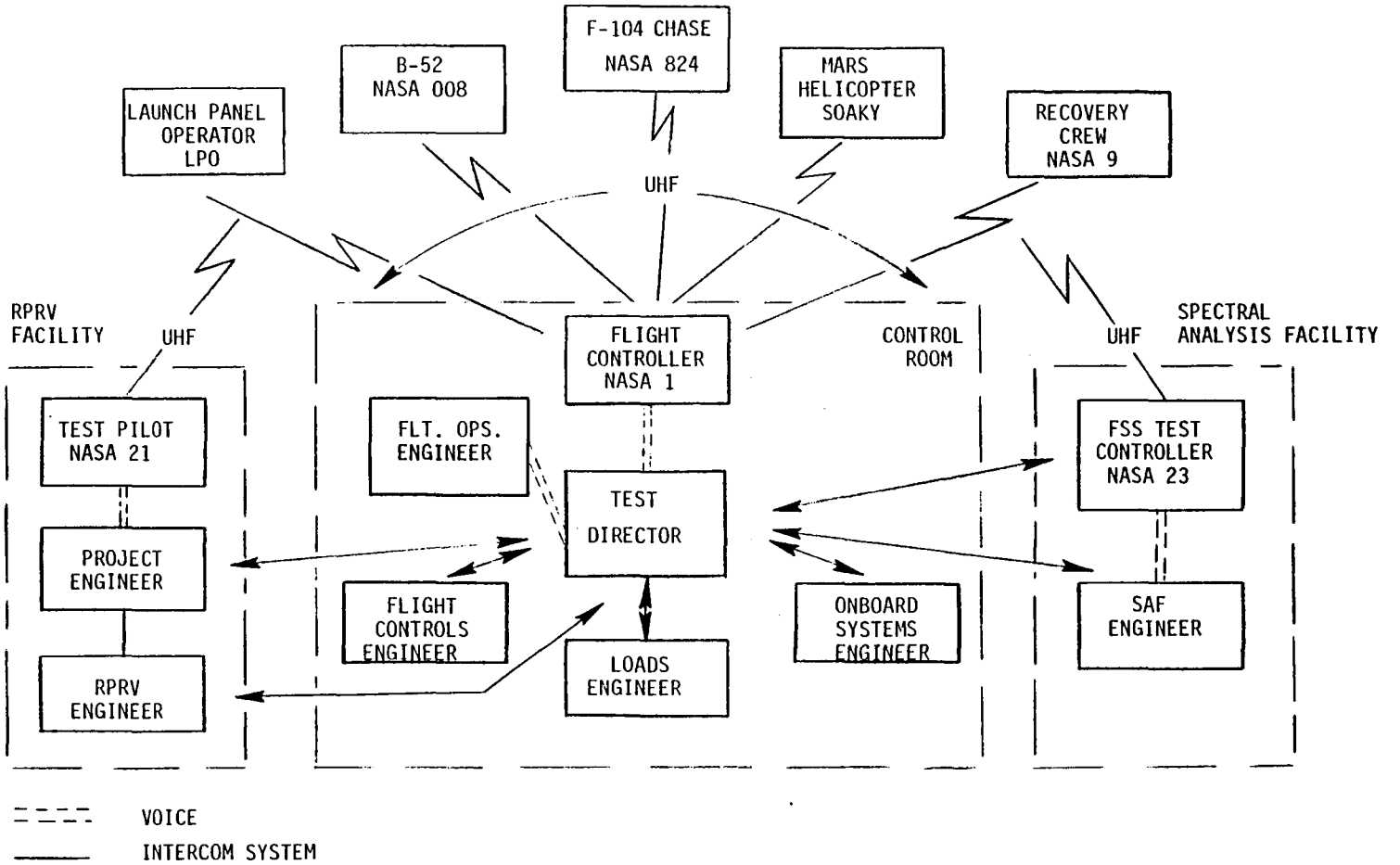

Figure 4.17. Communication channels between ground-based facilities and supporting aircraft systems.

CHAPTER 5

THE REMOTELY AUGMENTED VEHICLE (RAV) SOFTWARE DEVELOPMENT

Development and testing of the ground-based software is conducted in the simulation laboratory. A general purpose real time program is utilized for the development of the RAV flight control system and the validation of the test vehicle's flying qualities.

In this chapter a description is given of the simulation laboratory and the real time simulation capabilities this facility provides. The Cyber-73 and Varian real time programs are also described. The DAST-I ground-based software specification and testing are presented. A description of the DAST-I software control management is given.

5.1 The Simulation Laboratory

The simulation laboratory is located in the main building of the NASA Dryden Flight Research Center. The facility is utilized for the development and testing of the RAV control system, validation of the test vehicle's flying qualities, flight planning, and failure mode effects analysis. The laboratory also provides the ability to checkout and validate the actual flight tape that contains the RAV control system utilized in the RPRV facility during actual flight testing.

A layout of this facility is shown in figure 5.1. There are three cockpit stations linked to the Cyber-73 and Varian computers through special interface equipment. All three cockpits have interchangable side and front panels and are identical to the respective RPRV cockpits.

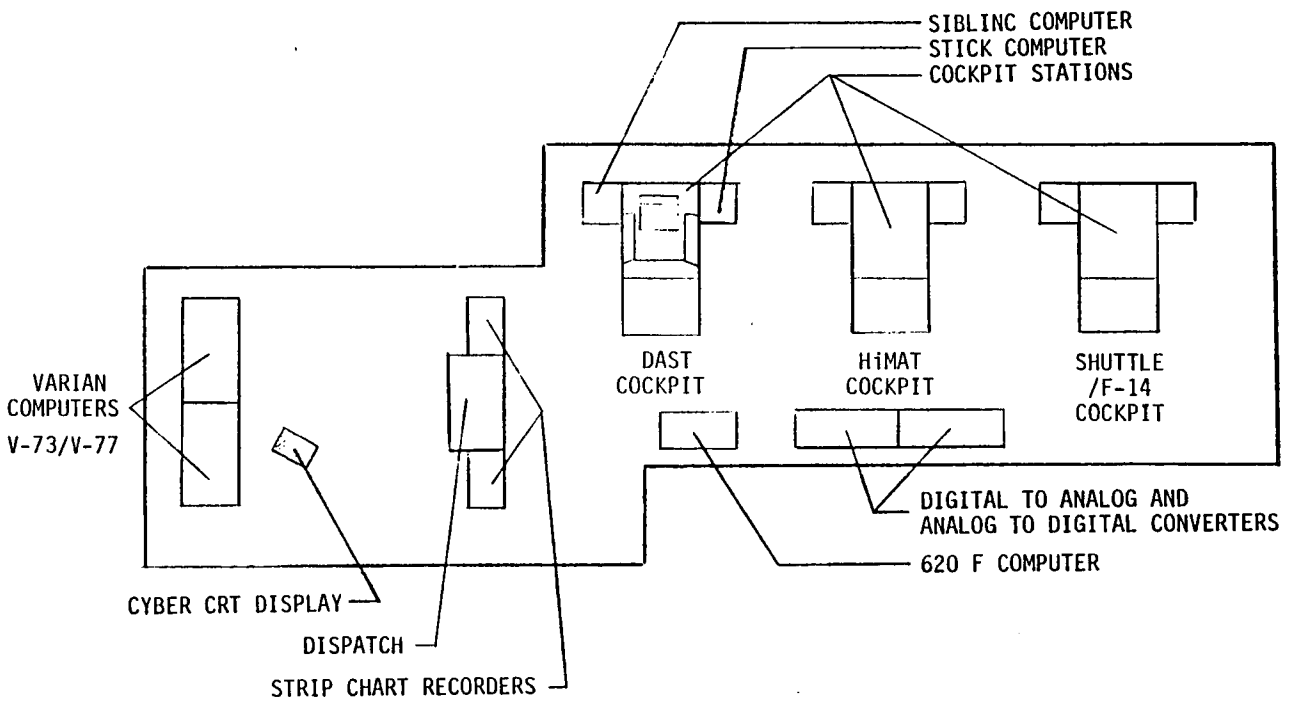

Figure 5.1. Layout of the simulation laboratory.

The Cyber-73 computer is utilized for the actual real time simulation. It has 131K 60-bit words of addressible memory.

The Varian computers, V-73 and V-77, have 32K 16-bit words of addressible memory each. These units are similar to the ones used in the RPRV facility. The dispatch system performs the necessary interface between the Varian and Cyber computers and the cockpit stations. Other systems such as the Siblinc interface computer, digtial-to-analog and analog-to-digital converters, buffers, and signal-conditioning equipment, are similar to the systems utilized in the RPRV facility.

The simulation laboratory provides basically two modes of operation for validation testing and flying qualities evaluation. These modes are known as the All-Cyber and Varian/Cyber configurations. In figure 5.2 a simplified diagram of the DAST-I flight test operation is compared with the two simulation configurations.

In the All-Cyber mode, the Cyber computer simulates the test vehicle along with the ground-based and onboard systems. In the Cyber/Varian configuration, the flight control system and cockpit instrument calculations are implemented in the V-73 computer. The V-77 computer simulates the decommutation of downlink parameters supplied by the Cyber. The interface between the cockpit station and the V-73 computer is representative of the interface in the RPRV facility.

The similarity between the simulation laboratory and RPRV facility allows the complete checkout and validation of the flight code that is utilized for RAV control during remotely piloted flight test operations.

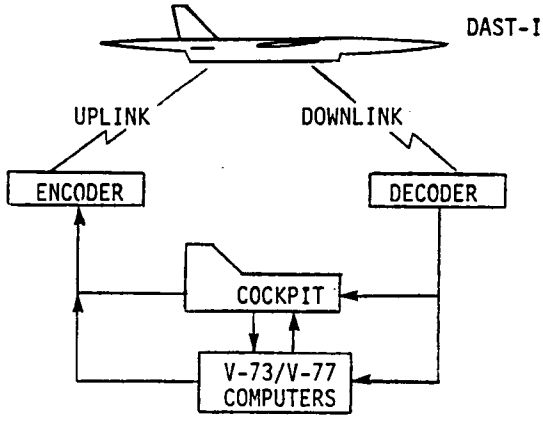

(a) Simplified RPRV operation.

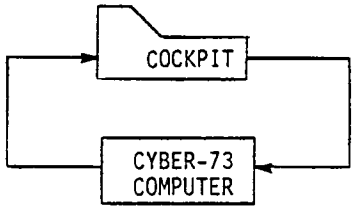

(b) All-Cyber configuration.

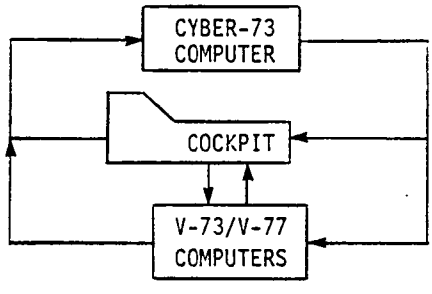

(c) Varian/Cyber configuration.

Figure 5.2. Simplified comparison between the actual flight test configuration and the real time simulation configurations.

5.1.1 Real Time Simulation Program

A simplified flow chart of the All-Cyber simulation program is presented in figure 5.3. This program consists of the following four major subsections:

- Non-real time initialization
- Primary loop
- Secondary loop
- Display functions

The first, non-real time, contains subroutines for the initialization of constants utilized in the real time sections of this program. It will also read and put into memory the aerodata package and the engine thrust and fuel flow tables.

The primary loop operates in real time and is subdivided into two sections. The first section simulates the test vehicle and the operation of all onboard systems. The second section includes control system and cockpit instrument calculations.

The primary loop has the highest execution priority. The secondary loop utilizes the remaining execution time. Calculations in the primary loop are updated every 18.75 milliseconds (msec). The secondary loop update rate is 56.25 msec. Both loops are driven by interrupts generated by the program itself.

The secondary loop performs the interface between the primary loop and the ground cockpit. A section of this secondary loop is utilized for real time print out.

The display functions code is a part of the real time program that is executed with the lowest priority. This program section allows the user to monitor the vehicle status in real time through a cathode-ray tube (CRT) display. It also provides the ability to

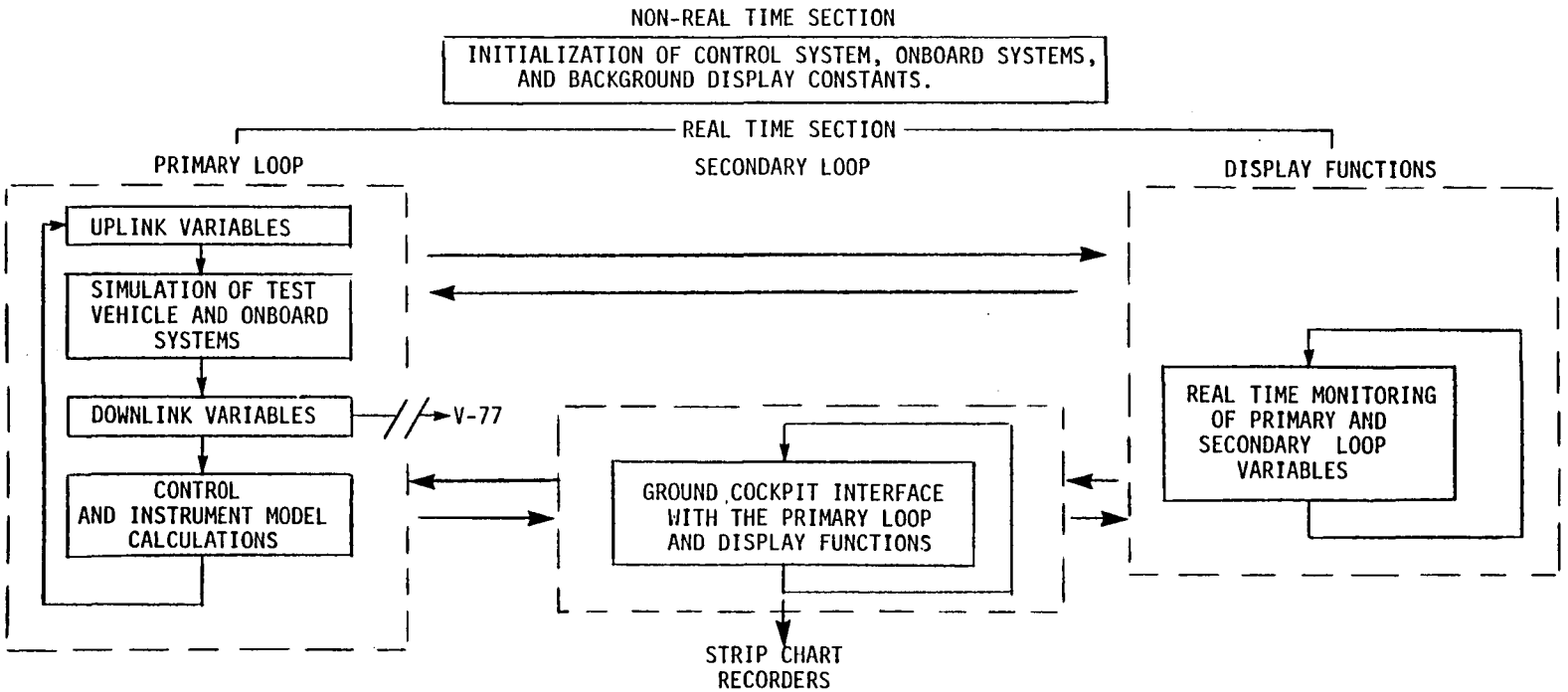

Figure 5.3. Simplified flow chart of the All-Cyber simulation program.

modify constants and initiate logic commands through the CRT display while the program operates in real time.

In the Varian/Cyber configurations, the control system and cockpit instrument calculations included in the primary loop will be executed by the V-73 computer. The output of the first section of the primary loop that simulates the test vehicle becomes the input to the V-77 computer. These data are equivalent to the downlink telemetry signal. The simulated downlink update rate is 18.75 msec.

A simplified flow chart of the program that is implemented in the V-73 computer is presented in figure 5.4. The actual code consists of two separate programs that run independently. The primary program contains the control law calculations while the secondary part of the code performs cockpit instrument calculations. Control law computations are performed on a split frame basis. The frame time is 18.75 msec. The V-73 receives an interrupt from the Babcock decoder every 9.375 msec. Within this time (split frame), part of the control system calculations are performed and the respective uplink commands updated. Calculations in the second part of the code are initiated upon reception of the following interrupt. The uplink signal will be fully updated every 18.75 msec.

Under normal operating conditions the computer will not utilize all 9.375 msec to compute each half of the control system. The remaining compute time from every split frame is used to calculate the secondary loop. Since the remaining time is a function of the amount of calculations performed in the primary loop, the actual time in which this secondary loop is calculated will be variable. The V-73 code checks the operation of the secondary loop. If the

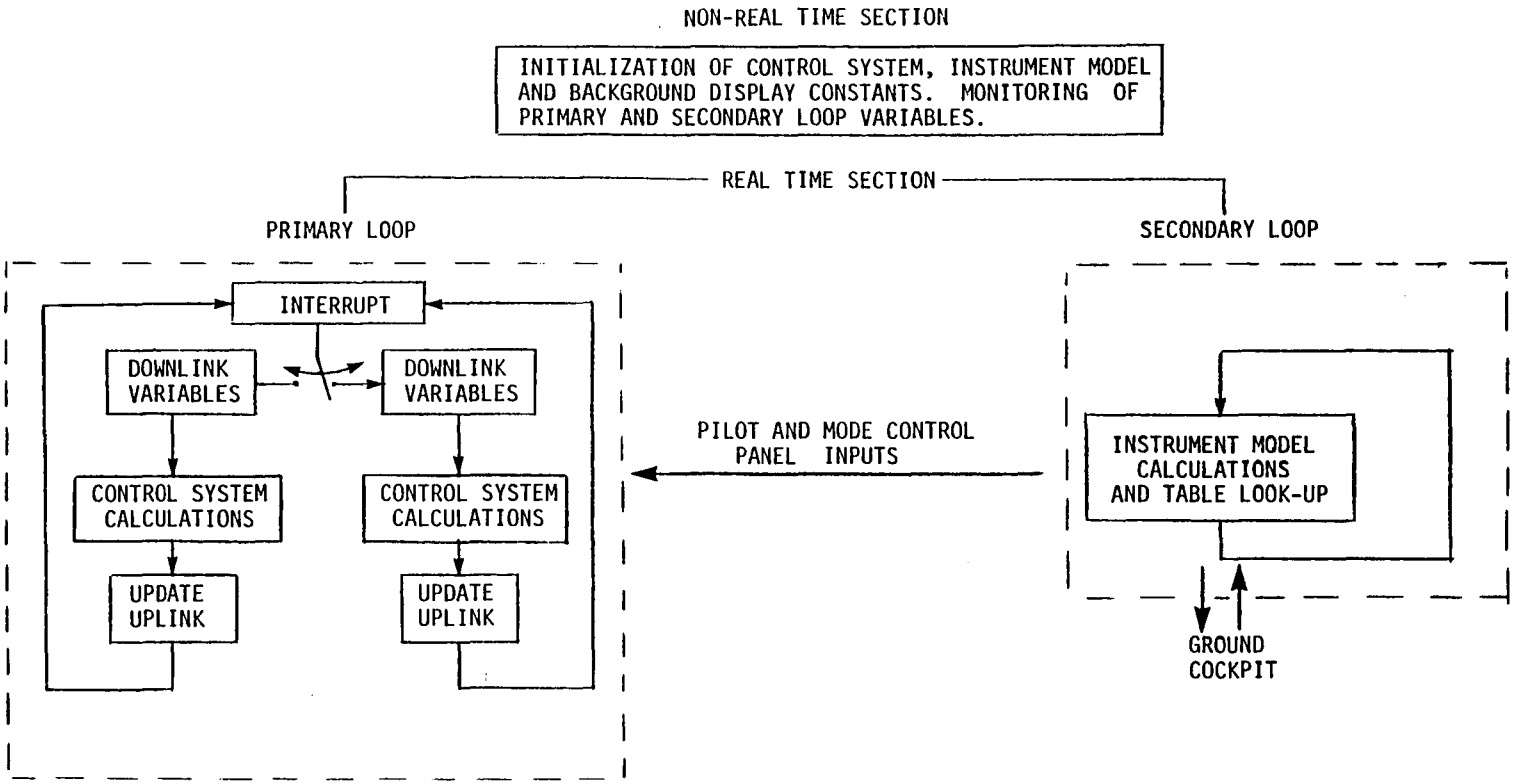

Figure 5.4. Simplified flow chart of the Varian program.

computations in this loop are not completed within 100 samples (1.875 sec) the computer will illuminate a computer fail light.

Because of the variable and low sample rate, the secondary loop contains functions that do not change rapidly with time.

The status of the control system and instrument calculations can be monitored through a CRT display only when the primary and secondary loops are not executed (out of real time).

5.2 RAV Software Specification

Software specification documents are generated to define special software requirements to be implemented in the Cyber simulation program and the V-73 Varian computer flight code. For the DAST-I the following specification documents were generated:

- Ground-based software
- Autopilot
- Recovery system and logic card

In this section a description is given of the ground-based software specification. The specification of the onboard systems is not presented since the respective documents reflect the descriptions given in section 2.4. The ground-based software specification document specifies the following areas:

- Background displays and initialization
- Real time functions
- Fault detection

A description of what is specified in each of the above areas is presented in the following sections.

5.2.1 Background Displays and Initilization

The simulation program provides the ability to monitor the real time operation through CRT displays. The background and initialization specification defines the information presented on these displays. It includes ground cockpit interface variables, downlink and uplink signals, initial conditions, and onboard system variables. Discrete and proportional signals are also included. In the All-Cyber configuration, the displays can be utilized while in real time operation. Display functions in the Varian program can only be monitored out of real time. This is done to keep the available computation time for the control system and instrument model to a maximum.

Initialization is a part of the Cyber and Varian program that is executed once prior to entering real time. The document specifies the values at which control system constants, such as feedback gains, limits and constants of the background displays, will be initialized.

The Cyber initialization code includes also subroutines for the initialization of onboard systems such as the autopilot and the recovery system. Discrete signals are also initialized in this part of the program.

5.2.2 The Real Time Functions

The real time functions are elements of the Cyber and Varian program that are included in the real time loop. The functions specified are:

- Input/Output Interface

- Cockpit Display Computations
- Real Time Analog Output
- Control Laws
- Pulse Panel
- Mode Switching And Fading

A simplified description of the specification of the above items follows:

The Input/Output Interface specification includes the proportional and digital downlink variables which form the input to the V-73 computer and uplink commands generated by the timing and control system. The DAST-I downlink parameters are shown in table 5.1. The uplink word is presented in figure 5.5.

TABLE 5.1 PROPORTIONAL AND DISCRETE DOWNLINK PARAMETER INPUTS TO THE VARIAN-77 COMPUTER

Symbol	Parameter proportional	RANGE
PHI	Bank angle	±180 deg
THA	Pitch angle	±80 deg
THAF	Pitch angle fine	±20 deg
P	Roll rate	±100 deg/sec
Q	Pitch rate	±60 deg/sec
R	Yaw rate	±40 deg/sec
ALP	Alpha	-12, +30 deg
AN	Normal acceleration	-3, +6 g
AX	Longitudinal acceleration	-1, +1 g
PSI	Static pressure	0-105 kgf/cm^2
QCI	Differential pressure	0-70.3 kgf/cm^2
FFR	Fuel flow	1.47, 23.6 kg/min
	DISCRETE	
TOPOFF	Fuel quantity reset	
LAUNCH	Launch	
AP	Autopilot	

	BITS 0 THROUGH 9	10	11	12	13	14	15
WORD 1	LEFT HAND STAB.	RECOVERY 1 (OFF)	AP CMD 0 (OFF)	EXCITATION ANTI-SYMMETRIC 1 (OFF)	CAMERA ON 0 (OFF)	FSS ON 1 (OFF)	PULSE ON 0 (OFF)
WORD 2	RIGHT HAND STAB.	EMERGENCY RECOVERY 1 (OFF)	TIP MASS EJECTION 0 (OFF)	FILTER IN 1 (OFF)	SMOKE 0 (OFF)	EXCITATION AMP. HIGH 1 (OFF)	SWEEP ON 0 (OFF)
WORD 3	RUDDER	RECOVERY 0 (OFF)	AP CMD 1 (OFF)	EXCITATION ANTI-SYMMETRIC 0 (OFF)	CAMERA ON 1 (OFF)	FSS ON 0 (OFF)	PULSE ON 1 (OFF)
WORD 4	THROTTLE	EMERGENCY RECOVERY 0 (OFF)	TIP MASS EJECTION 1 (OFF)	FILTER IN 0 (OFF)	SMOKE 1 (OFF)	EXCITATION AMP. HIGH 0 (OFF)	SWEEP ON 1 (OFF)

	RANGE
LEFT HAND STAB. δ_{h_l}	-7° to 12°
RIGHT HAND STAB. δ_{h_r}	-7° to 12°
RUDDER δ_r	$\pm$10°
THROTTLE THR	70 to 100 percent rpm

Figure 5 5. Uplink word format.

The specification of the Cockpit Display Computations defines the variables to be calculated in the secondary loop and be displayed on the ground cockpit instrument panel. In table 5.2 the instrument model calculations are presented.

The Real Time Analog Output specification defines the internal program variables that are required for monitoring purposes.

Specification of the Control Laws defines the control system calculations to be implemented in the primary computation loop. In section 5.3 a detailed description of the DAST-I control system calculations is presented.

The Pulse Panel is an option of the RAV system that provides the ability to add computer-generated step commands to the proportional outputs of the V-73 computer. Specification of the Pulse Panel defines four selectable step values for each proportional uplink word.

The Mode Switching and Fading specification defines the type of technique to be used to suppress transients caused by mode switching. For the DAST-I, a two-second fader is applied to all proportional uplink commands. Proper control system initialization and also reduce transients control system initialization will be applied whenever possible.

5.2.3 Fault Detection

Fault detection is required by the RAV system to prevent various failures from endangering the test vehicle.

The following fault detection schemes were specified for the DAST-I RAV operation:

Downlink checks were specified to protect the RAV system from sensor

failures, spurious signals, and possible signal loss. There is a rate and a limit check.

The rate check is performed on all V-73 downlink parameters prior to engineering unit conversion. The rate limit is set to 100 counts per 100 milliseconds. (The usual full range of a downlink parameter is equivalent to 1024 counts.)

The limit check prevents downlink parameters from exceeding the predefined range limits as shown in table 5.1.

TABLE 5.2 INSTRUMENT MODEL CALCULATION

Mach Number Subsonic: $\frac{P_t}{P_s} \leqq 1.893$	$M = \sqrt{5\left[\left(\frac{P_t}{P_s}\right)^{2/7} - 1.0\right]}$
Supersonic: $\frac{P_t}{P_s} > 1.893$	$M = .88128\sqrt{\left(\frac{P_t}{P_s}\right)\left(1 - \frac{1}{7M^2}\right)^{5/2}}$
Airspeed, m/sec	$KCAS = 761\sqrt{\left(\frac{P_t - P_s}{101325.} + 1.0\right)^{2/7} - 1.0}$
Altitude, m	$HP = -44332.\left[\left(\frac{P_s}{10332.}\right)^{.19026} - 1.0\right]$ $HP = 11000. - 6341.6\ \ell n\left(\frac{4.47712\ P_s}{10332.}\right)$
Altitude Rate, m/sec	$\dot{HP} = HP\left(\frac{10}{s + 10}\right)\left(\frac{s}{s^2 + 1.414s + 1.0}\right)$
Flight path acceleration, g	$FPA = (AX - \sin\theta)^* \cos\alpha - (AN - \cos\Theta * \cos\Phi) * \sin\alpha \left[\frac{1}{1 + \left(\frac{1.414}{3.1416}\right)s + \left(\frac{s}{3.1416}\right)^2}\right]$

Computer system checks are performed to prevent V-73 and/or V-77 failures from endangering the test vehicle.

The time-out counter is implemented in the V-73 code, and is designed to detect asynchronous operation between uplink and downlink. If such a situation is detected for a consecutive number of frames, the computer fail light will be illuminated.

The heartbeat monitor is a hardware device external to the computer, designed to detect V-73 failures. This system, also known as the missing pulse detector, receives a pulse from the V-73 every time an uplink interrupt is sent to this computer. The heartbeat monitor will illuminate the computer fail light if the V-73 computer fails to generate a pulse within a preset time interval.

The autopilot and computer fail circuitry is a hardware system external to the Varian computers. The system is designed to down mode remote control by disengaging the RAV system. Down moding will take place when the heartbeat monitor detects a computer failure or when the V-73 acknowledges onboard autopilot engagement. This feature will result in proper RAV control system reengagement whenever one of the above failures would occur temporarily during flight.

5.3 Ground-Based Control System Design and Characteristics

The original RAV control system reguirements for the DAST-I test vehicle were:

- Achieve level 1 flying qualities (MIL-8785B) in all axes at all flight conditions.
- Control the unstable pitchup characteristics of the unaugmented vehicle.

- Prevent the vehicle from exceeding the 2.5 g structural wing load limit.

The primary objective of the above requirements is to decrease the pilot's workload and prevent the vehicle from exceeding aerodynamic and structural limits.

Additional RAV control system requirements called for the design of an altitude hold and bank angle hold mode. Both modes are expected to further decrease the pilot's workload and enhance his ability to maintain constant flight conditions during FSS testing.

Most of the design requirements were met by developing the ground-based control system presented in this section.

A load limiter was developed and initially utilized during the first ARW-I flight, but was later deleted as it was determined that the pilot had good load factor control within the flight envelope and that deletion of this system would simplify the complexity and improve the characteristics of the control system. A description of the control system with the load limiter is presented in appendix B.

Control of the unstable pitchup characteristics was not obtained by means of an angle of attack limiter. Instead, an angle of attack warning system (audio buzzer) was designed. This warning system will be engaged whenever α exceeds the 6 degree limit.

The DAST-I flight control system is implemented as a digital system in the Cyber and Varian programs. Linear analysis was conducted in the z-plane. In order to simulate the time delays introduced by the asynchronous operation of onboard and ground-based systems, and signal processing equipment, a time delay of two samples (37.5 msec) was incorporated in the calculations.

A description of the DAST-I control system and its characteristics follows:

Longitudinal Axis

The RAV system can be selected through the mode control panel shown in figure 4.6. In the longitudinal axis the pilot has the ability to select four different modes.

The Computer Direct (CD) mode is automatically engaged when the RAV system (computer) is selected. The pitch axis control system is shown in figure 5.6. This figure indicates that the CD mode does not provide any augmentation. The computer allows the implementation in this mode of non-linear longituding stick gearing.

The Rate Damper (RD) mode provides pitch axis augmentation through pitch rate feedback. The feedback gain is selectable through the mode control panel. The lead-lag filter is a compensation term for the time delay introduced by the Varian computer. Linear analysis results are presented in figure 5.7. The s-plane root locations were determined by transforming the equivalent z-plane results. The figure shows the effect of the selectable pitch rate gain. In general, an increase in feedback gain will increase the damping of the short period. The phugoid is less sensitive to pitch rate feedback gain variation.

The Attitude Hold (ATTH) mode, shown in figure 5.6, provides pitch attitude feedback. Pitch attitude control is achieved through an integrator driven by a ground cockpit switch. The ATTH mode is initialized at the moment of engagement. The integrator output is set to zero and the pitch attitude value at the moment of engagement is subtracted as a constant from the pitch attitude feedback path.

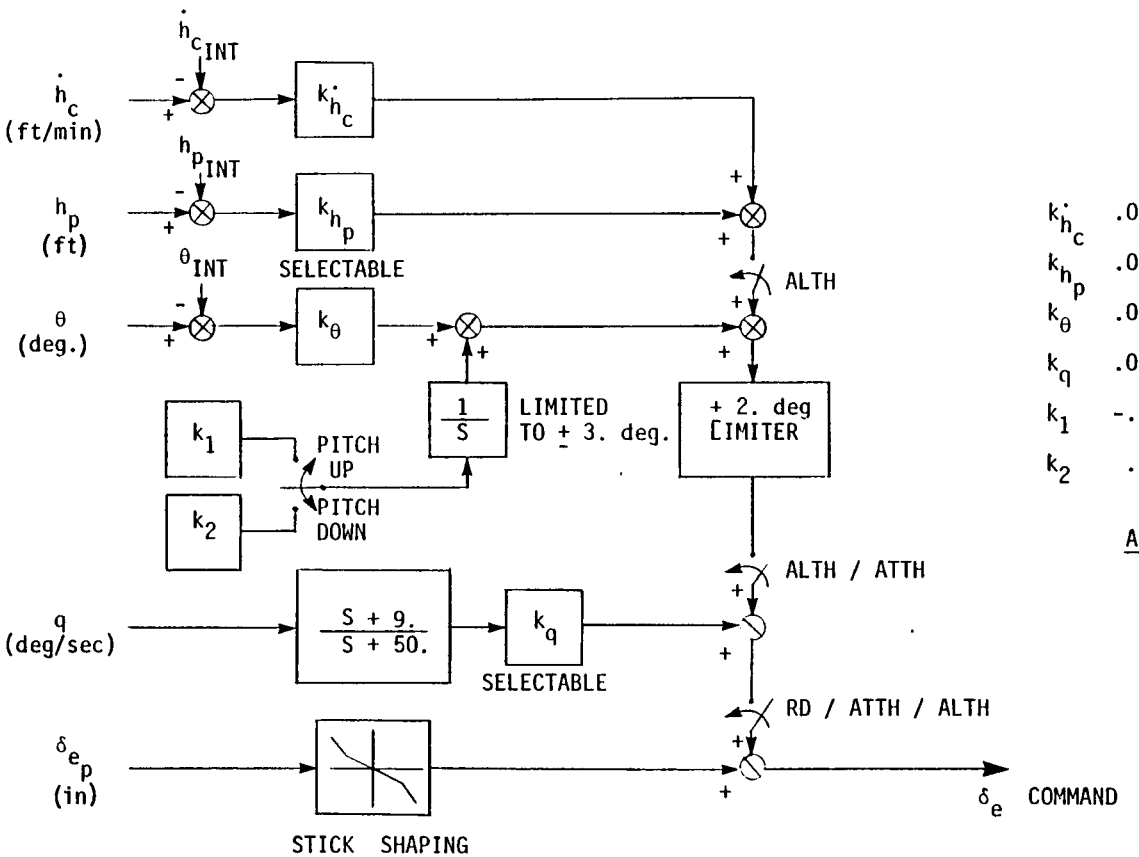

FEEDBACK GAIN VALUES

$k_{\dot{h}_c}$	.0002 (deg/ft min^{-1})
k_{h_p}	.0001/.0002/.0003/.0004 (deg/ft)
k_θ	.025 (deg/deg)
k_q	.05/.10/.15/.20 (deg/deg sec^{-1})
k_1	-.1 (deg sec)
k_2	.1 (deg sec)

ALTITUDE RATE CALCULATION

$$\dot{h}_c = V_T * (\theta - \alpha * \cos \phi)$$

Figure 5.6. Pitch axis control system.

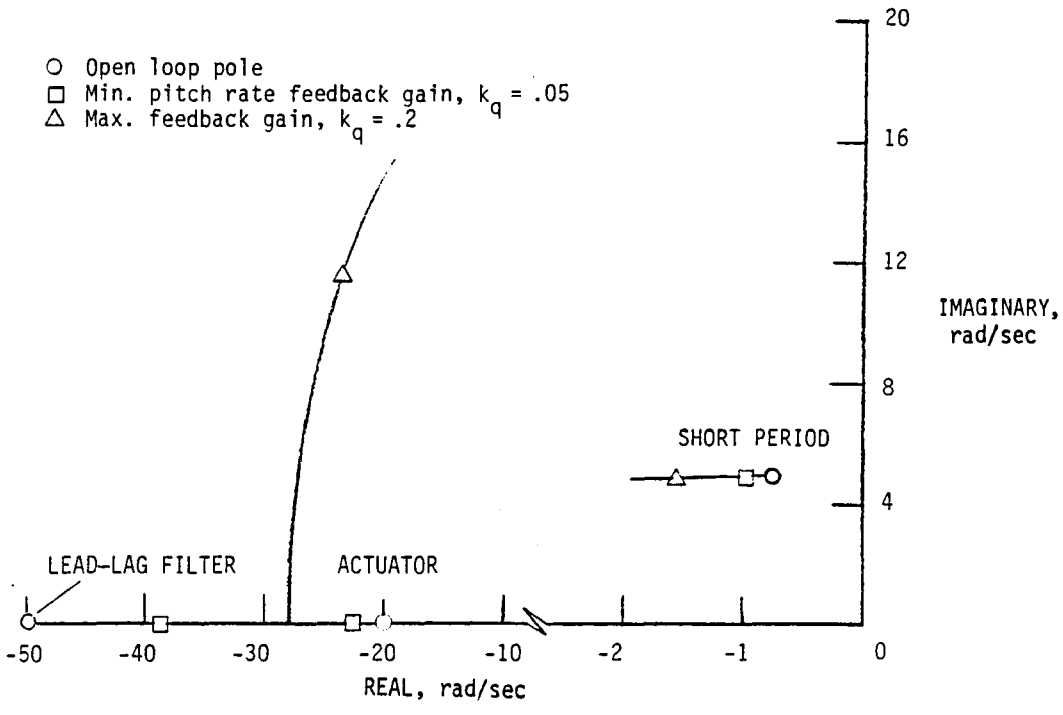

(a) Root locus.

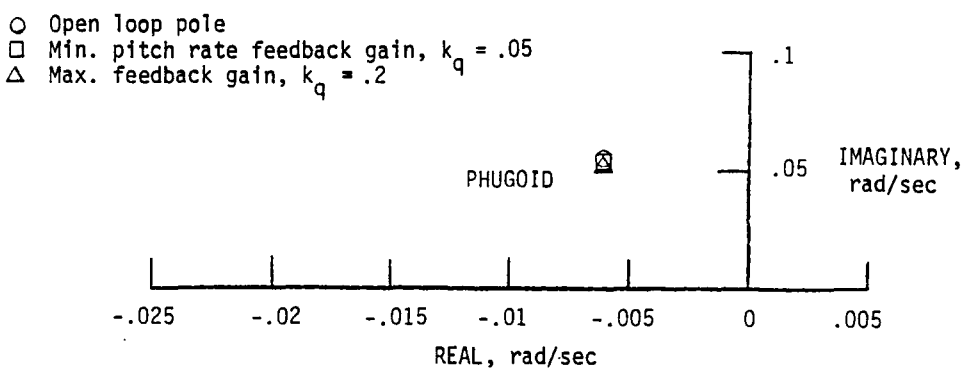

(b) Expanded view of root locus near origin.

Figure 5.7. Pitch rate damper mode root locus for maximum and minimum pitch rate feedback gain at full fuel conditions. W = 1008 kg; c.g. = 264.4 F.S.; h = 6096 m; Mach = 0.8.

Attitude corrections can be obtained through the constant rate integrator. The integrator output is limited to ±3 degrees. The rate is equal to .1 deg/sec. The output of the ATTH path is limited to ±2 degrees. This mode is designed to be used while changing altitude conditions. Altitude changes can be achieved in this mode by using either trim inputs or the attitude command integrator.

Linear analysis results are presented in figure 5.8. Root locations are given for a series of Mach numbers at two different altitudes.

The Altitude Hold (ALTH) mode is the most complex mode since it engages all previous modes. It provides in addition to pitch an attitude feedback, altitude and altitude rate feedback. The altitude feedback gain is selectable through a switch located on the left-hand side panel. The system is designed to maintain constant altitude. In this mode most of the FSS testing is conducted.

The altitude rate feedback signal is computed as follows:

$$\dot{h} = V_t * (\theta - \alpha * \cos \Phi) \qquad (5.1)$$

where

$\dot{h}$ altitude rate, ft/min

V_t true airspeed, ft/min

θ pitch attitude, rad

α angle of attack, rad

Φ bank angle, rad

The cosine term is a bank angle compensation term for altitude rate. This term will approximate the true altitude rate while the vehicle is in a turn.

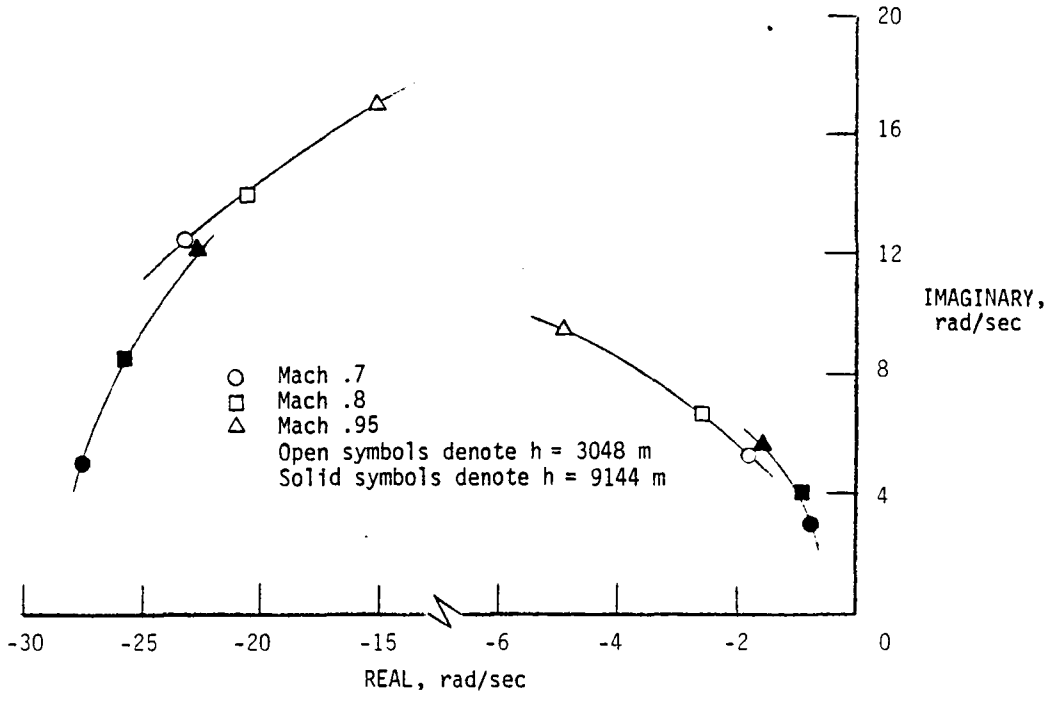

(a) Root locus.

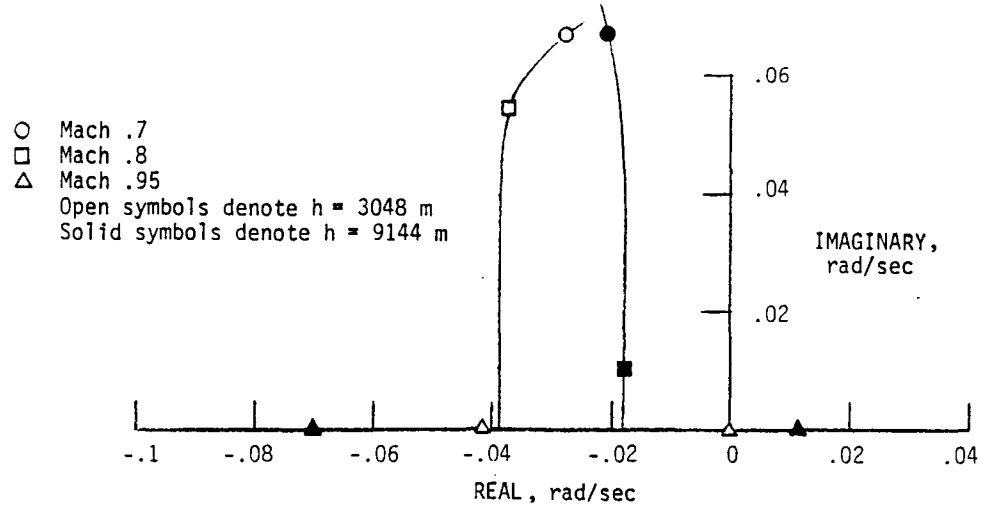

(b) Expanded view of root locus near origin.

Figure 5.8. Attitude hold mode root locus at selected flight conditions. W = 1008 kg; c.g. = 264.4 F.S.; k_q = .2.

Both altitude and altitude rate signals will be initialized at the engagement of the ALTH mode. This is achieved by subtracting the value of the input signal at the moment of engagement as a constant from the feedback path. In the ALTH mode the pitch attitude, altitude, and altitude rate paths are limited to ±2. degrees.

Linear analysis results are presented in figure 5.9. The root locations for several selected altitude and Mach conditions are presented.

In figure 5.10, open and closed loop root locations for full and empty fuel conditions are presented. This figure shows that the ATTH and ALTH modes improve the open loop characteristics of the vehicle. There is a considerable increase in phugoid frequency as a result of the altitude and altitude rate feedback. For all cases the decreasing fuel quantity will result in a slight increase in damping and decrease in frequency.

Lateral-Directional Axes

There are three selectable computer modes in the roll axis. The roll axis control system block diagram is shown in figure 5.11.

The Computer Direct mode is automatically selected upon RAV system engagement. This mode does not provide any augmentation. A non-linear gearing schedule for lateral stick inputs is implemented.

The Rate Damper mode provides augmentation in the roll axis through roll rate feedback. A gain switch located on the mode control panel provides four selectable roll rate feedback gains. Linear analysis results are given in figure 5.12. This figure shows the anticipated increase in roll mode damping achieved through roll rate feedback. The dutch roll and spiral modes are hardly a function of the variable feedback gain.

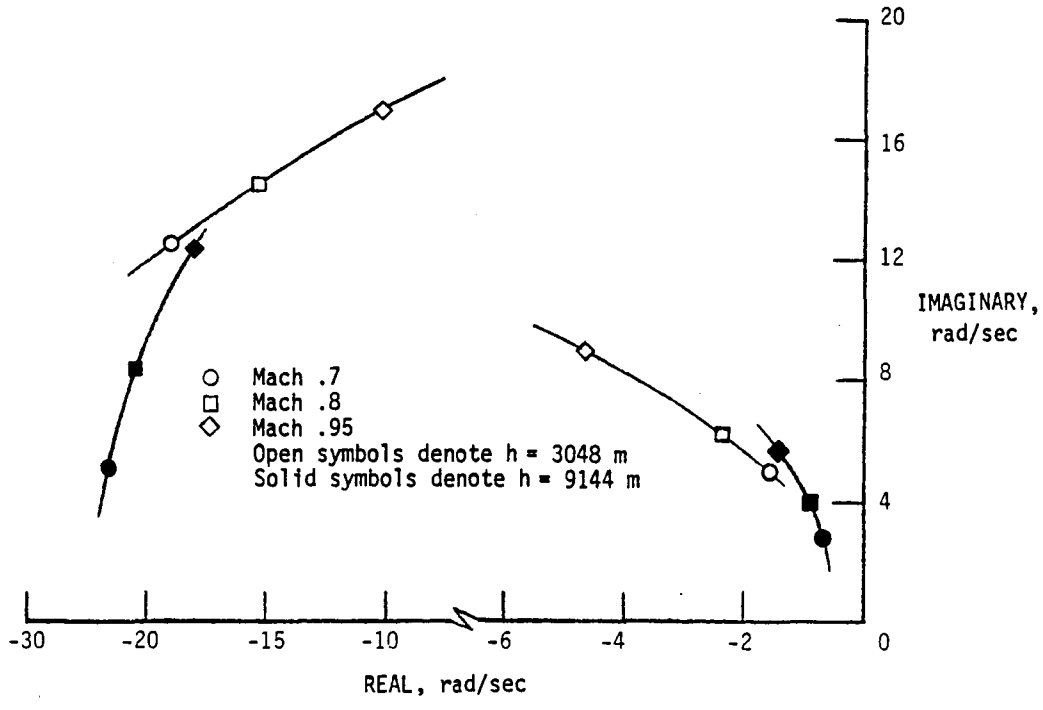

(a) Root locus.

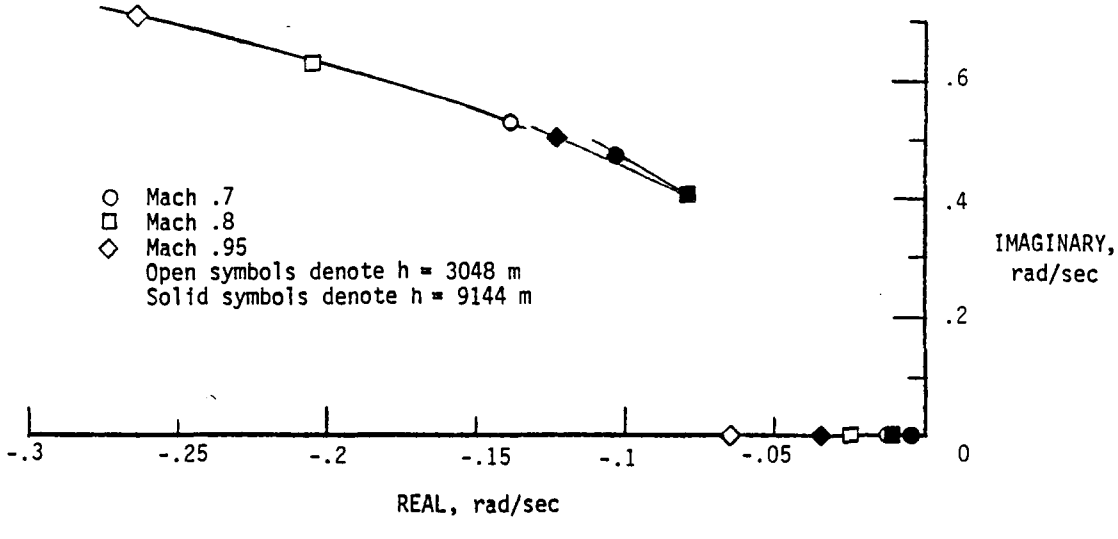

(b) Expanded view of root locus near origin.

Figure 5.9. Altitude hold mode root locus at selected flight conditions. W = 1008 kg; c.g. = 264.4 F.S.; k_q = .2; k_h = .0002.

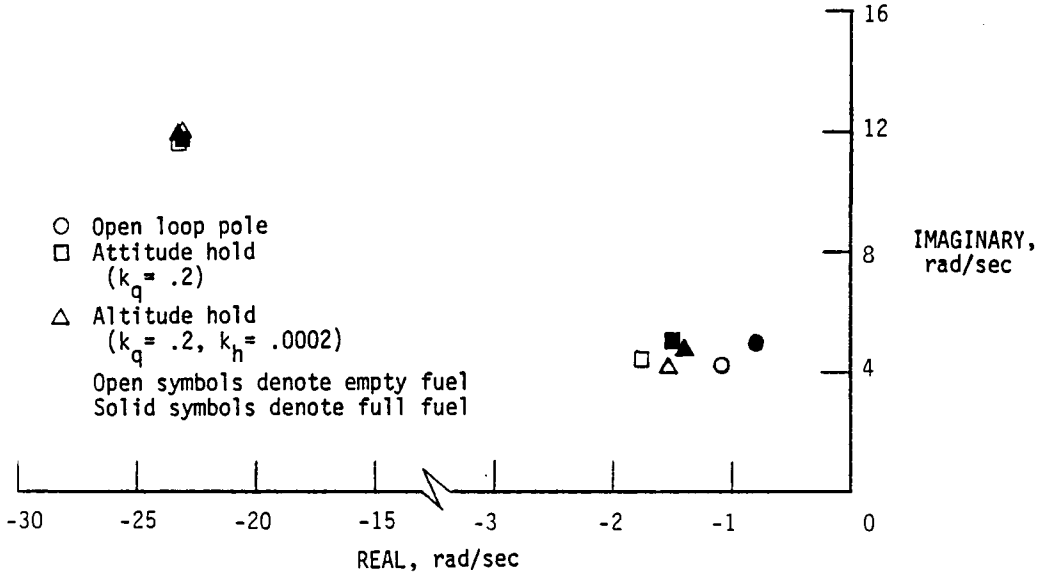

(a) Root locus.

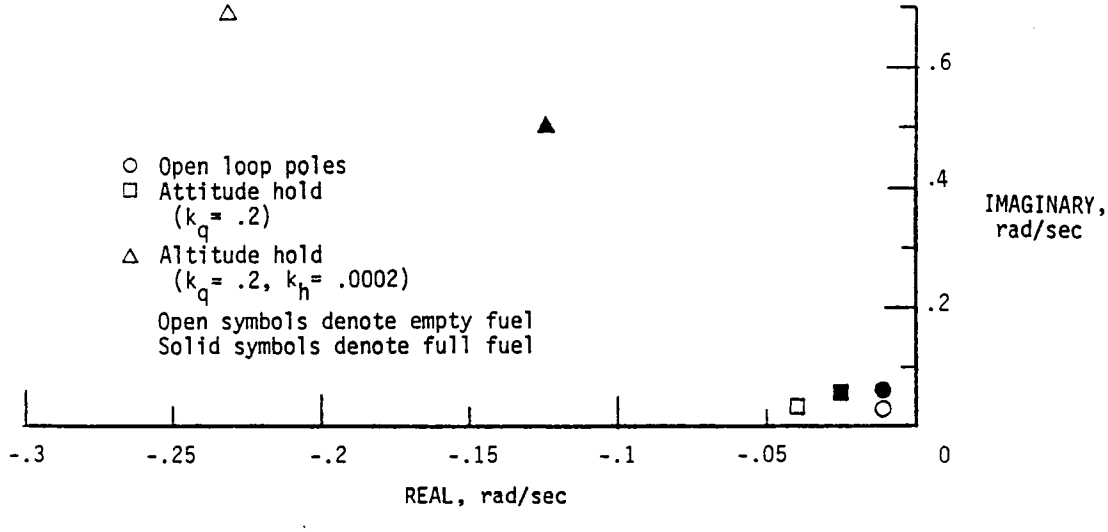

(b) Expanded view of root locus near origin.

Figure 5.10. Attitude and altitude hold mode root locations at full and empty fuel conditions. At full fuel W = 1008 kg, c.g. = 264.4; at empty fuel W = 870 kg, c.g. = 268.0 F.S.; Mach 0.8; h = 6096 m.

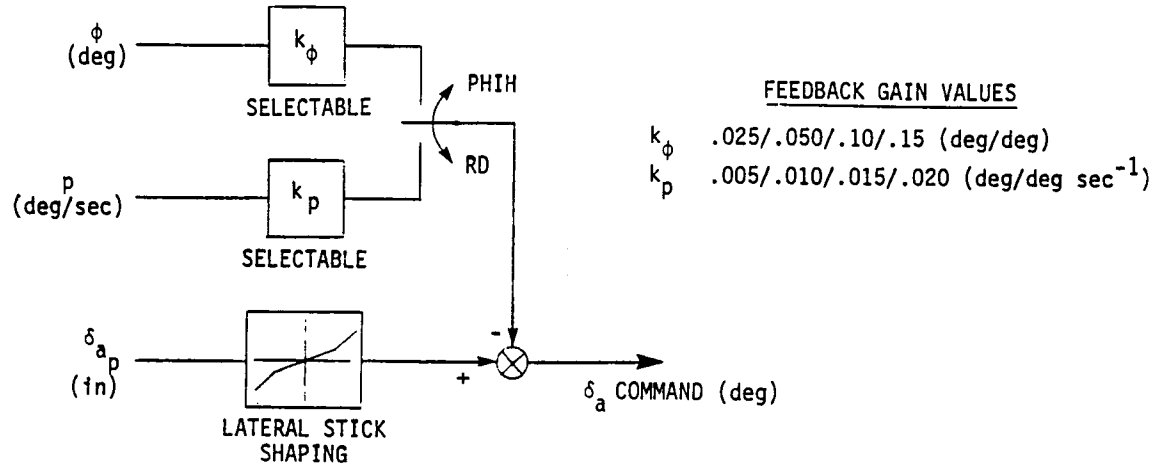

Figure 5.11. Roll axis control system.

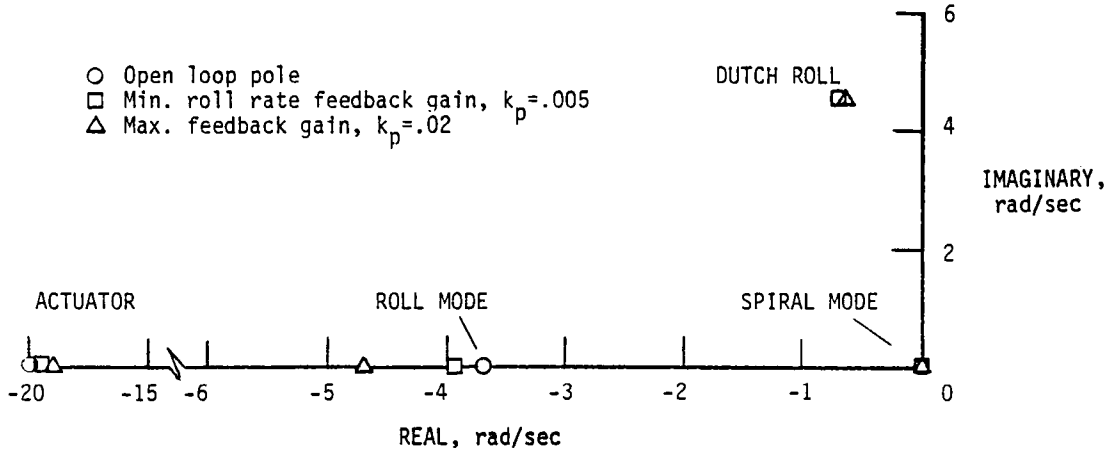

Figure 5.12. Roll rate damper mode root locus for maximum and minimum roll rate feedback gain. Mach = 0.8; h = 6096 m.

The Bank Angle Hold mode provides a wings-leveling capability that decreases the pilot's workload during straight and level flight. When this mode is selected, the roll rate feedback path is cut off while the variable roll rate feedback gain switch controls the variable bank angle feedback gain.

Linear analysis results, shown in figure 5.13, indicate the anticipated increase in spiral mode damping as a result of the increasing bank angle feedback gain. The roll mode time constant increases with increasing feedback gain. For the highest feedback gain, the spiral and roll mode form a complex set of poles (lateral phugoid). Dutch roll damping slightly increases with increasing bank angle feedback.

In the yaw axis, the control system provides only two selectable modes. The yaw axis block diagram is shown in figure 5.14.

In Computer Direct the computer implemented gearing schedule is linear and similar to the Babcock direct schedule. No augmentation is obtained in this mode.

The Rate Damper mode, shown in figure 5.14, provides yaw rate feedback with a selectable feedback gain. The gain switch is located on the mode control box. The washout filter in this feedback path is implemented to eliminate control system inputs in turns and constant yaw rate manuevers. Linear analysis results, presented in figure 5.15, show a considerable increase in dutch roll damping with increasing yaw rate feedback gain. A slight increase in roll mode damping is also obtained.

Throttle Control

Whenever the RAV system is engaged, throttle commands are

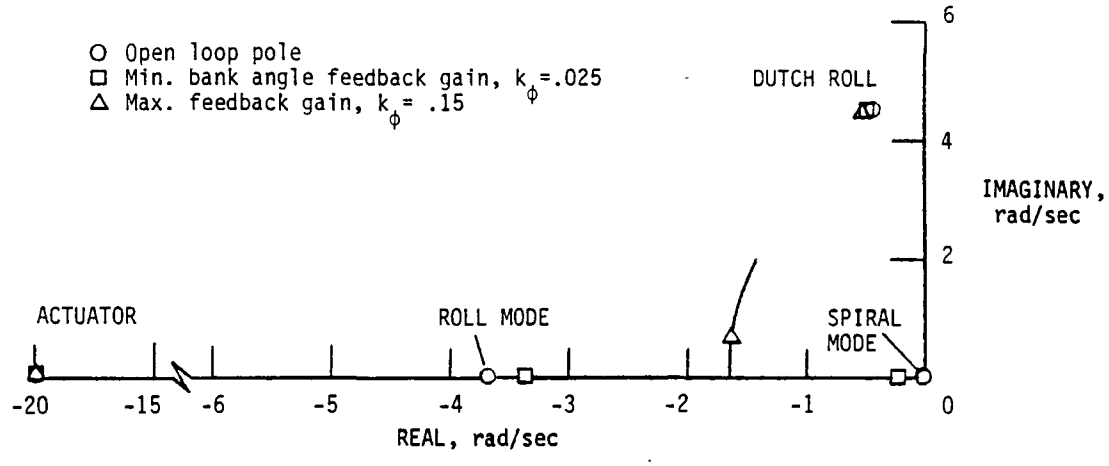

Figure 5.13. Bank angle hold mode root locus for minimum and maximum bank angle feedback gain. Mach = 0.8; h = 6096.

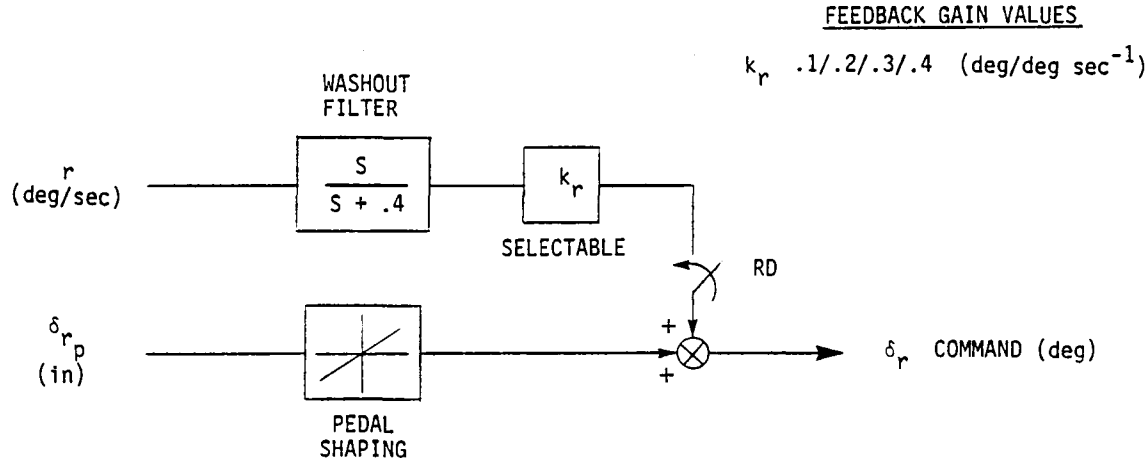

Figure 5.14. Yaw axis control system.

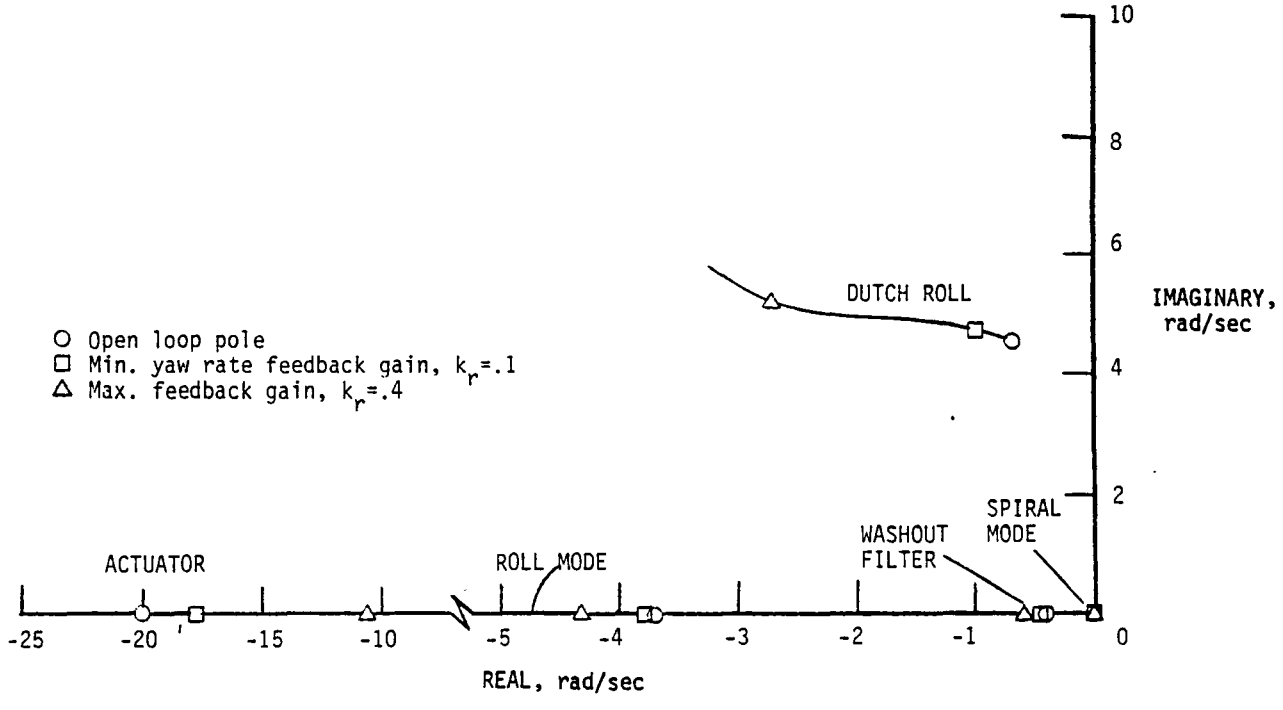

Figure 5.15. Yaw rate damper root locus for maximum and minimum yaw rate feedback gain. W = 1008 kg; c.g. = 264.4 F.S.; Mach 0.8; h = 6096 m.

directed to the V-73 computer. A computer-implemented schedule provides a linear throttle control through the throttle lever. The throttle authority is limited between 70 and 100 percent rpm.

5.4 Software Testing

Software testing, conducted in the simulation laboratory, has as a primary objective to verify the developed code implemented in the real time simulation program and validate the flying qualities of the test vehicle. Tests are also conducted to determine the effects of onboard and ground-based system failures. A summary of the DAST-I software tests follows:

Verification tests are conducted by simulation engineers and are meant to verify the code implemented in the Cyber real time simulation program. This code should reflect the requirements defined in all specification documents. Verification is obtained by visual inspection of strip chart recordings generated by the simulation program. Similar tests are conducted to verify the Varian code. In this case, strip chart recordings are compared to the recordings obtained from the All-Cyber verification tests.

All-Cyber and Varian/Cyber verification test results are included in a test report that is inspected and approved by the Software Control Board (SCB) prior to a flight. Verification tests are conducted once after a new RAV code is implemented and are repeated whenever the code is modified or updated.

Validation tests are conducted by research engineers. The objective of these tests is to validate the flying qualities of the simulated vehicle within the flight envelope. Tests are conducted first in the All-Cyber and later in the Varian/Cyber configuration.

Displayed cockpit instruments are also validated. Validation tests will be repeated whenever verification tests are performed. Test results are inspected and approved by the SCB.

Failure Model and Effects Test (FMET)

The purpose of these tests is to investigate the effects of onboard and ground-based failures and define possible actions in case such a failure would occur. Active participation of the test pilot is required for these tests. The objective is to familiarize the test pilot with most of the failures, define failure detection methods, and generate the appropriate actions.

Failures are simulated in several computer modes and other configurations, such as in autopilot and during the recovery. The failures that are considered are:

- Uplink faults (frozen or hardover)
- Downlink faults (frozen or hardover)
- Cockpit faults (instrument out stick failures)
- Ground software faults (computer failure)
- Onboard faults (instrument failures)
- Test results are included in a report that is presented to the SCB for inspection and approval.

Most of these tests are conducted in the All-Cyber configuration because of the flexibility this mode of operation provides. These tests are performed once for every flight test configuration. In general, part of these tests will be repeated prior to every flight in order to familiarize the test pilot with failure detection methods and actions.

5.5 Software Management

The DAST-I software management is established according to the policy and procedures specified in the "DFRC Software Control Management Policy" document. This document is the software control guideline for all programs conducted at the Dryden Flight Research Center. There are three levels of software management defined in this document. These levels are defined as follows:

Level A. When software failure could cause loss of life or limb, compromise public safety, or result in substantial financial loss.

Level B. When software failure could cause mission failure.

Level C. When software failure could cause inaccurate results or inefficient use of resources.

The DAST program requires a level B software control management. Software control is accomplished through the Software Manager and Software Control Board.

The Software Manager performs duties delegated by the overall responsible directorate or project manager. He is the only person immediately responsible for coordination, direction, documentation, and approval of all software activity.

The Software Control Board actions serve as a critical design review prior to any configuration changes. The board will review and approve all Program Change Requests (PCR's) and Program Change Notices (PCN's) prior to their incorporation into a new release. The failure mode effects test report and verification and validation reports are also reviewed by this board.

CHAPTER 6

PREFLIGHT PROCEDURES

In this chapter a description is given of the procedures followed prior to a test flight. These procedures include flight planning, vehicle tests, and system checkout. A description of the preflight briefings for project and center personnel is also presented.

6.1 Flight Planning

Flight planning is conducted in the simulation laboratory. The real time simulation is used to define and evaluate the flight track which will be followed during the actual test flight. Due to the limited range of the DAST-I vehicle, the primary objective of flight planning is to define a flight track that provides a maximum of flight test data within the available flight time.

In general, the following limitations will be considered during flight planning:

- Available fuel
- Antenna range and signal strength pattern
- Availability of air space
- Vehicle restraints, such as structural and aerodynamic limitations
- Termination of flight within the recovery area

Once the flight track is defined, the test pilot will try to gain experience in following the track and obtaining the flight

conditions required for FSS testing. When all test procedures are defined, a flight request is generated that describes in detail the flight track and flight conditions to be flown during the actual test flight. This request also includes alternate flight plans to be followed in case of an emergency caused by an onboard or ground-based system failure.

6.2 Preflight Tests

All preflight tests are conducted in the hangar of the Dryden Flight Research Center. A description of these tests is given in the following sections.

6.2.1 Ground Resonance Test (GRT)

The objective of the GRT is to demonstrate structural resonance and limit-cycle free operation of the DAST-I RAV system for up to four times the maximum specified feedback gain on the rate feedback loops.

The vehicle configuration during testing and the test procedures are defined in the DAST-I GRT document. This document also specifies the facilities required to be operational during testing and their configurations.

This test is conducted only once for a test configuration. Extensive structural or RAV system modifications may require repetition of these tests.

6.2.2 Ground Vibration Test (GVT)

The DAST-I GVT objective is to determine structural vibration modes

of the wing and fuselage. Vehicle excitation is obtained through two 25 kg MD shakers. GVT is conducted prior to flight testing a new configuration. For the DAST-I vehicle an abbreviated GVT is conducted after a test flight to verify that wing structural characteristics have not changed as a result of the wing loads experienced during flight.

The overall test configuration and test procedures are described in the DAST-I GVT procedures document.

6.2.3 Weight and Balance Tests (W&B)

Weight and balance tests are conducted prior to each flight with the objective of defining the empty and full fuel weight of the test vehicle and balancing the horizontal c.g. location to a predetermined value. Ballast weights in the forward and aft sections of the test vehicle provide the ability to shift the c.g. location by adding or subtracting weights.

6.3 Systems Checkout

In this section a description is given of the checkout procedures that verify the interface between ground-based facilities and the test vehicle.

6.3.1 Combined Systems Run (CSR)

The main objective of the CSR is to verify engine operation and control, telemetry links, and interface between the test vehicle and the ground-based facilities. During CSR checkout, the test vehicle is connected to a test cart through an umbilical. The test cart

provides the ability to checkout and monitor the operation of the engine and the recovery system.

The CSR includes the following tests:

- Test cart checks
- Ground facility and aircraft tests
- F-104 telemetry and autopilot tests
- Engine calibrations and operation tests
- Stand alone checks (test cart disconnected)

The CSR is conducted once prior to flight testing a new configuration.

6.3.2 RPRV Facility Preflight Checks

The RPRV preflight checks are conducted prior to each flight. The Varian software has to be available for these checks. The objective of the RPRV preflight checks is to verify the operation of the RPRV facility systems and the interface between this facility and the test vehicle.

The following checks are performed:

- Ground cockpit stick computer calibrations
- Operation of cockpit functions, such as the autopilot control and pulse panel
- Cockpit instrument calibrations and check out
- PCM downlink and uplink telemetry calibrations
- Closed loop software checks

Abbreviated RPRV preflight checks will be conducted only when the facility systems and ground-based software have not been modified since the previous flight.

6.3.3 Day of Flight Checks (DOF)

The DOF checks are conducted on the day of flight. During those tests the vehicle will be attached to the B-52 carrier. The test objective is to verify full systems operation prior to B-52 take off.

The checks performed are:

- Onboard system and instrumentation check out
- Uplink and downlink telemetry checks
- F-104 telemetry checks
- Operational checkout of all B-52 test, monitor and launch panels
- B-52 fuel top-off system checks
- FSS operational checks

The DOF check list describes in detail all checks, required actions and personnel assigned to conduct every individual test.

6.3.4 The Flight Check

The flight checklist describes the final preflight checkout up to the moment the vehicle is launched. Checks are initiated prior to B-52 engine start. At this point all facilities involved in the DAST-I RPRV operation will be fully operational.

The following are included in the DAST-I flight checklist:

- Final telemetry checks prior to taxi and take-off
- Ground cockpit checks including remote control
- Onboard systems checks (AP and Recovery)
- F-104 remote AP control checks
- FSS and TMR checks

- Refuel and power checks
- Final B-52 speed and heading corrections

The flight checklist includes a series of alternate procedures that will be followed during emergency situations prior to launch.

6.3.5 Captive Flight

A captive flight is conducted to evaluate ground-based and airborne system checkout procedures up to launch. Such a flight is only conducted when a new or highly modified test vehicle configuration is to be tested.

In general, a captive flight has the following objectives:

- Verify checkout procedures.
- Familiarize B-52 and F-104 crew with launch procedures.
- Verify sufficient signal strength along the predetermined flight track.

The CH-3E recovery helicopter is the only element of the DAST flight test operation that is not present during this test configuration. A captive flight ends with a simulated launch.

6.4 Briefings

Project and center personnel are informed about an upcoming flight through a series of briefings. These are:

The ground school briefing provides technical information to all project members. A list of subjects that are included in this presentation follows:

- Recent vehicle modifications
- Proposed testing
- Ground cockpit updates

- Software modifications
- Onboard system modifications
- Onboard system modifications
- Emergency procedures
- Mission rules

The technical briefing is organized by the project management and has the objective to inform project and center personnel about the test flight objectives and the way these objectives are to be accomplished. A technical briefing is held prior to every test flight.

The crew briefing is an operational briefing that is held just prior to the test flight and has the objective to review personnel assignments and present the flight checklist and time line for the day of flight. UHF frequencies are announced and weather predictions for the day of flight are given to all supporting aircraft crew members.

CHAPTER 7

DAST-I FLIGHT TEST RESULTS

The DAST program was initiated in 1976. The Firebee II drone, selected as a test bed for this program, was flight tested for the first time at the NASA Dryden Flight Research Center in July 1977 to familiarize center personnel with its operation. The Firebee II was flown in a target drone configuration that is extensively used by the U.S. Air Force and the Navy.

The vehicle was later modified to fulfill Dryden Flight Research Center test requirements. A description of the modifications is given in section 2.1.2.

This chapter describes the test flight of the modified Firebee II drone, known as the Blue Streak configuration, and the first and second flight of this drone fitted with the aeroelastic wing, a configuration known as the DAST-I or ARW-I.

7.1 Blue Streak Flight

The first DAST test flight with the modified Firebee II drone was conducted at NASA Dryden Flight Research Center, March 9, 1979. The test vehicle was fitted with an original Firebee II wing instrumented for loads measurements. This wing, instrumented by NASA Langley, is known as the Blue Streak because of a blue stripe painted across its surface.

A description of the objectives, the flight test plan, and the results obtained from this flight follows:

Flight Objectives

The principal flight test objectives of the Blue Streak flight were to evaluate the new onboard system, the RAV system, the interface between onboard and ground-based systems, and remote autopilot control stations (F-104 and ground cockpit). Other objectives were to familiarize ground personnel and supporting aircraft crews, in testing and monitoring the DAST-I operation, to obtain and evaluate wing pressure and loads data and to demonstrate the recovery system.

Flight Plan

Flight planning was conducted on the real time simulator. All flight conditions to be obtained during this flight were to remain below the drag chute dynamic pressure limits. This requirement would assure a safe drag chute deployment in case an emergency recovery should be commanded. The flight test conditions are shown in figure 7.1.

A summary of the submitted flight request for this flight follows:

Launch: Launch at 6100 m, Mach .4, and a throttle setting of 80 percent rpm.

Testing:

a. Level off at 6100 m and Mach .85. Perform elevon and rudder pulses in CD and RD, perform a windup turn of 2 and 4 g, and evaluate onboard autopilot control through the ground cockpit.

b. Accelerate to Mach .94 at 6100 m, perform elevon and rudder pulses in RD, and windup turn of 4 g.

c. Descend to 4525 m and maintain an airspeed of .94 Mach, perform pulses in RD.

d. Climb to 6100 m at .8 Mach, transfer command to the F-104 controller.

e. Evaluate F-104 backup control station control and vector the vehicle to the recovery area.

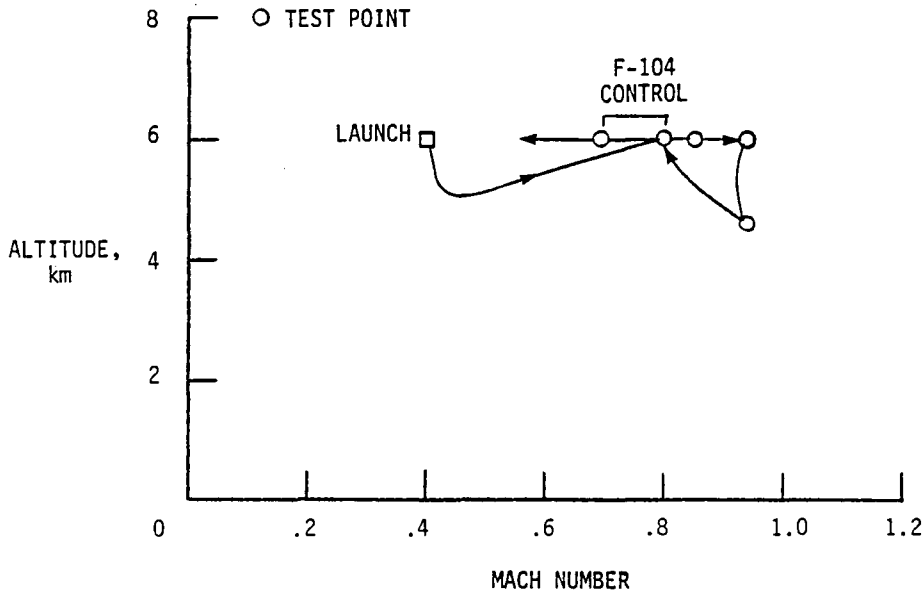

Figure 7.1. Planned flight test conditions for the Blue Streak test flight.

Recovery: Transfer command to the ground station and command recovery above the predetermined recovery area.

Pertinent information regarding this flight is presented in table 7.1.

TABLE 7.1 BLUE STREAK TEST FLIGHT

Flight number	Flt. 2-6
Date of flight	3/9/79
Test pilot	T. McMurtry
Launch	10.57 a.m.
Recovery	10.12 a.m.
Duration of flight	15.00 min
Max. speed	.97 Mach
Max. altitude	6100 m

Flight Test Results

The Blue Streak test flight was considered a successful operation. Due to some problems encountered during flight, the planned flight track was not completely followed. The actual and planned flight tracks are given in figure 7.2. The flight conditions obtained during this flight are shown in figure 7.3. Halfway through the flight the decision was made to shorten the flight track because of a problem encountered in controlling the engine rpm. The minimum commanded throttle setting resulted in a much higher rpm than anticipated. This enabled the pilot to obtain lower Mach conditions specified in the flight plan. The pilot has actual control of the engine fuel flow which is not directly related to the engine rpm. Altitude and airspeed will alter the actual rpm. The minimum throttle command was expected to result in 80 percent rpm. The experienced rpm at the same conditions was 86 percent. Uncertainties concerning the fuel consumption caused management to decrease the actual flight time.

A second problem was encountered when command was transferred to the F-104 backup station. The F-104 controller was unable to

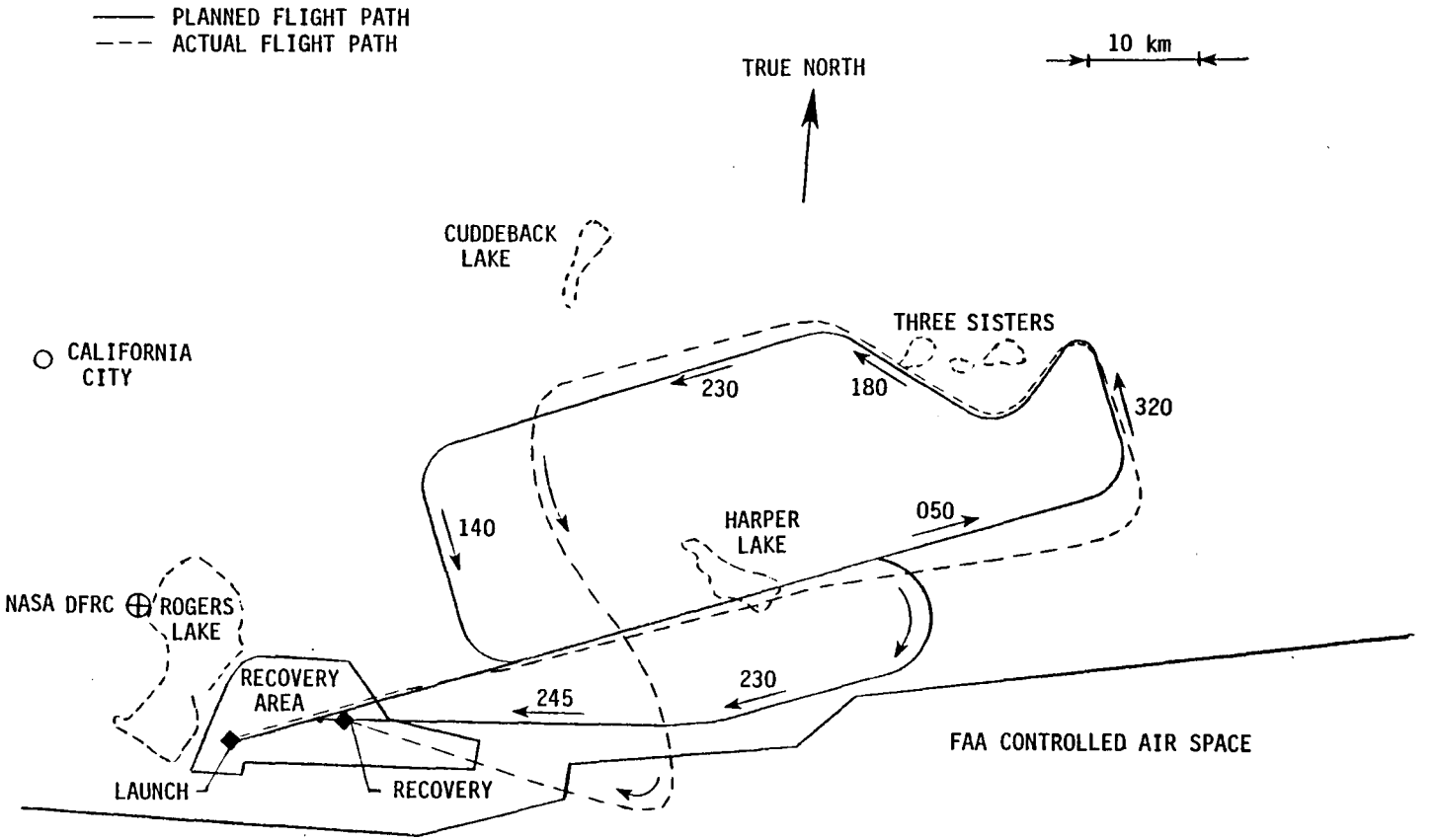

Figure 7.2. Planned and actual flight path of the Blue Streak flight.

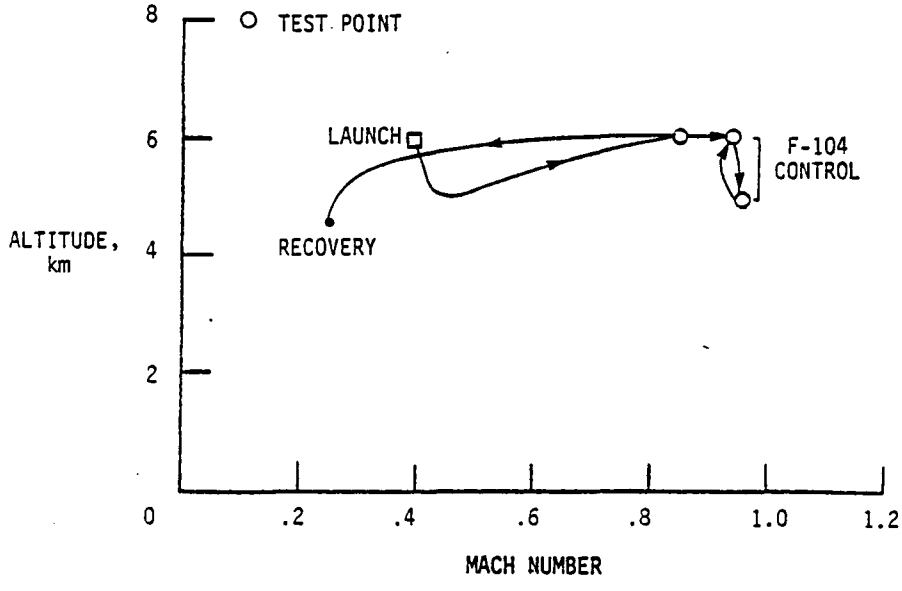

Figure 7.3. Flight conditions achieved during the Blue Streak flight.

achieve the required turn rate due to the fact that the maximum AP bank angle authority was less than anticipated. When this problem was recognized, command was transferred back to the ground cockpit. Post flight analysis indicates that the AP bank angle feedback signal was biased by 10. degrees, left wing down. This limited the bank angle authority to 30 degrees right wing down. The anticipated limit was 40 degrees. Simulation results indicate that, due to a 10 degree bank angle bias, the maximum AP turn rate is reduced by 40 percent.

During this flight the RAV system consisted of an unaugmented CD direct mode in all three axes and a rate damper mode also in all axes.

An instability was encountered in the roll axis at an altitude of approximately 6000 m and Mach .97. The selectable gain position was in position 2 at that point, representing a roll rate feedback gain of -.2 deg/deg sec^{-1}. Real time simulation tests did not indicate such an instability at gain values four times as high. The instability was attributed to the time delay that is introduced through the asynchronous operation of ground-based systems and other signal processing equipment. The V-73 computer will also introduce a delay equal to the computation time required to calculate the control laws. Linear analysis shows that the roll instability can be seen at the second gain position when the time delay reaches the value of two samples. In figure 7.4, the z-plane analysis results are given. The roll damper root locus is shown as a sampled-data system and as a sampled-data system with two time delays (2 x 18.75

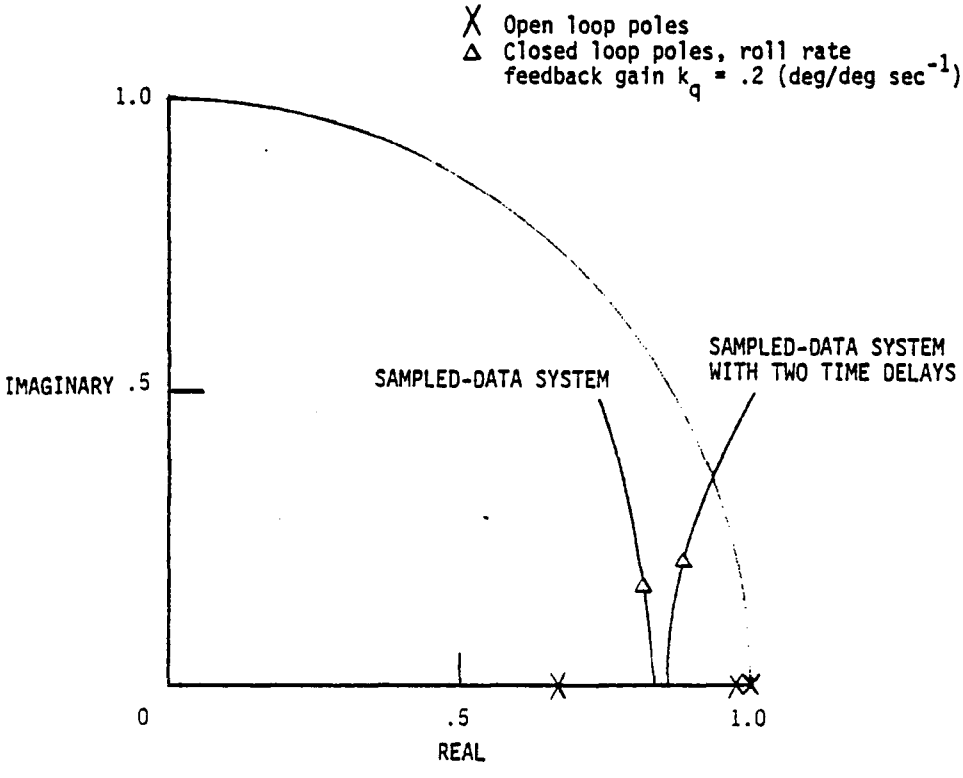

Figure 7.4. Root locus of the roll axis rate damper mode. h = 6100 m; Mach = 0.98.

msec). The tendency towards the instability at approximately 5. Hz is evident.

Concluding Remarks

The Blue Streak flight evaluated the new onboard systems and their interface with the ground based systems. This test flight provided valuable information for the DAST operation.

Problem areas, such as the throttle control and autopilot authority were identified. Valuable information was obtained for future control system analysis. Flight data provided sufficient information to verify the real time simulation performance and improve the areas that did require corrective action.

7.2 First ARW-I Flight

Following the Blue Streak flight the Firebee II drone was fitted with the aeroelastic wing ARW-I. The active flutter suppression instrumentation was installed and extensively tested.

Extensive simulation testing was conducted to validate the drone's flying qualities and the new RAV system (see appendix B). The ground cockpit and F-104 autopilot circuitry was modified to increase the control authority. The ground cockpit was fitted with the FSS panel for monitoring the testing.

Flight Objectives

The primary objectives of this flight were to validate the FSS equipment and characteristics and perform sub-critical flutter testing.

The FSS testing procedures would also be verified since this was the first operation in which the SAF would be actively involved

in the flight test operation. The modified RAV system included an additional mode in pitch that was designed to provide an altitude hold and load limiting function.

Flight Plan

Most of the testing conducted in this flight involved FSS tests. The test procedure would be to fly the vehicle at the predetermined flight conditions and conduct a 1 minute FSS test sequence including pulses and steps, with FSS on and off. Following the test sequence evaluation of the obtained data would take place through the HP Fourier analyzer. Positive results would clear the following condition. The test conditions for this flight are presented in figure 7.5. A simplified version of the flight request follows:

Launch: Launch at an altitude of 6096 m and Mach .4. The RAV system will be engaged at launch. Start in CD and upmode to RD as soon as possible.

Testing: a. Level off at 5180 m and Mach .7. Engage CAS mode and perform FSS test sequence (pulses and sweeps) at .7, .75, and .8 Mach. Perform stability pulses in CD at the .8 Mach condition.

b. Climb to 7620 m in RD and engage CAS at that altitude at Mach .75. Generate FSS test sequence at Mach numbers .75, .8, .85, .875, and .9. Stability pulses to be performed in CD at the .8 Mach condition.

Recovery: Decelerate to Mach .7 at 6096 m and initiate recovery above the predetermined area. In table 7.2 pertinent information regarding this flight is presented.

TABLE 7.2 FIRST ARW-I TEST FLIGHT

Flight number	Flt 3-8
Date of flight	10/2/79
Test pilot	T. McMurtry
Launch	10.33 a.m.
Recovery	10.41 a.m.
Duration of flight	8.00 min
Max. speed	.75 Mach
Max. altitude	5530 m

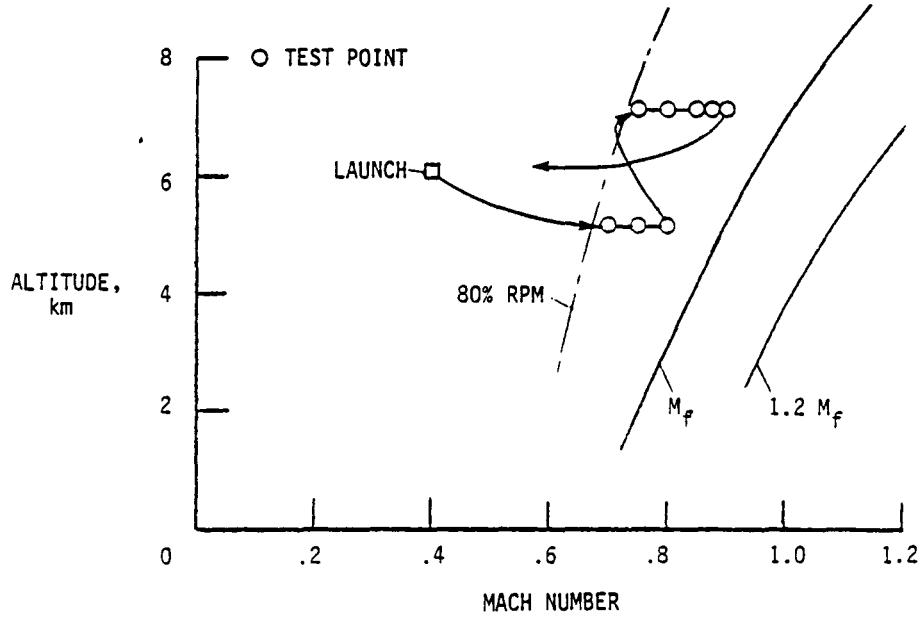

Figure 7.5. Planned flight test conditions for the first ARW-I test flight.

Flight Test Results

The first flight of the ARW-I was conducted October 2, 1979. This flight was beset by numerous difficulties. The flight was ended prematurely eight minutes after launch. The major problems encountered during this flight were:

- FSS hydraulic pump failure
- CAS mode lightly damped short period oscillation
- Numerous telemetry drop-outs and spurious commands

The spurious telemetry hits and loss of telemetry were a major problem in controlling the test vehicle from the ground cockpit. The premature end of this flight was attributed to a spurious hit causing an inadvertant recovery command.

The projected and actual flight paths are presented in figure 7.6. Five minutes into the free flight, the decision was made to deviate from the original flight path and return to the recovery area. At that point it became apparent that the low telemetry signal strength and spurious hits could result in the loss of the vehicle. Eight minutes into the flight an inadvertent recovery command was initiated while the test vehicle was located several kilometers away from the anticipated recovery area. Thanks to an exceptional effort of the CH-3E helicopter crew, coordinated by the flight controller, the vehicle was recovered in mid-air at an altitude of 1000 m, 8.5 minutes after the recovery sequence was initiated.

Within 90 seconds after launch the FSS hydraulic pump failed to what appeared to be a hydraulic fluid loss due to a major leakage. The hydraulic pump failure and the resulting loss of oil pressure

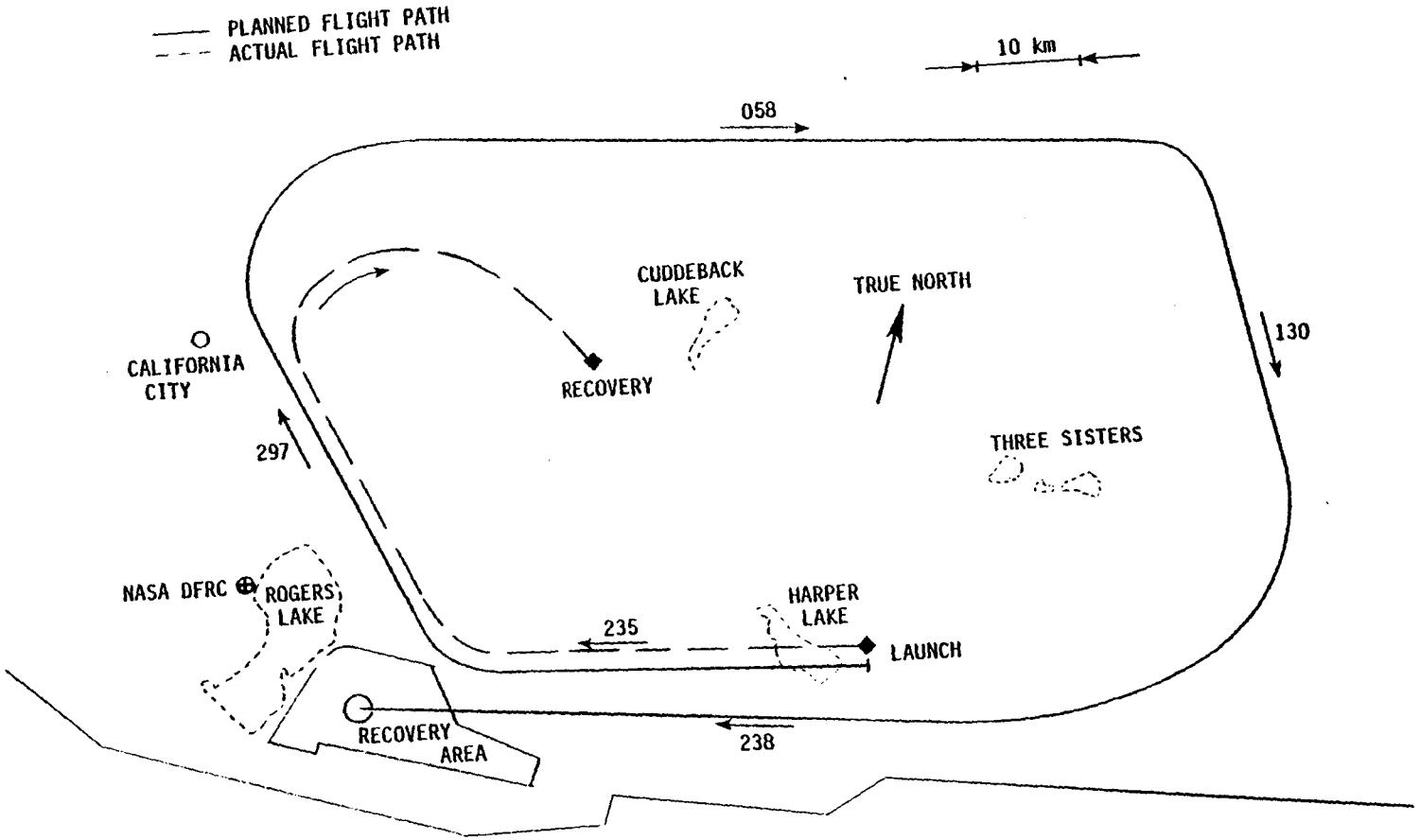

Figure 7.6. Planned and actual flight path for the first ARW-I flight.

caused the wing (FSS) ailerons to be forced fully trailing-edge up by the aerodynamic hinge moment. The surfaces maintained this position for the remainder of the flight.

Accelerometer information provided sufficient data concerning the wing motion. Two distinctive conditions were analyzed one at an altitude of 5180 m and Mach .7 and the second at an altitude of 5030 m and Mach .75. In both cases the wing was excited by aileron and elevator motion. The achieved flight conditions are presented in figure 7.7. The obtained results are given in figures 7.8 and 7.9. The symmetric root locus of the first wing bending, given in figure 7.8, shows the tendency to become unstable at approximately Mach .7. Analysis conducted by NASA indicates similar behavior only at a much higher Mach number.

Flight results presented in figure 7.9 show the antisymmetric root locus of the first wing bending mode to become unstable at Mach .75. Linear analysis indicates that the instability will occur at higher Mach numbers.

Control system performance in CD and RD modes in all three axes was as anticipated. The pitch CAS (Command Augmentation System) mode was engaged shortly after launch. In this mode the vehicle exhibited a lightly damped low frequency oscillation. This response was attributed to the high altitude rate feedback gain and to flexibility effects of the aeroelastic wing that result in a considerable reduction of the pitching moment coefficient, C_{m_α}. A possible reduction of $C_{m_{\bar{\alpha}}}$ due to the flexible wing was anticipated. The magnitude

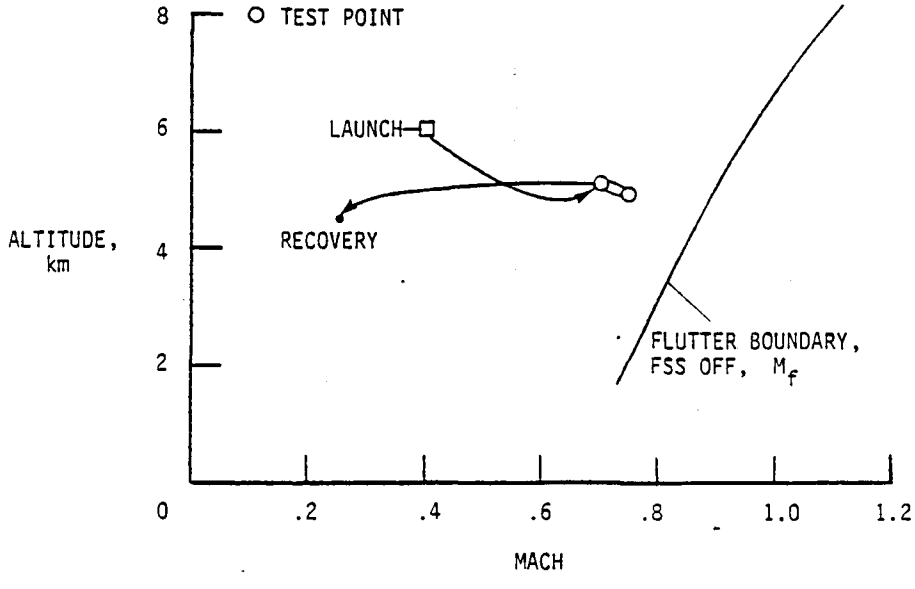

Figure 7.7. Flight conditions achieved during the first ARW-I flight.

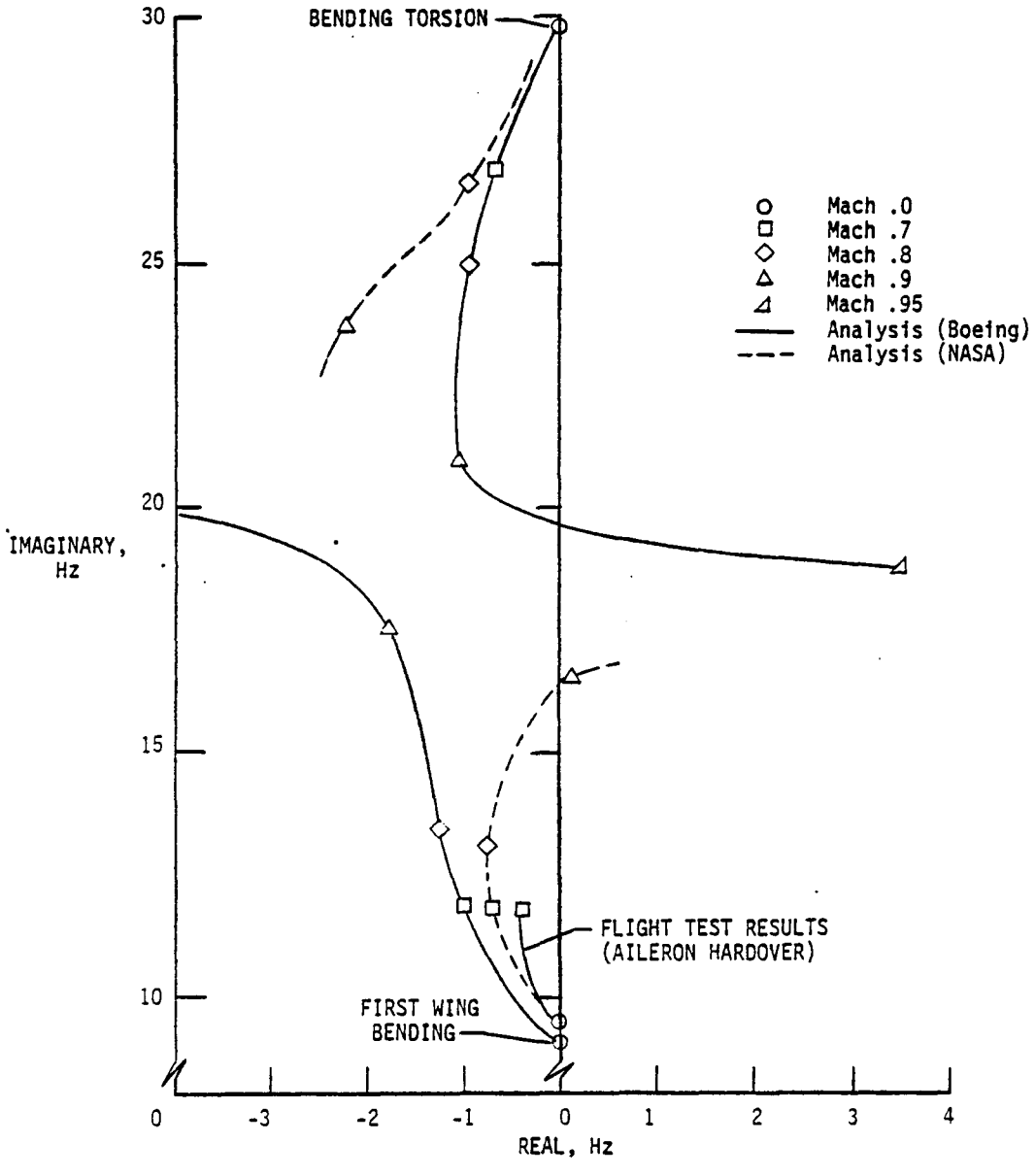

Figure 7.8. Symmetric root locus versus Mach number. h = 5180 m.

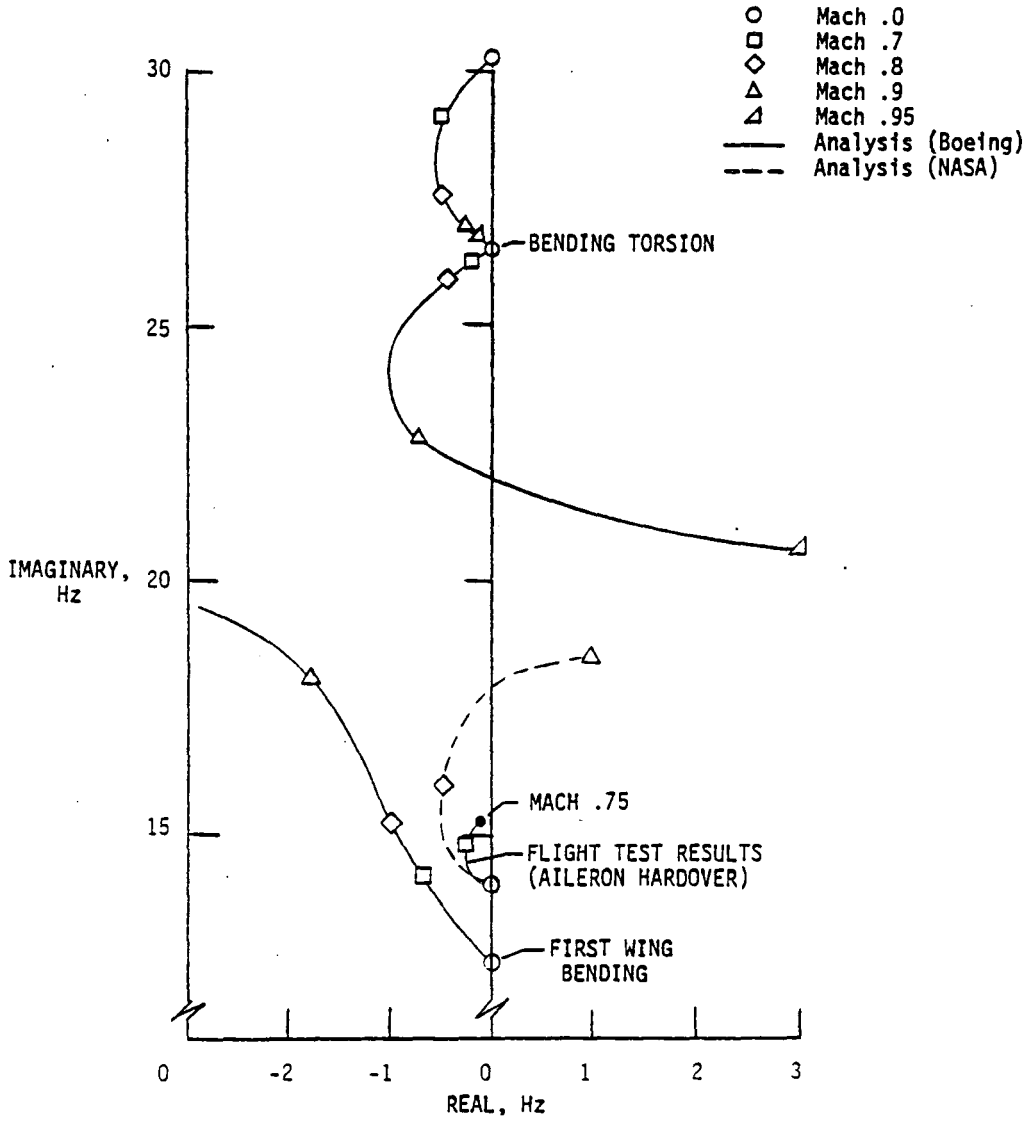

Figure 7.9. Antisymmetric root locus versus Mach number. h = 5180 m.

of the reduction was actually underestimated. Linear analysis results, presented in figure 7.10, show the effect of fuel quantity and pitching moment coefficient on the root locus of the short period. The results indicate that the short period locus approaches neutral stability at approximately 5 Hz, the frequency at which the vehicle was oscillating during flight.

The telemetry problems were caused by a malfunction of the onboard uplink receiver resulting in a low signal strength which in turn caused the numerous engagements of the onboard autopilot. Discrete signals were also affected by this malfunction. This resulted in random onboard system switching and other spurious commands such as the inadvertant recovery command. The loss of 1 bit resolution on all PCM-1 system parameters was attributed to the PCM power supply system that contained noise and provided poor regulation of internal power. All RAV system parameters are obtained from this PCM system. The degraded performance of the CAS mode can partially be attributed to this problem.

Concluding Remarks

Although the FSS system was not evaluated, open loop responses showed that the flutter boundary of the ARW-I was lower than predicted by as much as .1 Mach.

The flexibility effect of the aeroelastic wing would have to be evaluated and incorporated in future control system development and testing.

Pilot's ability to control the load factor of the vehicle well within the limits would result in the deletion of the load limiter implemented in the control system.

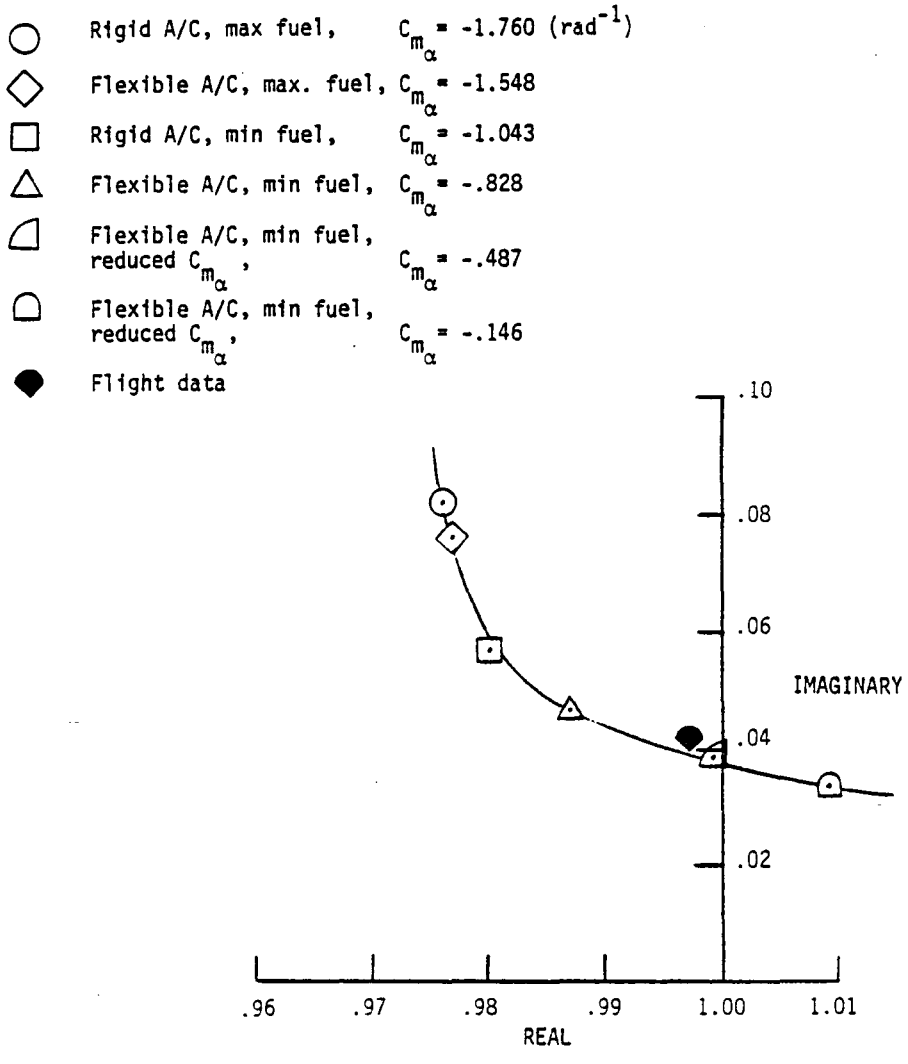

Figure 7.10. Command augmentation system short period root locus versus C_{m_α} and fuel remaining. h = 5180 m; Mach = 0.7.

The obtained flight data showed an excellant signal-to-noise ratio, promising good results from following flights.

7.3 Second ARW-I Flight

Prior to this flight several modifications were made to the test vehicle to eliminate problems encountered during the first ARW-I flight. The FSS hydraulic pump was replaced by the new ABEX pump, and the telemetry encoder, PCM system, and signal-conditioning devices were completely revised. The FSS ailerons were modified to decrease their moment of inertia about the hinge axis in order to increase actuator effectiveness. The RAV control system was also modified only in the pitch and roll axis. A description of the system is given in section 5.3.

The test flight took place March 12, 1980, six months after the first ARW-I flight.

Flight Objectives

The primary objective of this flight was to conduct the sub-critical flutter testing that was not accomplished during the first flight. Results from the previous flight indicated the reduction in flutter boundary speed. The new flight conditions were adjusted for the new flutter boundary.

Secondary objectives included the validation of the modified ground-based control system, the new hydraulic pump, and the wing's flexibility effects.

Flight Schedule

For this flight a different flight track was chosen. The total range was considerably reduced to minimize flying in low signal

strength areas that could result in telemetry loss. The flight track was positioned in such a way that a minimum of Air Force and Navy flight test areas would have to be scheduled for this flight. The previous flight was delayed as a result of the inability to schedule the required test areas on the day of the flight.

The flight track, shown in figure 7.11, indicates the race track concept adopted for this flight. This track would be followed twice during flight.

The respective flight test conditions are shown in figure 7.12. This figure indicates the narrow sub-critical test area, limited by the minimum throttle setting and the reduced flutter boundary speed.

A summary of the flight plan follows:

Launch: Launch at an altitude of 7010 m and Mach .41. (V_{CAS} = 181 kn)

Testing:

a. Level off at 6100 m and perform the following testing: Conduct FSS on and off test sequence including aileron pulses and sweeps at Mach numbers .7, .725, and .75. At the last Mach conditions, perform stability and control pulses.

b. Climb to 6860 m and Mach .75 repeat FSS test sequence.

c. Climb to 7620 m and perform FSS tests at Mach numbers .75, .8, .825, and .85. Stability and control pulses will be performed at the .75 Mach condition.

Recovery: Reduce speed to .7 Mach and initiate recovery within the recovery area. All FSS test sequences will be followed by a clearance call from the SAF.

Pertinent information for this flight is included in table 7.3.

TABLE 7.3 SECOND ARW-I TEST FLIGHT

Flight number	Flt. 4-10
Date of flight	3/12/80
Test pilot	T. McMurtry
Launch	9.33 a.m.
Recovery	9.58 a.m.
Duration of flight	25.00 min
Max. speed	.926 Mach
Max. altitude	7620 m

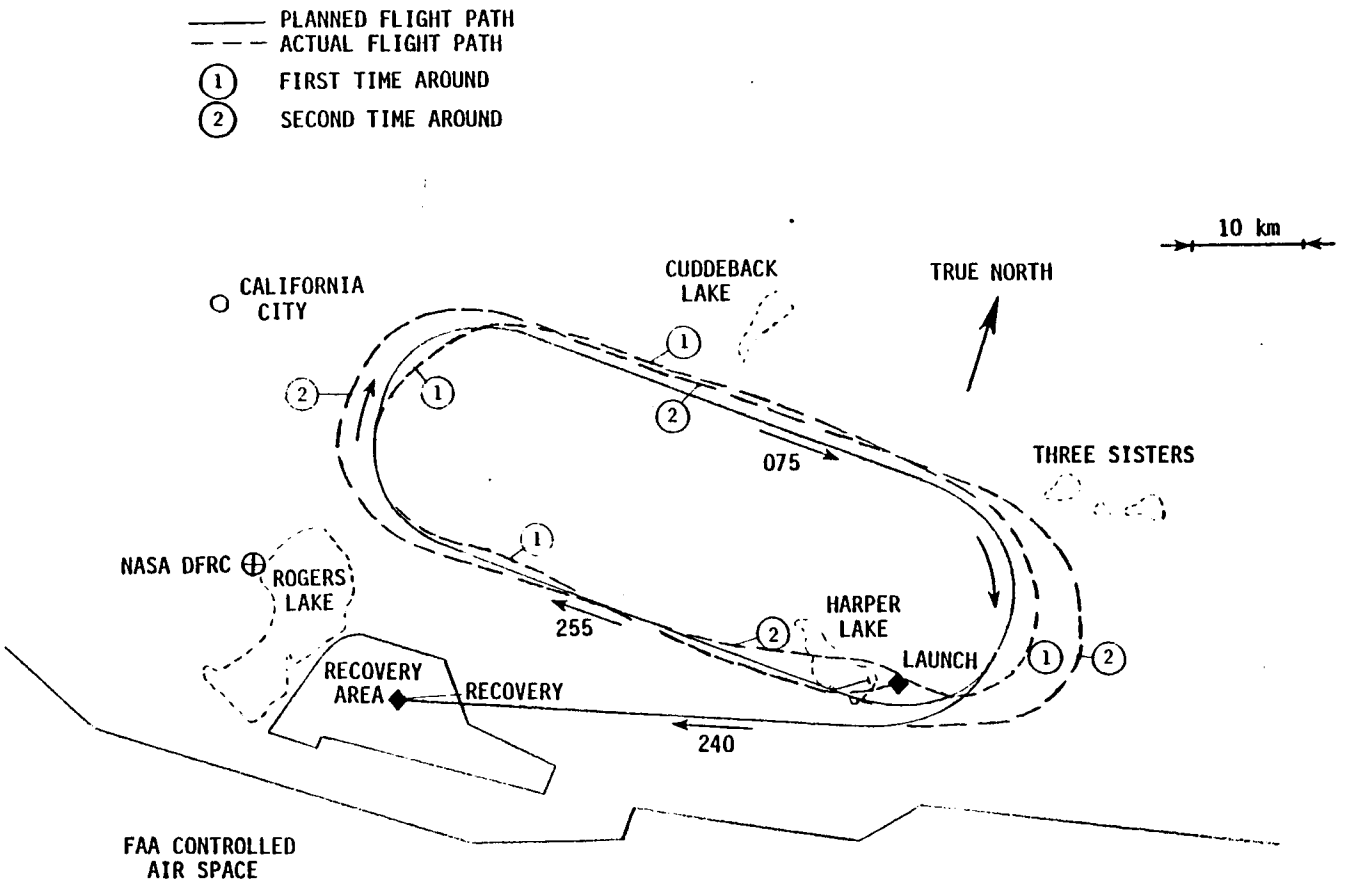

Figure 7.11. Planned and actual flight path of the second ARW-I test flight.

Flight Test Results

The second ARW-I flight was a very successful operation. Due to a hydraulic mode problem of about 200 Hz, FSS tests were terminated shortly after launch. The limited FSS engagement provided response data on only two frequency sweeps. A greater number of open loop frequency sweep response data were obtained than originally planned due to the available flight test time resulting from the deletion of all FSS tests.

The actual and planned flight tracks are shown in figure 7.11. The obtained flight conditions are given in figure 7.13. Tests on several conditions were conducted twice to verify repeatability of the obtained results.

Excellent aeroelastic response data were obtained from this flight. Analysis results presented in figure 7.14 show that the symmetric flutter boundary defined at an altitude of 7620 m is 1830 m higher than predicted. At the same altitude and Mach number, the antisymmetric flutter boundary was encountered and found to be 915 m higher than predicted. The predicted flutter boundaries presented here are based on updated GVT results obtained after the first ARW-I flight.

Frequency and damping ratios of the symmetric and antisymmetric first wing bending mode are presented in figures 7.15 and 7.16, respectively. Both figures show the damping decreasing to zero at a Mach number of approximately .92.

The symmetric and antisymmetric bending mode root loci versus Mach number are shown in figure 7.17. Analysis results generated by NASA are also given in this figure for comparison.

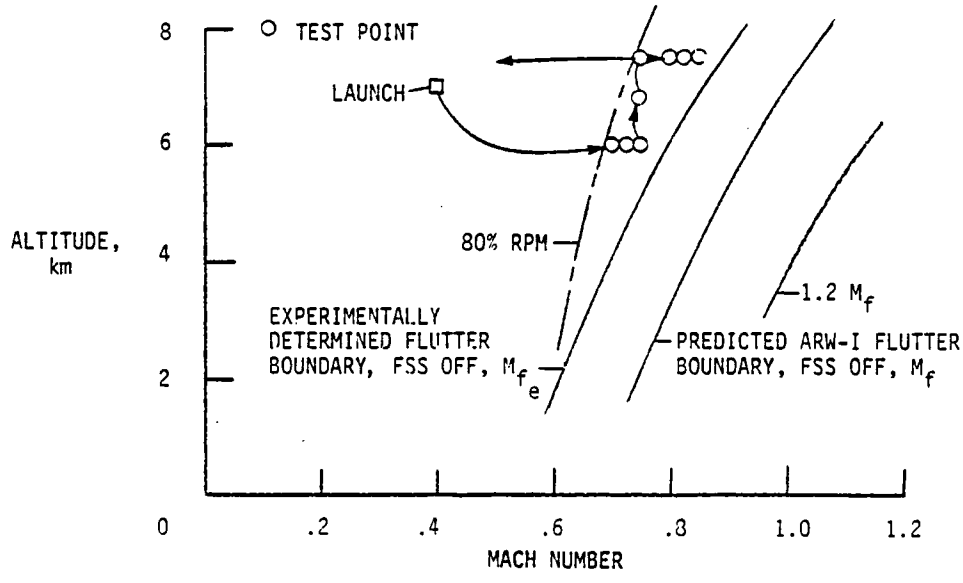

Figure 7.12. Planned flight test conditions.

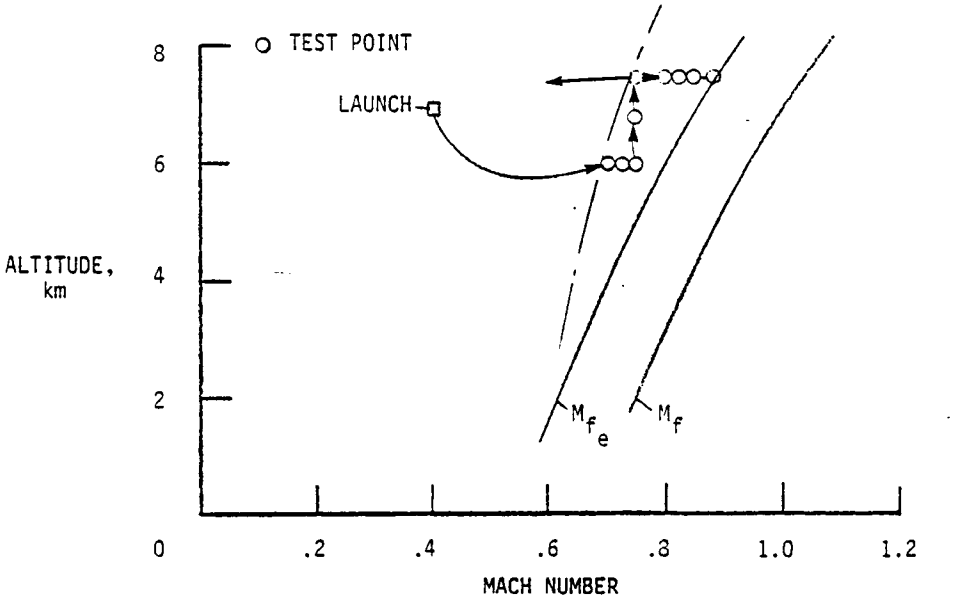

Figure 7.13. Obtained flight test conditions.

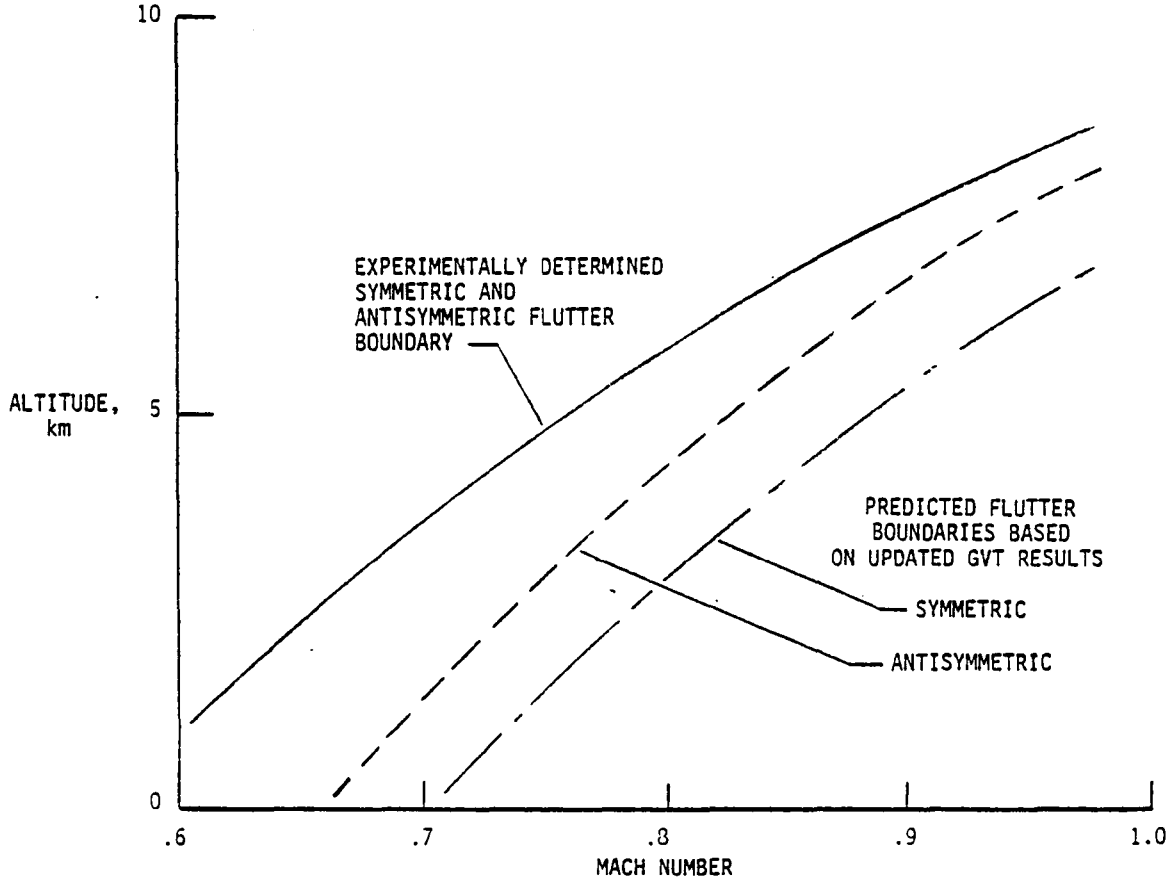

Figure 7.14. Predicted and experimentally determined ARW-I flutter boundaries.

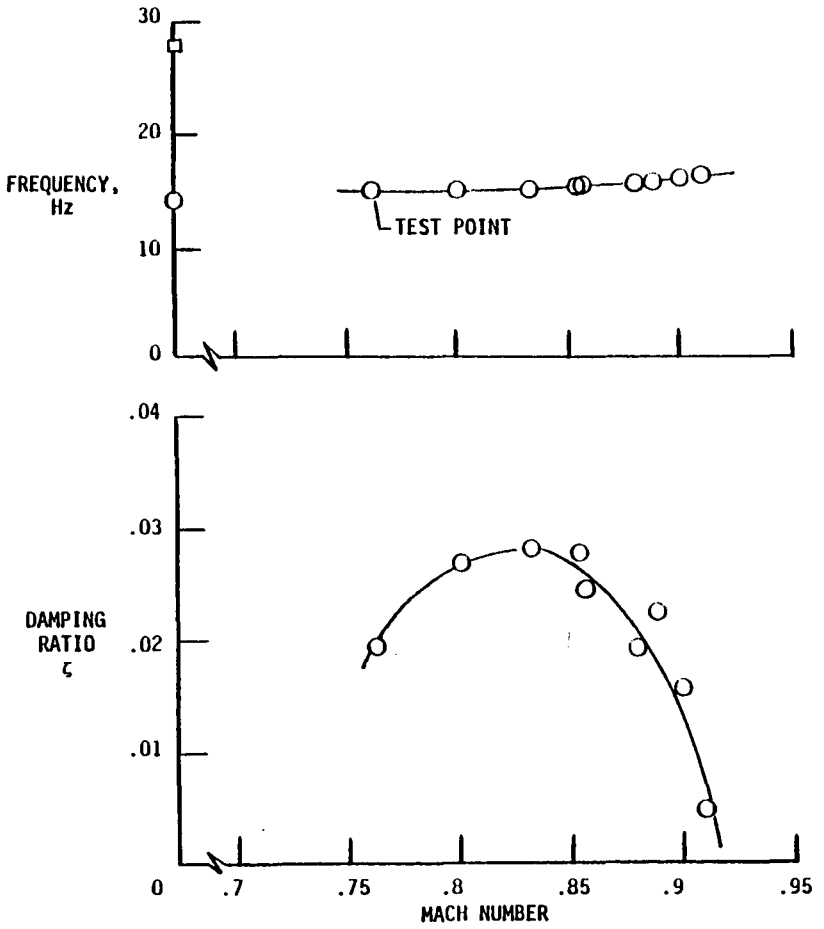

Figure 7.15. ARW-I symmetric bending mode frequency and damping at an altitude of 7620 meters.

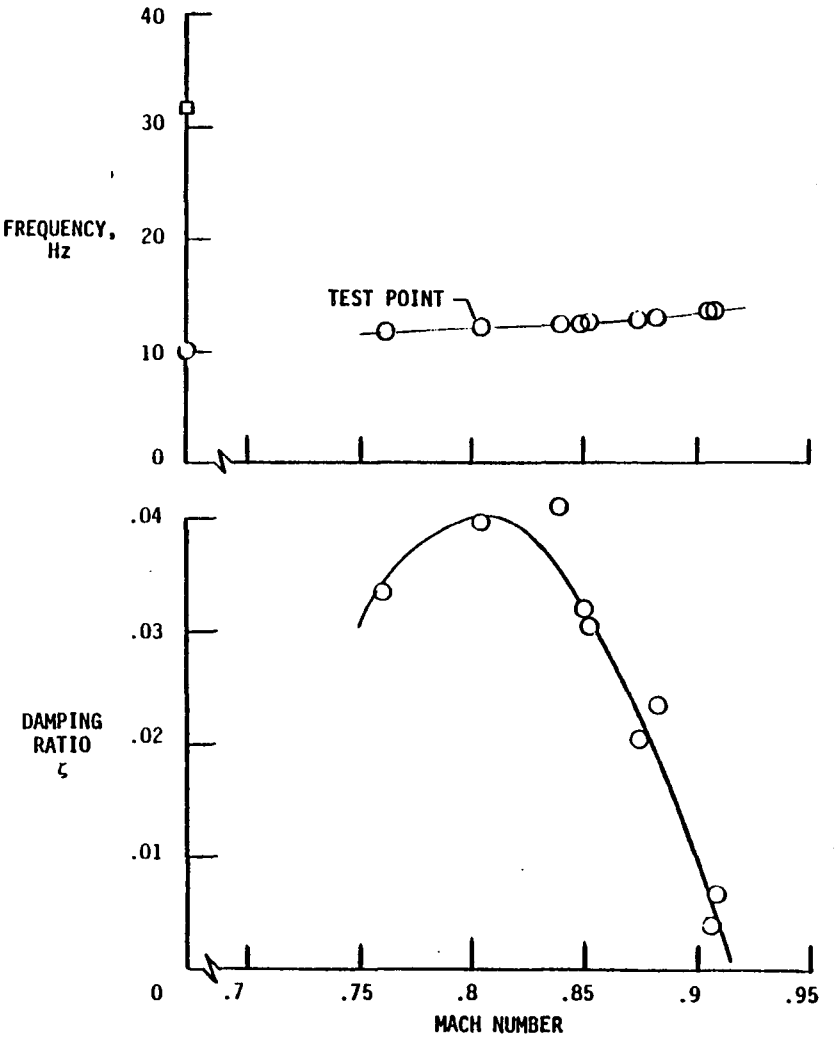

Figure 7.16. ARW-I antisymmetric bending mode frequency and damping at an altitude of 7620 meters.

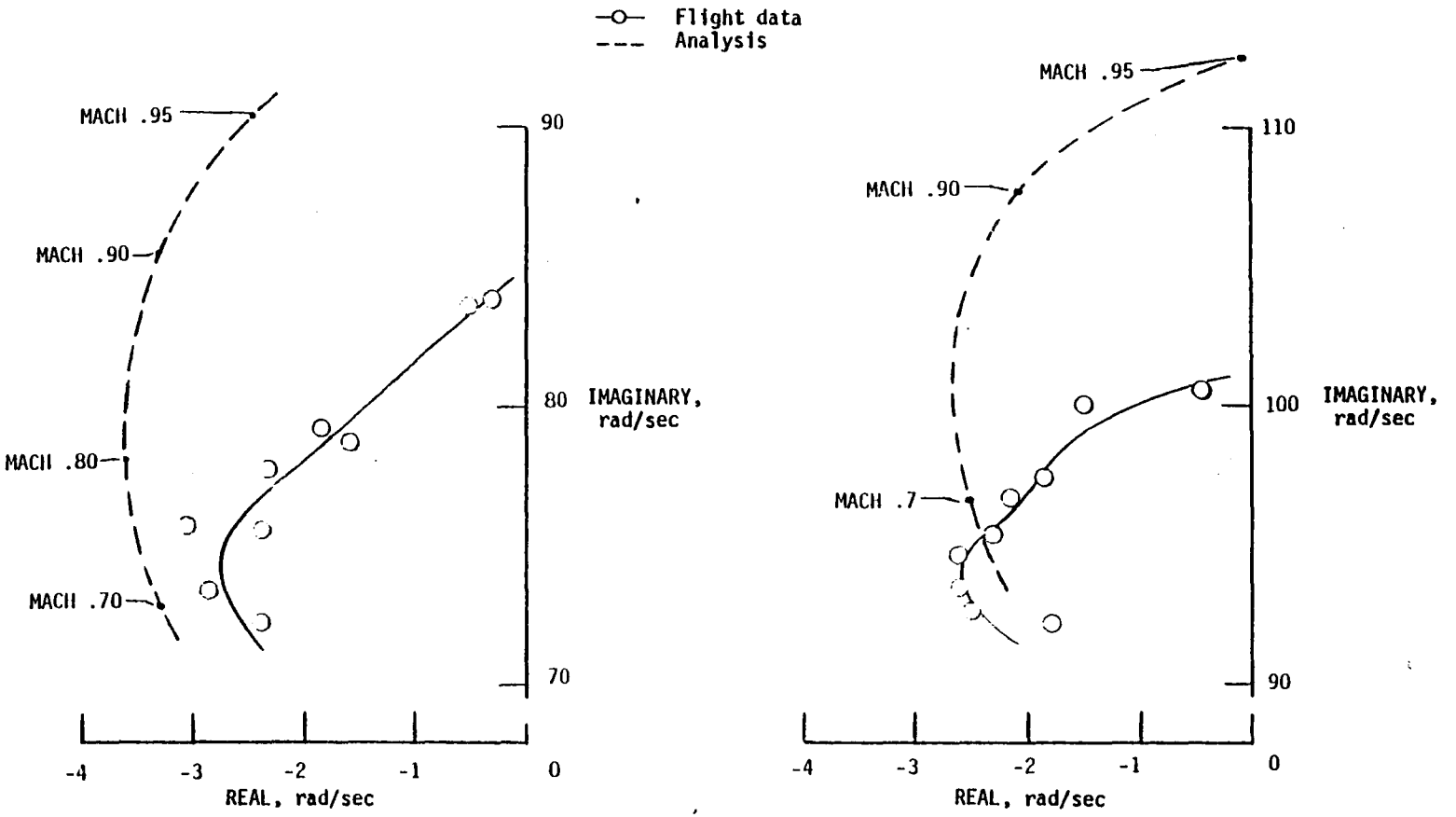

Figure 7.17. Comparison of predicted and experimentally determined bending mode root loci versus Mach number. h = 7620 m.

The limited FSS testing was able to provide data that validate the design of this system. The results given in figure 7.18 show increase in bending mode damping as a result of the FSS at an altitude of 6100 m and .7 Mach. Analysis results are also presented in this figure for comparison.

The flight was ended with a successfull mid-air recovery at the predetermined recovery area.

Concluding Remarks

This flight successfully validated the operation of ground-based monitoring and testing facilities and, in general, the flight test procedures for the DAST-I vehicle.

The excellent data obtained provided valuable information for future flights. The limited FSS results validated the design of this system. Modifications to the system are expected to eliminate all problems with the hydraulic system and result in a fully operational FSS for the next flight.

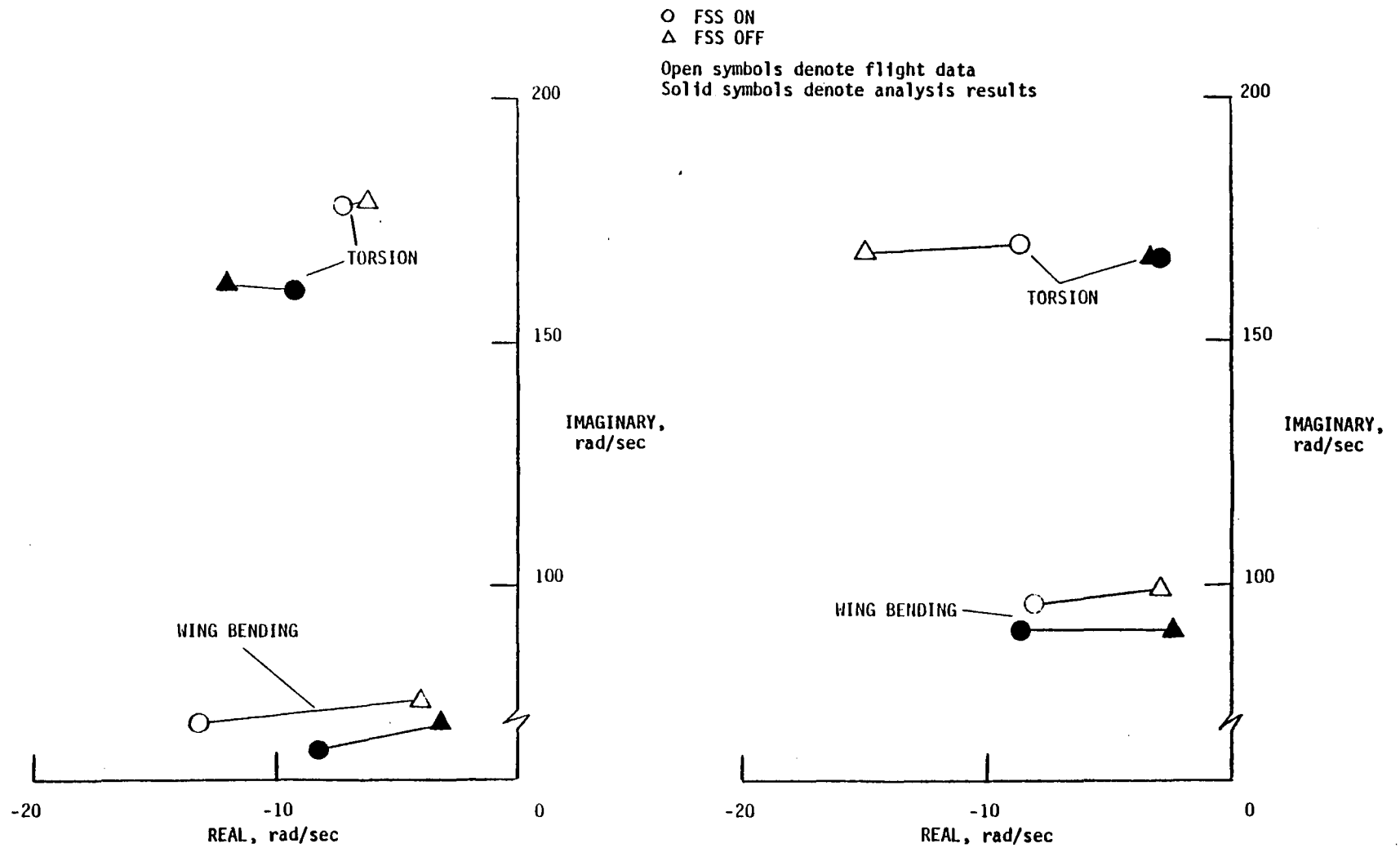

Figure 7.18. Symmetric and antisymmetric bending and torsion modes. h = 6096 m; Mach = 0.7.

CHAPTER 8

CONCLUDING REMARKS

In this section a summary is given of remarks concerning the DAST-I RPRV program.

Although at this stage of the program no concrete conclusions can be made concerning the performance of the FSS, the results obtained to date show evidence that the DAST-I program will provide valuable information for the active control technology.

The use of the RPRV concept for this program was undoubtedly the only alternative for such a high risk flight test program. The economical aspect of this concept is, however, questionable. The RPRV concept requires considerable ground-based and aircraft support, resulting in an operation that is as expensive as the flight testing of full-scale, manned vehicles.

Flight testing of the ARW-I was considerably delayed, and the anticipated flight test rate of one flight a month has not been achieved yet. This is the result of a number of problems that are common to research programs utilizing advanced hardware systems such as the FSS. The turn-around time is expected to decrease considerably following the third ARW-I flight.

Experience obtained from the DAST RPRV operation so far indicates that the concept of implementing the control laws in the ground computer shows limitations in controlling high frequency modes, due to the considerable time delays introduced by the asynchronous operation of ground-based and onboard systems. An alternative to

the present concept would be to implement the ground-based control system in an onboard micro-computer. This concept is presently under development and is expected to be utilized in future DAST experiments.

Flight test results from the FSS experiment will be reported jointly by NASA DFRC and NASA LaRC. Reporting will be accomplished during the six month period following the end of the DAST-I test program.

REFERENCES

1. T. A. Byrdsong, J. B. Hallisy. "Longitudinal and Lateral Static Stability and Control Characteristics of a 1/6 Scale model of a Remotely Piloted Research Vehicle With a Supercritical Wing." NASA TP-1360, May 1979.
2. D. L. Grose. "The Development of the DAST-I Remotely Piloted Research Vehicle for Flight Testing an Active Flutter Suppression Control System." NASA CR 144881, February 1979.
3. N. W. Matheny, D. H. Gatlin. "Flight Evaluation of the Transonic Stability and Control Characteristics of an Airplane Incorporating a Supercritical Wing." NASA TP 1167, February 1978.
4. J. W. Edwards. "A FORTRAN Program for the Analysis of Linear Continuous and Sampled-Data Systems." NASA TM X-56038, January 1976.
5. O. E. Visor, F. D. Sevart. "Preliminary Design Study of Flutter Suppression Control System for the BQM-34E/F Drone Aircraft With a Supercritical Wing--Final Report." NASA CR 132480, 1977.
6. I. Abel, B. Perry, H. Murrow. "Synthesis of Active Controls for Flutter Suppression on a Flight Research Wing." AIAA Guidance and Control Conference, Hollywood, Florida, August 1977.

APPENDIX A

DAST-I AERODATA

This appendix presents the DAST-I aerodata package used by the real time simulation program and for linear analysis. The data presented here are derived from computer implemented tables which give the aerodynamic derivatives as a function of Mach number and angle of attack. The derivatives presented here are referenced to the 1/4-chord point of the ARW-I.

The aerodata package was derived from data obtained from wind tunnel tests conducted by NASA Langley on a 1/6-scale model. The test procedures and results are presented in reference 1.

The derivatives C_m, C_L, and C_D are defined at every breakpoint as follows:

$$C_m = C_{m_o} + C_{m_\alpha} * \alpha_{B.P.}$$

$$C_L = C_{L_o} + C_{L_\alpha} * \alpha_{B.P.} \qquad (A.1)$$

$$C_D = C_{D_o} + C_{D_\alpha} * \alpha_{B.P.}$$

where $\alpha_{B.P.}$ is the angle of attack at every breakpoint.

Additional derivatives presented in this appendix are:

$C_{m_{\delta_e}}$, C_{m_q}, C_{m_α}

$C_{L_{\delta_e}}$

$C_{D_{\delta_e}}$

C_{ℓ_β}, C_{ℓ_r}, C_{ℓ_p}, $C_{\ell_{\delta_\alpha}}$, $C_{\ell_{\delta_r}}$

C_{n_β}, C_{n_r}, C_{n_p}, $C_{n_{\delta_\alpha}}$, $C_{n_{\delta_r}}$

C_{y_β}, $C_{y_{\delta_\alpha}}$, $C_{y_{\delta_r}}$

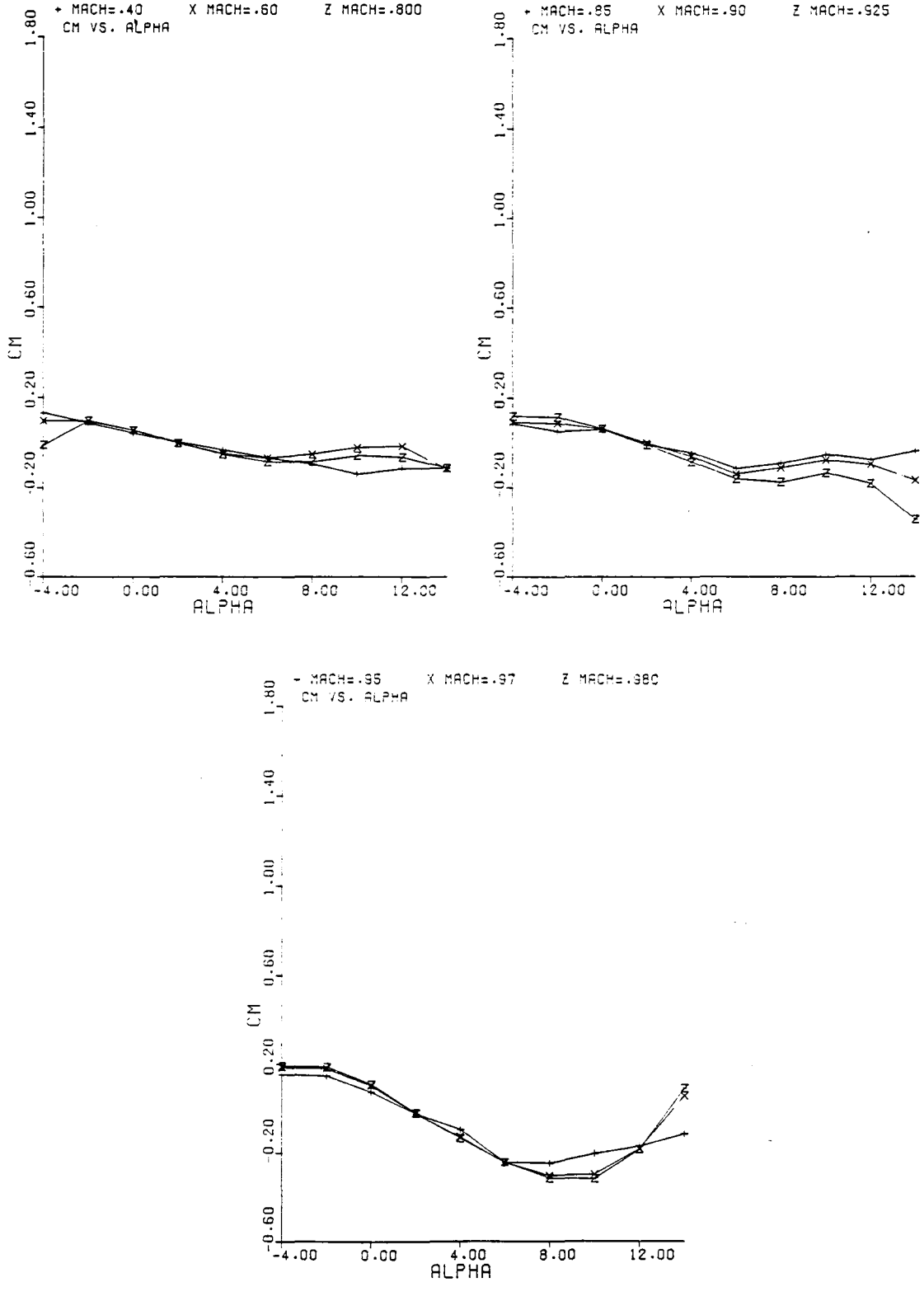

Figure A.1. Pitching moment coefficient, C_m, plotted against angle of attack, α. $C_m = C_{m_0} + C_{m_\alpha} * \alpha_{B.P.}$

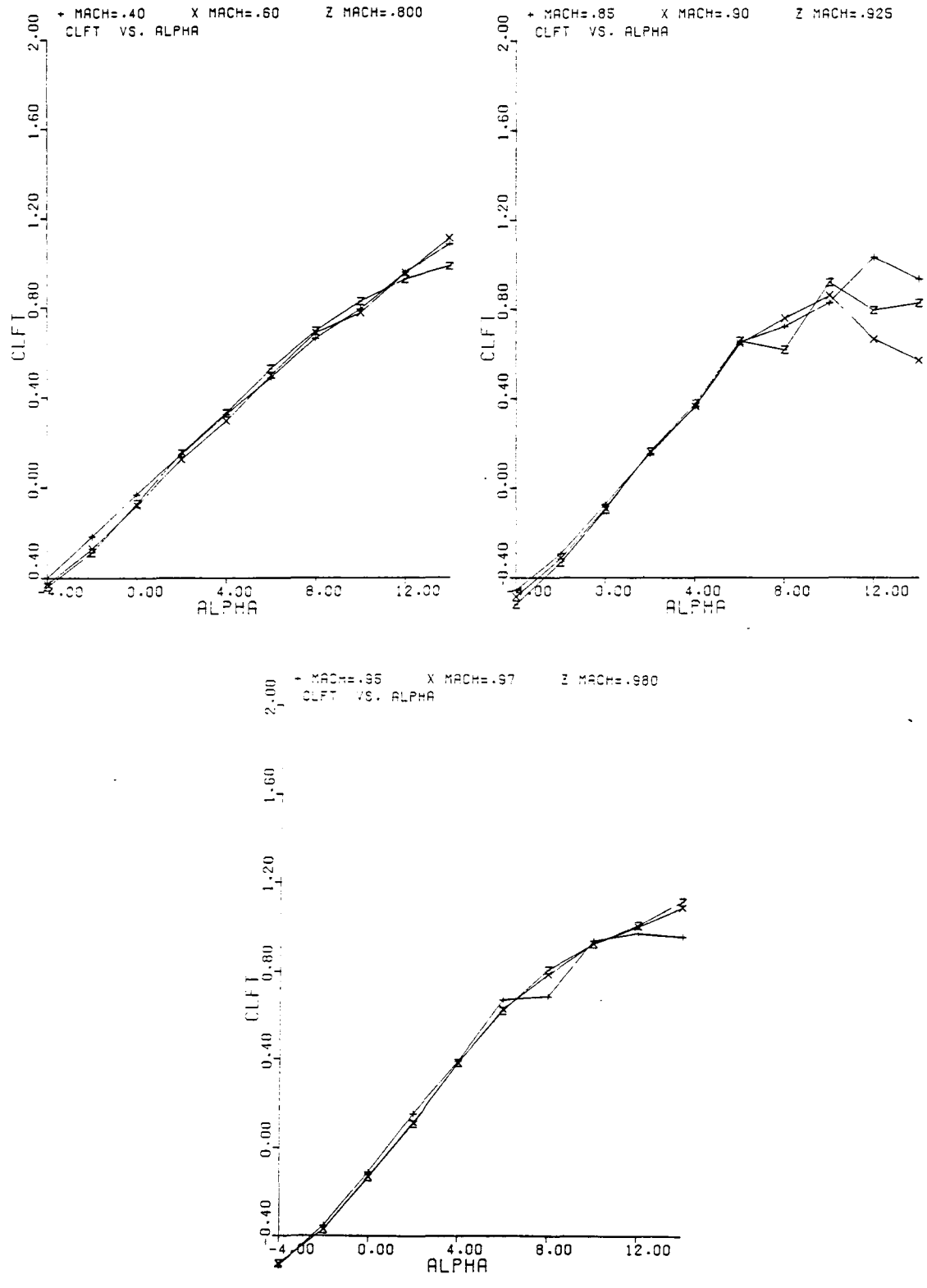

Figure A.2. Lift coefficient, C_L, plotted against angle of attack, α. $C_L = C_{L_0} + C_{L_\alpha} * \alpha_{B.P.}$

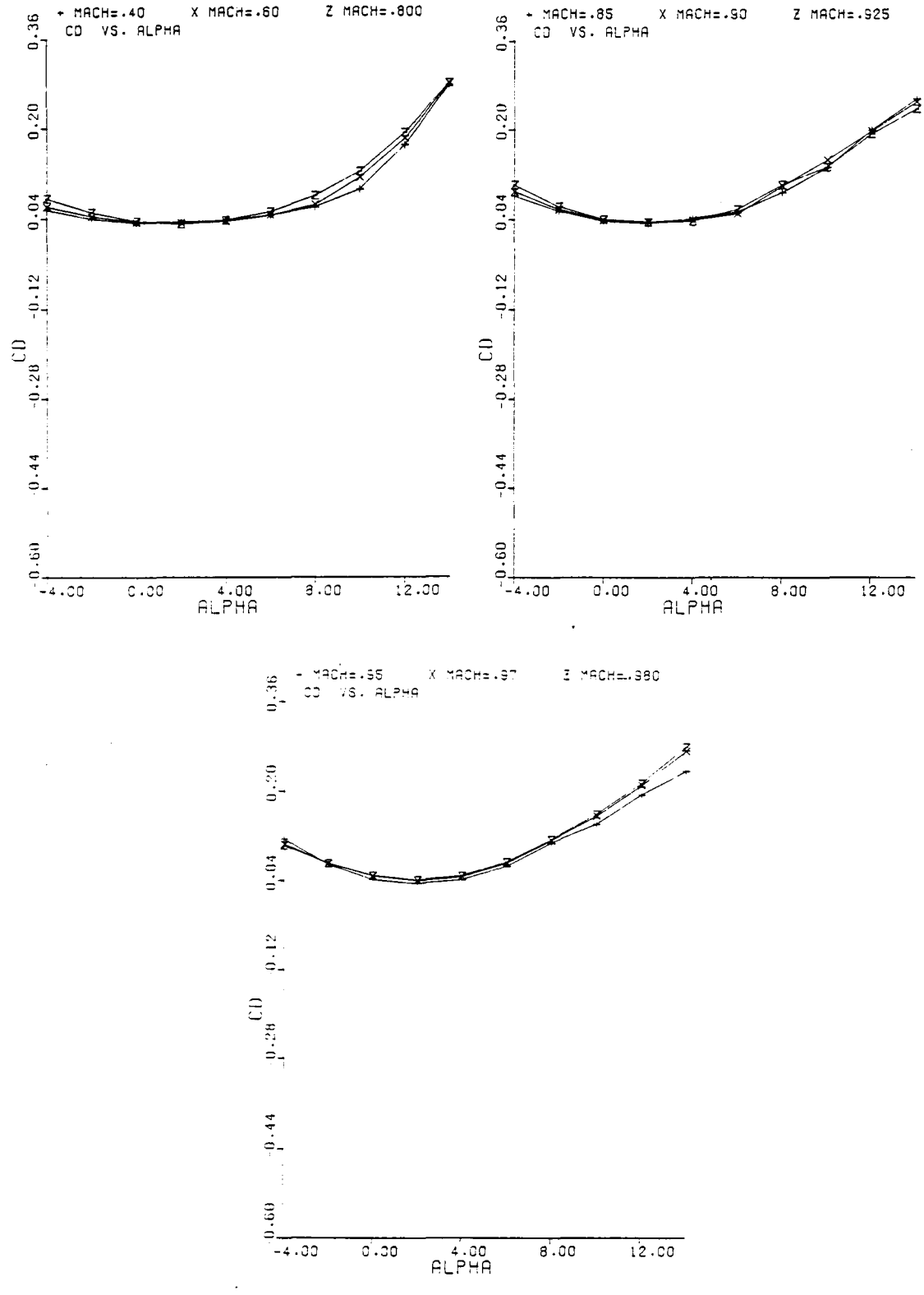

Figure A.3. Drag coefficient, C_D, plotted against angle of attack, α. $C_D = C_{D_0} + C_{D_\alpha} * \alpha_{B.P.}$

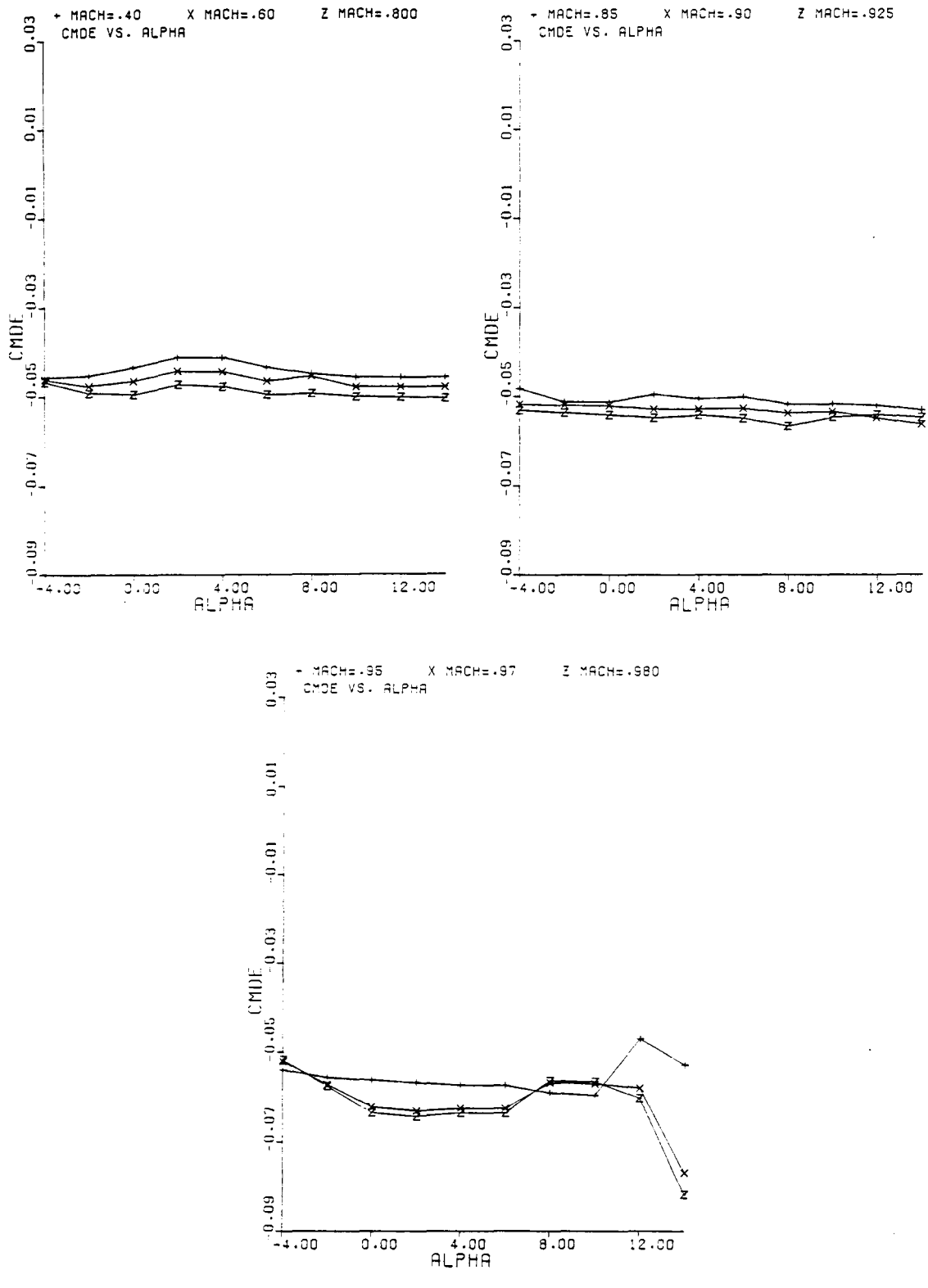

Figure A.4. Variation of pitching moment coefficient with elevator angle, $C_{m_{\delta_e}}$ (deg^{-1}), plotted against angle of attack, α.

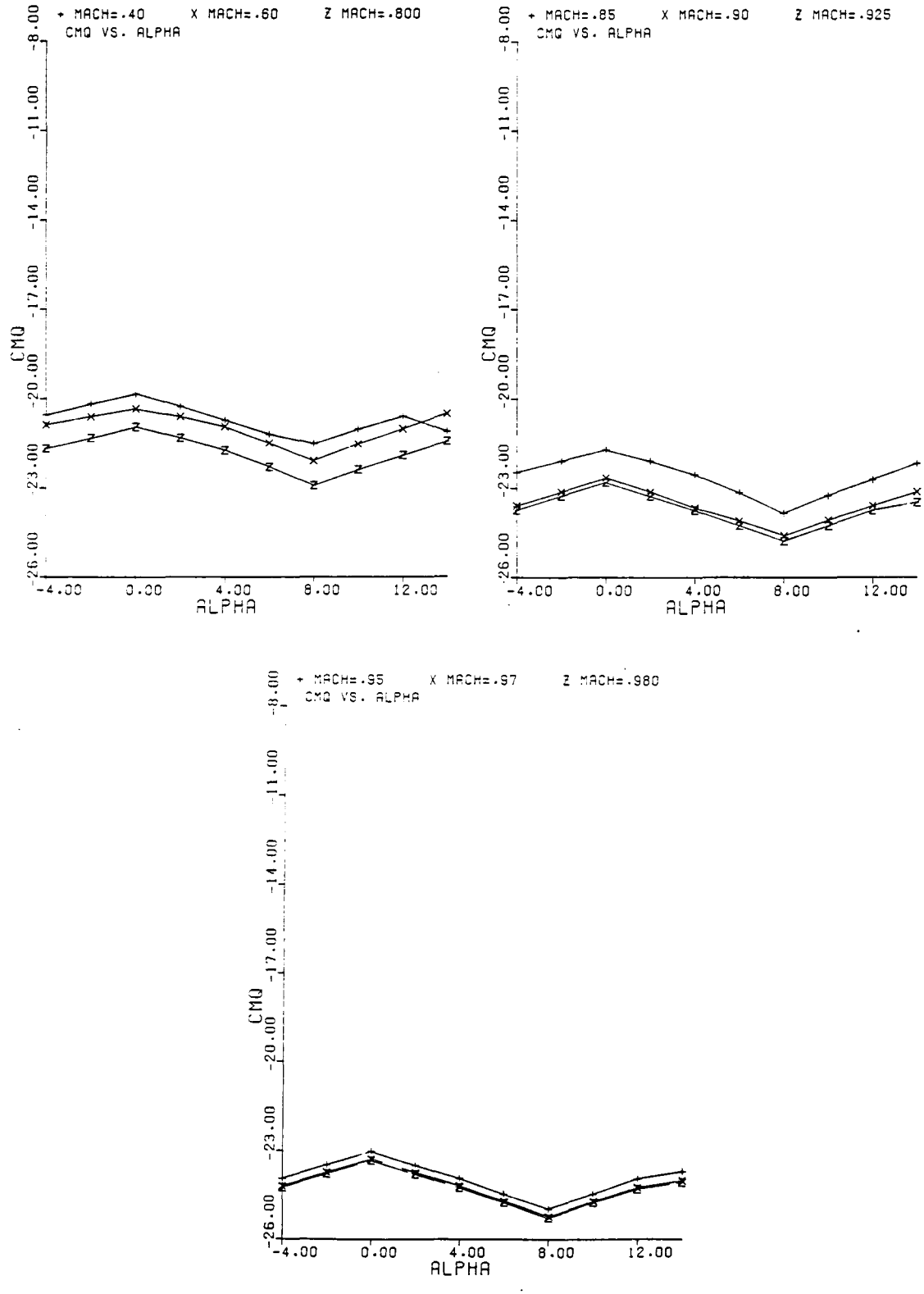

Figure A.5. Variation of pitching moment coefficient with pitch rate, C_{m_q} (rad^{-1}), plotted against angle of attack, α.

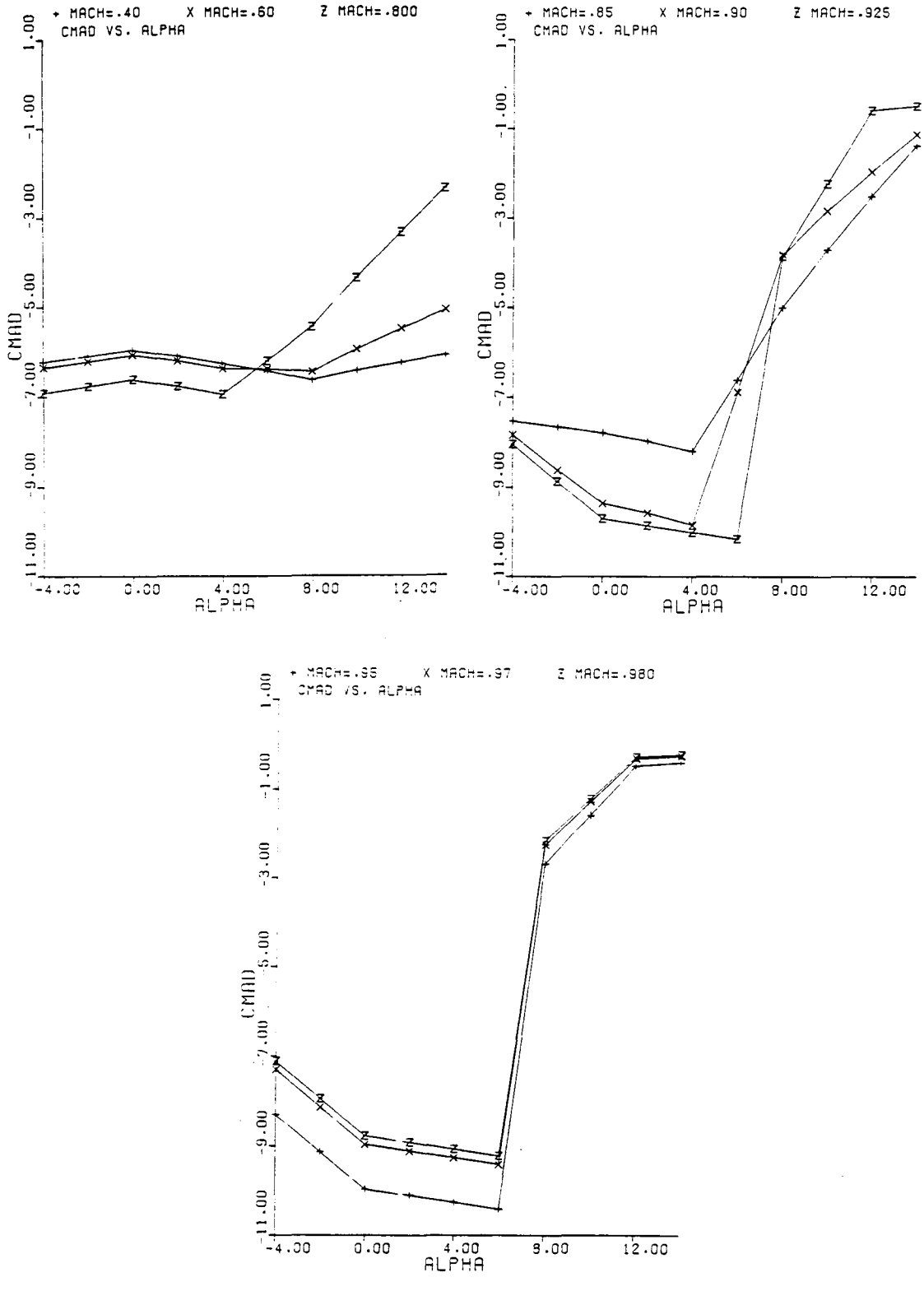

Figure A.6. Variation of pitching moment coefficient with angle of attack rate, $C_{m_{\dot{\alpha}}}$ (rad^{-1}), plotted against angle of attack, α.

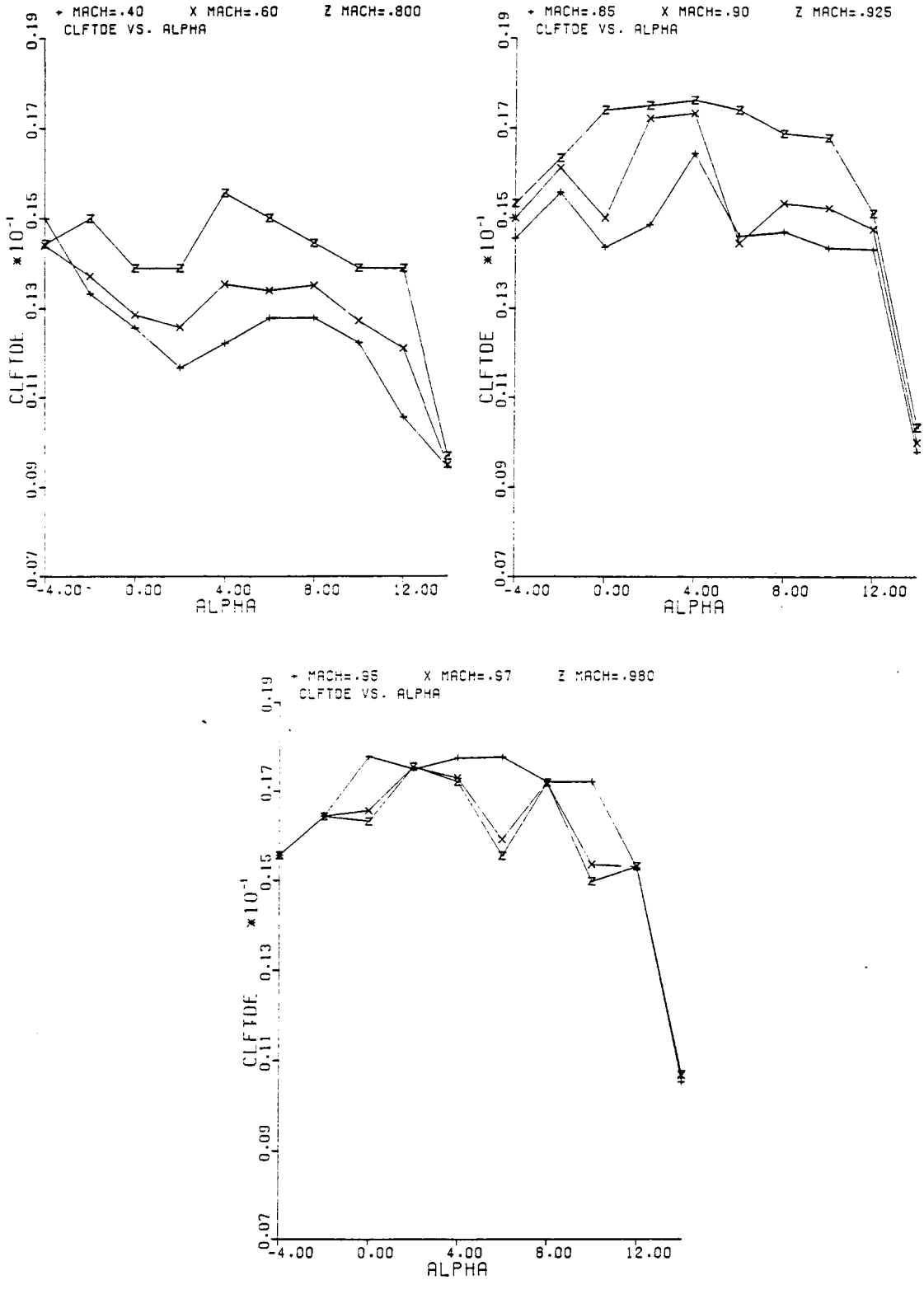

Figure A.7. Variation of lift coefficient with elevator angle, $C_{L_{\delta_e}}$ (deg^{-1}), plotted against angle of attack, α.

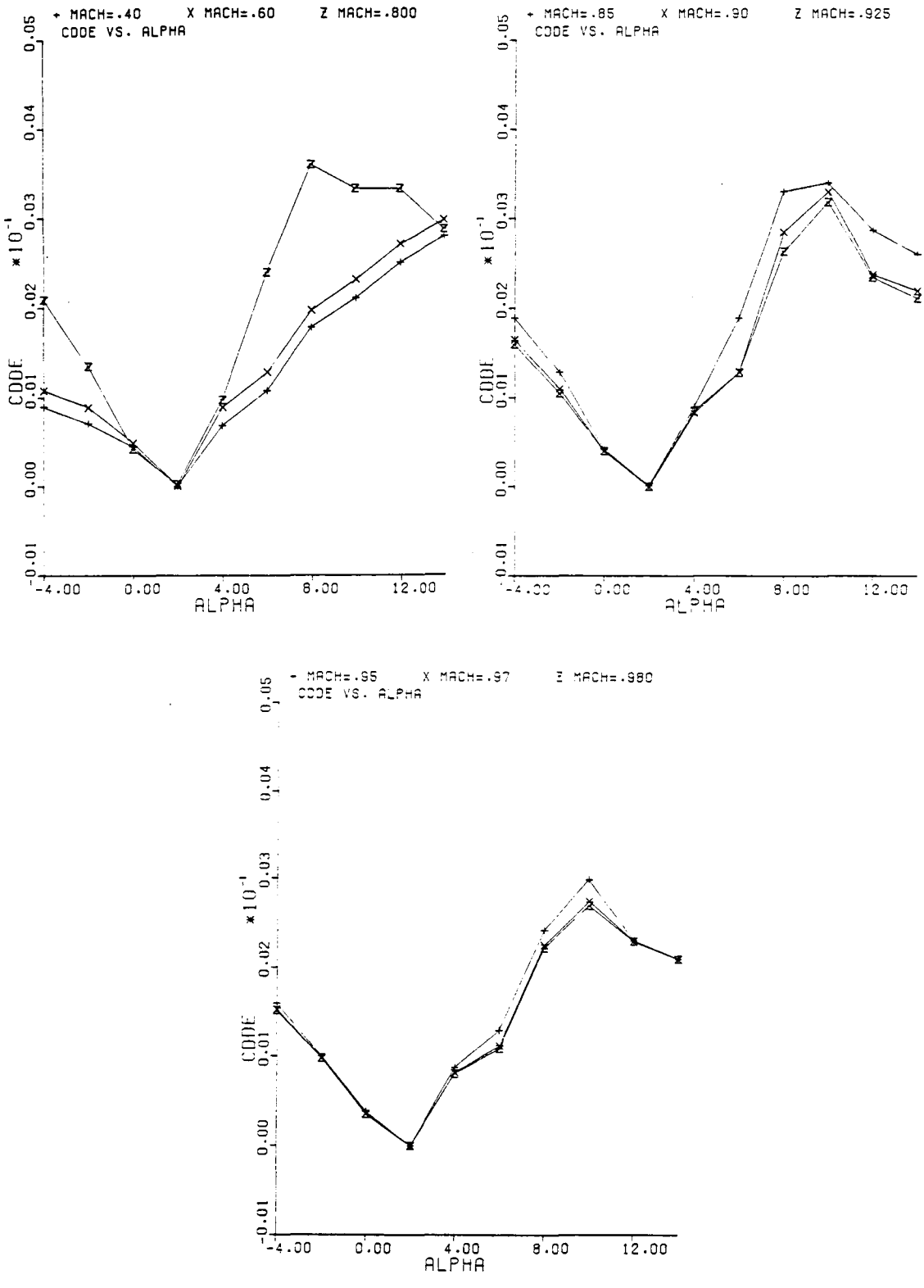

Figure A.8. Variation of drag coefficient with elevator angle, $C_{D_{\delta_e}}$ (deg^{-1}), plotted against angle of attack, α.

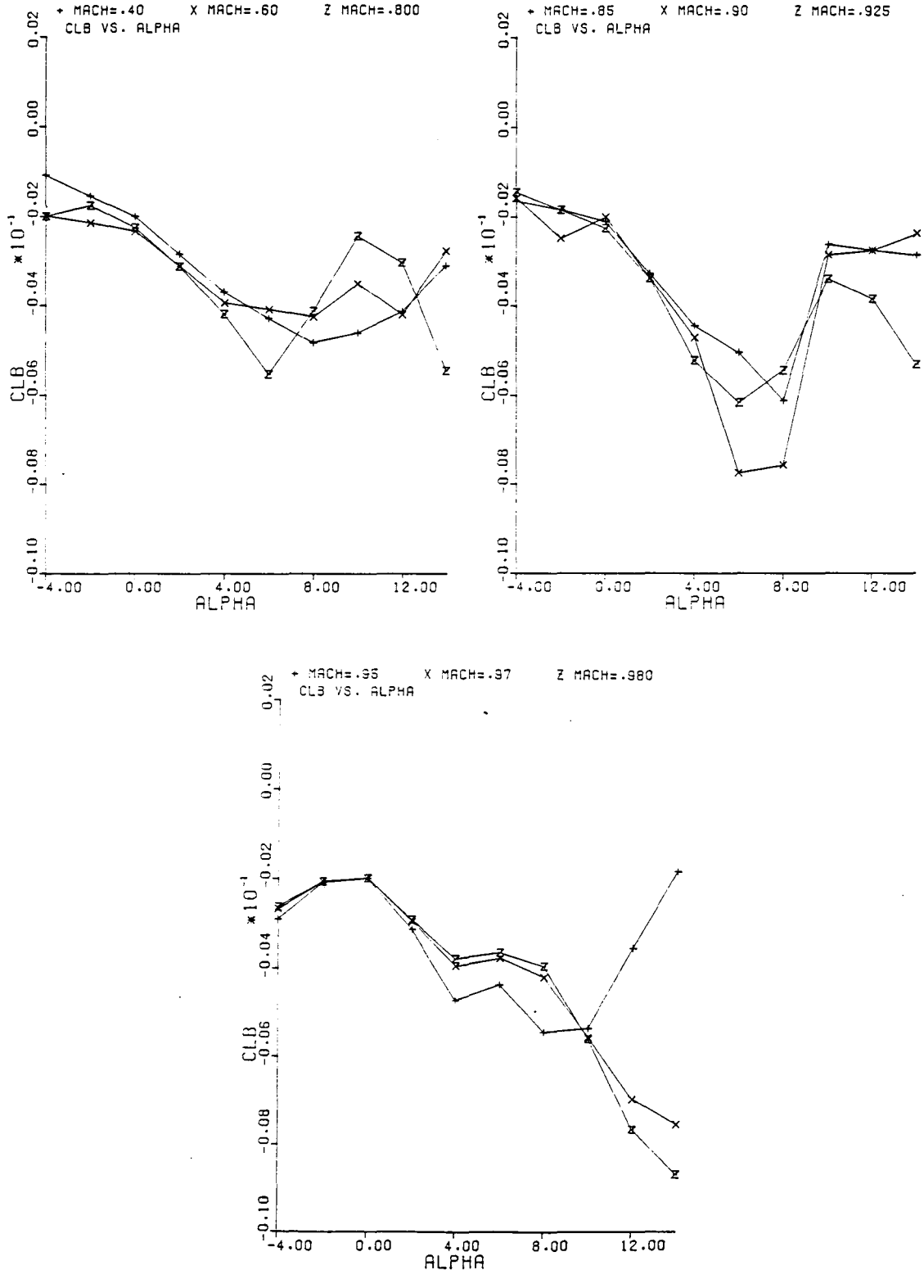

Figure A.9. Variation of rolling moment coefficient with sideslip angle, C_{ℓ_β} (deg^{-1}), plotted against angle of attack, α.

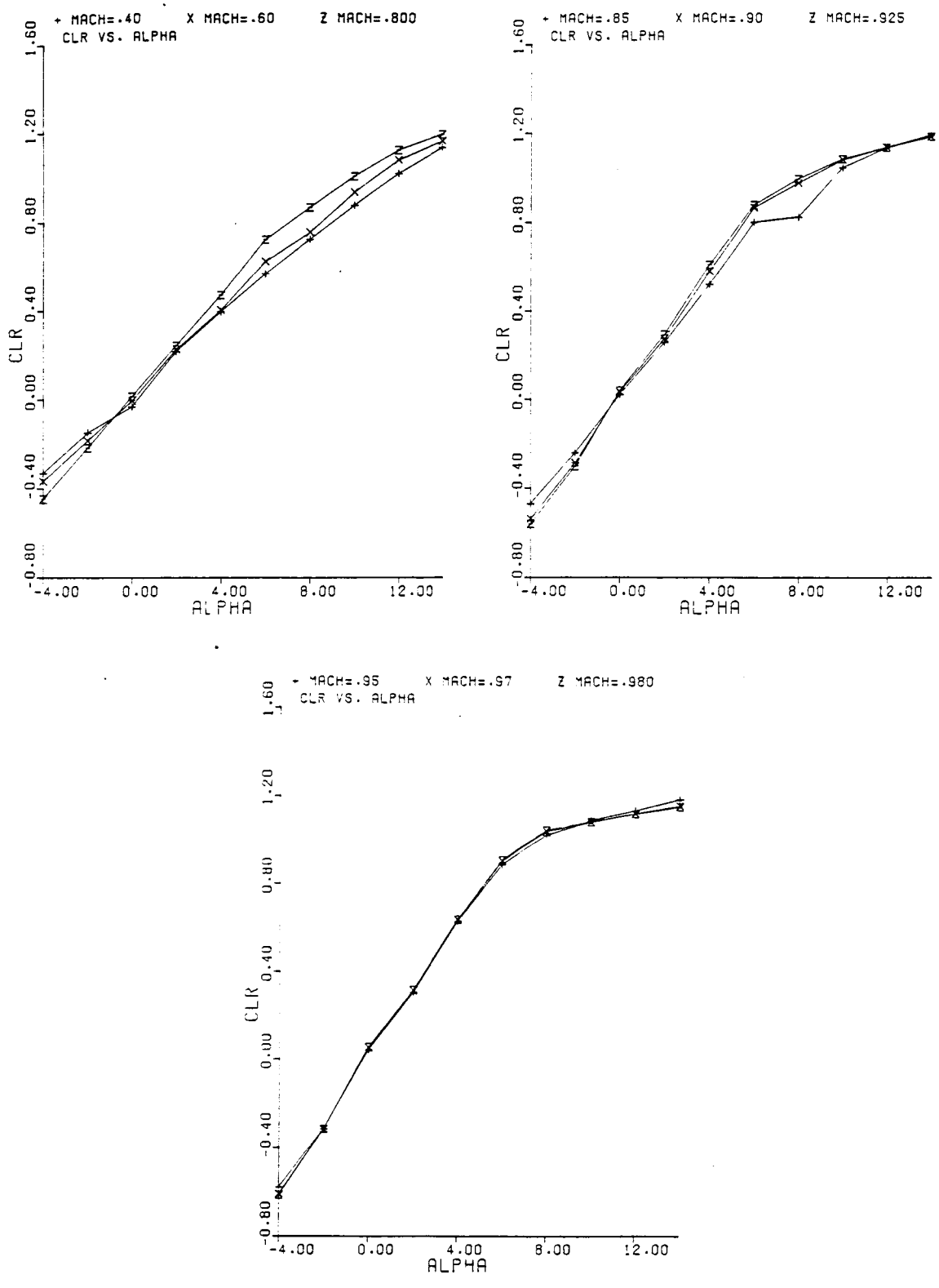

Figure A.10. Variation of rolling moment coefficient with yaw rate, C_{ℓ_r} (rad^{-1}), plotted against angle of attack, α.

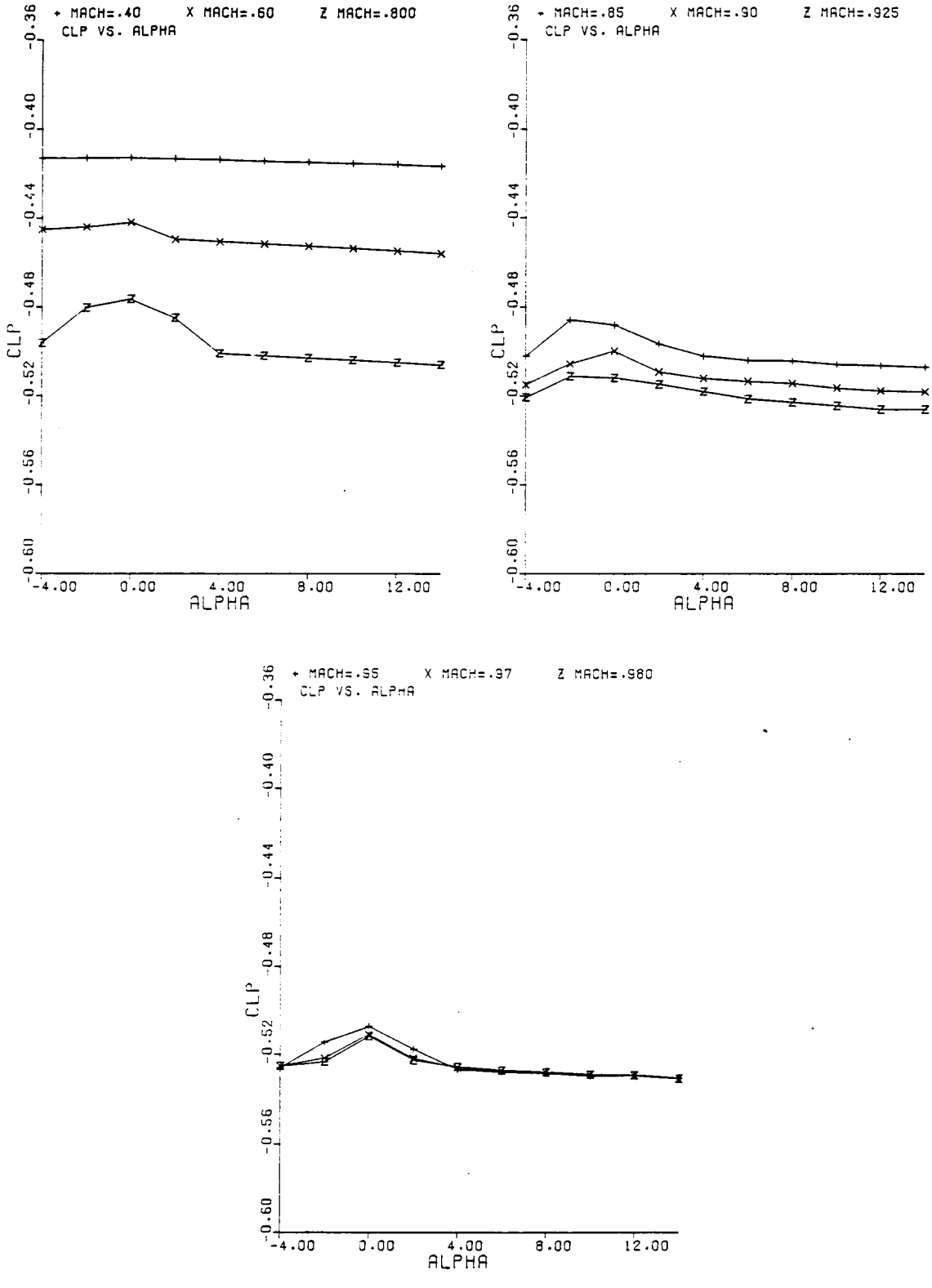

Figure A.11. Variation of rolling moment coefficient with roll rate, C_{ℓ_p} (rad^{-1}), plotted against angle of attack, α.

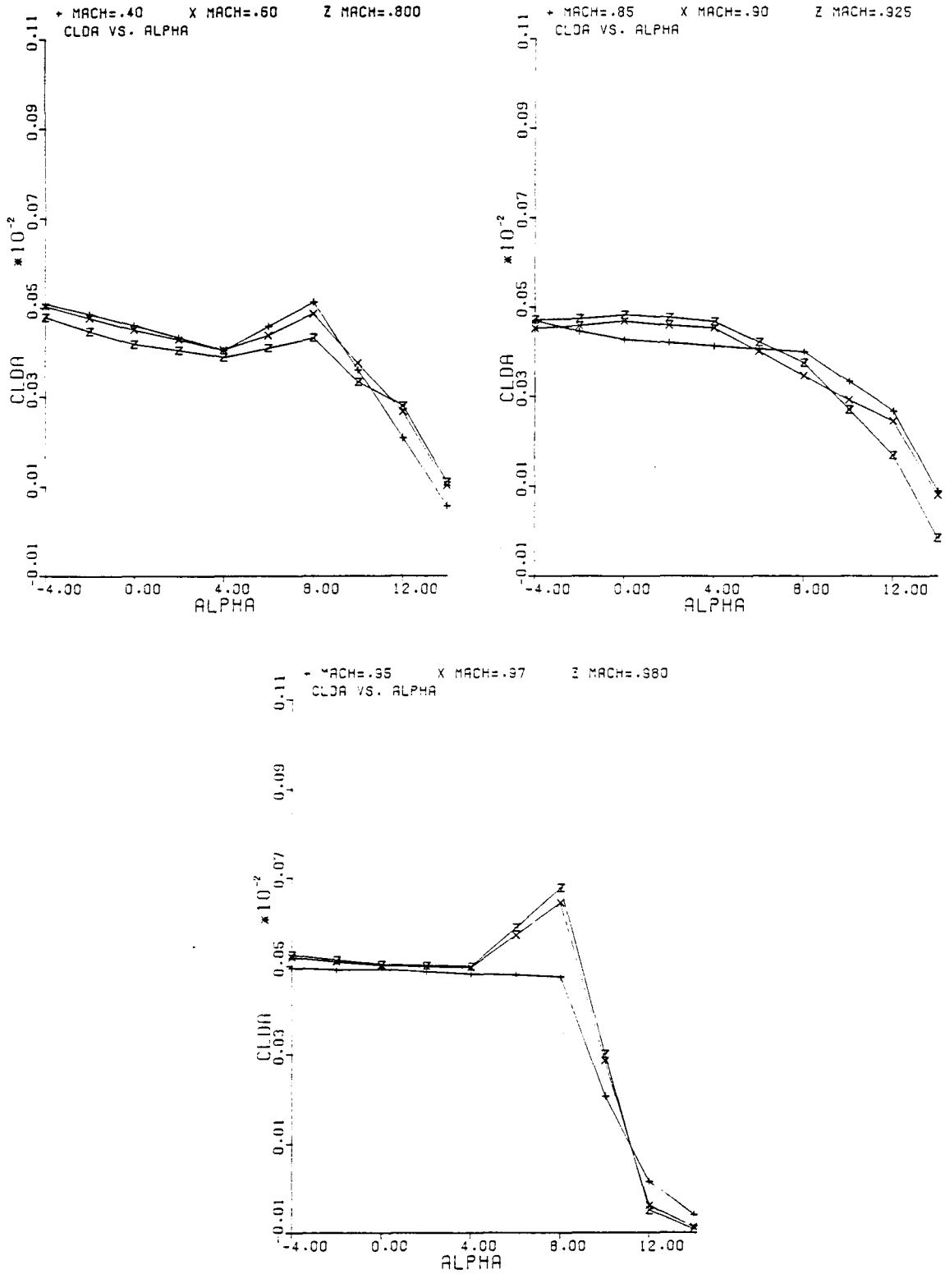

Figure A.12. Variation of rolling moment coefficient with aileron angle, $C_{\ell_{\delta_a}}$ (deg^{-1}), plotted against angle of attack, α.

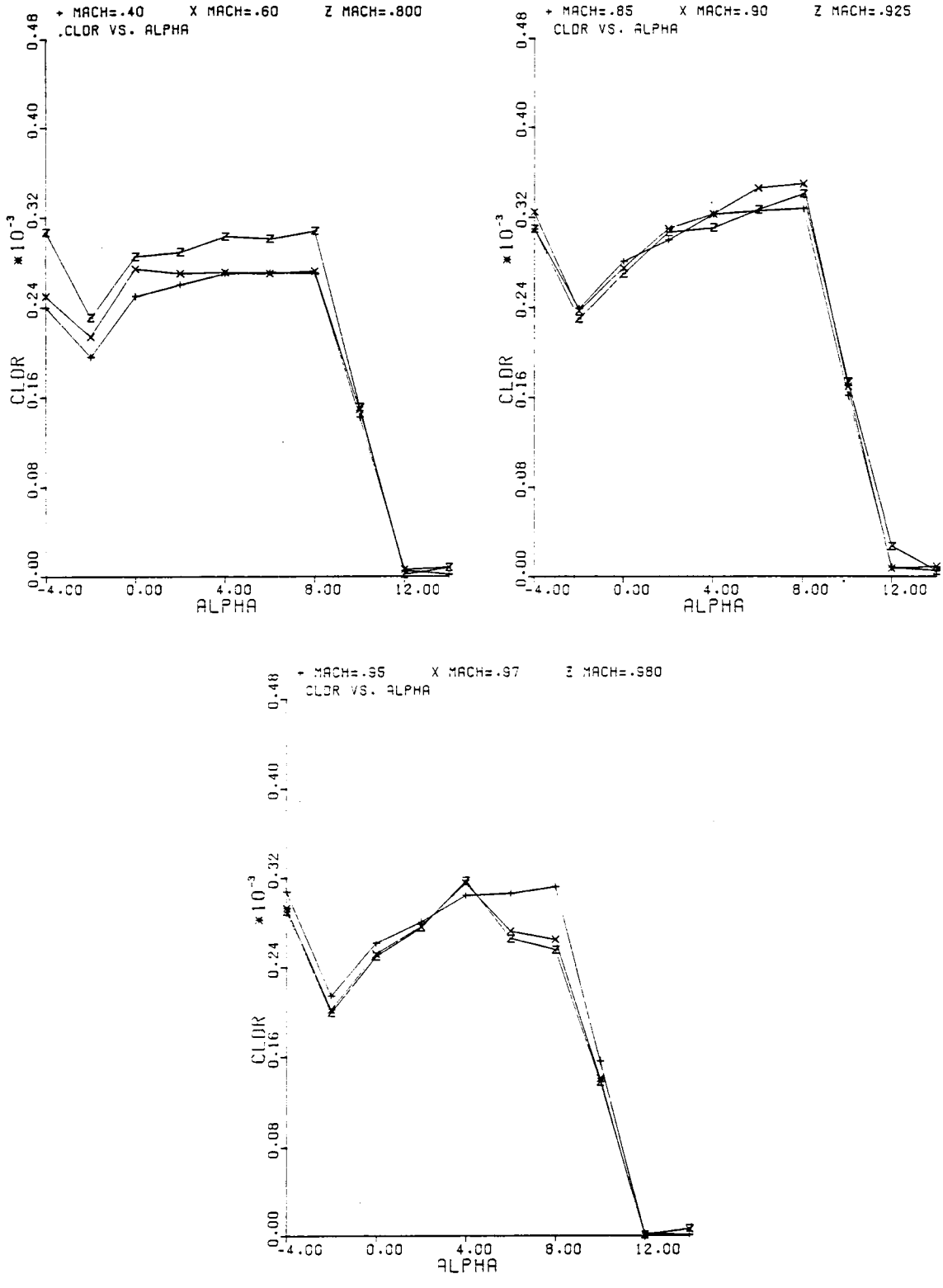

Figure A.13. Variation of rolling moment coefficient with rudder angle, $C_{\ell_{\delta_r}}$ (deg^{-1}), plotted against angle of attack, α.

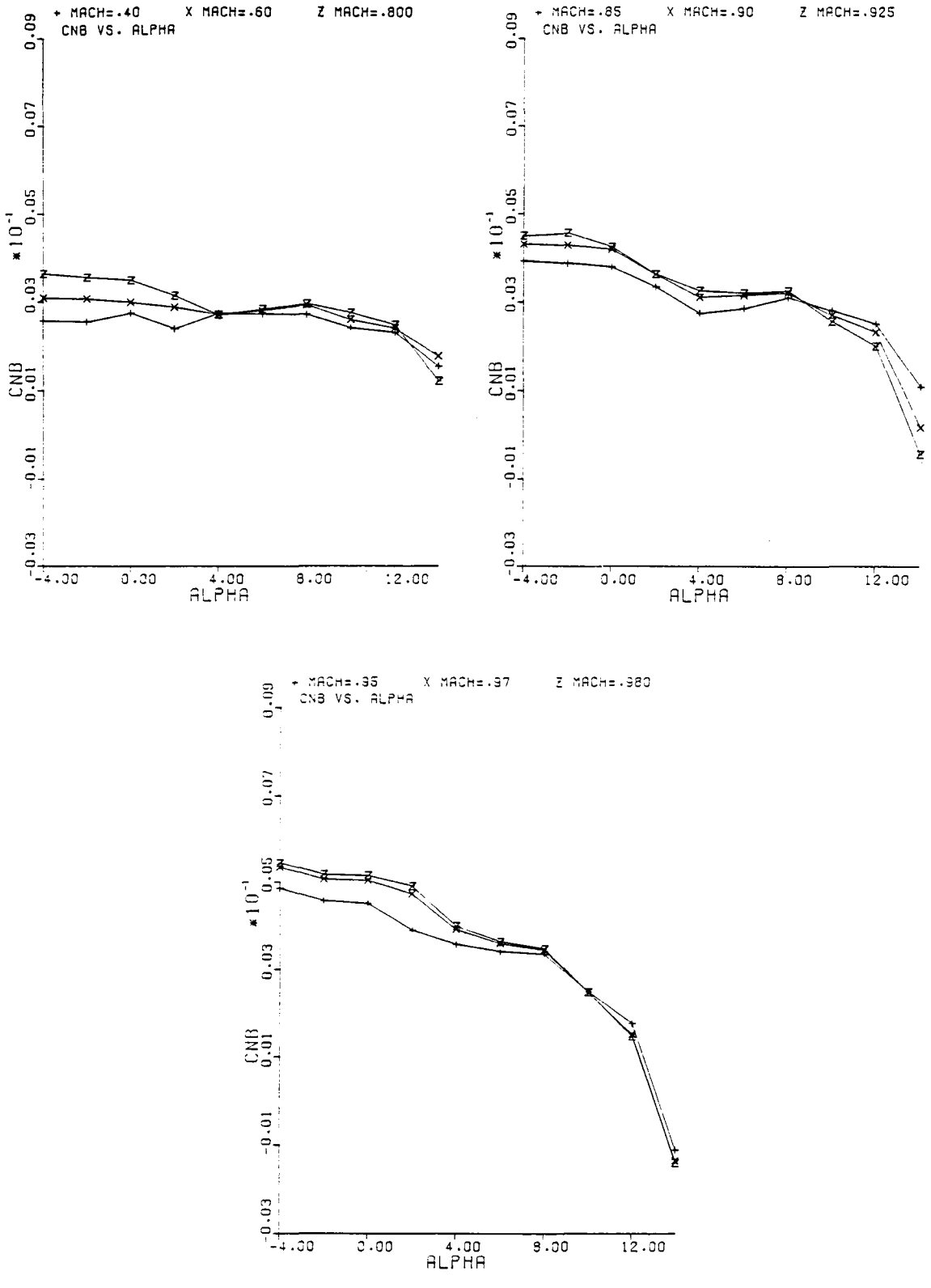

Figure A.14. Variation of yawing moment with sideslip angle, C_{n_β} (deg^{-1}), plotted against angle of attack, α.

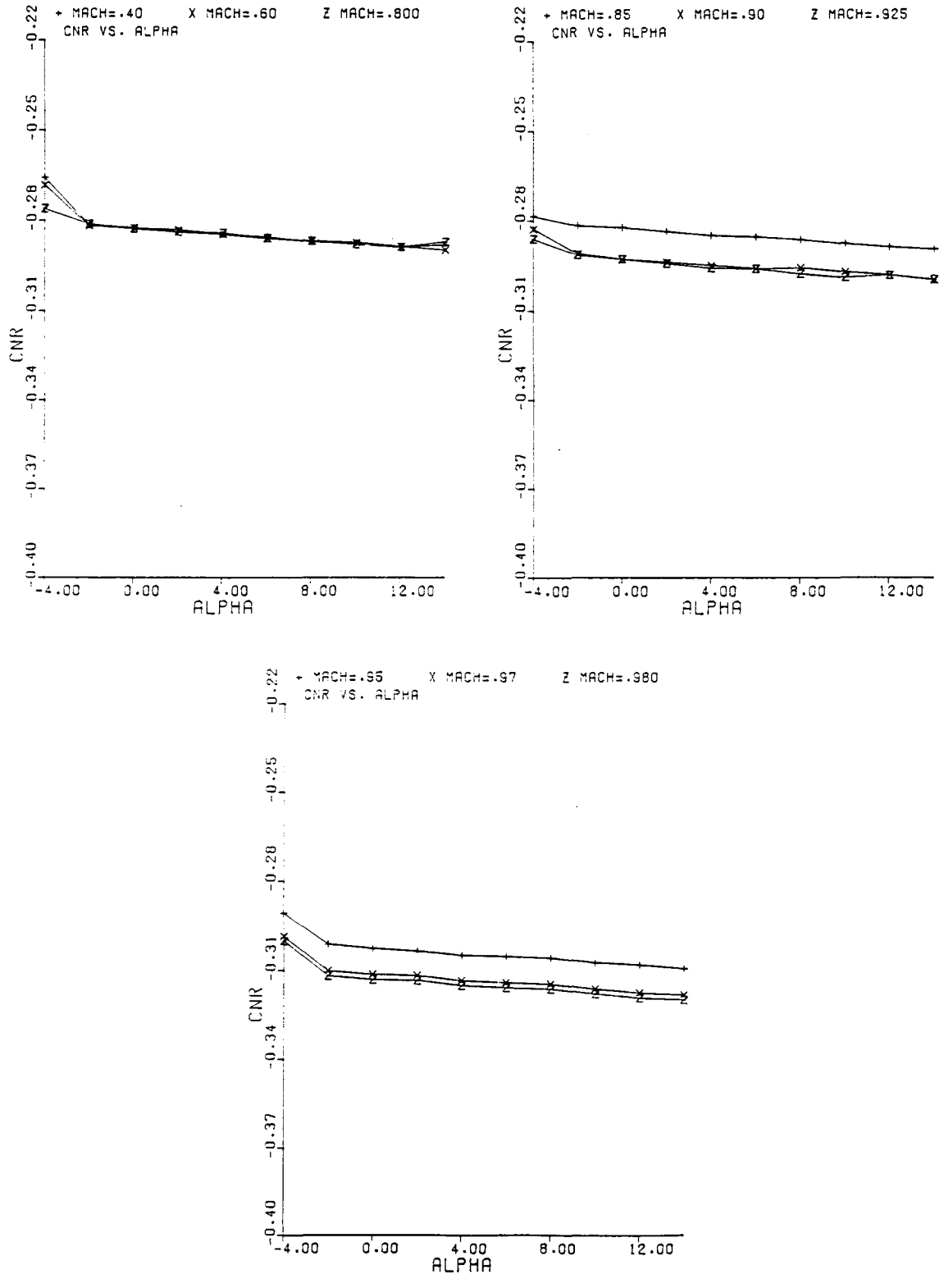

Figure A.15. Variation of yawing moment with yaw rate, C_{n_r} (rad^{-1}), plotted against angle of attack, α.

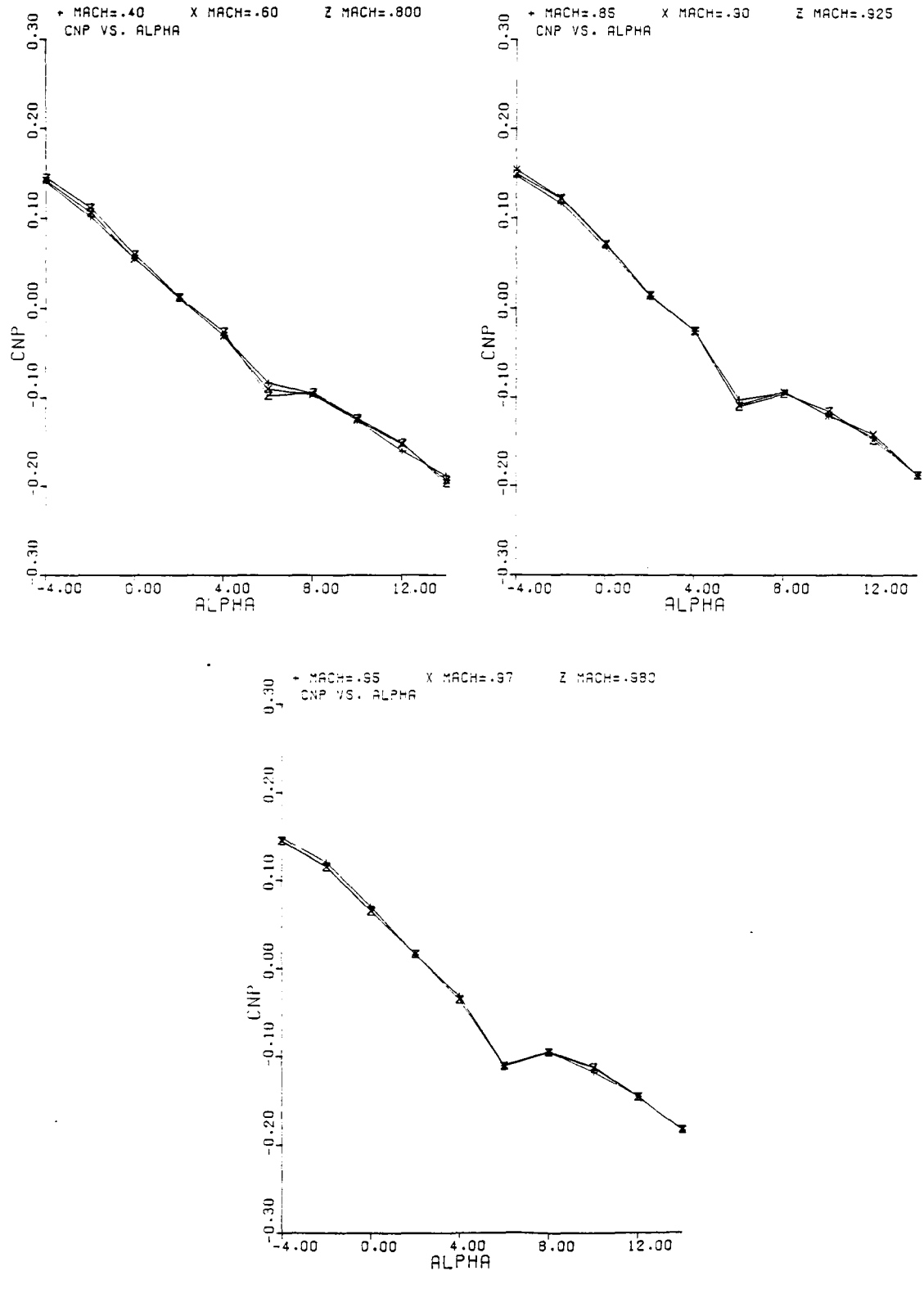

Figure A.16. Variation of yawing moment with roll rate, C_{n_p} (rad^{-1}), plotted against angle of attack, α.

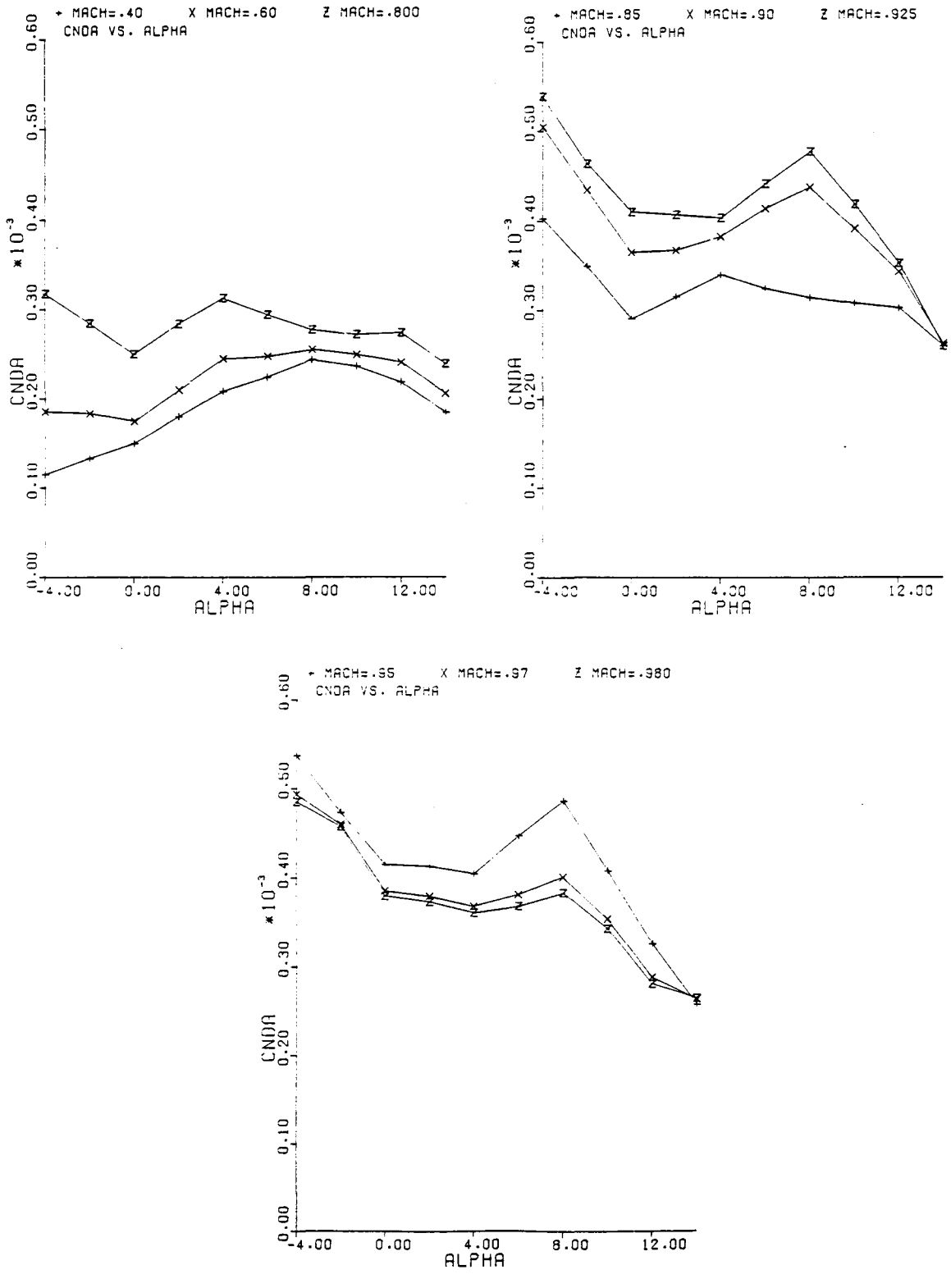

Figure A.17. Variation of yawing moment with aileron angle, $C_{n_{\delta_a}}$ (deg^{-1}), plotted against angle of attack, α.

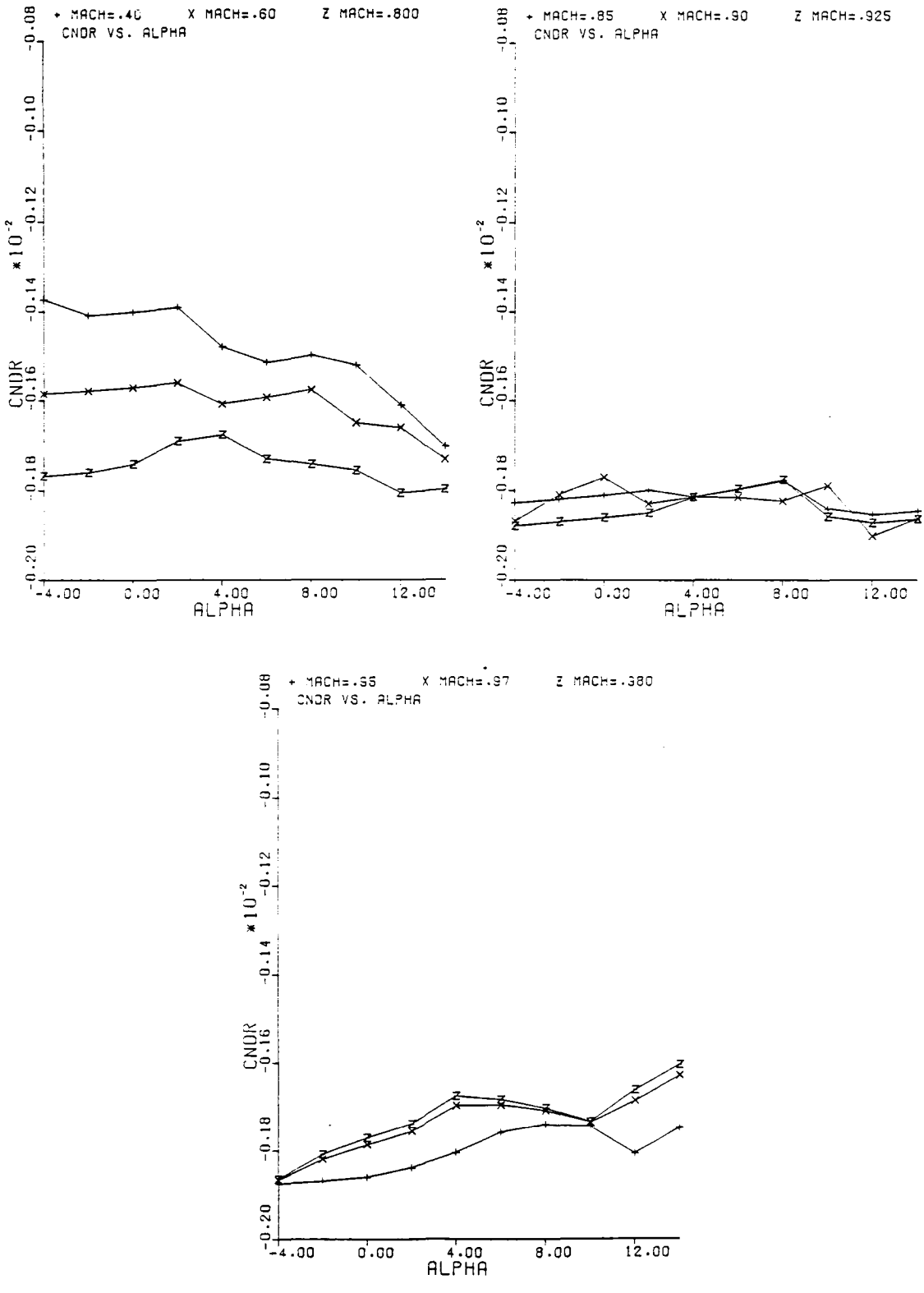

Figure A.18. Variation of yawing moment with rudder angle, $C_{n_{\delta_r}}$ (deg^{-1}), plotted against angle of attack, α.

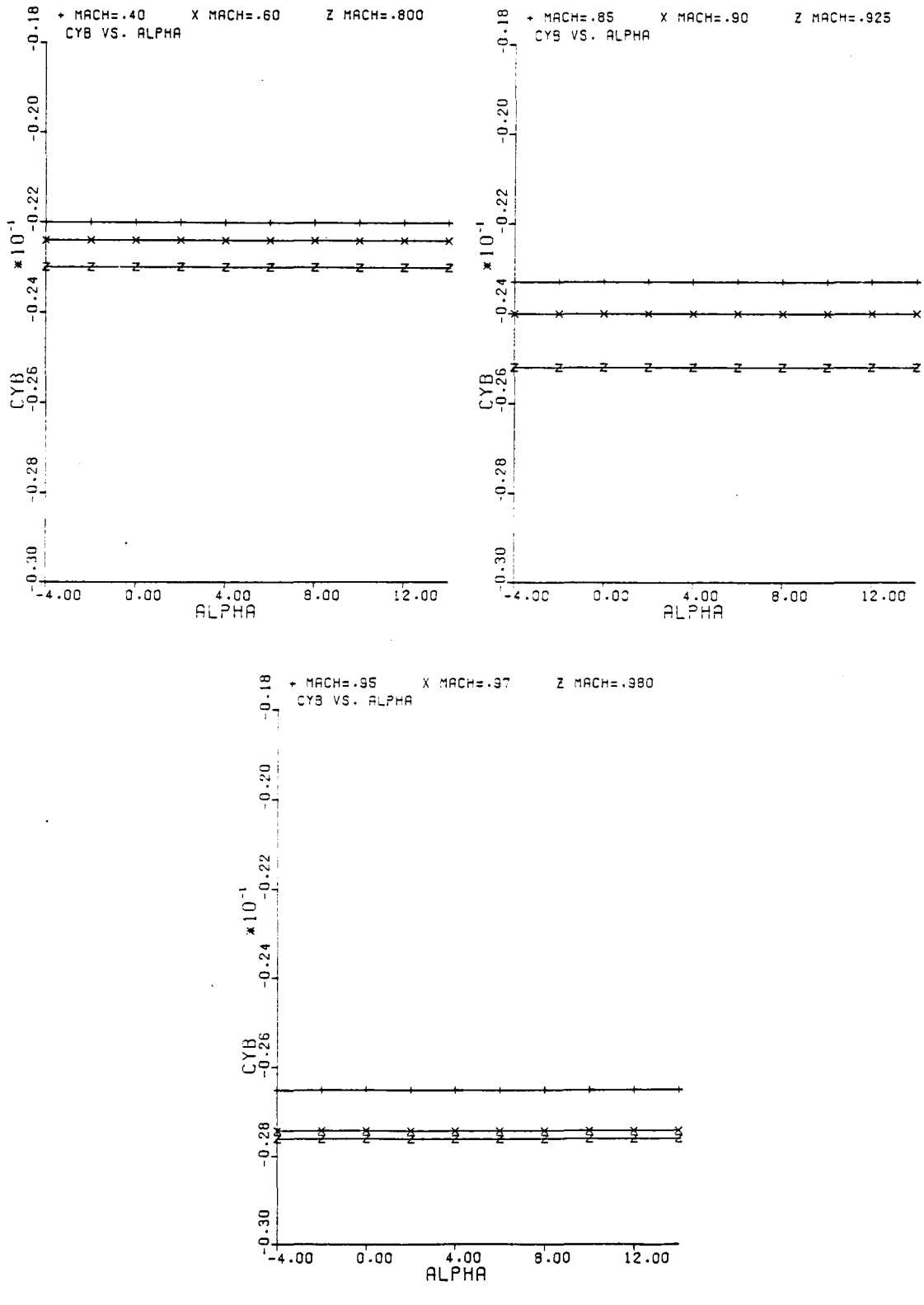

Figure A.19. Variation of side force coefficient with sideslip angle, C_{y_β} (deg^{-1}), plotted against angle of attack, α.

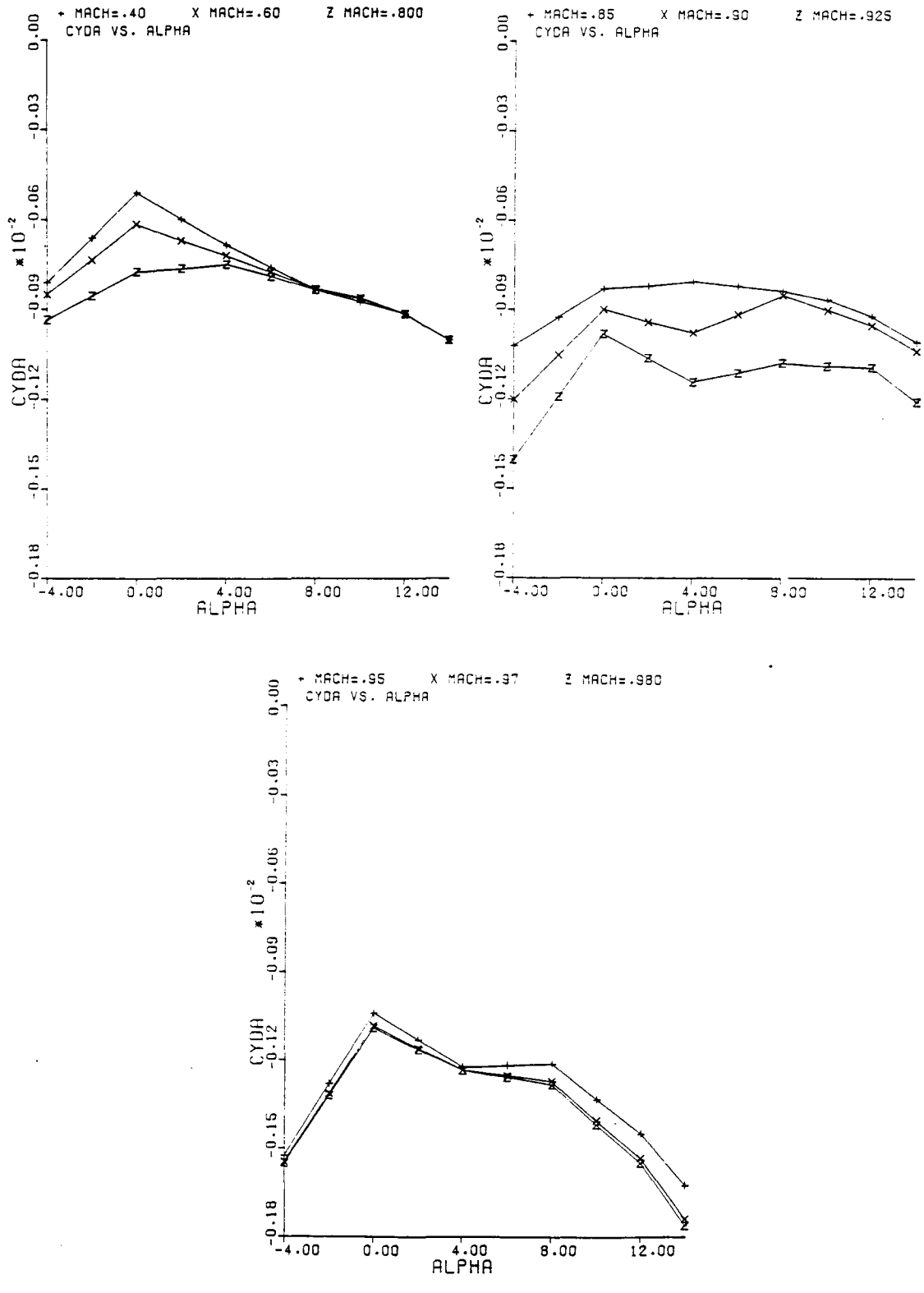

Figure A.20. Variation of side force coefficient with aileron angle, $C_{y_{\delta_a}}$ (deg^{-1}), plotted against angle of attack, α.

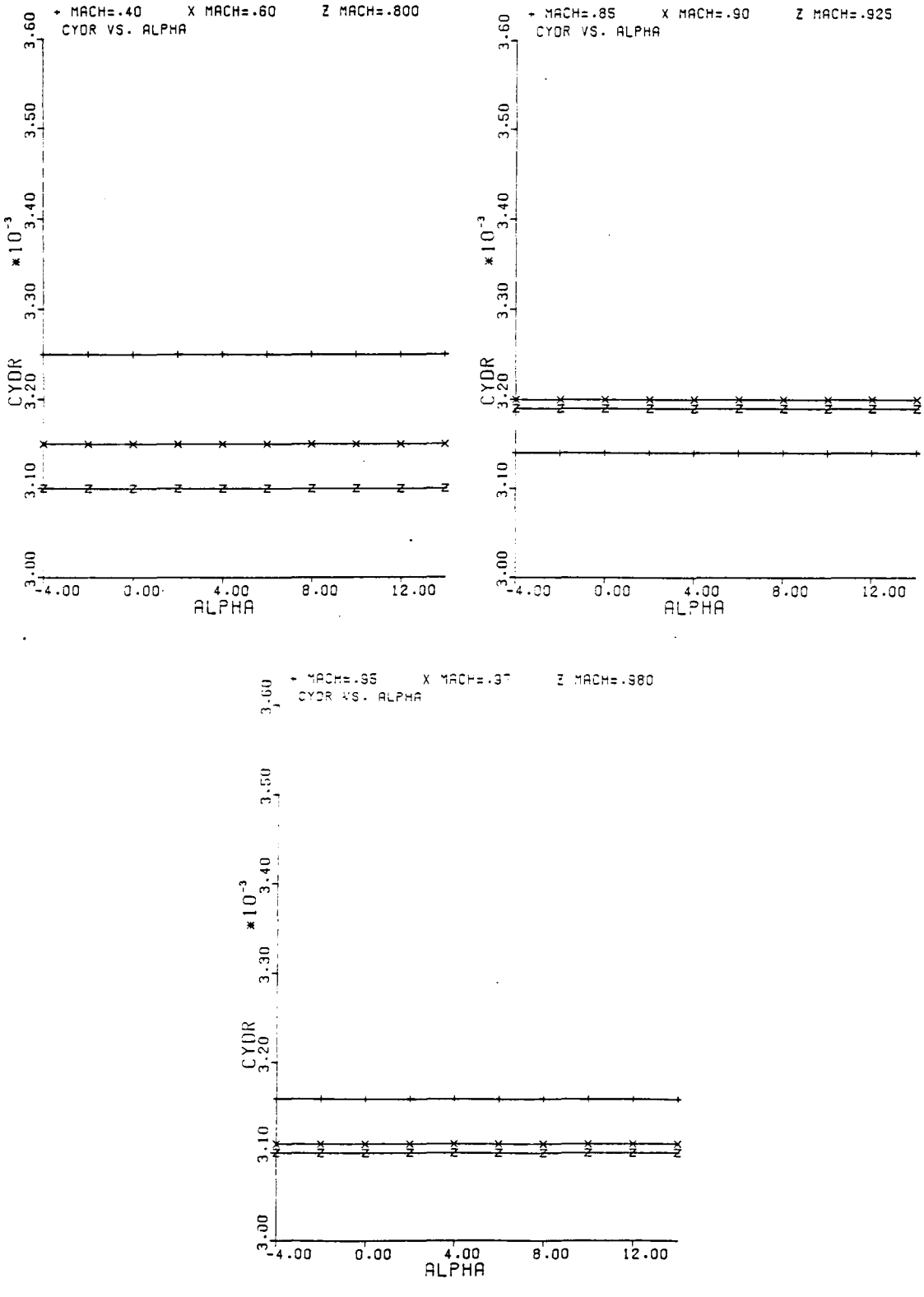

Figure A.21. Variation of side force coefficient with rudder angle, $C_{y_{\delta_r}}$ (deg^{-1}), plotted against angle of attack, α.

APPENDIX B

THE COMMAND AUGMENTATION SYSTEM (CAS)

This appendix describes the pitch axis augmentation system that was implemented in the Varian computer during the first ARW-I test flight. The system provided basically a load limiting and an altitude hold function. A block diagram of this mode is presented in figure B.1. The mode is presented here as an analog system to simplify the description. The system consists of the following feedback paths:

- The pitch rate feedback path is identical to the feedback path in the RD mode. The selectable feedback gains are also of the same magnitude.

- A direct plus integral altitude rate feedback path provides the altitude hold function. The altitude rate signal is computed as shown in section 5.3, equation 5.1. The multiplier gives full authority to this path between ±1000 ft/min (app. 305 m/min) and decreases the authority linearly to zero at ±2000 ft/min (610 m/min). This schedule provides the pilot with an override capability. The feedback path is initialized to zero at the moment of engagement to eliminate problems arrising from biases in the angle of attack and pitch angle signals. This initialization implies that this path will try to maintain the altitude rate at the moment of engagement.

- The positive and negative load limiter paths prevent the pilot from exceeding the 2.5 and -1.5 g structural load limits of the wing. The load limiting schedules are shown in figure B.2. As the pilot increases the load factor the schedule output will cause the maximum select switch to disengage the pilots input. As long as the pilot remains commanding a pitching up maneuver, the forward loop integrator will gradually drive the load factor to 2.5 g. The operation of the negative load limiter is similar.

- The pilots path in CAS has the same gearing as in CD and RD. The pilot has proportional plus integral control. In addition to the CD and RD mode, this path has a low pass filter and a deadband of ±.05 degrees. The deadband was introduced to avoid stick noise from upsetting the forward loop integrator. This path is initialized at the moment CAS is engaged. The longitudinal trim value at the moment of engagement is subtracted from this path as a constant to provide a zero signal at the

input of the maximum select switch. This will cause the maximum select switching to be independent of the flight condition at which engagement of the mode took place. In order to maintain the trimmed elevator position the subtracted trim value is added further down stream.

The CAS mode as presented here exhibited a low damped oscillation during flight. This was attributed to flexibility effects of the wing and the high altitude rate feedback gain. This mode was deleted following the first ARW-I flight, mainly because it was found that the load limiting function (which contributes considerably to the complexity of this mode) was not necessary.

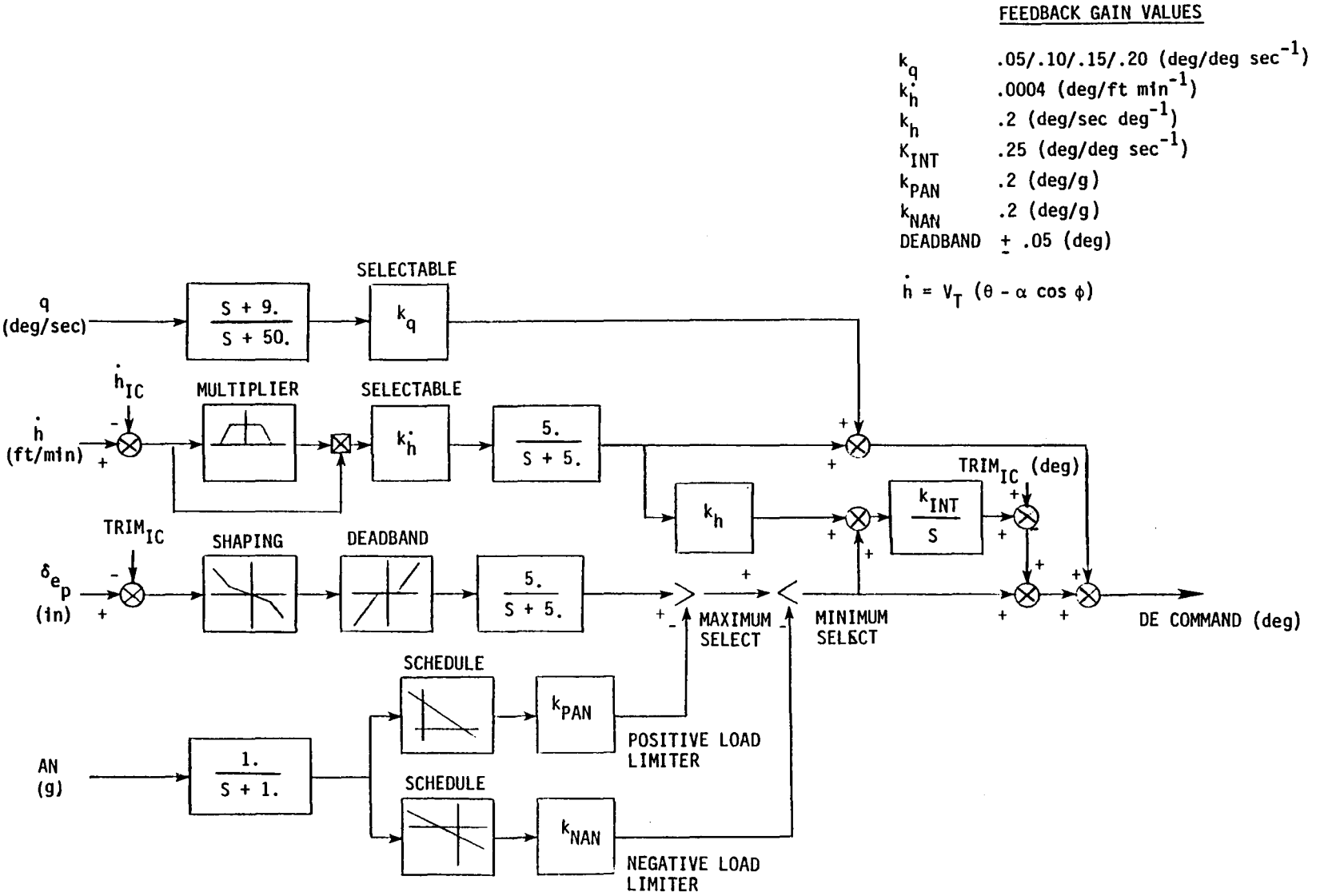

Figure B.1. Command augmentation system block diagram.

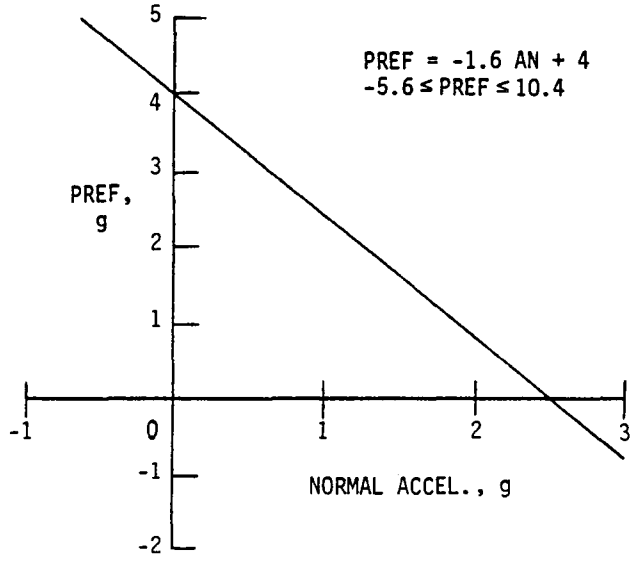

(a) Positive load factor schedule.

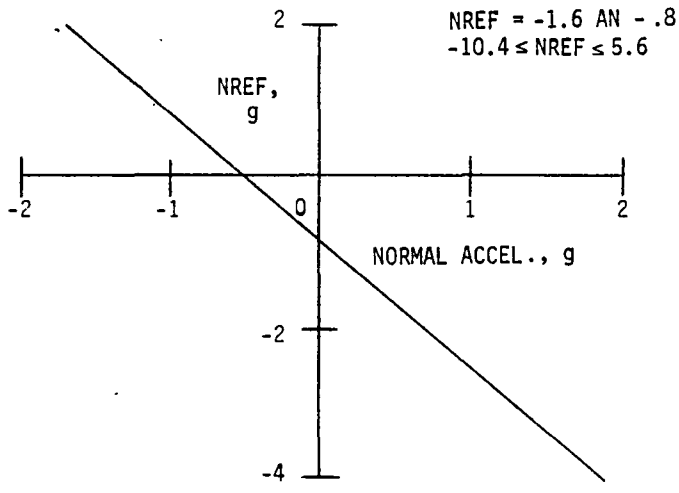

(b) Negative load factor schedule.

Figure B.2. Load limiter schedules.

1. Report No.	2. Government Accession No.	3. Recipient's Catalog No.
CR-163105		

4. Title and Subtitle	5. Report Date
THE DAST-I REMOTELY PILOTED RESEARCH VEHICLE DEVELOPMENT AND INITIAL FLIGHT TESTING	February 1981
	6. Performing Organization Code

7. Author(s)	8. Performing Organization Report No.
Alexandros Kotsabasis	
	10. Work Unit No.

9. Performing Organization Name and Address	11. Contract or Grant No.
University of Kansas Center for Research, Incorporated 2291 Irving Hill Drive Lawrence, Kansas 66045	NSG 4017
	13. Type of Report and Period Covered
12. Sponsoring Agency Name and Address	Contractor Report - Final
National Aeronautics and Space Administration Washington, DC 20546	14. Sponsoring Agency Code 505-33-54

15. Supplementary Notes

NASA Technical Monitor: Glenn B. Gilyard

16. Abstract

The development and initial flight testing of the DAST (Drones for Aerodynamic and Structural Testing) remotely piloted research vehicle, fitted with the first Aeroelastic Research Wing, ARW-I, are presented. A modified BQM-34E/F Firebee II supersonic aerial target drone is utilized as test bed. The ARW-I is a swept supercritical wing, designed to exhibit flutter within the vehicle's flight envelope. An active Flutter Suppression System (FSS) designed to increase the ARW-I flutter boundary speed by 20 percent is described. The development of the FSS was based on prediction techniques of structural and unsteady aerodynamic characteristics. A description of the supporting ground facilities and aircraft systems involved in the Remotely Piloted Research Vehicle (RPRV) flight test technique is given. The design, specification, and testing of the Remotely Augmented Vehicle (RAV) system are presented. A summary of the preflight and flight test procedures associated with the RPRV operation is given. An evaluation of the Blue Streak test flight and the first and second ARW-I test flights is presented.

17. Key Words (Suggested by Author(s))	18. Distribution Statement
DAST ARW-I Remotely piloted research vehicle Active flutter suppression	Unclassified - Unlimited Subject category 05

19. Security Classif. (of this report)	20. Security Classif. (of this page)	21. No. of Pages	22. Price*
Unclassified	Unclassified	229	$14

For sale by the National Technical Information Service, Springfield, Virginia 22161

End of Document